

Using Automation, Theory and Machine Learning to Gain Mechanistic Understanding of Chemical Glycosylation

Inaugural-Dissertation
to obtain the academic degree
Doctor rerum naturalium (Dr. rer. nat.)

Submitted to the Department of Biology, Chemistry and Pharmacy
of Freie Universität Berlin

by
Sooyeon Moon
February 2020

The work in this dissertation was performed between January 2016 and December 2019 under the supervision of Prof. Dr. Peter H. Seeberger in the Department of Biomolecular Systems, Max Planck Institute of Colloids and Interfaces, and the Department of Biology, Chemistry and Pharmacy, Freie Universität Berlin.

Date of defense: June 22, 2020

1st Reviewer: Prof. Dr. Peter H. Seeberger

2nd Reviewer: Prof. Dr. Kevin Pagel

Acknowledgement

Firstly, I would like to express my sincere gratitude to Dr. Kerry Gilmore and Prof. Dr. Peter H. Seeberger for their encouragement, ideas, patience and stimulating suggestions, which were invaluable for the feasibility of this research project and completing this thesis.

It was a complete stroke of luck and I was extremely lucky to have Dr. Sourav Chatterjee who worked with me during my Ph.D. project over the past four years. This collaborative interaction with him helped me discover my passion and enthusiasm on science.

A special thanks goes to Uwe Osswald for translating the summary of my thesis into German and Tanistha Gupta for providing me building blocks and having fruitful discussions with me.

Many thanks to all the members of the Biomolecular Systems Department, here at the Max-Planck-Institute of Colloids and Interfaces, for providing a nice working atmosphere and especially to Continuous Chemical Systems group members.

I am deeply indebted to my parents and my brother for their support and love. I will also like to take this opportunity to thank Dr. Kris Rathwell and Dr. Dominea Rathwell for encouraging me to pursue PhD and thus initiating a turning point in my life.

Last but not the least, I will like to thank Prof. Dr. Kevin Pagel for kindly agreeing to review my thesis.

Contents

List of Publications	IX
List of Abbreviations	XI
Summary	XV
Zusammenfassung	XVII
Chapter 1 Introduction	1
1.1 Carbohydrates – Easy to find, hard to make	1
1.2 Challenges facing glycosidic bond formation.....	4
1.3 Canonical methodology for carrying out glycosylation reactions.....	7
1.4 Using microreactor technology to gain control reaction conditions.....	8
1.5 Benefits of microreactor based continuous flow technology	9
1.6 Application of microreactor based continuous flow technology	10
1.6.1 Glycosidic bond formation.....	10
1.6.2 Functional group modification	15
1.6.3 Multistep synthesis	20
1.7 Goal of this thesis.....	25
Chapter 2 Instrumentation to provide increased control over glycosylation conditions	26
2.1 Introduction.....	26
2.2 Design of the automated flow platform.....	26
2.2.1 Microreactor Section	27
2.2.2 Automation Section	29
2.2.3 Analysis Section.....	33
Chapter 3 Factors effecting glycosylation	34
3.1 The Permanent and temporary factors affecting glycosylation.....	34
3.2 Controlled interrogation of factors affecting glycosylation through automation	36
3.3 Effects of Permanent Factors	37
3.3.1 Donor.....	37
3.3.2 Acceptor.....	42
3.4 Environmental Factors influencing glycosylation.....	46
3.4.1 Temperature	46
3.4.2 Stoichiometry	47
3.4.3 Activator	49
3.4.4 Water content	51

3.4.5 Solvent	53
3.5 Discussion.....	57
Chapter 4 Machine learning approach to glycosylation.....	60
4.1 Introduction.....	60
4.2 Numeric quantification of permanent factors	61
4.2.1 Donor	61
4.2.2 Acceptor.....	64
4.3 Numeric quantification of environmental factors	66
4.3.1 Activator	66
4.3.2 Solvent	67
4.4 Machine learning software development.....	68
4.5 Generation of a training set for machine learning.....	69
4.8 Default glycosylation conditions.....	73
4.9 Training and prediction of glycosylation.....	73
4.10 Generation of validation set for benchmarking.....	77
4.11 Comparison of four different algorithms	81
4.12 Conclusion	96
Chapter 5 Conclusion and Recommendations.....	97
5.1 Conclusion	97
5.2 Recommendations	100
Chapter 6 Experimental section.....	102
6.1 Total experimental data collected from the automated flow platform.....	102
6.2 Calibration curve for products	110
6.3 General procedure for performing glycosylations in the automated flow platform	113
6.4 Procedure for drying solvents	114
6.5 General experimental details for preparing building blocks	114
6.6 XYZ Coordinates	142

List of Publications

Book Chapter

Moon, S.; Gilmore, K.; Seeberger, P. H. (2018) The Controlled Synthesis of Carbohydrates. *Science of Synthesis: Flow Chemistry in Organic Synthesis*, Eds. Tim Jamison, Guido Koch. DOI: 10.1055/sos-SD-228-00279, page 399.

Journal Articles

Chatterjee, S.;[§] **Moon, S.**;[§] Hentschel, F.; Gilmore, K.; Seeberger, P. H. An Empirical Understanding of the Glycosylation Reaction. *J. Am. Chem. Soc.* **2018**, *140*, 11942-11953. (§Equal contribution)

Chatterjee, S.; **Moon, S.**; Rowlands, A.; Chin, F.; Seeberger, P. H.; Merboudh, N.; Gilmore, K. Click, Zoom, Explore: Interactive 3D (i-3D) Figures in Standard Manuscript PDFs. *ChemRxiv* **2019**, DOI: 10.26434/chemrxiv.7701695.

- Story in Chemistry World **2019**

(<https://www.chemistryworld.com/news/pdfs-dragged-into-digital-age-with-3d-interactive-chemical-structures/3010126.article>)

Marianski, M.; Mucha, E.; Greis, K.; **Moon, S.**; Pardo, A.; Kirschbaum, C.; Thomas, D. A.; Meijer, G.; Helden, G. v.; Gilmore, K.; Seeberger, P. H.; Pagel, K. Direct Evidence for Remote Participation During Glycosylations Revealed by Cryogenic Vibrational Spectroscopy. *Angew. Chem. Int. Ed.* **2020**, *Accepted*. DOI: 10.1002/anie.201916245

Moon, S.;[§] Chatterjee, S.;[§] Seeberger, P. H.; Gilmore, K. Predicting Glycosylation Stereoselectivity Using Machine Learning. **2020**, *Submitted*. (§Equal contribution)

List of Abbreviations

2F-EtOH	2,2-Difluoroethanol
3F-EtOH	2,2,2-Trifluoroethanol
Ac	Acetyl
ACN	Acetonitrile
Alloc	Allyloxycarbonyl
aq.	Aqueous
Area	molecule's total surface area (\AA^2) in a space-filling model
Bn	Benzyl
BPR	Back Pressure Regulator
Bu	Butyl
Bz	Benzoyl
BzCN	Benzoyl cyanide; Phenylacetonitrile; Benzylnitrile
C1	Anomeric carbon of pyranose
CB	Conjugate Base
CF	Continuous flow
CIP	Contact Ion Pair
CSA	Camphorsulfonic acid
DBU	1,8-Diazabicyclo[5.4.0]undec-7-ene
DCM	Dichloromethane
DFT	Density Functional Theory
DMF	Dimethylformamide
DNA	Deoxyribonucleic acid
ESI	Electrospray Ionization
Et	Ethyl
Et ₂ O	Diethyl Ether
Et ₃ NH	Triethylamine
EtCN	Propanenitrile; Propionitrile; Ethyl cyanide; Cyanoethane
Fmoc	Fluorenylmethyloxycarbonyl
GPR	Gaussian Process Regression
GUI	Graphical User Interface
H1-H2 j	³ J coupling constant of H1-H2
H2-H3 j	³ J coupling constant of H2-H3
H3-H4 j	³ J coupling constant of H3-H4
H4-H5 j	³ J coupling constant of H4-H5

HOMO	Highest Occupied Molecular Orbital (eV)
HPLC	High-Performance Liquid Chromatography
HRMS	High Resolution Mass Spectrometry
HSQC	Heteronuclear Single Quantum Coherence Spectroscopy
IR	Infrared
Log P	octanol water partition coefficient
LUMO	lowest unoccupied molecular orbital (eV)
M	Molar concentration; Molarity
MaxElPot	Maximum value of the electrostatic potential
Me	Methyl
MeCN	Acetonitrile
MinElPot	Minimum value of the electrostatic potential
Ms	Methanesulfonyl
MSE	Mean Square Error
MTBE	Methyl <i>tert</i> -Butyl Ether
NaOAc	Sodium Acetate
NIS	<i>N</i> -Iodosuccinimide
NMR	Nuclear Magnetic Resonance
O Shift	¹⁷ Oxygen NMR chemical shift of hydroxyl group
O ⁻ /N ⁻ area	Oxygen (O ⁻) or Nitrogen anion (N ⁻) exposed surface area in a space-filling model of the conjugate base
O/ α C area	Exposed surface area of oxygen or α -carbon in a space-filling model
O2O3	Dihedral Angle of O2-C2-C3-O3
O3O4	Dihedral Angle of O3-C3-C4-O4
O4C6	Dihedral Angle of O4-C4-C5-C6
OTf	Trifluoromethanesulfonate
PG	Protecting Group
Ph	Phenyl
Phth	Phthaloyl
PNP	<i>p</i> -Nitrophenol
Pr	Propyl
PSA	molecule's polar surface area (\AA^2) in a space-filling model
PTFE	Polytetrafluoroethylene
QTOF	Quadrupole Time of Flight
R ²	Coefficient of determination
RF	Random Forest
RMSE	Root Mean Square Error

RNA	Ribonucleic acid
RT	Regression Tree
rt	Room Temperature
sat.	Saturated
SSIP	Solvent Separated Ion Pair
SVM	Support Vector Machine
TBAB	<i>tetra-n</i> -Butylammonium bromide
TBDMS	<i>tert</i> -Butyldimethylsilyl
TCA	Trichloroimidate
Tf	Triflic
TFA	Trifluoroacetic acid
TfO ⁻	Triflate
THF	Tetrahydrofurane
TLC	Thin Layer Chromatography
TMSOTf	Trimethylsilyl
Tol	Tolyl; Methylphenyl
Troc	2,2,2-Trichloroethoxycarbonyl
Trt	Trityl; Triphenylmethyl
UHPLC	Ultra High Performance Liquid Chromatography
UV	Ultraviolet
VI	LabVIEW Virtual Instrument
Volume	Molecule's total volume (Å ³) in a space-filling model
X1O2	Dihedral Angle of X1-C1-C2-O2
αC	α-Carbon

Summary

Carbohydrates are one of the most abundant biomolecules on earth. These molecules range from single monomers such as glucose, measuring 180 Da, that serve as a basic energy source of plants and animals, to hundreds or even thousands of monomers joined together to form gigantic polymeric structures such as cellulose that are a staggering >15 kDa forming the structural backbones of plant cell walls. In addition to providing energy and structure, carbohydrates also serve fundamental biological functions such as cell-cell signaling, cell recognition, and signaling pathways. Extracting carbohydrates from nature is a tedious biochemical and enzymatic process often resulting in mixtures of compounds. The chemical synthesis of carbohydrates provides the opportunity to obtain defined chemical structures to aid in understanding the specific roles, their functional relationships, and advancing the field of carbohydrate research.

However, the mechanism behind the formation of the glycosidic bond, and critically the control over the stereoselectivity, is one of the central challenges in organic chemistry dating back to the seminal paper of Fischer in 1893. This bond formation joins two monomers into a disaccharide. Many factors including the temperature, nature of solvent, water content, reaction time, and stoichiometry potentially influence the yield and stereochemical outcome of the reaction. To date no a systematic study of these factors has been pursued. Compounding the problem is the irreproducibility of the reaction, which stems from the sensitivity and lack of control over the reaction conditions. Flow chemistry and automation provides significant promise in control and reproducibility of chemical reactions.

Hence, in this thesis, a fully automated flow chemical platform was built for the exhaustive study of glycosylation reactions, systematically interrogating the factors and reaction conditions influencing the yield and stereochemical outcome of glycosylation. The thesis, divided into six chapters, introduces the challenges in understanding the mechanism of glycosylation, before describing the tools utilized to address the challenges, an automated flow chemical platform for studying chemical glycosylation and the development of Random Forest based machine learning model for predicting the stereoselectivity of glycosylation reaction.

Chapter 1 introduces the problem of understanding the glycosylation mechanism, the identity of the various factors affecting the selectivity of glycosylation, and the relevant flow chemical approach to obtain greater control over the reaction. *Chapter 2* introduces methodologies details and the design of the automated flow platform for interrogating and controlling glycosylations. The detailed application of this machine, along with systematic interrogation of various factors influencing the stereochemical outcome, is described in *Chapter 3*. This systematic study led to a high degree of stereoselective control of a model glycosylation and allowed for our comprehensive empirical understanding of the glycosylation mechanism. Additionally, for the first time, more than 300 reproducible data points systematically populating the relevant chemical space were generated. This allowed for the application of Random Forest based machine learning algorithm for creating a model capable of predicting the stereoselectivity of glycosylations, described in detail in *Chapter 4* of this thesis. The research concluded in *Chapter 5* and an outlook on the immediate future work is suggested. All the experimental data described in this thesis is given in *Chapter 6*.

Zusammenfassung

Kohlenhydrate sind die am weitesten verbreiteten Biomoleküle auf der Erde. Diese Moleküle können von einem einzigen Monomer wie Glucose, welche als grundlegende Energiequelle für Pflanzen und Tiere dient, bis hin zu Hunderten oder Tausenden Monomeren reichen, welche riesige Polymerstrukturen wie Zellulose bilden, die das strukturelle Rückenrad der pflanzlichen Zellwand darstellen. Kohlenhydrate sind neben den Funktionen als Energielieferant und Strukturelement auch in grundlegende biologische Funktionen wie zelluläre Signale, Zellerkennung und Signalwege involviert. Die Gewinnung von Kohlenhydraten aus der Natur ist ein langwieriger, komplizierter biochemischer Prozess und führt sehr oft zu einer Mischung von Verbindungen. Die chemische Synthese von Kohlenhydraten bietet die Möglichkeit, eine definierte chemische Struktur von hoher Reinheit zu erhalten, was es ermöglicht, die einzelnen biologischen Funktionsbeziehungen zu verstehen und den Bereich der Kohlenhydratforschung weiter zu entwickeln.

Das Kontrollieren der Glykosylierung, der Reaktion die zwei Zuckerbausteine unter Bildung einer glykosidischen Bindung verknüpft, und damit der Stereoselektivität ist eine der Herausforderungen in der modernen organischen Chemie, und basiert auf den bahnbrechenden Erkenntnissen von Emil Fischer im Jahr 1893. Viele Faktoren wie Temperatur, Lösungsmittel, Wassergehalt, Reaktionszeit und Stöchiometrie beeinflussen die Ausbeute der Reaktion und die stereochemische Zusammensetzung des Produkts. Bisher wurden keine umfassenden systematischen Untersuchungen aller dieser Faktoren durchgeführt. Eine große Herausforderung ist die Reproduzierbarkeit der Glykosylierung, die auf die Sensibilität der Reaktion und mangelnde Kontrolle über die Reaktionsbedingungen durch den Experimentator zurückzuführen ist. Durchflusschemie und Automatisierung bieten hier erhebliche Möglichkeiten die Kontrolle und damit die Reproduzierbarkeit chemischer Reaktionen zu optimieren.

Daher wurde in dieser Dissertation eine vollautomatische durchflussschemische Plattform für die umfassende Untersuchung von Glykosylierungsreaktionen entwickelt, in der systematisch die Reaktionsbedingungen variiert und deren Einfluss auf Ausbeute und stereochemischen Zusammensetzung des Produkts untersucht werden können. In dieser sechs Kapitel umfassenden Arbeit werden die Herausforderungen beim Verständnis des Glykosylierungsmechanismus vorgestellt, und die zur Bewältigung verwendeten Werkzeuge

beschrieben. Dazu gehören die automatisierte durchflussschemische Plattform zur Untersuchung der chemischen Glykosylierung und die Entwicklung eines zufälligen „Random Forest“ basierten Modells für maschinelles Lernen, das der Vorhersage der stereochemischen Zusammensetzung des Produkts dient.

Kapitel 1 erörtert die Herausforderungen beim Verständnis des Glykosylierungsmechanismus, und die verschiedenen Faktoren, die das Ergebnis der Glykosylierung beeinflussen, um damit im durchflussschemischen Ansatz eine größere Kontrolle über die Reaktion erhalten zu können. *Kapitel 2* stellt die Methodik und das Design der automatisierten Flow-Plattform für Glykosylierungen vor. Die detaillierte Anwendung dieser Maschine wird in *Kapitel 3* beschrieben, zusammen mit systematischen Fragen zu den verschiedenen Faktoren, die die stereochemische Zusammensetzung des Produkts beeinflussen. Durch diese systematische Studie konnte ein sehr hohes Maß an Kontrolle über die Modell-Glykosylierung und ein umfassendes empirisches Verständnis des Reaktionsmechanismus erworben werden. Außerdem wurden zum ersten Mal mehr als 300 reproduzierbare Datenpunkte systematisch im chemischen Raum erstellt. Dies ermöglichte es, mittels einem „Random Forest“ basierten maschinellen Lernalgorithmus ein Modell zu erstellen, das die stereochemische Zusammensetzung des Produkts vorhersagen kann, welches in *Kapitel 4* dieser Arbeit detailliert beschrieben wird. Eine Zusammenfassung und ein Ausblick finden sich in *Kapitel 5*. Alle in dieser Arbeit beschriebenen experimentellen Daten sind in *Kapitel 6* aufgeführt.

Chapter 1 Introduction

1.1 Carbohydrates – Easy to find, hard to make

Carbohydrates represent an extremely important class of biomolecules, constituting about 75% of the earth's mass.¹ They have a wide range of structural complexity, from a monomer unit consisting of a single monosaccharide such as glucose, which serves as a major energy source in plant and animal cells, to hundreds of glucose monomers units linked together forming cellulose, giving the structural framework of plant cell wall.²⁻³ A substitution of an acetyl group at the C2 position of glucosamine and subsequent polymerization forms chitin, which serves as the outer hard shell of insects and crabs in the animal world (Figure 1.1).⁴

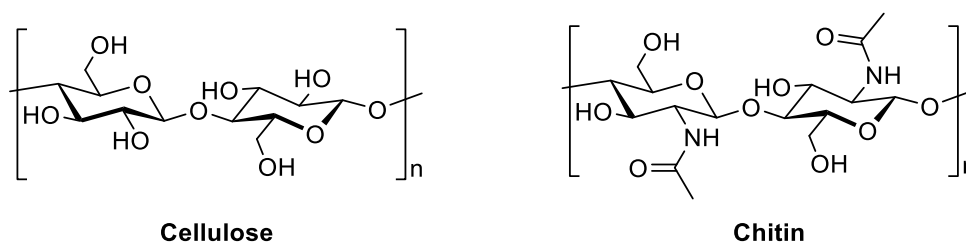


Figure 1.1: Examples of common polysaccharides of glucose (cellulose) and acetyl glucosamine (chitin).

These mammoth structures serve diverse functions such as forming a capsular polysaccharide of a pathogen, cell recognition, cell to cell communication and cell signaling.⁵ Even the table sugar we use daily as an important food flavoring agent is a disaccharide of glucose and fructose. At the very heart of the diversity and structural complexity of carbohydrate molecule lies the formation of glycosidic bond that joins two carbohydrate molecules generating two possible anomers, the axial α -anomer and the equatorial β -anomer (Figure 1.2).

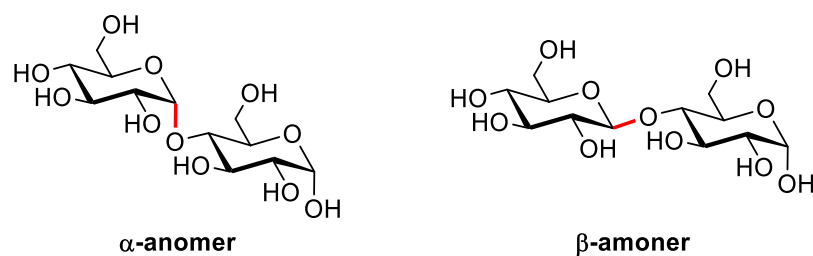


Figure 1.2: Example of α - and β -anomers of glucose disaccharides.

To understand the difficulties in the formation of a glycosidic bond involving two monosaccharides needs to be designed, which upon reaction will generate the desired disaccharide. This reaction happens in nature using enzymatic transformation and usually needs glycosyltransferases. For example, two reactants – UDP (uridine diphosphate) galactose and mannose – could be joined forming a β -disaccharide by S_N2 reaction using mannose $\beta(1,4)$ galactosyltransferase (Figure 1.3).⁶

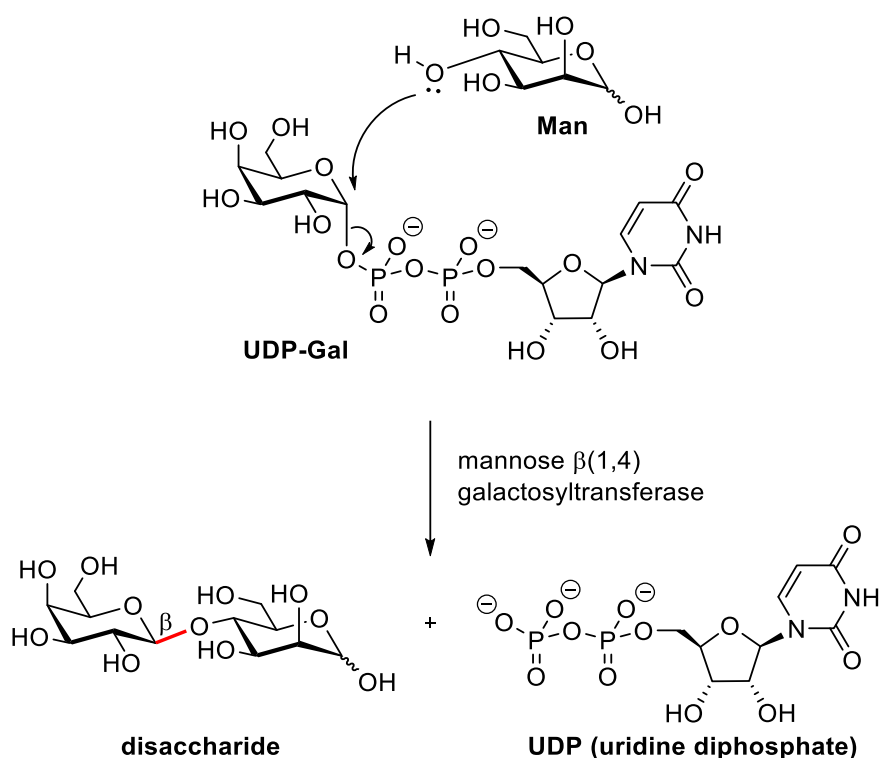


Figure 1.3: Enzymatic disaccharide formation using UDP-galactose and mannose to form a β -disaccharide with mannose $\beta(1,4)$ galactosyltransferase. Figure adapted from ref 6.

However, chemical synthesis of the above disaccharide is difficult due to the presence of several unprotected hydroxyl groups. Upon analysis the above structure, it can be observed that the typical unprotected sugar molecule contains three distinct classes of

hydroxyl groups, the one at C-6 position is primary, C-2, C-3, C-4 represents the secondary and the C-1 is the anomeric hydroxyl group (Figure 1.4).

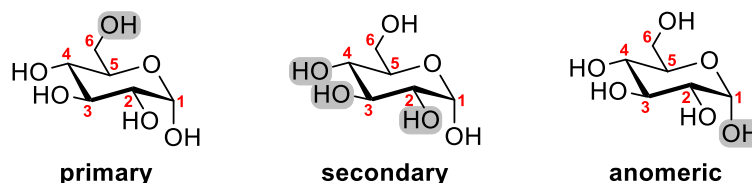


Figure 1.4: Three types of hydroxyl groups in carbohydrates: the primary hydroxyl group ($-\text{CH}_2\text{OH}$) which for D-glucose is at C-6; the secondary hydroxyl groups ($-\text{CH}(\text{OH})-$) which in D-glucopyranose are at C-2, 3, 4; the anomeric hydroxyl group which is at C-1.

Synthesizing a disaccharide can be possible by linking the two monomers by forming a glycosidic bond between them. This can be achieved by a simple displacement of a leaving group at the anomeric position of one of the coupling monosaccharide, which in this case is called a glycosyl donor using the second coupling partner, the glycosyl acceptor, which is the nucleophile. The chemical glycosylation was first reported by Fischer in 1893 (Figure 1.5).⁷ It is the glycosylation using unprotected carbohydrates and simple alcohols (methyl-, benzyl-, and allyl-) with Brønsted/Lewis acid.

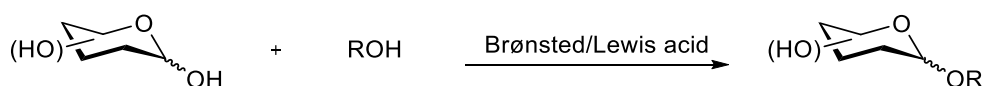


Figure 1.5: Fischer glycosylation using unprotected carbohydrates.

The synthesis of oligosaccharides is very sensitive and the stereochemical outcome of the reaction depends on numerous factors including building blocks accounting for variants of hydroxyl substitution and stereochemistry on the pyran/furan core.⁸ The number of possible structures is further significantly increased by the fact that each glycosidic bond generates a stereogenic center where two diastereomers (α or β) can be formed (Figure 1.6).⁹ Controlling this stereoselectivity towards a specific anomeric configuration is a central challenge in the field of carbohydrate chemistry¹⁰ and has been studied for more than 100 years.⁷

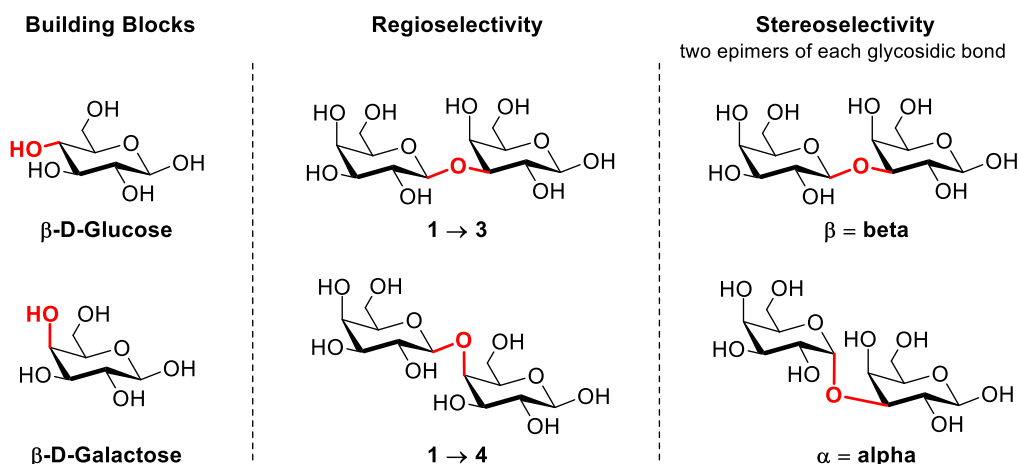


Figure 1.6: Three types of structural parameters contribute to the inherent complexity of glycans. Figure adapted from ref 9.

In the case of chemical glycosylation to form a disaccharide, all hydroxyl groups need to be protected in both glycosyl donor and acceptor except for only one of the hydroxyl groups in the glycosyl acceptor which needs to act as a nucleophile, otherwise, a mixture of disaccharides will result (Figure 1.7).

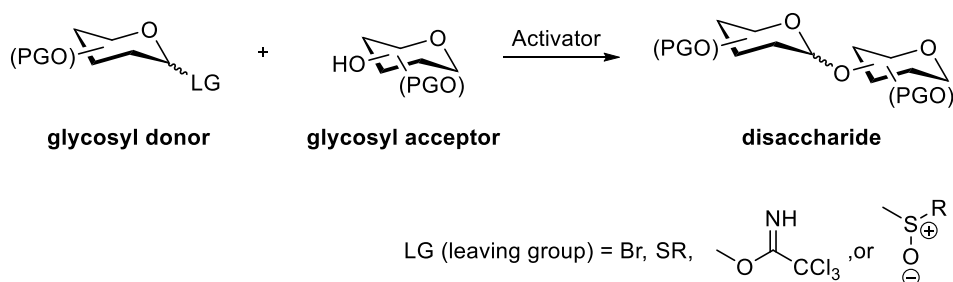
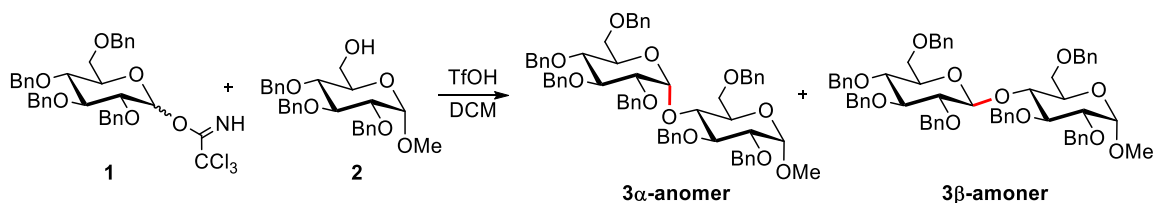


Figure 1.7: General chemical glycosylation using protected carbohydrates.

1.2 Challenges facing glycosidic bond formation

The control of stereoselectivity - selectively forming either α - or β -anomer in the glycosylation reaction - is particularly challenging.¹⁰ In order to fully appreciate the complexity of a relatively simple glycosylation reaction, let us consider the glycosylation reaction perbenzylated glucosyl donor **1** with triflic acid (TfOH) and coupling it with a C6-glucosyl acceptor **2**, forming α - and β -disaccharides **3** (Scheme 1.1).

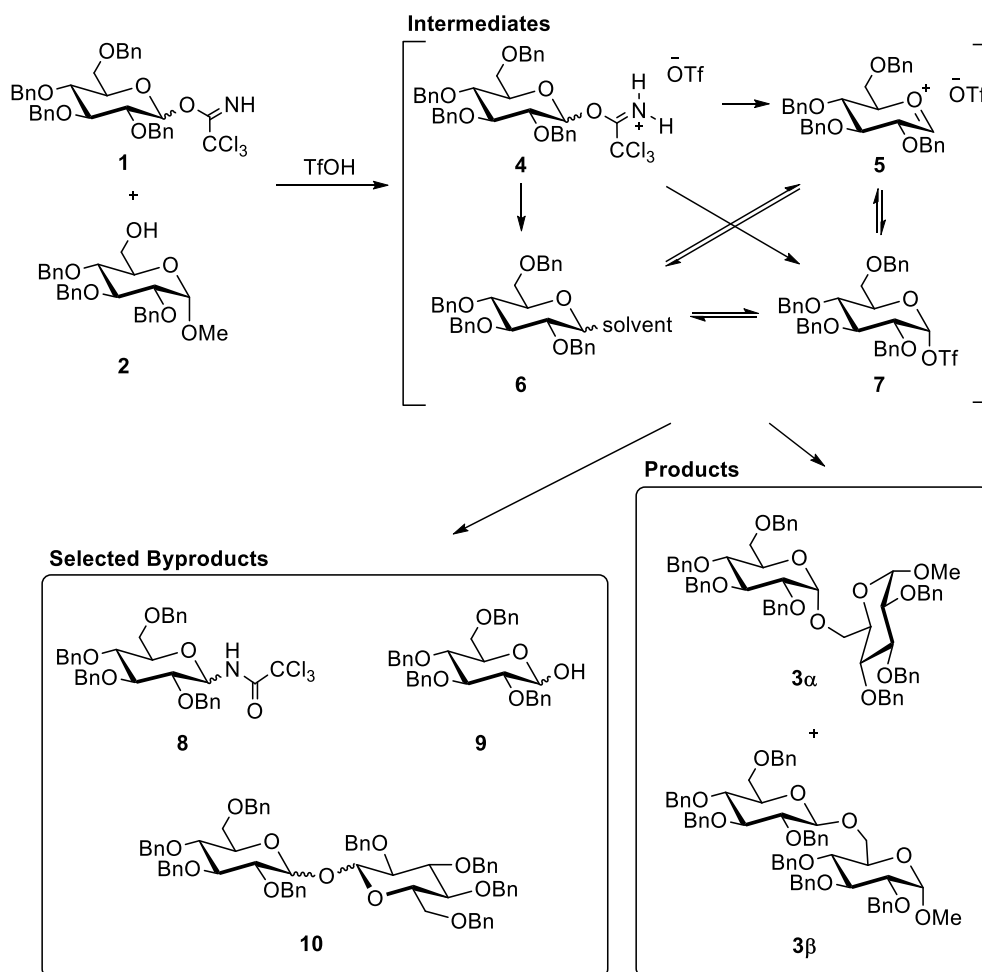


Scheme 1.1: Glycosylation reaction with glucose donor **1** and C6 hydroxyl glucose acceptor **2**.

The reaction mechanism involves the formation of several intermediates in equilibrium, which dictates the final stereochemical outcome of the product formed. The donor **1**, upon activation with TfOH can undergo several intermediate reaction steps (Scheme 1.2). Upon activation, the glycosyl trichloroacetimidate donor **1** generates an oxocarbenium ion species,¹¹⁻¹² which, being highly reactive electrophile, can combine with different nucleophiles present in the vicinity to form different intermediates **4-7**. For example, it can combine with the triflate conjugate, generated from the activator TfOH, to form an α -triflate intermediate **7**,¹³ which can be in equilibrium with the oxocarbenium ionic state **5**. The α -triflate intermediate can also coordinate with the reaction solvent **6**, which can in turn give rise to solvent effects. The imidate ion generated after activation can also act as a potential nucleophile and can combine with the oxocarbenium ion to give rise to rearranged donor **8**. The complexities of this transformation are manifold including the requirement of complete water free/anhydrous reaction condition. Water can compete as a potential nucleophile with the glycosyl acceptor, forming a hydroxyl donor **9** that is a common byproduct of the reaction. Numerous methodologies have been developed to keep the reaction mixture anhydrous, including removing all water from the reagents and adding molecular sieves in the reaction mixture to absorb water. Temperature is another important parameter that can have a profound effect on the stereoselectivity and yield of the reaction.¹⁴

Due to this myriad of both independent and interdependent factors influencing the reaction pathway, controlling the yield and selectivity of glycosylations is a significant challenging. Impeccable control of over reaction conditions, including residence time, temperature, and maintaining anhydrous condition is critical to obtain reproducible results.

Hence the yield and selectivity of a glycosylation reaction is influenced by several factors including the choice of donor, its protecting groups and the leaving group, choice of the acceptor and the position of the free hydroxyl group, represents the factors which cannot be changes during a typical glycosylation reaction and can be grouped as permanent factors. The other important factors affecting the yield and stereoselectivity are the type of activator, equivalents of donor, acceptor and activator, reaction solvent, mixing, presence of water and Temperature and reaction time. These factors can be easily manipulated during the course of a reaction and can be called as environmental factors. The permanent factors and environmental variables are discussed in greater detail in *Chapter 3* of this thesis.



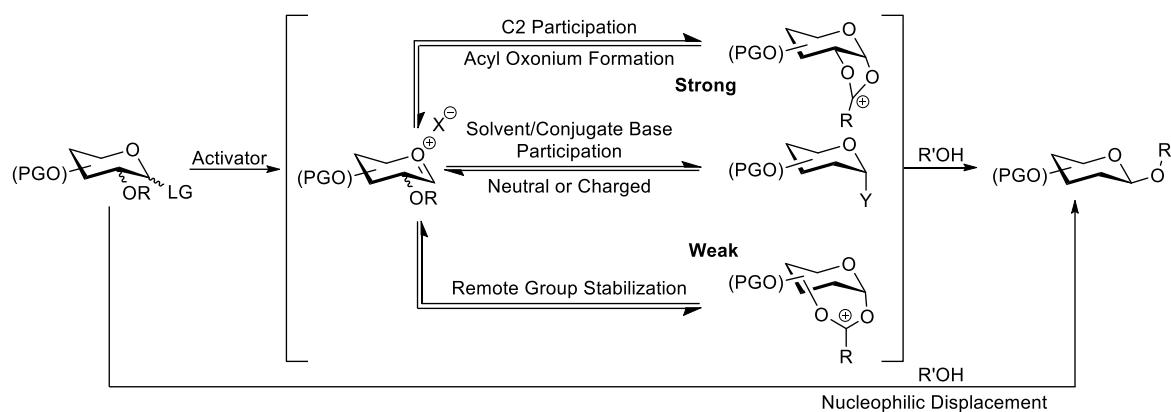
Scheme 1.2: The mechanistically poorly understood series of pathways leading from the donor and acceptor to either the α - or β -anomer of the glycosylation product.

Carbohydrate chemistry in flow is slowly becoming a field of research having immense potential. Microfluidic based flow systems, generally have very high surface to volume ratio due to the very large interfacial area created by the microscale domain, is advantageous in terms of precise control of flow conditions, uniform temperature gradients, excellent heat and mass transfer, and high throughput. In addition, inline analytics such as HPLC and FlowNMR could be coupled with flow system to perform ad hoc analysis of reaction progress, greatly simplifying the process of rapid screening and identification of optimized reaction conditions.

1.3 Canonical methodology for carrying out glycosylation reactions

Glycosylation reactions are traditionally carried out in round-bottom flasks, using a magnetic stirrer to mix and a water/oil bath to heat the reaction mixture or dry ice/acetone mixtures to cool. Precise and reproducible control of temperature and mixing are difficult to attain in this type of setup. In addition, the general reaction protocol followed in the literature involves starting the reaction at a defined low temperature and slowly warming to a higher reaction temperature prior to quenching. This default protocol where a sensitive reaction is performed over a temperature range eliminates any selectivity potentially gained, merely ‘averaging out’ the selectivities obtained at different temperatures.

Over the years, several chemical strategies have been developed to prevent these additional pathways, thus making the glycosylation more robust by decreasing the influence of several factors in an effort to obtain the desired anomeric product with high selectivity and yield. Nevertheless, these strategies have also introduced additional problems and complexity to an already complex transformation. One of the popular choices in dictating stereoselectivity is the use of participating protecting groups on the glycosyl donor.¹⁵ This strategy involves installing an ester protecting group at the C2 position of the glycosyl donor, which during the reaction, traps intermediates with carbocationic character at the C1 position, reversibly forming a more stable anomeric carboxonium ion (Scheme 1.3). This strategy can chemoselectively generate trans-1,2 products, however the methodology can also result in the formation of other byproducts by the mechanism of trapping of the acyloxonium ion.¹⁶ Stereoselectivity can also be controlled by the use of halogen such as bromide and chloride as leaving groups in the glycosyl donors. These can selectively undergo S_N2 reactions.¹⁷ Other methodologies for reducing mechanistic ambiguity involves steering the reaction through α -triflate intermediates,¹⁰ or using acetonitrile effect of solvents.¹⁸⁻¹⁹ Remote participating groups can also be utilized in promoting/stabilizing key intermediates and conformations (Scheme 1.3).



Scheme 1.3: Common strategies for controlling/influencing the anomeric selectivity.

Successful implementation of these strategies will also require proper control of reaction conditions. In addition to that, very specific modification of glycosyl donor/acceptor is often needed for implementing these strategies, which are both laborious and time consuming endeavors.

1.4 Using microreactor technology to gain control reaction conditions

To tackle the problem of precise control of reaction conditions, the concept of process intensification can be implemented, which was successfully introduced by Colin Ramshaw during the 1970s.²⁰⁻²¹ Upon dramatic reduction of dimension of existing process equipment, in this case the round bottom flask reactor, a significant advantage can be gained in heat and mass transfer performance (Figure 1.8).

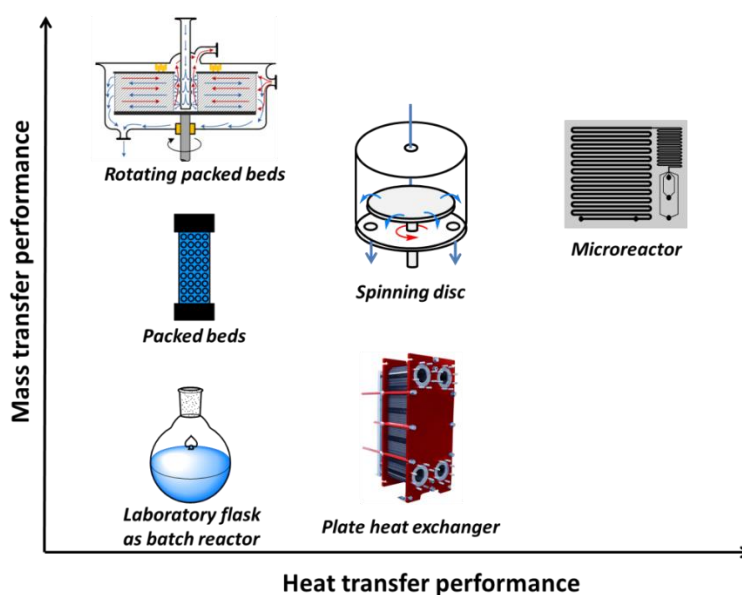


Figure 1.8: Performance of different reactor systems.²⁰⁻²¹

Reduction of the diameter of the reactor increases the surface to volume ratio in the order of 9000–15000 m²/m³ for a typical microreactor system.²² This translates to a significant increase in heat and mass transfer rates in the reactor. The reactor operates in near isothermal mode with negligible heat and mass transfer gradients. To remove the non-uniformity of concentrations of reagents and temperature within the reactor. Typical microreactors are shown below (Figure 1.9).



Figure 1.9: A typical microreactor. **a.** 4 way jet mixing device (left) and HPIMM (right) from Institut für Mikrotechnik Mainz (IMM) GmbH. **b.** Glass microreactor XXL from MERCK.

Microreactors are usually operated in a continuous mode. The reagents are continuously introduced in the micro channel of the microreactor, by means of syringes or HPLC pumps. The fluid eventually passes through different sections of the reactor, such as the mixing section, where continuous flow is coupled with constant bend in the flow lines. These rapid bends, in addition to continuous flow, generate controlled vortices in the flow. Enhanced mixing produces highly reproducible flow patterns which translate to better mixing, and reproducible flow profiles in the microreactor.²³⁻²⁴

1.5 Benefits of microreactor based continuous flow technology

The use of continuous flow microreactor and microfluidics technologies been successfully demonstrated in tackling complex chemistries in flow.^{23, 25-27} In addition to the dramatic improvement in efficiency in the microreactor, inline integration of analytical tools such as FlowIR and HPLCs with the microreactor platform presents itself as a powerful tool for controlling and studying complex chemical reactions with high reproducibility.²³

A typical continuous flow module is broken down into eight basic zones: fluid & reagent delivery, mixing, reactor, quenching, pressure regulation, collection (or connection to the next module), analysis, and purification (Figure 1.10). Reagents are delivered into the system in a continuously and reproducible manner via syringe, HPLC, peristaltic pumps or mass flow controllers for gasses. The flow rate of fluids, coupled with the dimension of reaction channel, is used to estimate and maintain reactor residence time. Reagents and solvents can be dosed by multiple pumps and mixed in a mixing unit to control the stoichiometry.

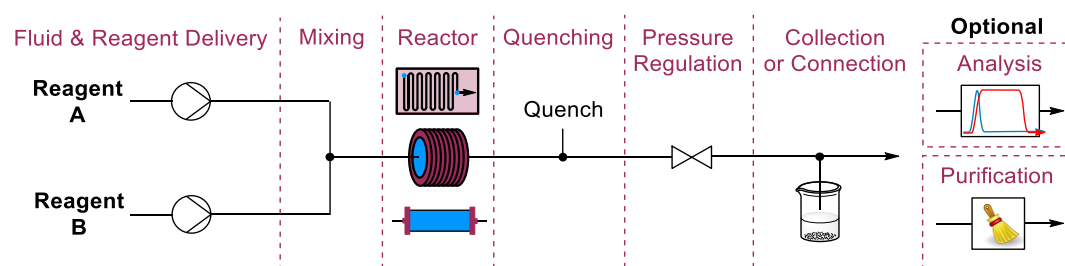


Figure 1.10: Reaction Zones of a Continuous-Flow Module.²³

The core of every flow module is the reactor unit – generally a (micro) chip, coil, or packed bed – to which the respective reaction conditions (heating, cooling, irradiation, etc.) are applied. A number of additional units can also be added including pressure regulators, collection equipment, in- or online analysis, or further reaction modules.

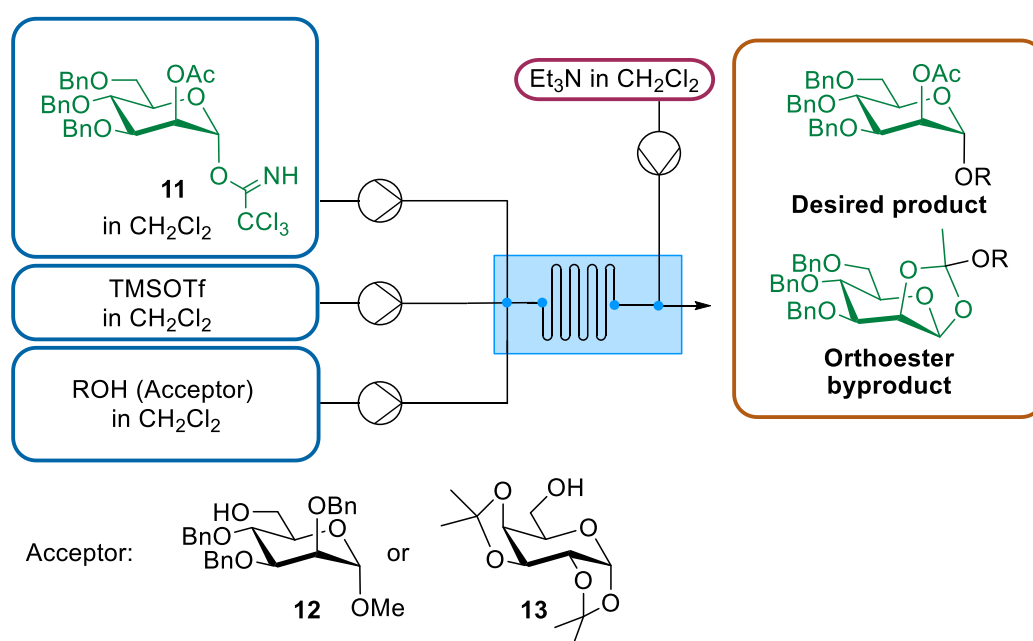
1.6 Application of microreactor based continuous flow technology

1.6.1 Glycosidic bond formation

As discussed in the previous section, flow chemistry holds numerous advantages over batch systems in terms of control of reaction conditions, minimization of concentration and thermal gradients, and better mixing. In the following sections, previous studies involving single glycosylations in a continuous flow environment are presented, utilized for screening of reaction conditions, improvements in yields and/or selectivity, reproducibility.

Application of continuous microreaction technology in carbohydrate chemistry was first demonstrated by Seeberger et al. for the study of α -mannosylations (Scheme 1.4).¹⁶ They screened various reaction conditions which directly or indirectly influence the overall yield and byproduct formation for the glycosylation. Mannosylation was performed with

acceptors **12**, **13** and the trichloroacetimidate donor **11**, activated using 0.2 equivalents trimethylsilyl trifluoromethanesulfonate (TMSOTf) in anhydrous dichloromethane. The microreactor had a volume of 78.3 μL ; hence it was possible to screen different reaction conditions using small amount of reagent. Using offline HPLC analysis of the crude samples, the reaction temperature was screened from -78 to 20 $^{\circ}\text{C}$, using glycosyl donor **11** at residence times of 26.7, 53.4, 106.8 and 213.5 seconds. It was observed that temperature influences the overall yield of the reaction by either aiding or suppressing the formation of the orthoester byproduct. By using a continuous microfluidic system, the importance of temperature and residence time was revealed, which affects the overall yield and byproduct formation.



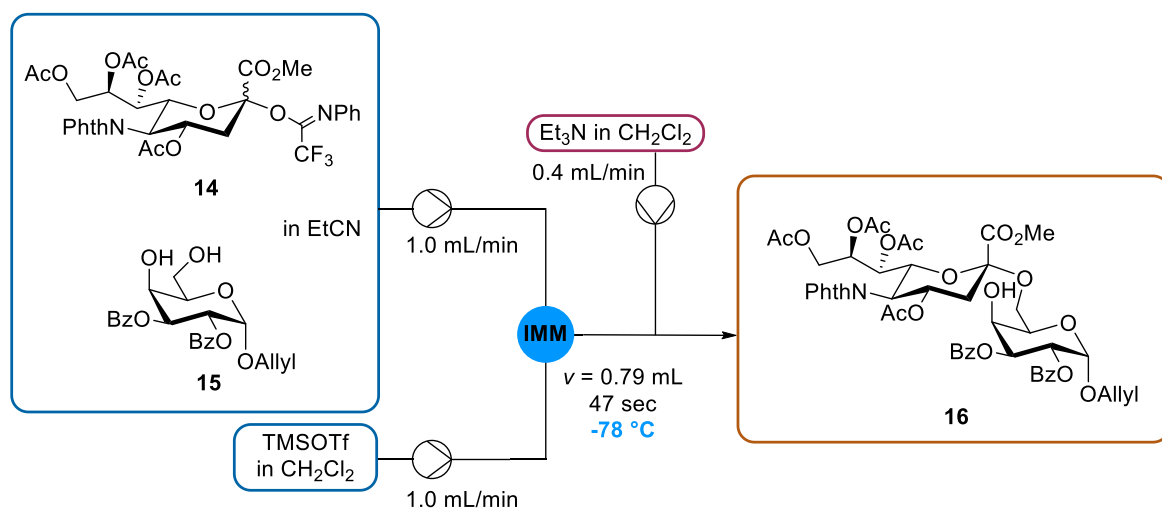
Scheme 1.4: Sample glycosylation of glycosyl donor **11** and nucleophile (acceptor) **12**, **13** to fashion disaccharide (desired product and orthoester side product).

In the second example, a highly α -selective sialylation of sialic acid *N*-phenyl trifluoro acetimidate, when sialylated with galactose acceptors and carried out on 50 mg in batch, yielded 92% α -product. However, reaction scale up was accompanied by significant glycol byproduct formation and yielded only 60% α -product. The decreased yield and selectivity is mainly due to high donor reactivity. In addition, the efficiency of the glycosylation reaction is influenced by both reaction scale and the speed of the addition of activator, where slow addition of the Lewis acid for large scale sialylation reduce the yield of the reaction.²⁸

When sialylations are performed in microfluidic flow platforms allow facile screening of the concentrations of donor, acceptor, and activator to quickly identify the best reaction conditions. For example, a sialylation was carried out in a microfluidic environment using glycosyl donor **14** and glycosyl acceptor **15** in propionitrile as solvent and TMSOTf as the activator in dichloromethane. Mixing was achieved using an IMM micromixer. The reaction temperature was fixed at -78°C (Table 1.1).²⁸

After exiting from the reactor section, the reaction was quenched by an excess solution of triethylamine in dichloromethane, added using a T mixer. The mannosylation in a mixed solvent system of EtCN:DCM in the ratio of 1:1, gave similar yield and α selectivity when compared to the batch system. However, by quickly scanning through the reaction conditions in the microfluidic setup, the optimal concentration of the Lewis acid was identified as 0.15 M, which gave an increased yield of the target α -sialysidediacaride **16** up to 88%. The final optimum quantitative yield of **16** was obtained when the concentration of donor **8** was increased from 0.15 M to 0.2 M (Table 1.1).

Table 1.1: Optimization of α -(2-6)-sialylation using IMM micromixer.



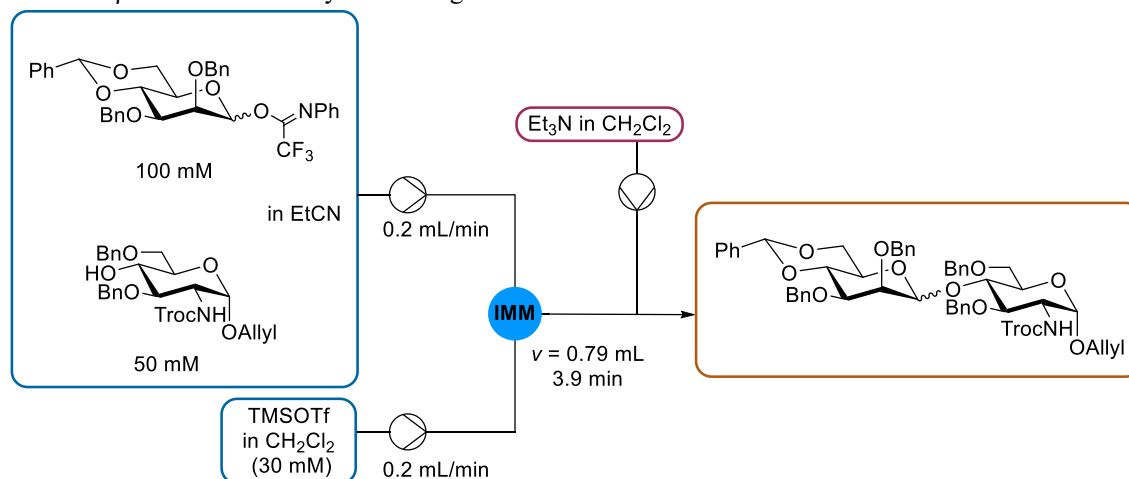
Entry	Donor 14 (M)	Acceptor 15 (M)	TMSOTf (M)	Yield (%)	$\alpha:\beta^a$
1	0.15	0.1	0.08	14	α only
2	0.15	0.1	0.15	88	α only
3	0.2	0.1	0.15	>99	α only

^aBased on ^1H NMR analysis.

The critical role that the rate of activator addition has in both glycosylation yield and anomeric selectivity was noted also in the synthesis of β -mannoside linkages. The chemoselective formation of this bond is highly important for a range of oligosaccharide

syntheses.²⁹ The study screened the influence of 30 sets of variables, investigating the concentrations of donor and activator, the temperature of mixing and reaction, as well as the residence time.²⁹ As can be seen in Table 1.2, while the selectivity can be improved by mixing at low temperatures, the yield was poor ($\alpha:\beta = 1:2.3$ with 16% yield at -78 °C). This relationship inverts at warmer temperatures (-20 °C), with higher yields (48%) obtained but with less of the desired β -anomer (Table 1.2).

Table 1.2: β -Selective mannosylation using TMSOTf under microfluidic conditions



Entry	Temp (°C)	Yield (%) ^a	$\alpha:\beta$ ^b
1	-78	17	1:2.3
2	-50	38	1:2.1
3	-20	48	1:1.8

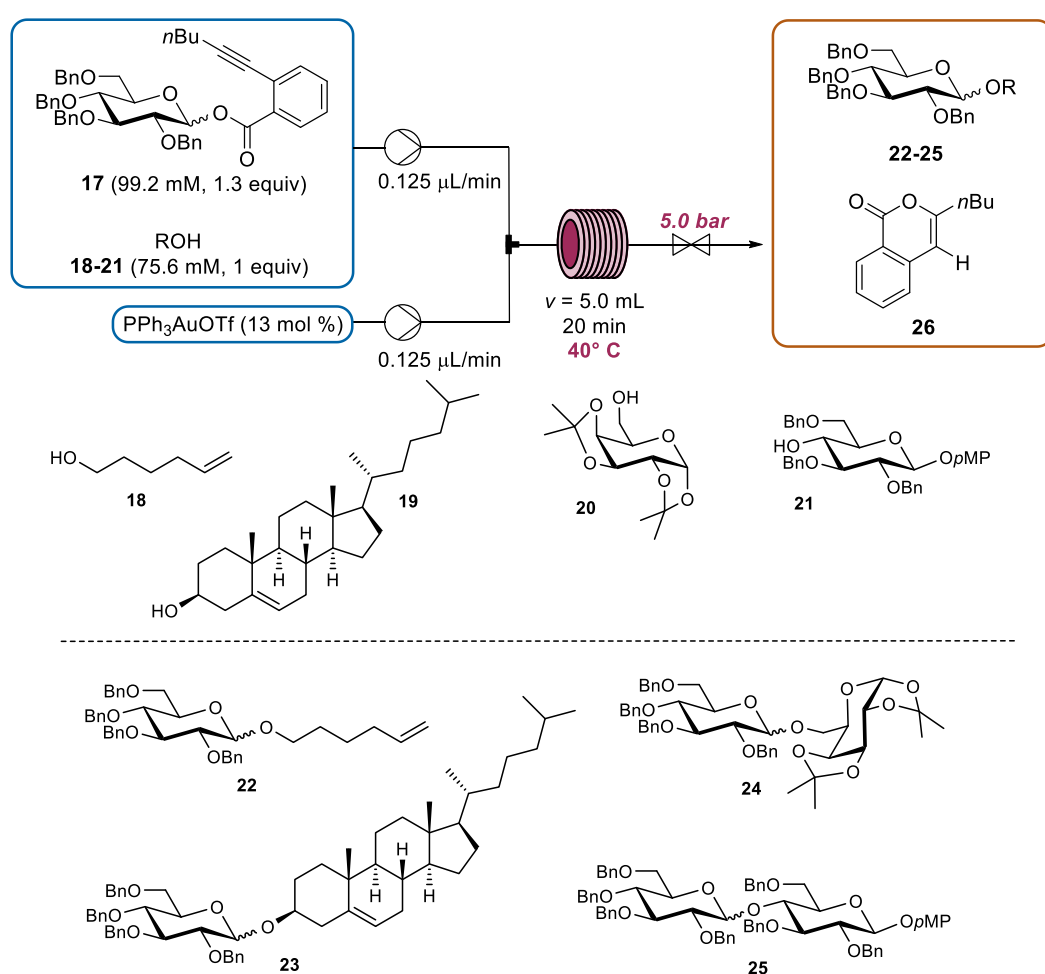
^a Isolated yields as a mixture of α - and β -isomers.

^b ^1H NMR and HPLC analysis determined the $\alpha:\beta$ ratio.

The glycosylation reactions discussed here, and nearly all other glycosylations, are generally carried out using reagents and activators in stoichiometric proportions involving harsh reaction conditions. Often these demanding and harsh reaction conditions are incompatible with labile protecting groups and make the processes challenging to scale up.³⁰⁻³¹ Hence, it becomes necessary to find alternative approaches for the synthesis of oligosaccharides using mild reaction conditions. One of the approaches can be the use of a gold catalyst to perform glycosylations in flow.³² Alkynyl building blocks, activated using a gold (I) catalyst, were shown to be an effective way to synthesize glycosides using short reaction time in the order of 20 minutes, giving excellent control on reaction conditions (Table 1.3).

The continuous glycosylation was achieved using setup as shown in Table 1.3. The glycosyl donor was mixed with the glycosyl acceptor solution and gold (I) catalyst in the form of PPh_3AuOTf solution via two syringe pumps respectively and subsequently added into a 5mL PFA reaction loop, maintained at the reaction temperature. The reaction temperature was generally maintained at 40 °C, which is higher, when compared to batch counterpart, to facilitate shorter reaction times of 20 minutes (the reaction takes hours in batch). Using this setup, glycosylations were carried out for alkynyl C_2 ester protected and perbenzylated building blocks and good yields were obtained (Table 1.3).

Table 1.3: Glycosylations using perbenzylated building block **17**.



Entry	Acceptor	Product	Solvent	Yield (%)	$\alpha:\beta^a$
1	18	22	CH_2Cl_2	73	1:02
2	19	23	CH_2Cl_2	84	1:01
3	19	23	Et_2O	88	4:01
4	20	24	CH_2Cl_2	92	1.25:1
5	20	24	Et_2O	48	5:01
6	21	25	CH_2Cl_2	36	2:01

^a ^1H NMR analysis determined the $\alpha:\beta$ -ratio.

1.6.2 Functional group modification

The multiple hydroxyl groups of a monosaccharide exhibit similar reactivity, making regioselective functionalization and coupling essentially impossible for carbohydrates in non-enzymatic processes. Therefore, protecting group (PG) manipulations are one of the fundamental reactions in carbohydrate synthesis. Multiple hydroxyl groups, usually present in unprotected monomers and oligosaccharides, have similar properties. Hence, to form glycosidic bonds at a desired oxygen position, other hydroxyl groups have to be protected with protecting groups. After the desired glycosidic bond formation, the final oligosaccharide can be deprotected.

The synthesis of the protected monosaccharide requires long reaction times and multiple reaction steps, involving multiple purifications and workup procedures. Kawakami et al. accelerated this process, synthesizing monosaccharide **27** by combining glycosylation and fluorous phase extraction by continuous microreaction technology (Figure 1.11).³³ First, a peracylated glucose derivative was coupled with a perfluorinated hydrocarbon glycerol ether moiety. The tag was sufficient to pull the target into a fluorous solvent, separating the product from all non-fluorinated byproducts and the excess reagents that remained in the organic phase. Using this strategy, the authors performed six individual transformations in Teflon tubing. Following the reactor, the fluorous solvent was added along with an organic solvent for quenching and separation. The biphasic stream exited into a separatory funnel, where the fluorous phase was removed and evaporated to yield clean, crude product to be used in the next step. A six-step synthesis was realized of C4-OH protected glucose **27** in 11%, with no intermediate purifications and only one final column chromatography (Scheme 1.5).

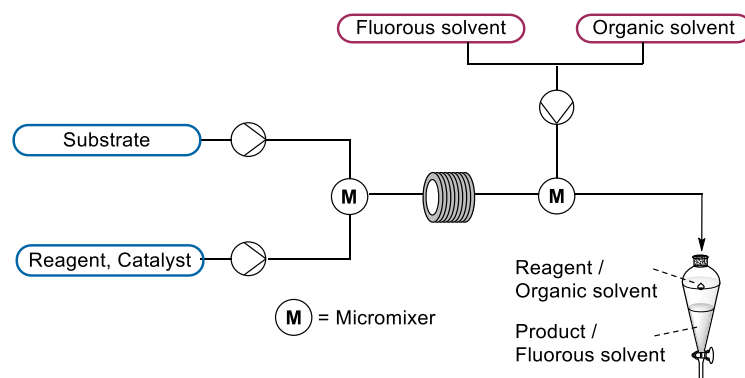
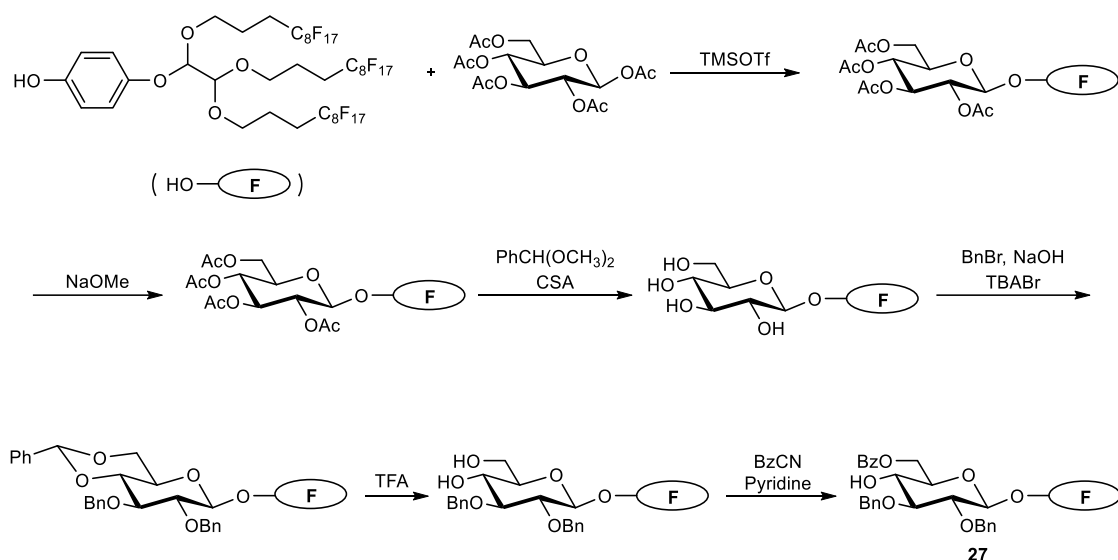


Figure 1.11: Microreactor system for fluorous-tag biphasic extraction.



Scheme 1.5: synthesis of monosaccharide unit **27** with a fluorinated hydrocarbon chain.

Benzyl ethers and benzylidene acetals are some of the most common protecting groups in the field of carbohydrate chemistry for non-reaction sites.³⁰ Their wide usage is mainly due to their stability towards various reaction conditions and facile deprotection by mild reaction conditions such as hydrogenolyses.¹⁵ However, batch reactors are commonly used for such deprotection reactions that require long reaction times, posing significant disadvantages associated with slow and laborious optimization for identifying proper reaction conditions. Hence, continuous flow systems can provide an efficient alternative to provide a faster reaction time and facile optimization of reaction conditions. The use of continuous flow systems for deprotection of several carbohydrate derivatives containing benzylidene and benzyl protecting groups was carried out by using a continuous flow (CF) hydrogenation reactor.³⁴ The CF hydrogenator consists of a water reservoir to produce hydrogen from electrolysis, which is an alternative to the batch system where a pressurized hydrogen gas bottle is necessary. This makes the CF process inherently safer. The sample in the hydrogenator is pumped via HPLC pump and, after mixing with hydrogen gas, is passed through a catalyst packed bed (Figure 1.12). This also essentially removes the catalyst recovery step which is necessary in the batch system.

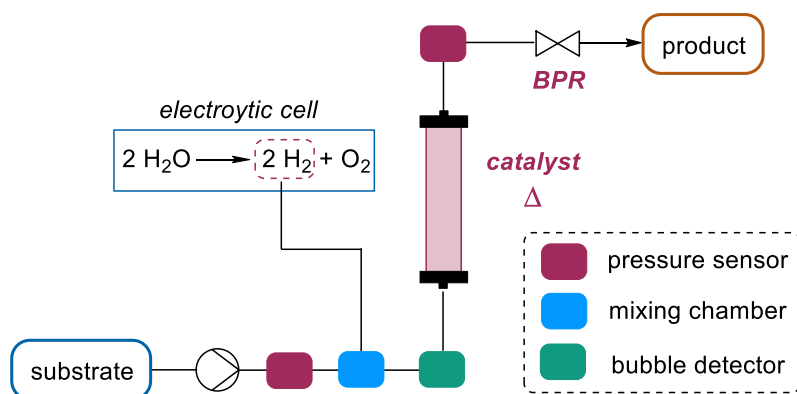


Figure 1.12: Basic diagram of H-Cube hydrogenations via the on-demand generation of H₂ via hydrolysis of water.²³

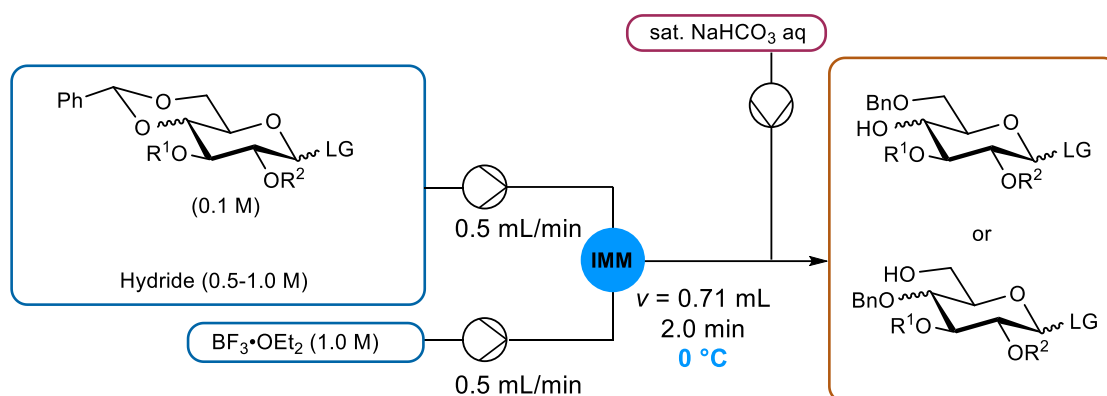
Another advantage of the CF hydrogenator is the facile process of changing temperature and hydrogen pressure which can be used to rapidly screen reaction conditions for the deprotection reaction. Ekholm et al. found that global deprotection of benzyls and benzyldines can be achieved selectively in the presence of both silyl and acyl protecting groups in high yield (>90%, Table 1.4). All reactions were completed using a 30 mm Pd/C preppacked cartridge reactor with a flow rate of 1 ml/min and 40 bar H₂-pressure at 80 °C.³⁵

Table 1.4: Deprotection of benzyl/benzyldene protected carbohydrates.

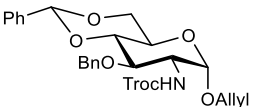
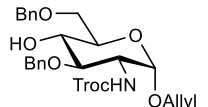
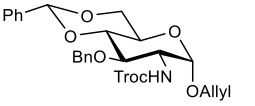
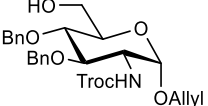
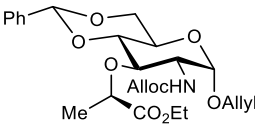
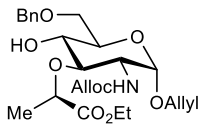
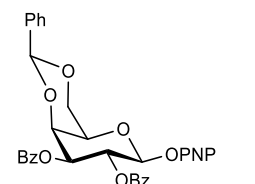
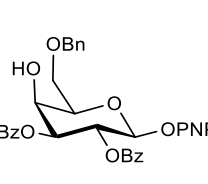
$\text{BnO} \begin{array}{c} \diagup \text{O} \diagdown \\ \text{---} \end{array} \xrightarrow[80\text{ }^{\circ}\text{C}]{\text{Pd/C, H}_2\text{ (40 bar)}} \begin{array}{c} \diagup \text{O} \diagdown \\ \text{HO} \end{array}$			
Entry	Substrate	Product	Yield (%)
1			95
2			95
3			95
4			90

Reductive ring openings of 4,6-O-benzylidene acetals are also important deprotections, as these acid and/or hydride mediated reactions are among the key transformations in carbohydrate chemistry. However, these reactions are often exothermic and it becomes imperative to prevent the subsequent acid-catalyzed hydrolysis reaction of the benzylidene groups by carefully optimizing the rate at which the acid is added in these reactions. Furthermore, the yields obtained in such reaction are often irreproducible and vary widely with scale. Often hydrolyzed byproducts such as 4, 6-diols are formed in larger scale systems. In order to improve the overall efficiency of the reaction, it is critical to precisely control temperature and mixing. Reductive opening of 4,6-O-benzylidene acetals was performed in a continuous microfluidic environment for fast optimization of reaction conditions (Table 1.5).³⁶

Table 1.5: Reductive opening of benzylideneacetals under microfluidic conditions.

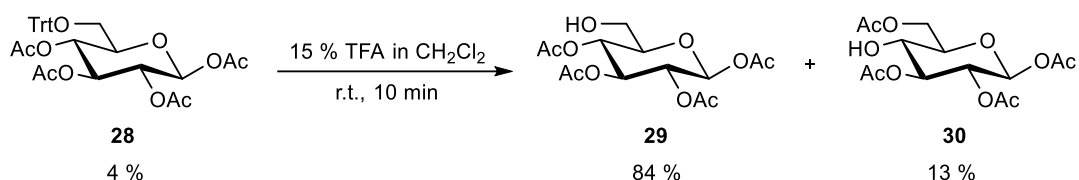


Entry	Substrate	Reducing agent	solvent	product	Yield (% microfluidic) ^a	Yield (% batch) ^{a,b}
1		Et_3SiH (1.0 M)	DCM		93 ^c	58
2		$\text{BH}_3 \cdot \text{Et}_2\text{NH}$ (0.5 M)	DCM		100	90

3		Et ₃ SiH (1.0 M)	DCM		91	83
4		BH ₃ ·Et ₂ NH (0.5 M)	DCM		100	86
5		BH ₃ ·Et ₂ NH (0.5 M)	ACN		100	NA ^d
6		Et ₃ SiH (1.0 M)	DCM		91	62

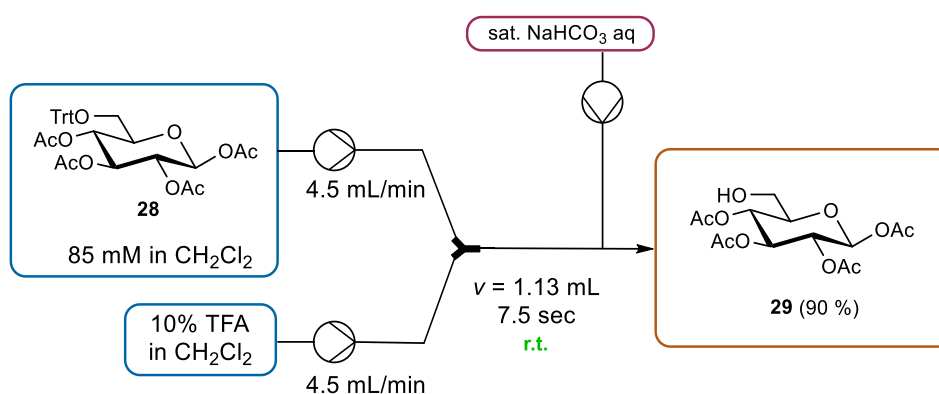
^a Isolated yields. ^b Reaction was performed at 100-500 mg scale. ^c 4-*O*-Benzyl derivative was obtained in 5% yield. ^d 60-70% yields for the case of corresponding *N*-Troc derivative. ^e PNP: p-nitrophenol.

The formation of byproducts during protection and deprotection reactions of oligosaccharides poses another challenge in the field of carbohydrate chemistry. The installation of the trityl group as a protecting group is important for the formation of 1,6-glycosidic bonds, e.g. in the synthesis of β -glucans.³⁷ Under batch conditions acetyl migration takes place right after the trityl group is deprotected from the 6-position of **28** due to the attack of the carbonyl group at 4-position acetyl group by the 6-position hydroxyl group (Scheme 1.6).



Scheme 1.6: Deprotection of the trityl group of **28** in batch condition.

To prevent such migrations, control of reaction time, temperature, and flow rate becomes necessary. Attaining such reaction conditions in batch is often not feasible. This dictates the usage of continuous flow microreactor for carrying out such transformations. Using continuous microfluidics, deprotection reactions of trityl protecting group for **28** were carried out screening reaction time, substrate concentration, and flow rate were optimized (Scheme 1.7). With these optimized reaction parameters, the deprotection could be successfully carried out in the microreactor system with the final deprotected product yield of 90%.



Scheme 1.7: Deprotection of the trityl group of **28** in microflow reaction system.

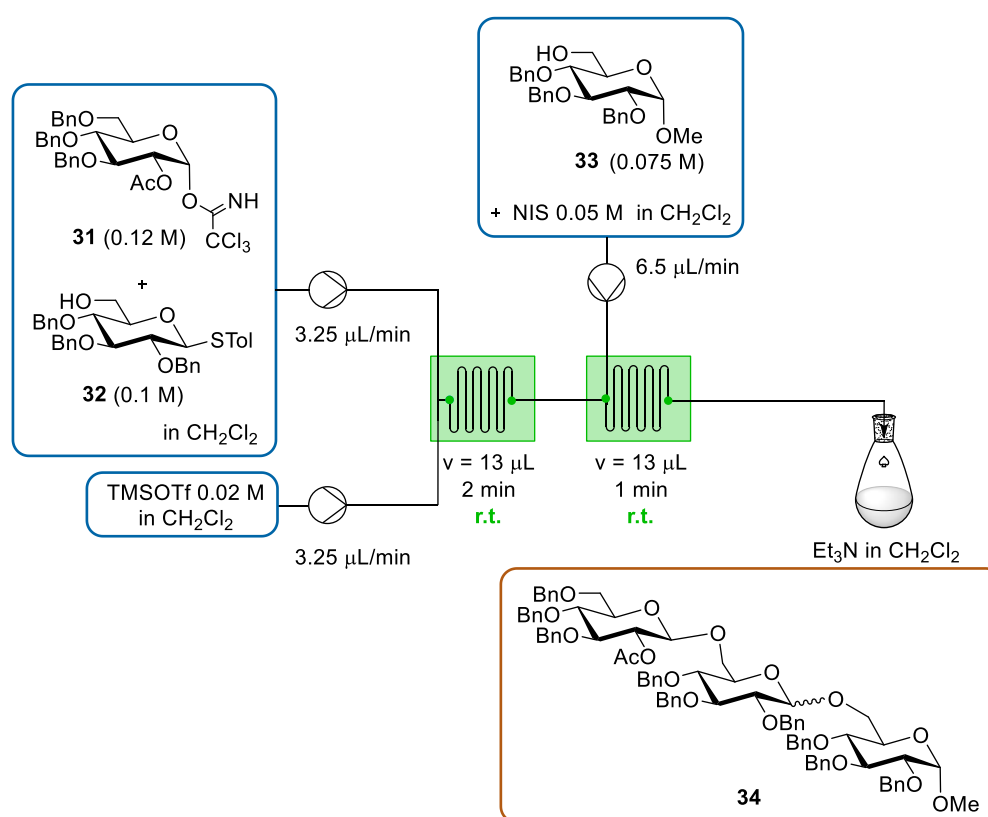
1.6.3 Multistep synthesis

The synthesis of oligosaccharides under microfluidic continuous flow conditions is not restricted to only single glycosylations to produce disaccharides. One of the main advantages of continuous flow systems is the ability to combine microreactors in series to facilitate multistep synthesis, which removes the necessity of isolating intermediate compounds after each reaction step.³⁸ This makes the overall synthesis a lot faster as compared to the respective batch process. Oligosaccharides can be synthesized conveniently as a single flow system combining more than one microreactors in series or by iterative glycosylations.

The synthesis of a trisaccharide is facilitated by utilizing the difference in the method of activation of different leaving groups such as trichloroacetimidates and thioglycosides.³⁹ For the synthesis of a trisaccharide, the first glycosylation reaction is carried out by selective activation of trichloroacetimidate donor **31** in the presence of **32** using TMSOTf and subsequently glycosylated with glycosyl acceptor **32** in DCM using a two minutes residence time at room temperature in the first microreactor. After the first glycosylation, the solution

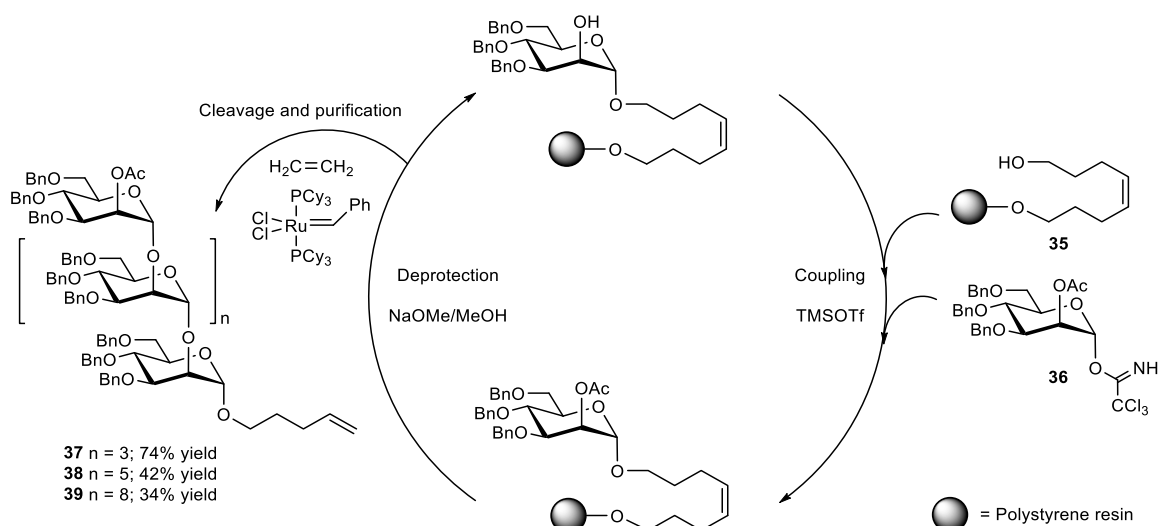
of the product containing the disaccharide thioglycoside donor **31+32** and TMSOTf were directly fed into the second microreactor along with DCM solution of glucosyl acceptor **33** together with NIS (*N*-Iodosuccinimide) which is co-activator for thioglycoside donor (Scheme 1.8).

The final trisaccharide **34** solution was obtained from the outlet of the second microreactor in 51% yield after quenching the remaining TMSOTf with trimethylamine. While the batch process gave similar selectivities to those observed in flow, the yield was generally lower and required anhydrous DCM, whereas reagent grade could be used in the flow reactors (Scheme 1.8).



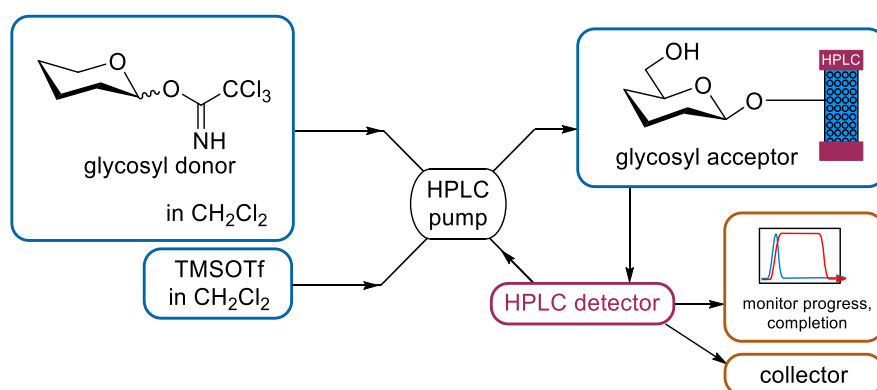
Scheme 1.8: One-flow multi-step synthesis of oligosaccharides **34** under microfluidic conditions.

While the above approach relies on orthogonal leaving group reactivities to synthesize tri- and even tetrasaccharides, the efficiency decreases – and technical challenges greatly increase – for larger and more complex compounds. Traditionally, the complexity and highly laborious syntheses of large oligosaccharides was only achieved by a handful dedicated laboratories. However, in 2001 Seeberger and coworkers adapted the iterative solid-phase approach (Figure 1.14) utilized for peptides and DNA/RNA to develop an automated means of oligosaccharide synthesis from the reducing end (Figure 1.13).⁴⁰ Using



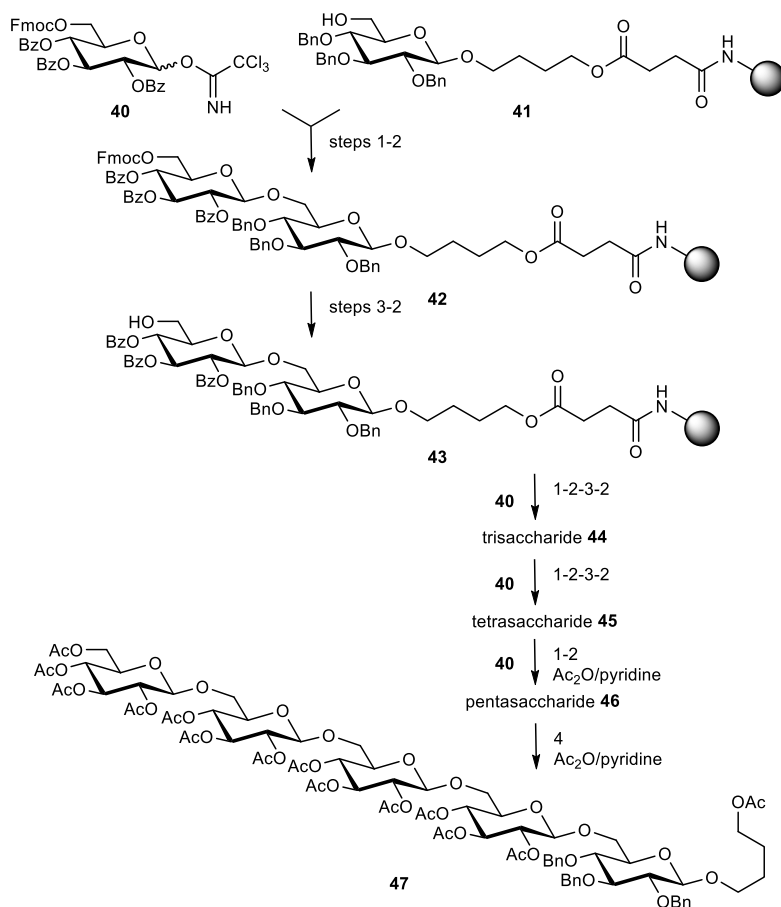
Scheme 1.9: Automated oligosaccharide synthesis with trichloroacetimidates.

Solid phase synthesis of oligosaccharides can be also achieved under continuous flow conditions when the acceptor-functionalized resin is loaded into a packed bed reactor (Scheme 1.10).⁴⁵⁻⁴⁶ Here, donor and activator are flown into the packed bed, where they mix in the presence of an acceptor with a very high effective molarity. Once enough material passes through the bed to react with all available sites – as determined by the inline HPLC UV detector – the subsequent washing and deprotection cycles can take place, preparing the column for the next iteration. A number of linear polysaccharides have been prepared with this method, including pentasaccharides. Upon completion of the synthesis, the product is released from the resin using sodium methoxide (Table 1.6).



Scheme 1.10: Set-up for HPLC-assisted synthesis using a packed-bed reactor with glycosyl acceptors.

Table 1.6: Experimental Data for the HPLC-Assisted Synthesis of Pentasaccharide **47**.



Operation	Action	Flow rate (mL/min)	Total volume (mL)	Time (min)
1. Glycosylate (acceptor 41)	Pump B: 39 mM 40 in CH ₂ Cl ₂ Pump C: 0.28 M TMSOTf in CH ₂ Cl ₂	0.3 B/C = 4/1	18	60
2. Wash	Pump A: CH ₂ Cl ₂	2	20	10
3. Deprotect 42	Pump C: piperidine/ DMF (1/5, v/v)	0.5	2.5	5
2. Wash	Pump A: CH ₂ Cl ₂	2	20	10
Repeat 1		0.3	18	60
2	As above, trisaccharide 44 is obtained	2	20	10
3		0.5	2.5	5
2		2	20	10
Repeat 1		0.3	18	60
2	As above, trisaccharide 45 is obtained	2	20	10
3		0.5	2.5	5
2		2	20	10
Repeat 1		0.3	18	60
2	As above, trisaccharide 46 is obtained	2	20	10
4. Cleave of to obtain 47	Pump C: 0.1 M NaOCH ₃ in CH ₃ OH/ CH ₂ Cl ₂	1	5 (recirc.)	60

1.7 Goal of this thesis

The stereoselective control and manipulation of carbohydrates represents one of the most difficult classes of transformations in organic chemistry due to a host of dependent and independent environmental factors, intrinsic and poorly understood molecular preferences, high sensitivity, and a range of competing side reactions. In addition, no systematic studies and interrogation of these factors has been published to date. Flow chemistry offers a significantly enhanced degree of control over the reaction and its environmental conditions. Improved control has proven highly beneficial in the synthesis of carbohydrates, whether it is the improved mixing resulting in more selective glycosylation or the high surface-to-volume ratios for better temperature control. In particular, the ability to couple multiple steps together has allowed for the rapid synthesis of molecules in hours in a fully automated fashion what would have taken a team of scientists years to achieve. The application of flow chemistry for tackling challenges in glycosylation were discussed in this chapter. Still, many fundamental question remain unanswered in the literature. Some of the question below were addressed in this thesis:

- 1) Will I be able successfully interrogate and study various factors influencing the stereochemical output of glycosylation is an automated flow platform?
- 2) Can the automated flow platform give me reproducible glycosylation data?
- 3) Can I generate a thorough understanding of the mechanism of glycosylation using such a platform?
- 4) Can I predict the stereoselectivity of a glycosylation reaction by application of flow chemistry, automation and machine learning techniques?

Chapter 2 Instrumentation to provide increased control over glycosylation conditions

2.1 Introduction

In an effort to demystify glycosylation reactions and guide synthetic chemists towards optimal reaction conditions without prior reaction optimization, general guidelines regarding the selection of appropriate reaction conditions based on the intrinsic preferences of the coupling partners are urgently needed. However, before these can be determined, each of the factors influencing glycosylation reactions must be identified first and categorized, before interrogatory experiments are devised and performed in a controlled, reproducible environment in as isolated a manner as possible. This reproducibility can be achieved using minimal amounts of material in microreactor flow chemistry setup. *Chapter 2* describes the development and utilization of an automated microreactor/HPLC platform capable of varying reactant ratios, temperature, and reaction time autonomously. This instrument was used for the rapid and reproducible isolation and interrogation of variables influencing the stereoselectivity, providing an unprecedented, systematic, and quantifiable view of glycosidic bond formation from 270 experiments. The identification of, and factors providing control over, specific intermediates of the glycosylation reaction is outside the scope of this work.

2.2 Design of the automated flow platform

The heart of the reaction optimizer platform is a 78.2 μL silicon microreactor comprised of a separate addition port for donor, acceptor, and activator. Each of these lines is driven by two syringe pumps for reagent and solvent, allowing for both line purging and changes in concentration in any of the reagents (Figure 2.1). The combined solution passes through a mixing zone before entering the reaction zone. A quench is added prior to the reaction mixture exiting the chip to ensure the reaction is only occurring at the desired temperature. Once steady states reached after ten reactor volumes, a sample is automatically removed via a 1 μL HPLC injection loop. The temperature in the chip is maintained reliably within a range from -55 to +70 $^{\circ}\text{C}$ within ± 0.1 $^{\circ}\text{C}$ by a surrounding aluminum block cooled or heated using a thermostat.

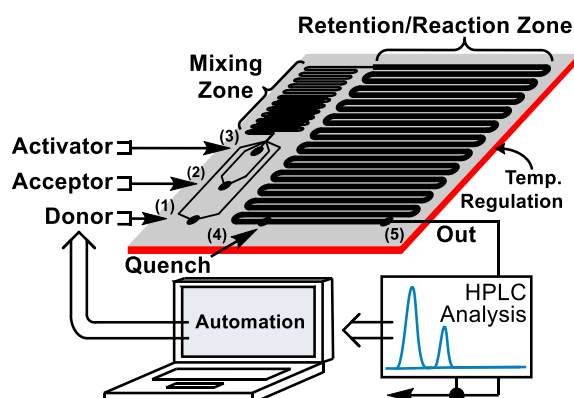


Figure 2.1: Schematic of automated glycosylation instrument consisting of three sections: reaction section, HPLC analysis, and automation.

2.2.1 Microreactor Section

The heart of the reactor section is the microreactor (Figure 2.2), which was housed inside a thermostat, made of an aluminum block. Thermal oil was circulated via closed loop inline thermostat system (Huber Unistat) through the thermostat to ensure proper control of reactor temperature ranging between -50 to 70 °C. The reactor is shown in Figure 2.3, and the detailed design of this reactor is described elsewhere.¹⁶ The reactor's volume of 78.2 μL consists of ports for introducing solutions of donor (port 1), acceptor (port 2), and activator (port 3) respectively. Solutions were introduced with the help of air tight glass syringes (Hamilton) driven by seven syringe pumps (Harvard Pump 11 Elite). Fluid connections between the syringes and the microreactor ports were done by 1/16 inch PTFE tubing as shown in Figure 2.4. The reactants were thoroughly mixed in the mixing section of the reactor and then introduced into the reaction zone. At the end of the reaction zone (port 4) excess activator was neutralized with a quench solution and the products exited via the out port (port 5). Subsequently, an 1 μL of sample from the reactor outlet was automatically injected in the HPLC system by an inline six port inline injection valve from VICI Valco, equipped with 1 μL sample loop. In total, seven syringe pumps (Harvard apparatus Pump 11 Elite) were used to control flow in the microreactor chip (Figure 2.3).

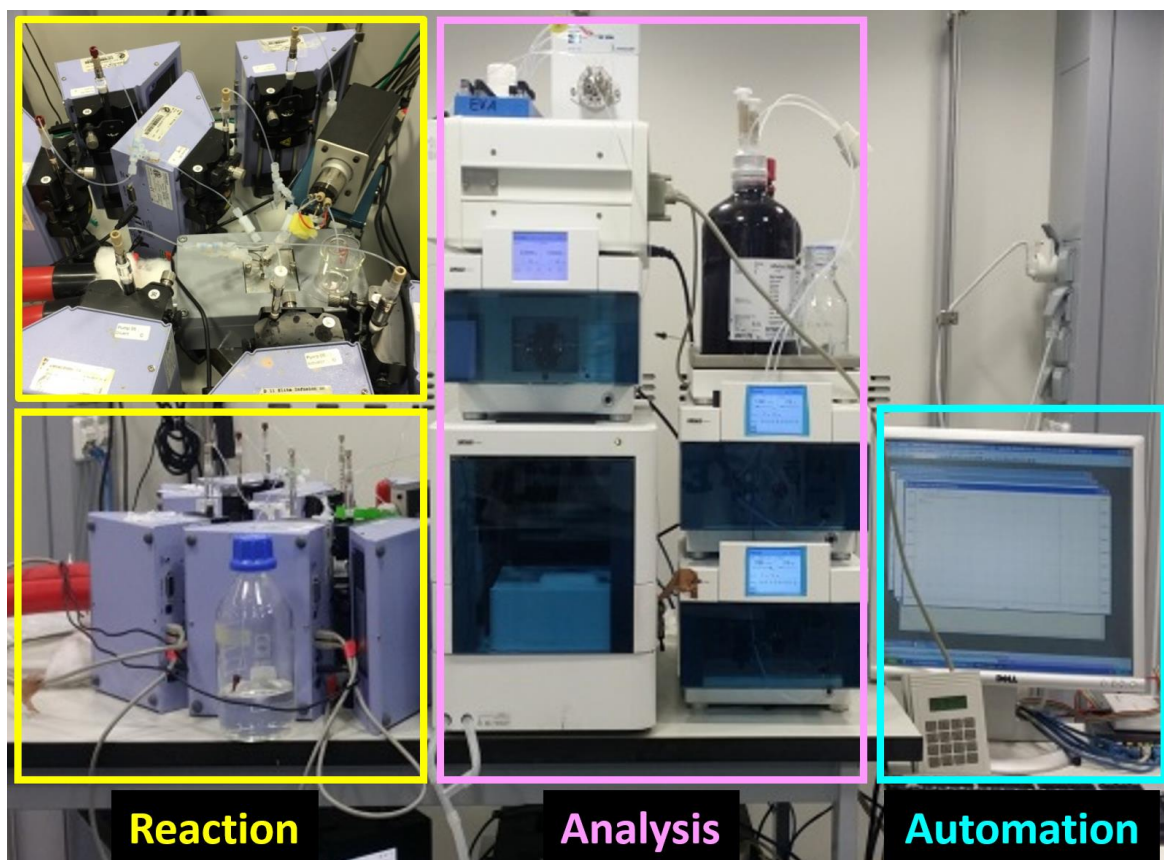


Figure 2.2: The automated flow platform. Reactor section showing seven syringe pumps, thermostat and inline injection valve, inline HPLC (analysis), LabVIEW software (automation).

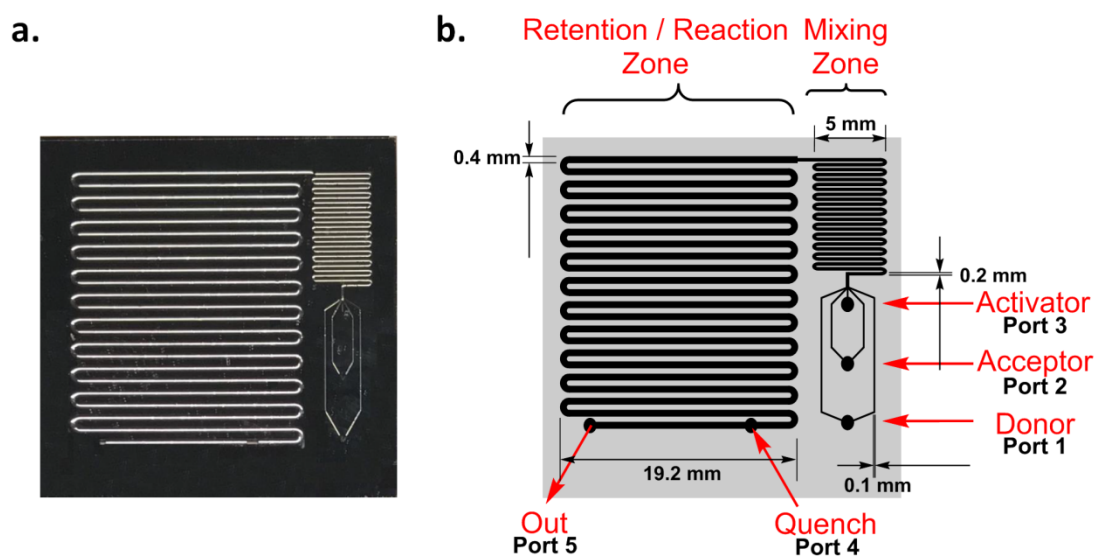


Figure 2.3: Microreactor for automated glycosylation.

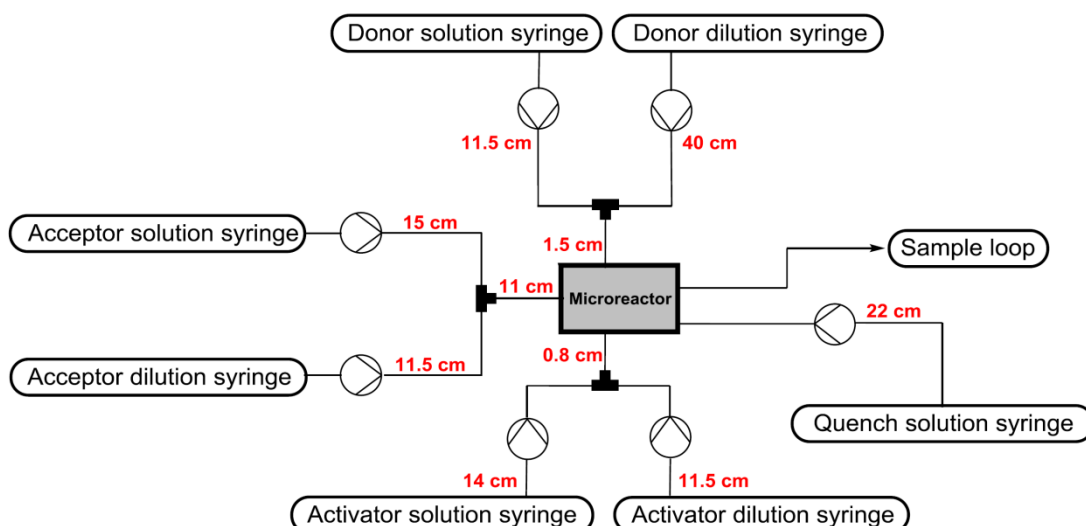


Figure 2.4: Reactor section showing all the connection and lengths of tubes.

2.2.2 Automation Section

The system is capable of automatically running a series of experiments with an on-line HPLC analysis set-up that ensures separation of the α/β diastereomers for a given donor/acceptor pair. The LabVIEW software controls a platform (Figure 2.5) consisting of syringe pumps, chiller, injection valve, HPLC, and autosampler controlled via a graphical user interface. Design of experiments is achieved via the graphical user interface. This programming was written by my collaborators Felix Hentschel and Dr. Sourav Chatterjee and is described in detail below.

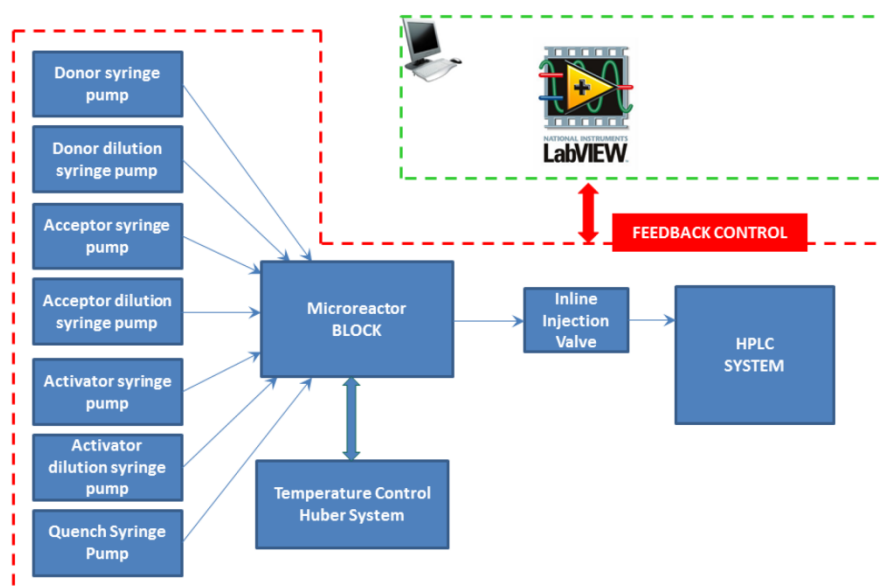


Figure 2.5: Schematics of overall automation of the system

The seven syringe pumps, the Huber unistat for temperature control, the inline HPLC injection valve for injecting the sample in HPLC, and triggering of the HPLC were automated and controlled by software, developed in LabVIEW 2014. Individual driver files for syringe pumps, thermostat, and HPLC trigger were written as separate Virtual Instrument (VI) files in LabVIEW 2014. In total 80 VIs were written and these individual subroutines were utilized in a Master VI, which handled the queuing system to control all the instruments in a timely manner. All the user input was handled with the data input VI, with its own Graphical User Interface (GUI) (Figure 2.6). The MasterVI also contains important status information of the overall system which are the syringe pump flowrate, temperature information, and current run indicators.

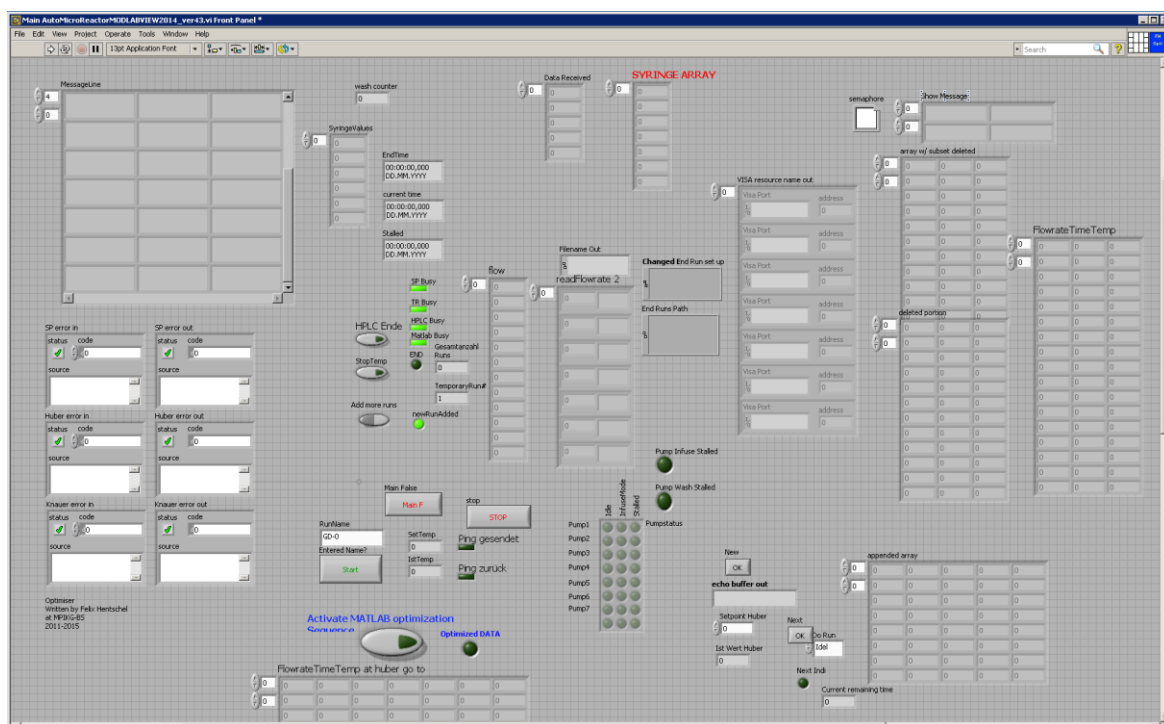


Figure 2.6: Graphical User Interface for the Master VI

The graphical user interface (GUI) of the software controls the automated flow platform. This GUI consists of several panels, including the central queuing panel and a series of indicator LEDs for different parts of the machine, such as the current state of the syringe pumps, temperature equilibration, and the HPLC status. To start the machine, at first the start button, which is highlighted in the GUI, needs to be clicked. Once the start sequence is initiated, the software is ready to receive the experimental conditions from the user and the GUI for the data input VI is initiated.

In the Data Input VI of the GUI shown in Figure 2.7, concentration of the donor, acceptor, activator, quench syringes are entered in the fields, labelled (1-1). The desired reaction concentration of the donor, acceptor, activator in the microreactor are subsequently entered in the fields, labelled (1-2). Residence time, desired reaction temperature are entered next in the fields, labelled (1-3). Lastly, the equivalents of quench are entered in the field labelled (1-4). Once these necessary values are entered in the VI, the ‘Table ready’ button, labelled (1-5) is activated which triggers the VI to calculate the flowrates of the reagents for that experiment. These flowrates are automatically entered by the VI into the run Table, labelled (2). In this way, multiple runs can be entered into the data input VI. After the desired number of reactions has been entered, the OK button under “Start Table (1-6)” needs to be clicked. This puts the automated flow platform in the run mode. The system then goes back to the GUI of the Master VI (Figure 2.6).

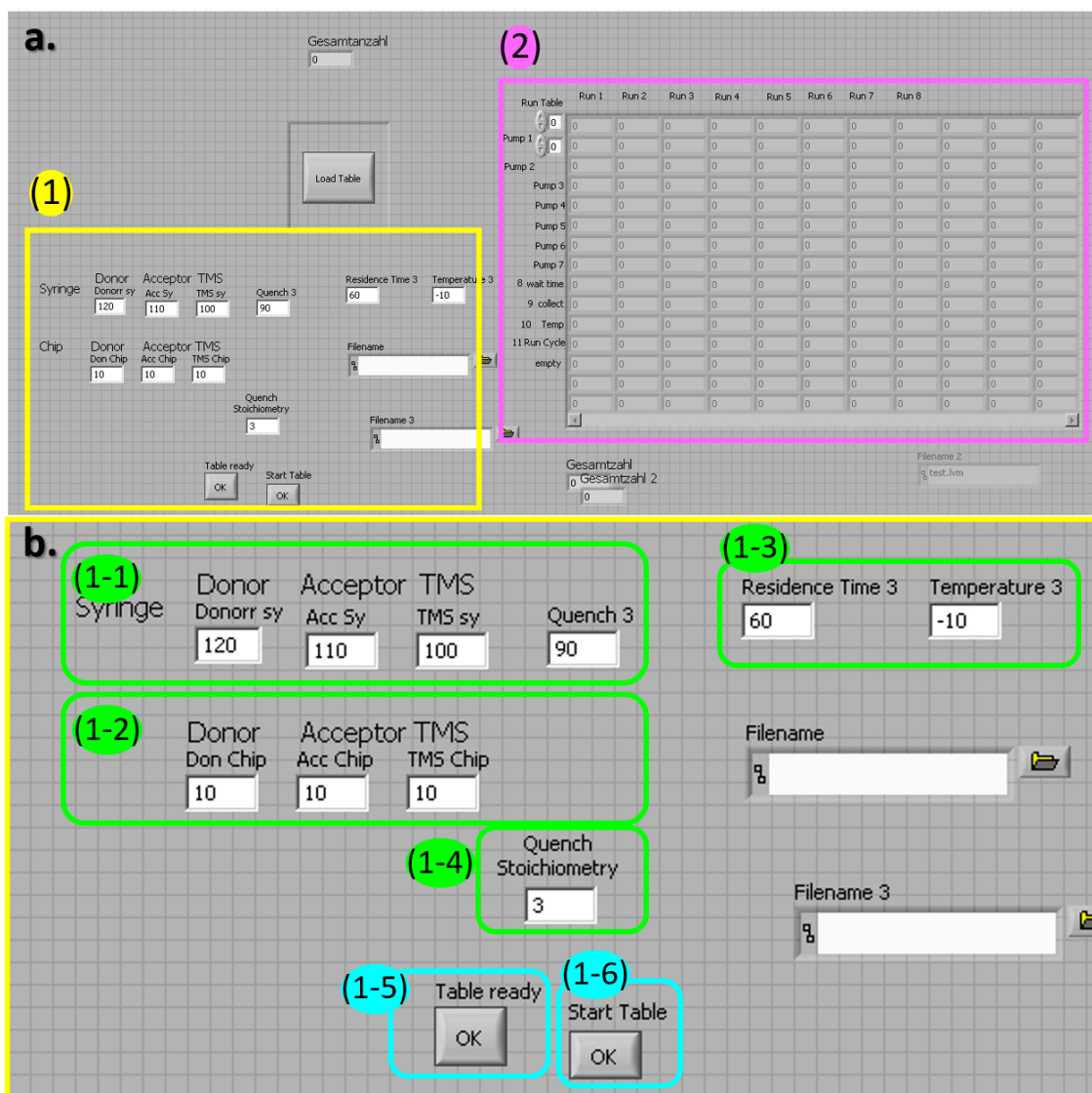


Figure 2.7: a, GUI of Data input VI software displaying the automated experiments to run. b, section (1) of a.

The system then runs automatically, going through a series of checks including washing the reactor system and equilibration of temperature, before the first reaction commences and the cycle continues, until the end of the table of the data input VI is reached. The control algorithm runs through a series of automation steps. (Figure 2.8).

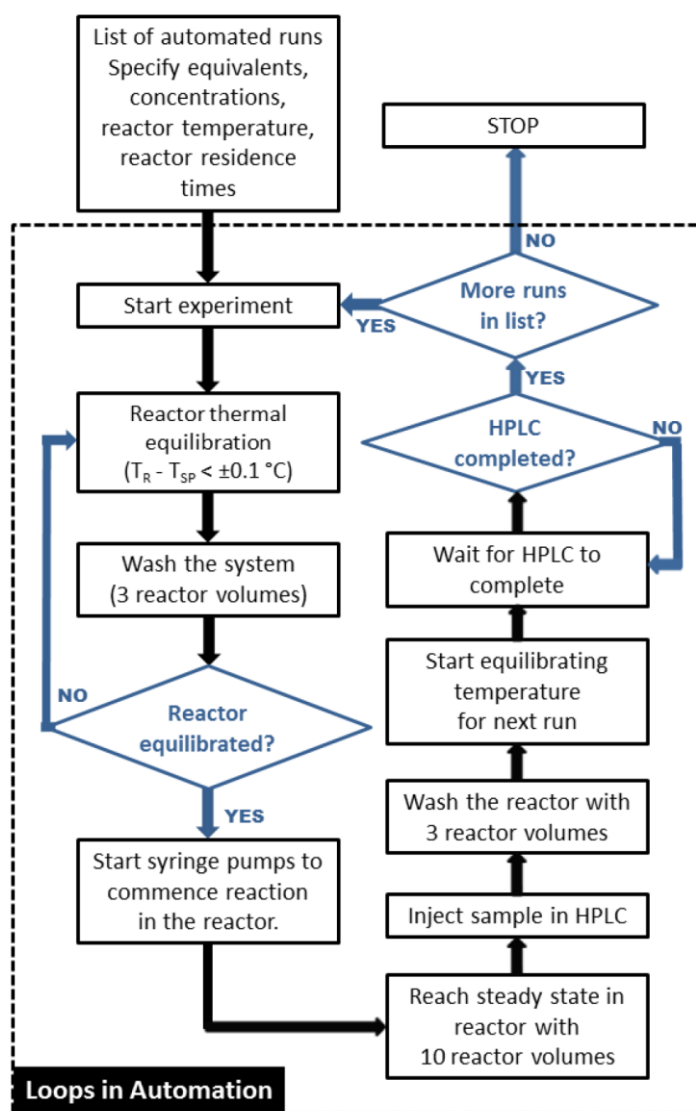


Figure 2.8: Flowchart showing the steps in automation.

After the software receives the table of experiments from the user, the control algorithm initiates the start of the experiments. It sends the reaction temperature to the temperature thermostat of the system, which starts equilibrating the temperature set point for the reactor. After the correct temperature is reached, the control algorithm initiates the reactor wash cycles, washing the reactor with three reactors volume of reaction solvent. After termination of the wash cycle, the algorithm re-checks the temperature equilibration and starts the syringe pumps to begin the first experiment. Upon completion of the reaction,

the sample is automatically injected in the HPLC and the software waits until the HPLC run is finished. Once the HPLC run is completed, the HPLC sends a signal back to the software and the next run of the table is started in the similar way. The algorithm runs until the last experiment in the table.

2.2.3 Analysis Section

The reactions were monitored using HPLC. The HPLC system used was a Kanuer Plating Blue system, equipped with a UV detector (254 nm). The column used was Macherey-Nagel Nucleosil 100-5 OH diol column with particle size of 5 μm . The column has an I.D. of 4.6 mm and length of 250 mm. The column was housed inside a column oven, and was maintained at 20 $^{\circ}\text{C}$ for all analysis. The mobile phase was gradient mixture of HPLC grade ethyl acetate and hexane, which was pumped with a constant flowrate of 1 mL/min. The gradient system of the mobile phase was developed and programmed into the HPLC. Depending on the molecule, either HPLC method A, HPLC method B or HPLC method C was used to separate and analyze the compounds in this study. The HPLC methods are discussed in *Section 6.3 of Chapter 6*.

Chapter 3 Factors effecting glycosylation

3.1 The Permanent and temporary factors affecting glycosylation

In spite of the lack of understanding regarding the underlying mechanism of the glycosylation reaction, as discussed in *Section 1.2 of Chapter 1*, the stereochemical outcome of the reaction is dictated, or at least influenced, by the coupling partners. These coupling partners, once fixed cannot be changed during the reaction and hence can be called “permanent factors”. The reaction conditions such as choice of solvent, temperature, choice of activator, concentration of reagents, and chemical equivalents can be “ad hoc” manipulated and controlled during the reaction. These categories can hence be called “environmental factors”(Figure 3.1).

Permanent	Environmental		Influence
Leaving Group: trichloroacetimidate thioether, phosphate	Temperature: -50 → 70 °C	Activator: TfOH, MsOH, FSO ₃ H, (Tf) ₂ NH	Stabilities: Conformers Intermediates Product(s)
Acceptor: MeOH, EtOH, <i>i</i> PrOH, <i>t</i> BuOH, di/trifluoroethanol	Concentration: 4.8 → 20 mM	Solvent: DCM, ACN Toluene, MTBE	Activation: Leaving Group Types of Intermediates Reaction Pathways
Donor: C2/C4: Glucose Galactose, Mannose	Residence Time: 45 → 270 sec	Water: Anhydrous → 0.25 equiv.	Mechanism: S _N 1- vs S _N 2-like Nucleophilicity Reaction Rates
	Acceptor Equiv. 0.8 → 10		

Figure 3.1: A selection of the permanent and environmental factors of glycosylation reactions, with the specific examples examined in this study, as well as how these factors potentially influence the stereoselectivity.

The donor contains five stereocenters, four of which can influence the activation as well as the stability and conformations of intermediates by hyperconjugation.⁴⁷⁻⁵² The presence of protecting groups at each of these four positions can directly⁵³⁻⁵⁴ or indirectly⁵⁵⁻⁵⁶ influence the stereoselectivity of the glycosylation. The presence of an electron donating protecting group, such as an ethers, influences the stereoselectivity by increasing the reactivity. This is called “arming” of a glycosyl donor, whereas presence of electron withdrawing groups such as esters results in “disarming” due to a reduction in reactivity of the donor (Figure 3.2).¹⁸



Figure 3.2: Outline of the armed-disarmed strategy discovered by Fraser-Reid.

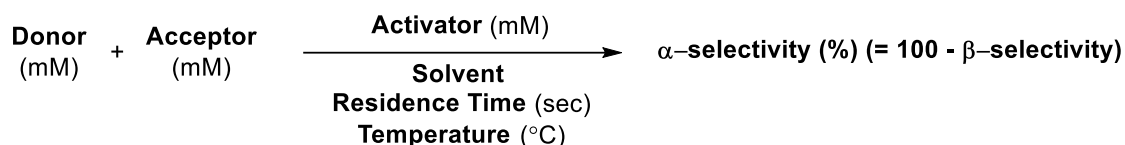
The stereoselectivity can also be influenced by restricting conformational freedom via bridged structures to influence reactivity.⁵⁷⁻⁶⁰ The choice of leaving group can also play a role in stereochemical outcome, activation of which leads to creation of neutral or charged byproducts.⁶¹⁻⁷⁰ As the vast majority of glycosylations are C-O couplings, the choice of acceptor also plays a significant role. The nucleophilicities of primary and secondary alcohols can depend on the orientation. In case of glycosyl acceptors the orientation is axial/equatorial, of the alcohol, the adjacent protecting groups,⁷¹⁻⁷² and by structural changes induced by conformational locking⁷³ or electronic modification.⁷⁴⁻⁷⁵ The sterics of the acceptor nucleophile can also potentially influence the stereochemical outcome by influencing the rate of reaction.

The reaction environment strongly influences the mechanistic path these coupling partners follow, as well as the intermediates which are formed. The choice of solvent can influence bond cleavage, stabilization of intermediates, and influence reaction pathways. The conjugate base generated from the activator can influence the formation of intermediates via contact-ion pairs or by forming covalent intermediates such as α -triflates.⁷⁶⁻⁷⁷ The temperature will impact the stability of intermediates, the reaction pathways followed, and product composition. Lastly, traditional reaction parameters such as concentration,⁷⁸ stoichiometry,⁷⁹⁻⁸⁰ reaction time, and mixing²⁹ can have an impact on the yield of the reaction as well as the resulting stereoselectivity.

Glycosylation is a deceptively simple reaction that is a technically very demanding transformation. Optimization is necessary for every new reaction with precise control of various reaction parameters. However, the lack of understanding, of *what influence* the factors have on the stereochemical outcome, coupled with scarcely reproducible data has left the selection of initial reaction parameters such as the choice of anomeric leaving group, protecting groups, solvent, temperature, and activating agent, often more of a matter of personal preference than knowledge-based decision making.

3.2 Controlled interrogation of factors affecting glycosylation through automation

The design and working of the automated system is described in *Chapter 2* of this thesis. This automated system in hand, a model glycosylation reaction system was chosen to investigate the factors influencing the stereoselectivity (Scheme 3.1).



Scheme 3.1: A model reaction in an automated microreactor flow platform.

When discussing the permanent factors initially, three pyran cores – glucose, mannose, and galactose – were chosen as donors to probe the effects of the C2 and C4 positions, respectively. Hydroxyl groups, except at the anomeric position, were protected as non-participatory benzyl ethers.

Three of the most widely used leaving groups, namely trichloroacetimidate, ethylthioether, and *n*-dibutylphosphate were systematically investigated. Glycosyl trichloroacetimidates as leaving group were particularly appealing, owing to relatively easy activation with catalytic amounts of activator, as compared to the NIS-TfOH activating system of thioglycosides or the requirements for stoichiometric activators for phosphates. Glycosyl trichloroacetimidates were activated with TfOH rather than TMSOTf to limit the potential reaction pathways, as TfOH is the catalytic activating species for both activation methods. To study the effect of acceptor nucleophilicity and sterics, a systematic interrogation was planned by utilizing primary, secondary and tertiary alcohols as model acceptors, specifically methanol, ethanol, 2,2-difluoroethanol, 2,2,2-trifluoroethanol, isopropanol, and *tert*-butanol, exploring a range of steric and electronic effects.⁸¹⁻⁸² The temperature ranges that were investigated were limited by the reactivity of the donor and the melting and boiling points of the solvents. The detail methodologies for the synthesis and preparation of reagents, drying of solvents are all described in detail in *Chapter 6*.

Glass syringes containing solutions of the donor (50-110 mM), acceptor (60-110 mM), and the activator (22.6-120 mM) feed lines were diluted as desired via accompanying syringe pumps prior to mixing in the reactor. The reaction temperature, reagent concentration, stoichiometry, as well as the residence time were all set with the aid of the

developed software. After reaction completion and inline quenching with pyridine, the reaction products were monitored by an automated injection into the online HPLC.

The results discussed below are based on 270 glycosylation reactions that were performed as part of this thesis. All reactions exhibited yields greater than 60% (Table 6.1 in *Chapter 6*). The results of these investigations are discussed as isolated factors with respect to the change in temperature, starting with the permanent factors, followed by environmental factors. For a detailed discussion of the experimental preparations and procedures, see *Chapter 6*.

3.3 Effects of Permanent Factors

3.3.1 Donor

3.3.1.1 Interrogating Permanent Donor Leaving Group (C1)

Over the past century, a host of different leaving groups and corresponding activators to induce anomeric cleavage have been introduced as part of the quest for mild, selective, and high-yielding glycosylation reactions.⁶¹⁻⁷⁰ For the systematic exploration of the effects different leaving groups have on the stereochemical outcome of glycosylation, a perbenzylatedglucosyl α -trichloroacetimidate (Schmidt donor), glucosyl β -ethanethio ether, or glucosyl α -*n*-dibutylphosphate were reacted with isopropanol as model acceptor in DCM at temperatures ranging from $-50 \rightarrow 30$ °C (Figure 3.3). To minimize differences in the conjugate bases/byproducts present in the solution, the activation conditions for each leaving group were chosen such that triflate anions were present in all cases. All other variables were kept constant (*e.g.* pyran core: glucose, acceptor: *i*PrOH, conjugate base: triflate (TfO⁻), solvent: DCM). The glucosyl donors with the three classes of explored leaving group gave nearly identical stereochemical outcomes under the conditions studied. Differences were in conversion and yield at low temperatures. A rapid drop of glycosylation yields was observed for thioglucosides from 88% at 10 °C to 45% at -10 °C. Glucosyl phosphate donors behaved similarly, exhibiting a 60% yield at -10 °C, which subsequently dropped to 30% at -30 °C. Along with the drop in yield, a slight decrease ($< 7\%$) in α -selectivity is observed as compared to the trichloroacetimidate donor.

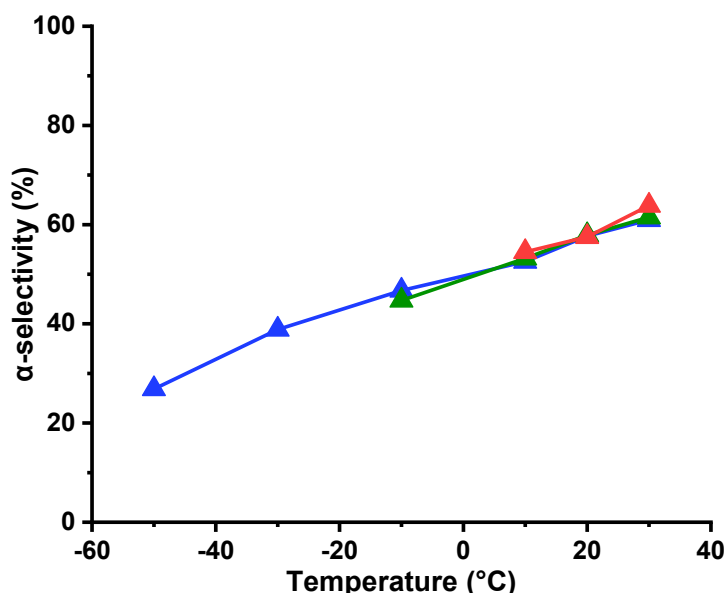
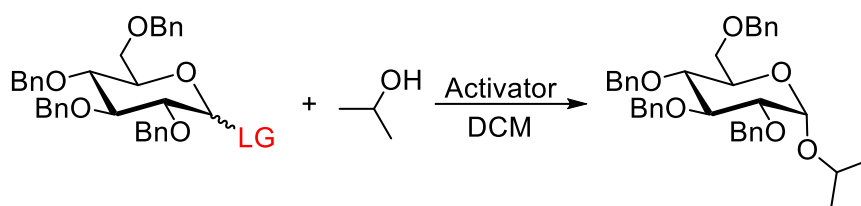
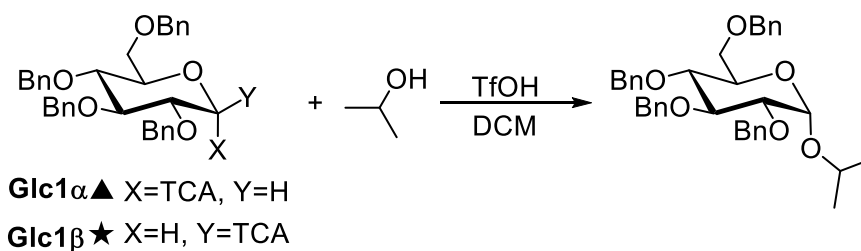


Figure 3.3: Comparison of stereoselectivities for glycosylations for glucose, bearing one of three leaving groups, with $i\text{PrOH}$ as acceptor in DCM . For full experimental details, see entries 13-18, 41-44, 313-317 of Table 6.1 in *Chapter 6*. Figure code: Glucose (▲); Trichloroacetimidate (blue) with TfOH (0.2 equiv.); ethyl thioether (red) with TfOH (0.2 equiv.) and N -iodosuccinamide (1.2 equiv.); n -butylphosphate (green) with TMSOTf (1.2 equiv.).

3.3.1.2 Influence of donor C1 position stereochemistry

The influence of the stereochemistry of the C1 position of the donor was investigated. A model glycosylation reaction involved coupling both α - and β - glucosyl trichloroimidate (TCA) with isopropanol in DCM and studied for the entire temperature range of the solvent (Figure 3.4). It can be seen that stereochemistry of the C1 position of the donor has no influence on the stereoselectivity of the reaction. This, however, is not always the case, as will be discussed in detail in *Section 4.1 of Chapter 4*.



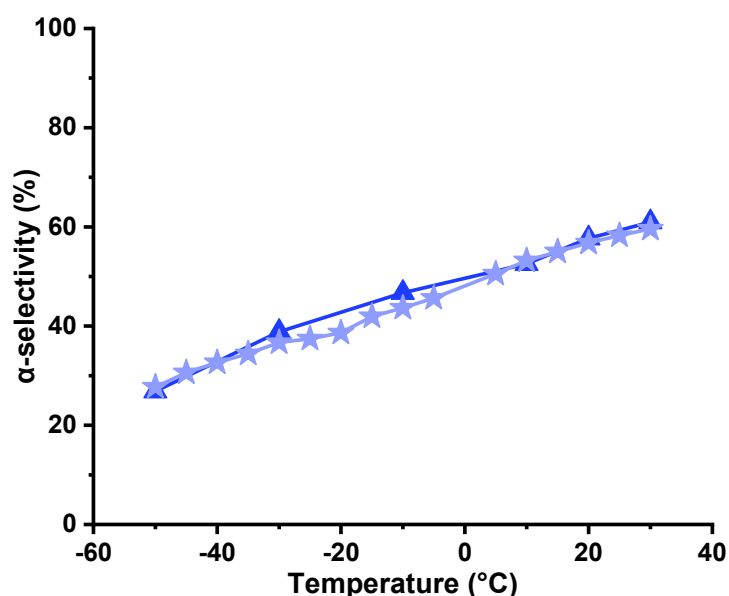


Figure 3.4: Comparison of C1 position stereochemistry of donor (perbenzylated glycosyl α - and β -trichloroacetimidates) on the stereochemical outcome of the reaction in DCM. *i*PrOH was used as acceptor and TfOH as activator. For full experimental details, see entries 13-34 of Table 6.1 in Chapter 6. Figure code: α -trichloroacetimidate glucose; (blue ▲); β -trichloroacetimidate glucose (pale blue ★)

3.3.1.3 Implication of leaving groups

After systematic studies of the effect of glycosyl donor leaving groups at different temperatures, it can be seen that the choice of leaving group does not affect the stereoselectivity of the reaction (Figures 3.3 and 3.4). Hence, for the rest of our systematic study identifying the influence of other factors glycosyl trichloroacetimidates were used, due to their facility of activation and broad reaction range. It was revealed that there is almost a linear relation between stereoselectivity and temperature, when model glycosylations were performed in DCM. For DCM, the lowest temperature studied is -50 °C due to the cooling limitation of the automated platform. The upper temperature range of solvent was dictated by the boiling point, for DCM the upper temperature examined was 30 °C. It was observed that the selectivity of the coupling of glucose and isopropanol in DCM, favors the formation of the β -product at -50 °C, with a selectivity of 73%. The alpha selectivity increases linearly with an increase in temperature, and at 30 °C the α -product was the major product (61% selectivity). This temperature sensitivity (the slope of the plotted data) was calculated at 0.41%/°C. These values serve as a comparison benchmark for all other variables examined herein. While the stereochemistry of some trichloroacetimidate donors, when reacted with TfOH, has been shown to have an influence

on the stereochemical outcome of glycosylations,⁸³⁻⁸⁴ under the standard conditions in DCM, no difference was observed between the α - and β -glucose donor.

3.3.1.4 Donor Stereochemistry (C2 and C4)

To probe the effect of donor stereochemistry at the C2- and C4-positions, model glycosylations were studied using glucose, galactose, and mannose donors. The stability of the intermediate and the activity of the donor can be influenced by through-bond or through-space hyperconjugation of the ether groups of the pyran core. For donors having non-participating groups, the C2 position has a huge influence, generating conformationally locked and unlocked glucose (equatorial C2 ether)/mannose (axial C2 ether) derivatives (Figure 3.5),⁸⁵ as well as for less common derivatives such as gluco-/mannosamine and the C2 fluorinated derivatives.⁸⁶

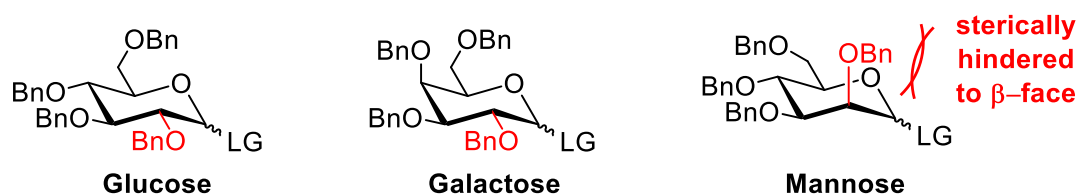


Figure 3.5: Comparison of three different monomers – glucose, galactose and mannose. In the case of mannose, axial C2 ether obstructs β -bond formation.

In order to investigate this aspect further, coupling of isopropanol with the α -glucosyl and mannosyl trichloroacetimidates were compared in DCM. A significant (30%) decrease in temperature sensitivity was observed when the C2 benzyl ether is axial, as is the case for mannose (Figure 3.6). The α -product were favored for mannose, and the selectivity is less sensitive to temperature, with α : β ratios ranging from 48:52 (-50 °C) to 61:39 (30 °C). Monosaccharides differing with respect to the C4 position, galactose (axial C4 ether) and glucose (equatorial C4 ether), exhibit similar temperature sensitivities ($T_{\text{sens}} = 0.43\%/^{\circ}\text{C}$) although galactose is 1.13 times more likely to give the β -product (9% more β -product formed) than glucose, ranging from 81% α -selectivity at -50 °C to 49% at 30 °C (Figure 3.6).

It can be inferred from the results that there are inherent preferences of glycosylating agents concerning mechanistic pathways and stereoselectivity. At low temperatures the β -product is favored by glycosyl donors, exhibiting a moderate degree of temperature

sensitivity and follows a more S_N2 -like reaction pathway as temperature decreases.⁸⁷⁻⁸⁸ Galactosyl donors have a higher preference for the formation of the β -product. However, the C2-position is a significantly influential functionality, and the formation of the α -product was favored in case of mannose which proceeded via a more S_N1 -like pathway (Figure 3.6). After the mannose donor is activated by TfOH, it forms a solvent separated ion pair mannosyl triflate.⁸⁷⁻⁸⁸ These inherent preferences can be enhanced or overridden by the other reaction variables from -50 °C to 30 °C (*vide infra*). This temperature depends on the solvent used for the glycosylation reaction.

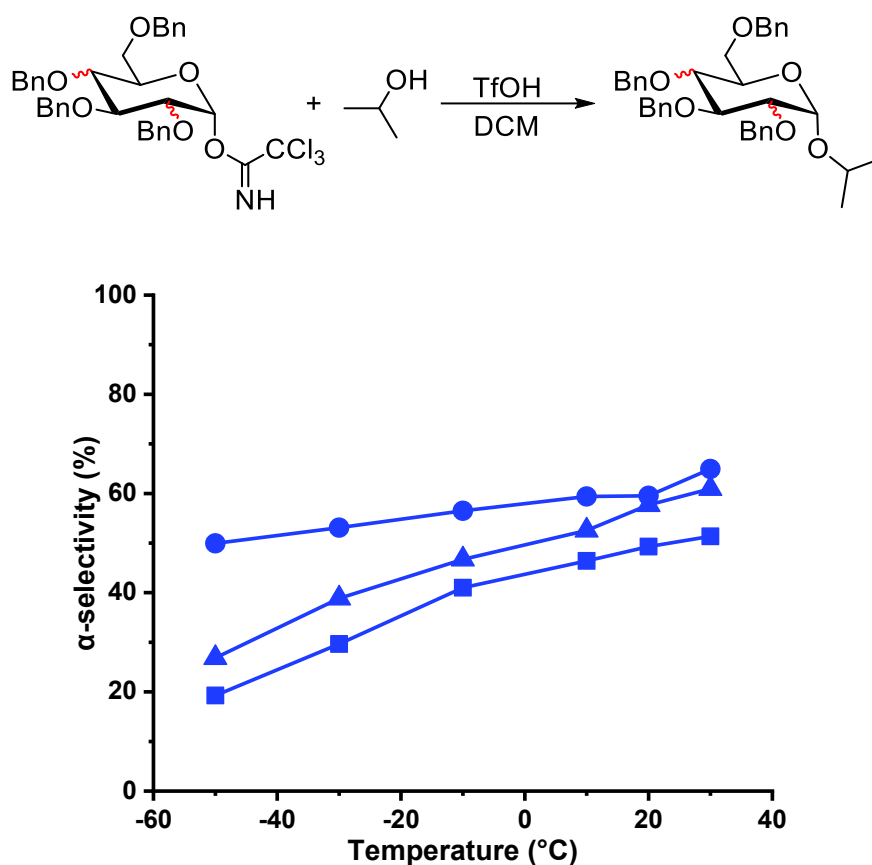


Figure 3.6: Comparison of the stereochemical outcome of three different trichloroacetimidates donors – glucose, galactose and mannose – reacting with isopropanol and TfOH. For full experimental details, see entries 13-18, 149-154, 232-237 of Table 6.1 in Chapter 6. Figure code: Glucose (▲); Galactose (■); Mannose (●); DCM (blue).

3.3.2 Acceptor

3.3.2.1 Acceptor Sterics and Electronics

To probe the influence of acceptor on the stereochemical output of glycosylation, model acceptors were chosen varying sterics and electronics properties: methanol, ethanol, isopropanol, *tert*-butanol, 2,2-difluoroethanol, and 2,2,2-trifluoroethanol. These nucleophiles were reacted with the glucosyl, galactosyl, and mannosyl trichloroacetimidate donors, respectively, in DCM across the accessible temperature range (Figure 3.7). A clear linear trend is observed in the series EtOH/*i*PrOH/*t*BuOH, exhibiting average stepwise increases of ~6.7% and ~8.2% in the α -selectivity, respectively, while a near identical rate of change with respect to temperature is maintained. However, methanol with its lack of C-C bond adjacent to the hydroxyl, shows a decrease in average temperature sensitivity when compared to EtOH (+0.3% α /°C vs +0.48% α /°C) and selectivities ranging from 30% α at -50 °C to 53% α at 30 °C.

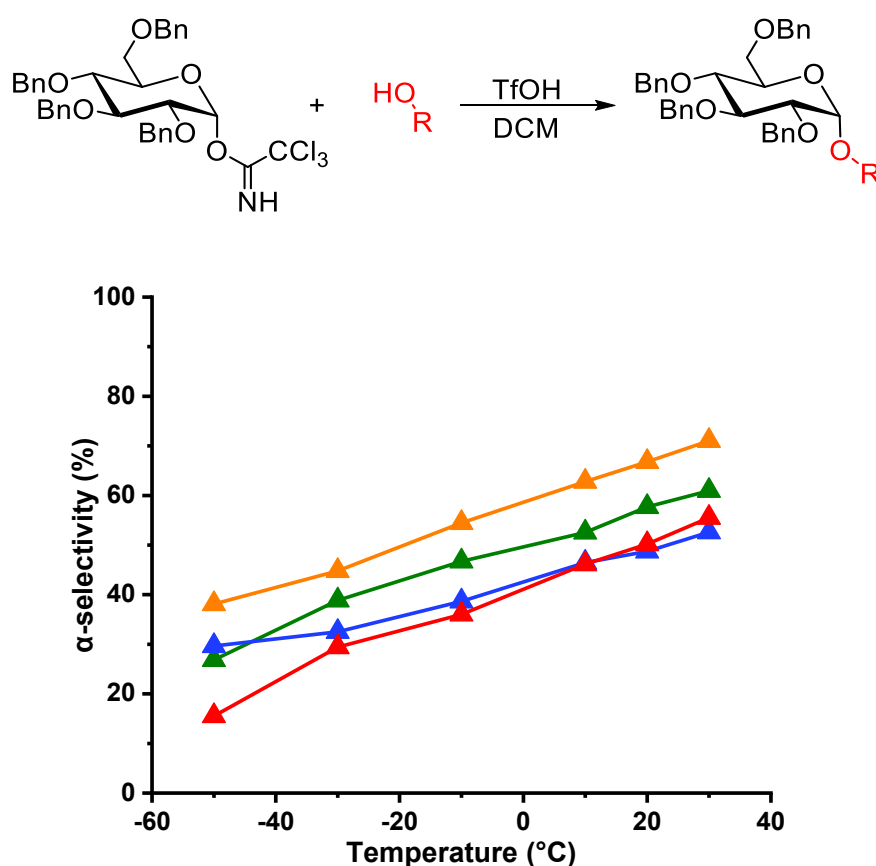


Figure 3.7: Comparison of different acceptors with perbenzylated glucosyl trichloroacetimidate. For full experimental details, see entries 1-18, 35-40 of Table 6.1 in *Chapter 6*. Figure code: Glucose (▲); MeOH (blue); EtOH (red); *i*PrOH (green); *t*BuOH (orange).

The acceptors tested exhibit less α -selectivity with galactose when compared to glucose, as was observed with isopropanol (Figure 3.8). While the α -selectivity increases in the EtOH to *t*BuOH series (4.8% and 4.2%), the temperature sensitivity is not as constant as it is in the glucose series. With increasing sterics of the acceptor, the rate of change of α -selectivity with respect to temperature declines, from +0.51% $\alpha/^\circ\text{C}$ (EtOH) to +0.4% $\alpha/^\circ\text{C}$ (*i*PrOH) to +0.27% $\alpha/^\circ\text{C}$ (*t*BuOH). Compared to the glucosyl donor with MeOH coupling, the coupling of galactosyl donor and MeOH is more temperature sensitive than the rest of the series, with the α -selectivity ranging from 14% at -50°C to 59% at 30°C ($T_{\text{sens}} = +0.56\%$ $\alpha/^\circ\text{C}$).

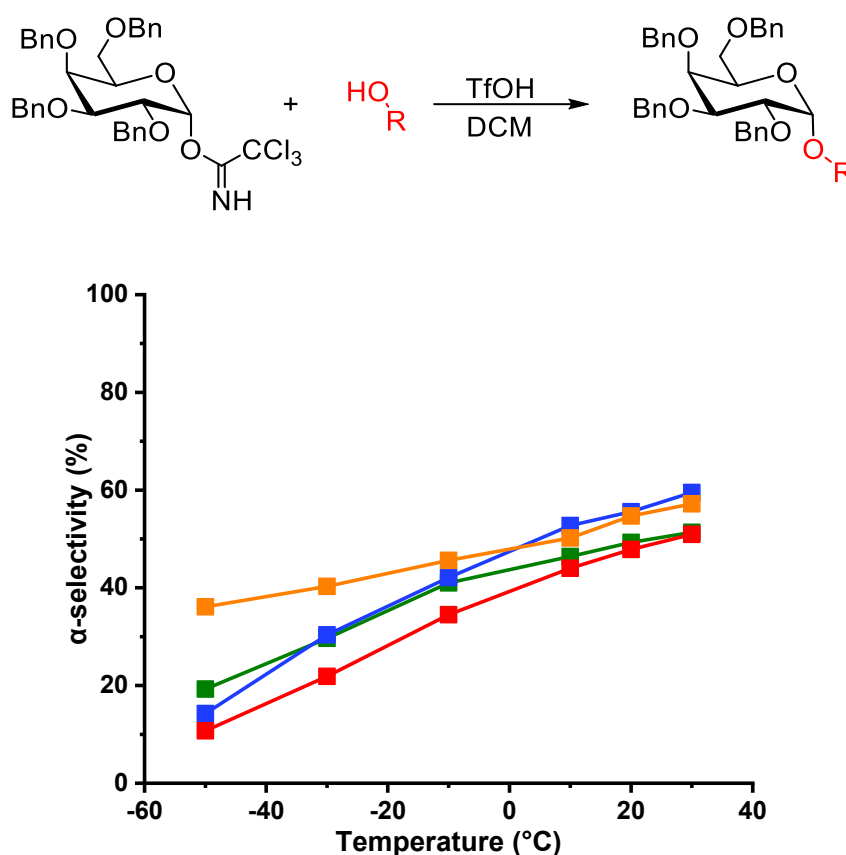


Figure 3.8: Comparison of different acceptors with perbenzylated galactosyl trichloroacetimidate. For full experimental details, see entries 136-141, 143-160 of Table 6.1 in *Chapter 6*. Figure code: Galactose (■); MeOH (blue); EtOH (red); *i*PrOH (green); *t*BuOH (orange).

The coupling of mannose with *i*PrOH was much less temperature sensitive than for glucose and galactose (Figure 3.9). The stereoselectivity of mannose couplings is also much less sensitive to substitution of the acceptor. Methanol, ethanol, and isopropanol all behave similarly with average selectivities ranging from around 50% α at -50°C to 63% at 30°C (average $T_{\text{sens}} = +0.17\%$ $\alpha/^\circ\text{C}$) and only with the increased sterics of *t*BuOH was deviation

was observed. *tert*-butanol essentially behaves similar to the other acceptors below 10 °C, with a stepwise increase of ~5% in α -selectivity, however, above 10 °C, a rapid change is observed, reaching 95% selectivity for the α -product at 30 °C.

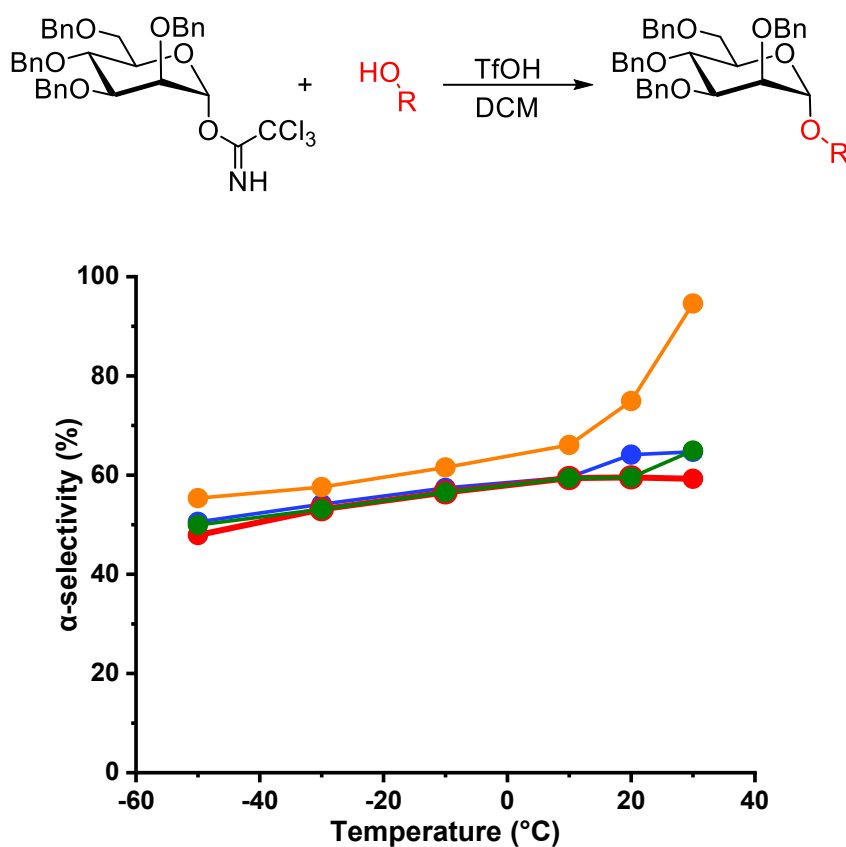


Figure 3.9: Comparison of different acceptors with perbenzylated mannose trichloroacetimidate. For full experimental details, see entries 220-243 of Table 6.1 in *Chapter 6*. Figure code: Mannose (●); MeOH (blue); EtOH (red); *i*PrOH (green); *t*BuOH (orange).

The electronics of the acceptor can be further tuned by insertion of electron withdrawing fluorines onto the β -carbon of nucleophiles (Figure 3.10).⁷⁴ The significant reduction of acceptor nucleophilicity has a pronounced effect on the stereoselectivity, favoring the formation of the α -product (Figure 3.11).

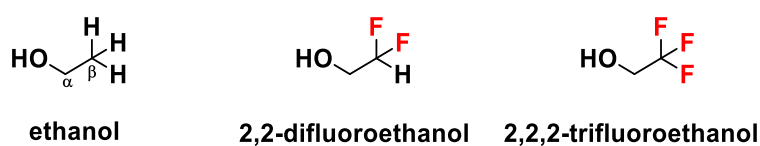


Figure 3.10: The nucleophiles lists to investigate electronics effect with similar sterics by inserting fluorines on β -carbon.

This influence on the stereochemical outcome was also systematically investigated with respect to temperature, by coupling galactose with 2,2-difluoroethanol. It was seen that there was significant drop of temperature sensitivity compared to ethanol ($T_{\text{sens}} = +0.15$ vs $+0.51\%$ $\alpha/^{\circ}\text{C}$) and more α -product is formed overall, ranging from 48% -50°C to 59% at 30°C . In the case of mannosylation, complete α -selectivity was shown when coupled with 2,2,2-trifluoroethanol from 50°C to 30°C (Figure 3.11).

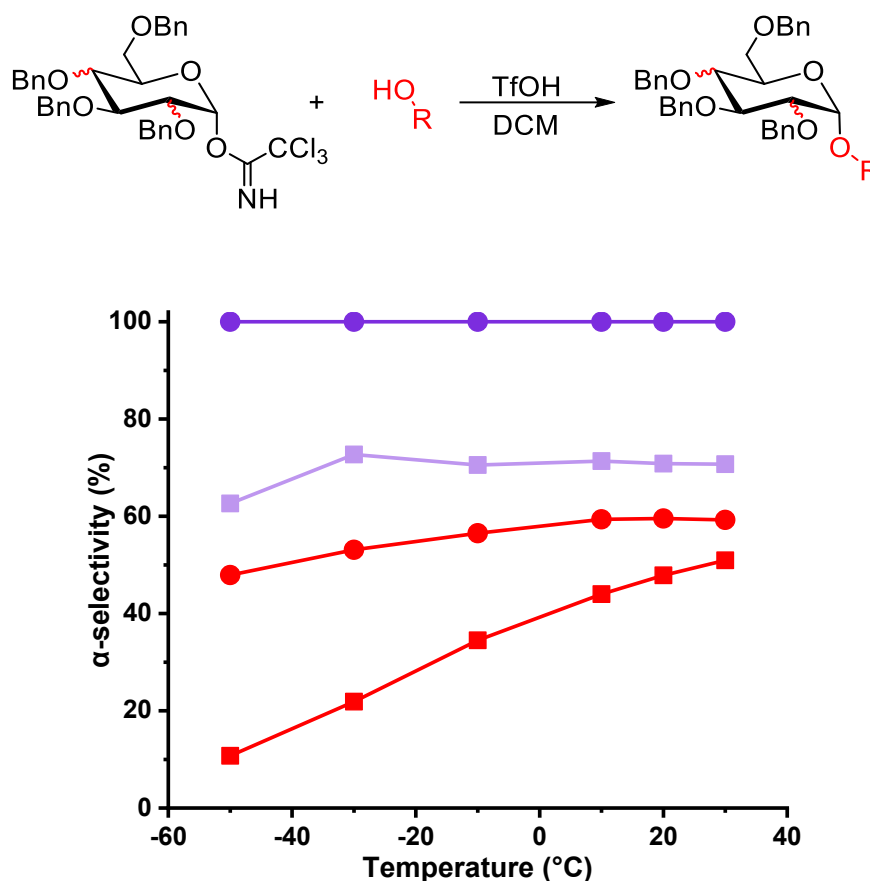


Figure 3.11: Comparison of different acceptors with glucosyl and mannosyl trichloroacetimidate. For full experimental details, see entries 143-148, 166-171, 226-231, 291-296 of Table 6.1 in *Chapter 6*. Figure code: Galactose (■); Mannose (●); EtOH (red); $\text{CF}_2\text{HCH}_2\text{OH}$ (light purple); $\text{CF}_3\text{CH}_2\text{OH}$ (dark purple).

3.3.2.2 Acceptor Sterics and Electronics Implication

The stereoselectivity of glycosylation reaction is a coupled problem, with respect to the individual influence of both the glycosyl donor and acceptor. For donors such as glucose and galactose, changes in acceptor nucleophilicity have a pronounced effect on the observed stereoselectivity, with stronger nucleophiles favoring the β -product at low temperatures and exhibit strong temperature sensitivity (Figures 3.7 and 3.8). The stereoselectivity of mannose couplings is dominated by the influence of the C2 position, favoring α -product formation, which overrides the subtle differences in the nucleophile (Figure 3.9). Only

major changes in nucleophilicity and sterics result in significant modifications to stereoselectivity of mannose couplings. With a large decrease in the nucleophilicity ($\text{CF}_3\text{CH}_2\text{OH}$ vs $\text{CH}_3\text{CH}_2\text{OH}$), the inherent favorability of mannose (α -formation), coupled with that of the low-nucleophilic acceptor, results exclusively in the α -product (Figure 3.11).

3.4 Environmental Factors influencing glycosylation

The environment under which the reaction is run has a profound influence on the stereoselectivity of glycosylation reactions, with the ability to enhance, diminish, or even override the intrinsic selectivities of a given donor/acceptor pair. Five factors were observed to strongly influence the reaction: temperature, stoichiometry, choice of activator, presence of water, and the choice of solvent. The other factors such as residence time, activator equivalents and donor concentration have only a minor influence.

3.4.1 Temperature

Temperature has a profound effect on the stereoselectivity of the glycosylation reaction. Systematic interrogation of stereochemical outcome with respect to temperature shows that in general, lower temperatures favor the formation of β -product. This is presumably (due to an increased proportion of $\text{S}_{\text{N}}2$ -like pathways from activated donors, such as intermediates like α -triflates. The temperature influence can be overridden when the $\text{S}_{\text{N}}1$ pathway becomes dominant. Similarly, at higher temperatures the more thermodynamically stable α -product is formed. Hence the degree of variance observed in the stereoselectivity of a glycosylation as a function of temperature¹⁶ emphasizes the need for precise temperature control. Temperature variation provides the most straightforward means of manipulating and control the stereoselectivity.

3.4.2 Stoichiometry

The stereochemical outcome and temperature sensitivity depends on the reagent stoichiometry for couplings involving S_N2-like mechanisms. Normally, the donor is used in excess in glycosylations⁸⁹ to obtain high yields. However, the addition of more equivalents of acceptor can influence both yield and selectivity.⁷⁹⁻⁸⁰ The effect of acceptor stoichiometry on stereoselectivity was investigated by reacting the perbenzylated galactosyl trichloroacetimidate with the poorly nucleophilic 2,2-difluoroethanol. With only one equivalent of acceptor, the process is temperature independent, favoring α -formation (~73%). At a higher temperature (30 °C), little change is observed when five or ten equivalents of acceptor are added. However, at -50 °C, increased amounts of acceptor results in decreases in α -product selectivity (62%, 58% and 50%, with one, five, and ten equivalents, respectively, Figure 3.12).

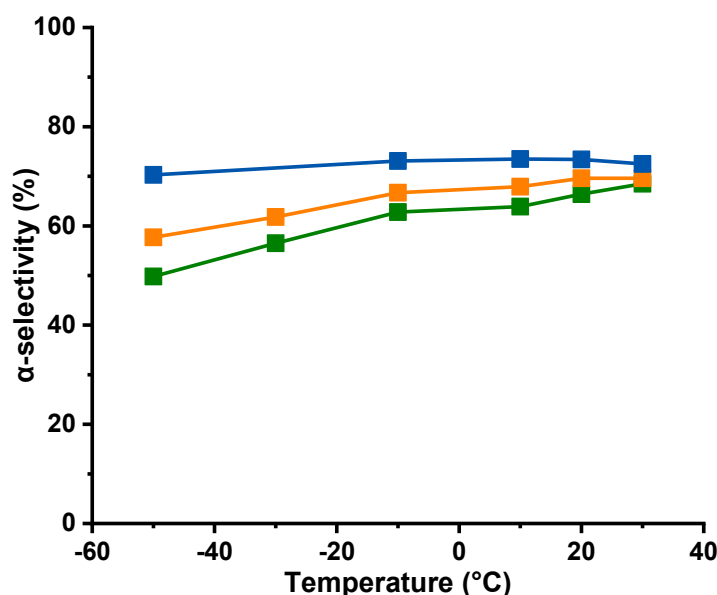
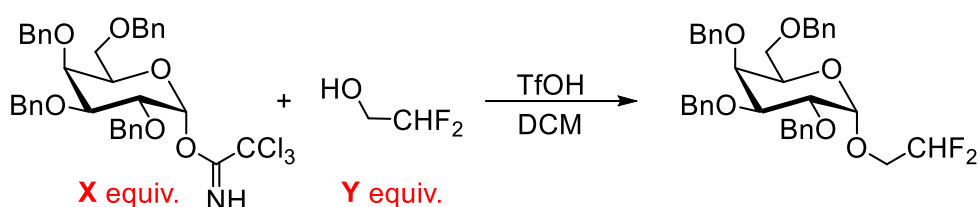


Figure 3.12: Comparison of acceptor stoichiometry in the reaction of galactosyl trichloroacetimidate with 2,2-difluoroethanol in DCM. For full experimental details, see entries 201-219 of Table 6.1 in *Chapter 6*. Figure code: Galactose (■); X:Y = 1:1 (blue); X:Y = 1:5 (orange); X:Y = 1:10 (green).

It can be inferred that for donors such as glucose and galactose that favor the S_N2 pathway, the formation of β -product can be enhanced by increasing the equivalents of the acceptor. A substantial increase in β -selectivity is seen even for poor nucleophiles, and even larger differences can be expected for stronger nucleophiles: a 26% increase in the β -selectivity is observed when ten equivalents of methanol were reacted with galactosyl trichloroacetimidate at 30 °C as compared to the 0.8 equivalents used in our standard experiments (Entries 141-142 of Table 6.1 in *Chapter 6*). However, this effect is not completely transferable to other glycosylations such as mannosylations. The perbenzylated mannosyl donor exhibited negligible difference with one and five equivalents of isopropanol in toluene across the -50 ~ 70 °C temperature range (Figure 3.13).

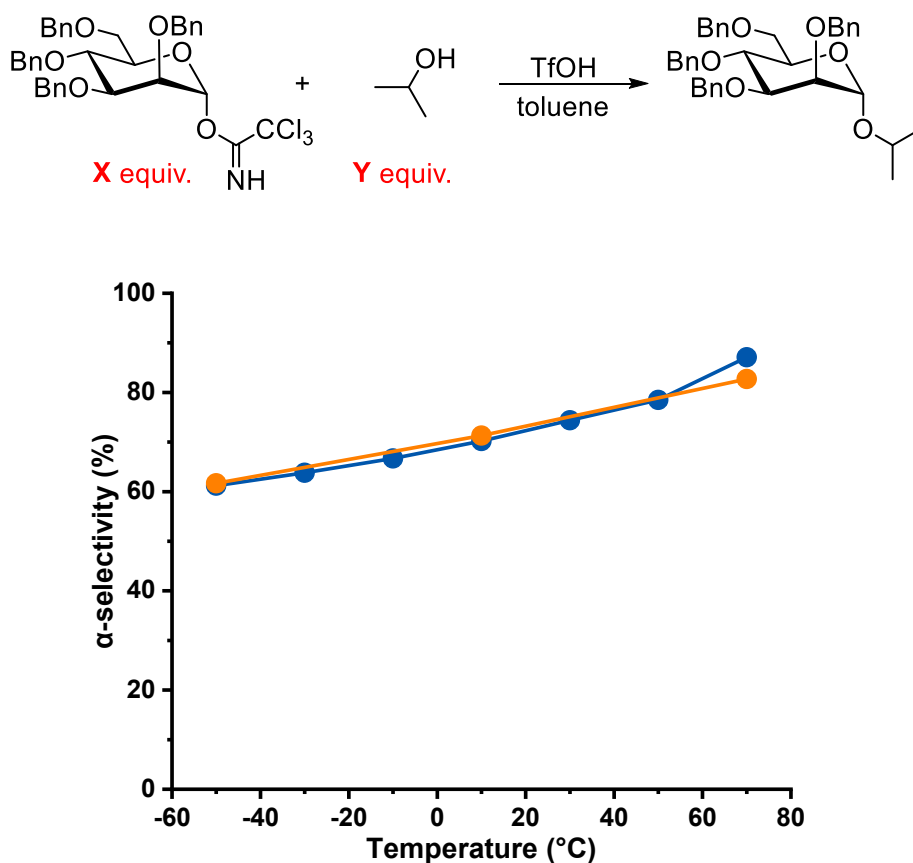


Figure 3.13: Comparison of acceptor stoichiometry in the reaction of mannosyl trichloroacetimidate with iPrOH in toluene. For full experimental details, see entries 271-277, 310-312 of Table 6.1 in *Chapter 6*. Figure code: Mannose (•); X:Y = 1.2:1 (blue); X:Y = 1:5 (orange);

3.4.3 Activator

The nature of the activator influences glycosylations in multiple ways, from the native species activating the leaving group to the conjugate base stabilizing charged intermediates. The conjugate base is able to trap these intermediates by reversible covalent bond formation, called a contact ion pair (CIP). This CIP intermediate is in equilibrium with solvent-separated ion pair (SSIP) and that equilibrium changed by properties of the activators (Figure 3.14).

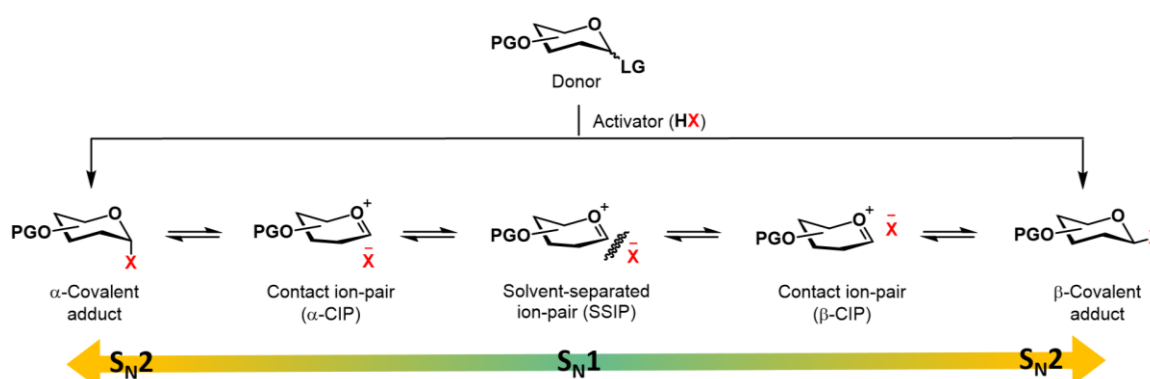


Figure 3.14: Mechanisms to explain effect on the stereochemistry of intermediates by influence of the activator.

To investigate the influence the activator exerts on stereoselectivity,⁹⁰⁻⁹² a range of activators (Tf_2NH , TfOH , MsOH and FSO_3H), were screened with perbenzylated mannose donor using *t*BuOH as model acceptor in DCM. When fluorosulfuric acid (green) or methanesulfuric acid (orange) were used as the activators, ~3:2 ratios of α : β anomers were maintained and a loss in temperature sensitivity is observed at higher temperatures (Figure 3.15). On the other hand, when the less electron-rich triflimide (Tf_2NH) is used, a significant change is observed. The behavior below -10°C was similar to triflic acid, fluorosulfuric acid, and methanesulfuric acid, however, sensitivity of α -selectivity as a function of temperature, exponentially increases and ratio of products approaches near complete α -selectivity above $+10^\circ\text{C}$.

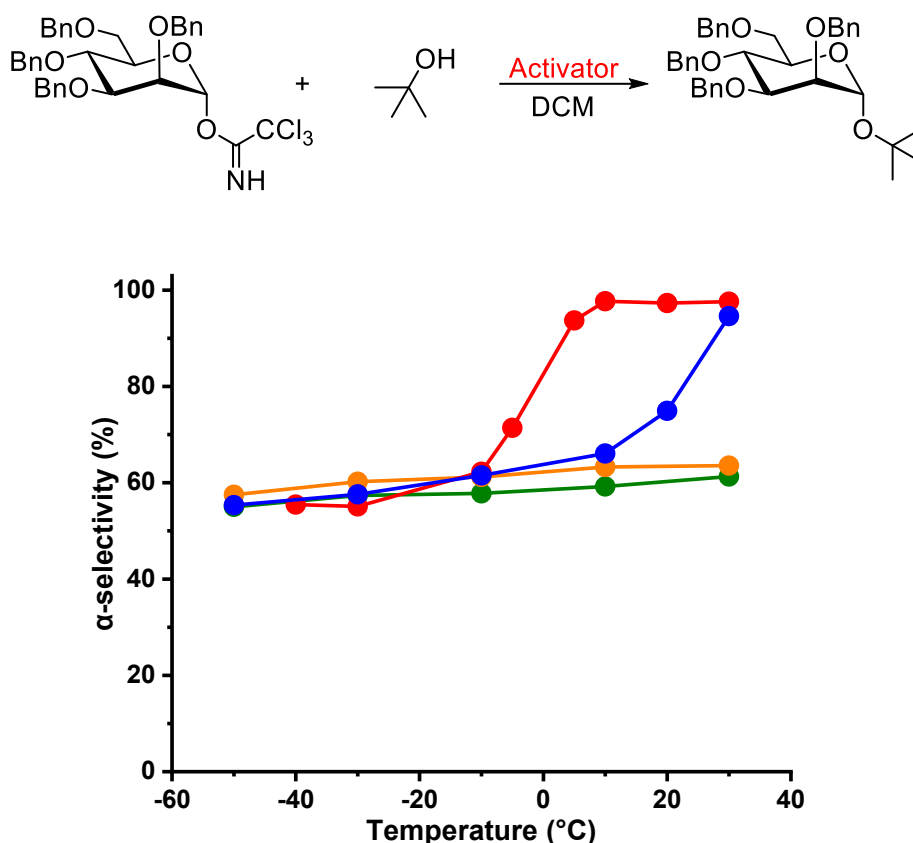


Figure 3.15: Comparison of different activators on the coupling of mannosyl trichloroacetimidates with *t*BuOH. For full experimental details, see entries 238-261 of Table 6.1 in *Chapter 6*. Figure code: Mannose (●); Tf₂NH (red); TfOH (blue); MsOH (orange); FSO₃H (green).

The influence of the acceptor was also investigated using a glucosyl donor, examining the unique influence of Tf₂NH activation on stereochemical outcome under the same reaction conditions. In the case of TfOH, poor selectivity was observed ranging from 40% α -product at -50 °C to 60% at 30 °C when glucosyl donor and *t*BuOH were used as coupling partners in DCM. Interestingly, when the activator is changed to Tf₂NH, α -product formation was suppressed and the reaction exhibited more β -selectivity (95%) at -50 °C and, moreover, sensitivity by temperature was about 1.5 times more than TfOH (Figure 3.16). By changing the conjugate base of the activator, the inherent stereoselective preference of the donor can be enhanced. Thus, when Tf₂NH is used instead of TfOH, the mannose donor prefers to form α -product and this behavior is strengthened as temperature increased. However, for glucose, the opposite trend is shown by favoring β -product formation at lower temperature.

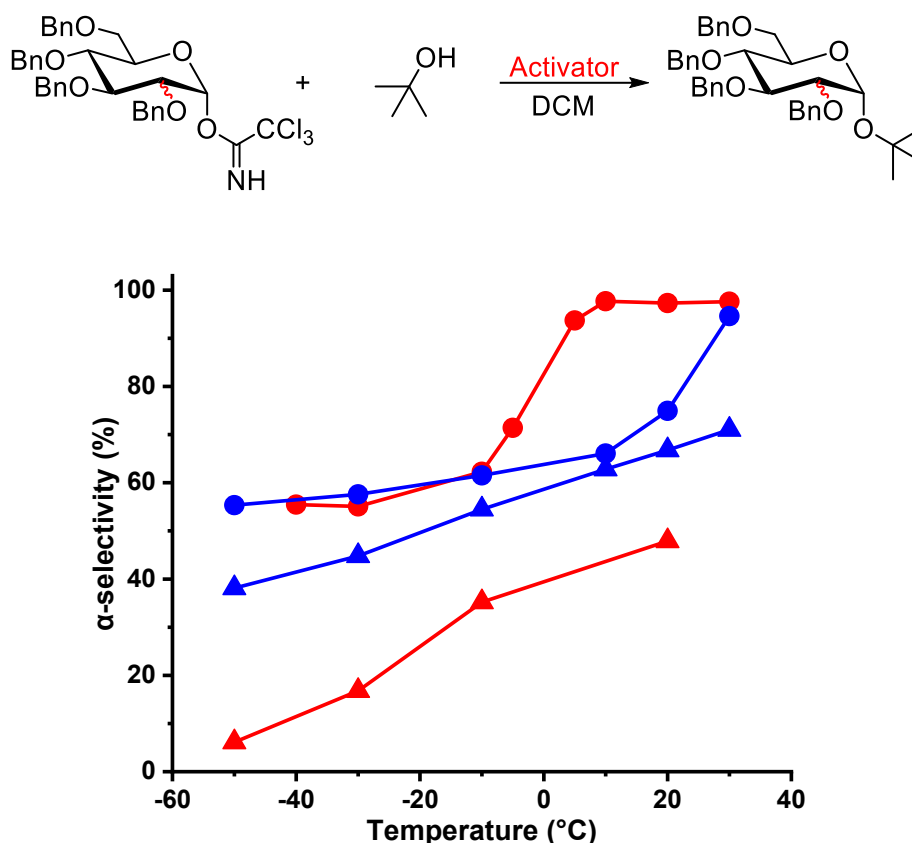


Figure 3.16: Tf_2NH enhances the inherent stereoselective favorabilities of donors. For full experimental details, see entries 35-40, 45-48, 238-243, 254-261 of Table 6.1 in *Chapter 6*. Figure code: Glucose (\blacktriangle); Mannose (\bullet); Tf_2NH (red); TfOH (blue).

3.4.4 Water content

The removal of residual water from glycosylating agents is an important procedure because water can act as a potential nucleophile and is detrimental to activation and yield of glycosylations. In this thesis, all glycosylating agents were azeotroped with toluene and all nucleophiles and solvents were dried to less than 3 ppm water content to avoid this unproductive pathway. The detailed methodology of drying of solvents is given in *Section 6.4 of Chapter 6*.

In addition to reduced glycosylation yields, it was discovered in the course of my work that the presence of substoichiometric amounts of water in the reaction can affect the stereoselectivity of the glycosylations. Under the standard “anhydrous” conditions, the mannosylation with *t*BuOH exhibits low temperature sensitivity until 10 $^{\circ}\text{C}$. Nevertheless, a rapid change is observed until almost complete α -selectivity is achieved at 30 $^{\circ}\text{C}$ (Figure 3.17). However, after the addition of 0.25 equivalents of water to the solvent, a complete loss of temperature sensitivity is observed. Unexpectedly, no difference on stereoselectivity

was observed in glucosylation with *i*PrOH under “anhydrous” conditions or in the presence of 0.25 equivalents of water (Figure 3.17). The yields for the two respective coupling conditions for mannose and glucose couplings were similar.

Large amounts of water present in the glycosylation medium can result in the competitive trapping of intermediates to form hydrolyzed donor, which is an irreversible reaction. However, 0.25 equivalents of water changes the reaction pathway without significant increase in byproduct formation. As such, mannosylation with *t*BuOH in DCM, is affected by small amounts of water in the medium, which reduces the α -selectivity from a complete α -selective pathway.

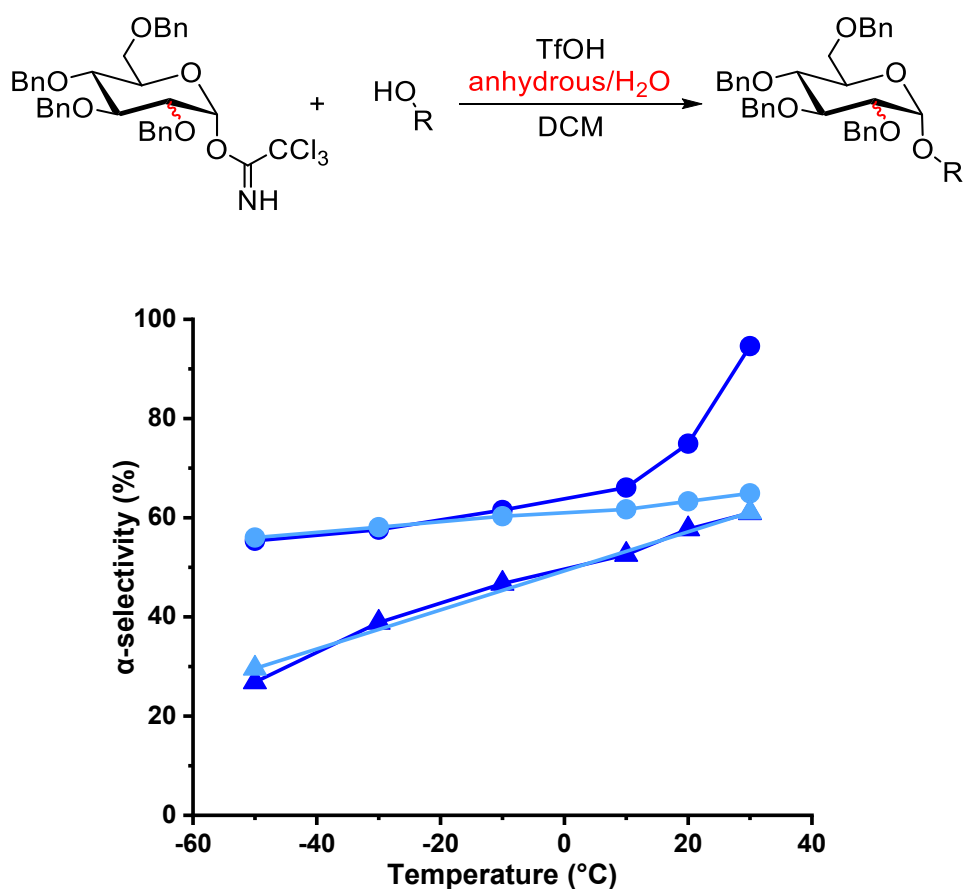


Figure 3.17: Comparison of stereoselectivities of glucosyl trichloroacetimidate with *i*PrOH and mannosyl trichloroacetimidate with *t*BuOH under “anhydrous” conditions and in the presence of substoichiometric amounts of water. For full experimental details, see entries 13-18, 107-108, 238-243, 303-308 of Table 6.1 in Chapter 6. Figure code: Glucose (▲); Mannose (●); DCM (blue); DCM + 0.25 equiv. H₂O (light blue).

3.4.5 Solvent

Solvent greatly influences the stereoselectivity⁹³ of glycosylation reactions. The influence of solvent ranges from stabilization of intermediates by coordination or by changing conformation and distribution of ion pairs.⁹⁴ The study of solvent effects reported in the literature reveals that α -linkages can be formed preferentially by coordinating ether solvents from the β side of the glycosyl donor, whereas, β -linkages are formed in acetonitrile due to the “nitrile effect” type coordination from α side (Figure 3.18).^{92, 94}

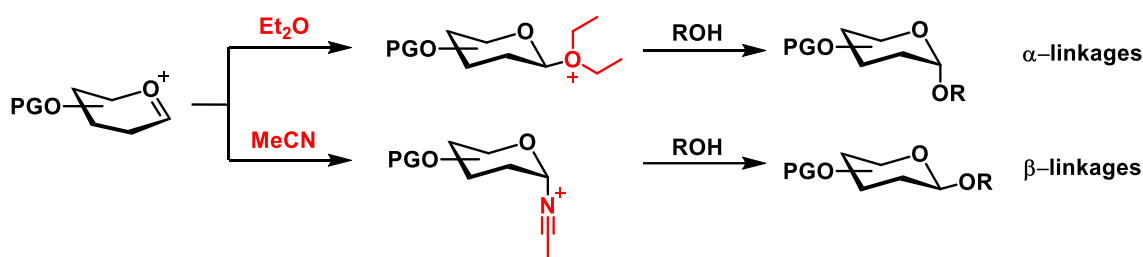


Figure 3.18: Solvent effect on glycosylation via different direction of coordination.

In order to systematically study the influence of solvents and how they can enhance, suppress, or override various factors influencing glycosylation stereoselectivity, model glycosylations were performed with glucose, galactose and mannose glycosyl donors in four solvents: dichloromethane (DCM), acetonitrile (ACN), toluene, and methyl *tert*-butyl ether (MTBE). Studies involving the effect of donor, acceptor, and activator on stereoselectivities reported in the previous sections of this chapter were conducted in DCM. Therefore, the results from the present solvent study were compared to DCM.

3.4.5.1 Solvent effect for glucose donor

Similar to the methodology followed in the earlier sections in this chapter, glucose trichloroimidate donor was coupled with isopropanol as a model acceptor using TfOH as activator. The stereoselectivities across the accessible temperature ranges in the four solvents is shown in Figure 3.19 and the following analysis compares each solvent to the results obtained in DCM. A significant increase in the formation of β -product is observed in acetonitrile, ranging from 10% α at -30 °C to 42% α at 70 °C. The temperature sensitivity of glucosylation is dampened in acetonitrile. On the contrary, toluene exhibits a stronger impact of temperature on stereoselectivity compared to DCM (19% \rightarrow 62% vs 27% \rightarrow 61%)

within the temperature range from -50 °C to 10 °C. Nevertheless, the gradual saturation of alpha selectivity from 10 °C to 70 °C in toluene can be due to two distinct mechanistic pathways appear to be occurring above and below 10 °C. In toluene, S_N2-like pathways are favored at lower temperatures whereas S_N1-like at higher temperatures. The solvent exhibiting the smallest influence of temperature on stereoselectivity was MTBE, where it was seen to be almost constant. It can be inferred here that MTBE is known as ester type solvent and has broad temperature scope when compared to diethyl ether, favoring α -product formation (85% α at -50 °C \rightarrow 82% α at +50 °C). It can be concluded here that by altering four different solvents, α -selectivity can be controlled between 10% and 90% at specific temperatures for the coupling of perbenzylated glucose donor and isopropanol using TfOH as activator.

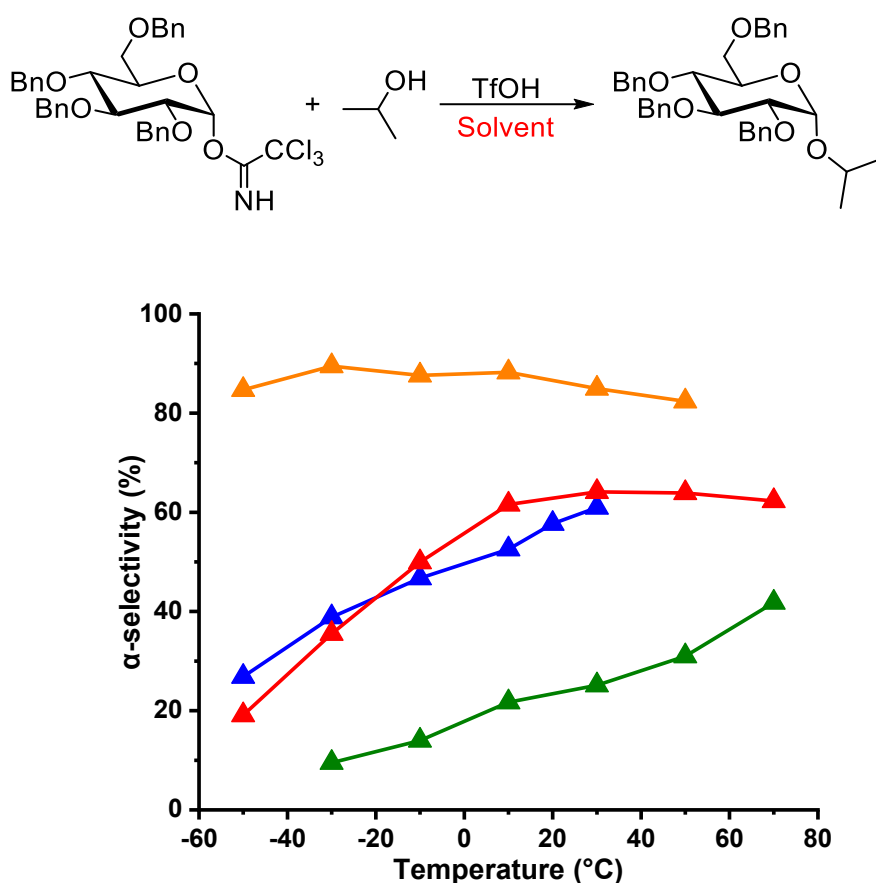


Figure 3.19: Comparison of four different solvents for the coupling of glucosyl trichloroacetimidate with *i*PrOH using TfOH as activator. For full experimental details, see entries 13-18, 61-67, 89-100 of Table 6.1 in Chapter 6. Figure code: Glucose (▲); DCM (blue); Toluene (red); ACN (green); MTBE (orange).

3.4.5.2 Solvent effect for galactose donor

The same methodology was followed to investigate the effect of solvent for a galactose donor (Figure 3.20). Galactose has the inherent preference for the β -formation due to the presence of the axial C4-O-benzyl ether. Similar to the nitrile effect observed with glucose donor, acetonitrile gives higher β -selectivities with decreased temperature sensitivities than seen for galactose in DCM (16% α \rightarrow 29% α vs 30% α \rightarrow 51% α , over a temperature range of -30 °C to 30 °C). In contrast to glucosylation in toluene, galactosylation shows a selectivity plateau above 50 °C, giving a broad range of selectivities, from 10% α at -50 °C to 69% α at 70 °C. While the formation of the α -product is increased in MTBE, and galactosylation exhibits higher temperature sensitivity compared to glucosylation in MTBE. The α -selectivity scope varies from 10% α to 78% α for the coupling between perbenzylated galactose donor and isopropanol using TfOH as activator.

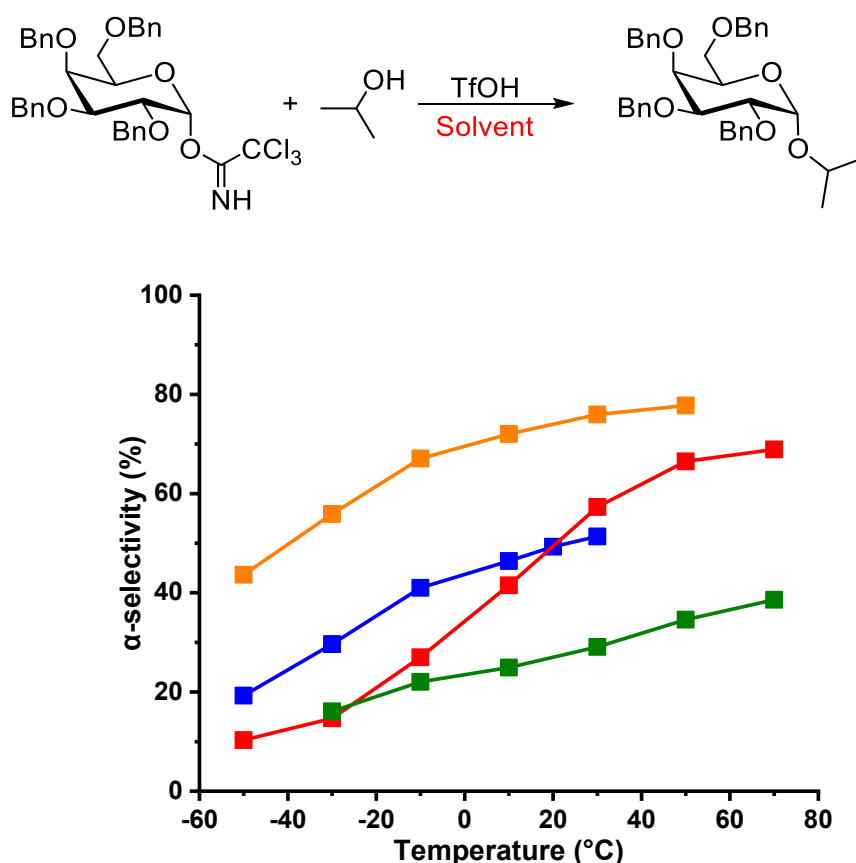


Figure 3.20: Comparison of four different solvents for the coupling of galactosyl trichloroacetimidate with i PrOH using TfOH as activator. For full experimental details, see entries 149-154, 172-190 of Table 6.1 in Chapter 6. Figure code: Galactose (■); DCM (blue); Toluene (red); ACN (green); MTBE (orange).

3.4.5.3 Solvent effect for mannose donor

Compared to glucose and galactose, mannose strongly prefers α -product formation due to the axial C2-O-benzyl ether, and this effect is present for all solvents. Unlike glucosylation and galactosylation, near stepwise increase in α -product selectivity by 10% are seen in the DCM/toluene/MTBE progression, with low temperature sensitivities in these three solvents. However, in the case of acetonitrile, it enhanced the inherent preference of the mannose donor, similar to what is observed for mannosylation with *t*BuOH using Tf₂NH in DCM. At lower temperatures, the selectivity is constant at 65% α -product. Above 10 °C, a rapid increase in temperature sensitivity (+1.1% α /°C) is observed as compared to the low temperature data, reaching near complete α -selectivity above 30 °C. The α -selectivity scope varies from 50% α to 98% α for the coupling between perbenzylated mannose donor and isopropanol using TfOH as activator (Figure 3.21).

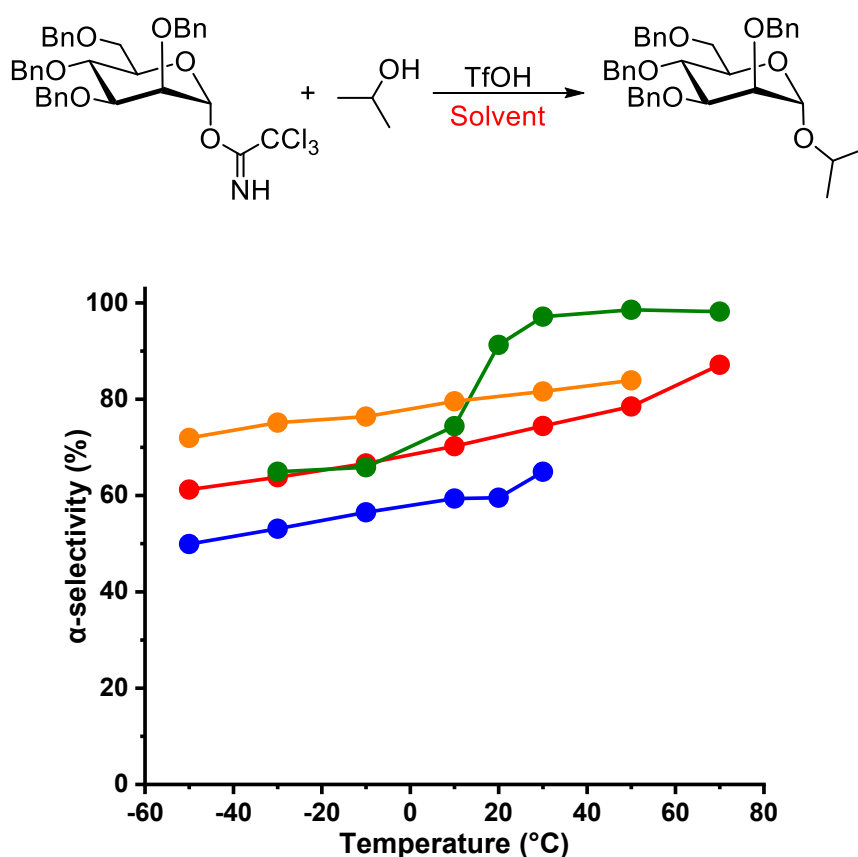


Figure 3.21: Comparison of four different solvents for the coupling of mannosyl trichloroacetimidate with *i*PrOH using TfOH as activator. For full experimental details, see entries 232-237, 271-290 of Table 6.1 in Chapter 6. Figure code: Mannose (●); DCM (blue); Toluene (red); ACN (green); MTBE (orange).

The solvent has different effects on the resulting α/β -selectivity with each glycosylating donor – glucose, galactose, and mannose. Acetonitrile enhances the inherent donor preferences, providing higher proportions of the β -product for glucose/galactose and α -product for mannose – similar to the reaction using $\text{ Tf}_2\text{NH}$ in DCM. Toluene gives the broadest temperature scope and establishes strong temperature sensitivity especially to glucose and galactose. Methyl *tert*-butyl ether enhances the α -formation for all donors. Glucose is particularly susceptible; Mannose is resistant to influence by solvents, but does exhibit increased proportions of the α -diastereomer in MTBE. The overall trend – glucose > galactose > mannose in α -selectivity – was shown in the solvents study.

3.5 Discussion

The various factors influencing the stereoselectivity of glycosylations is difficult to identify and decouple. In addition, irreproducible results due to the sensitivity of glycosylations to environmental factors has compounded the problem. While some aspects of glycosylations have been studied in great depth, the interrelationship of these factors and their degree of influence has remained unclear. In this thesis, utilizing a microreactor-based automated flow platform, model glycosylation reactions were performed to systematically and reproducibly interrogate several of these factors. My research generated the most complete picture to date of what these influencing factors are, what their effect is, and how they directly compare to one another, including how the degrees of influence of these factors rank with respect to one another (Figure 3.22). The most important take home message this work revealed that the donor and acceptor coupling partners possess inherent preferences for the formation of either the α/β -stereoisomer, and that these preferences can be enhanced, diminished, or overridden by environmental variables. The most important of the variables, dictated by coupling partners, is the stereochemistry of the C2 position of the donor, acting as a mechanistic divergent point in the coupling.

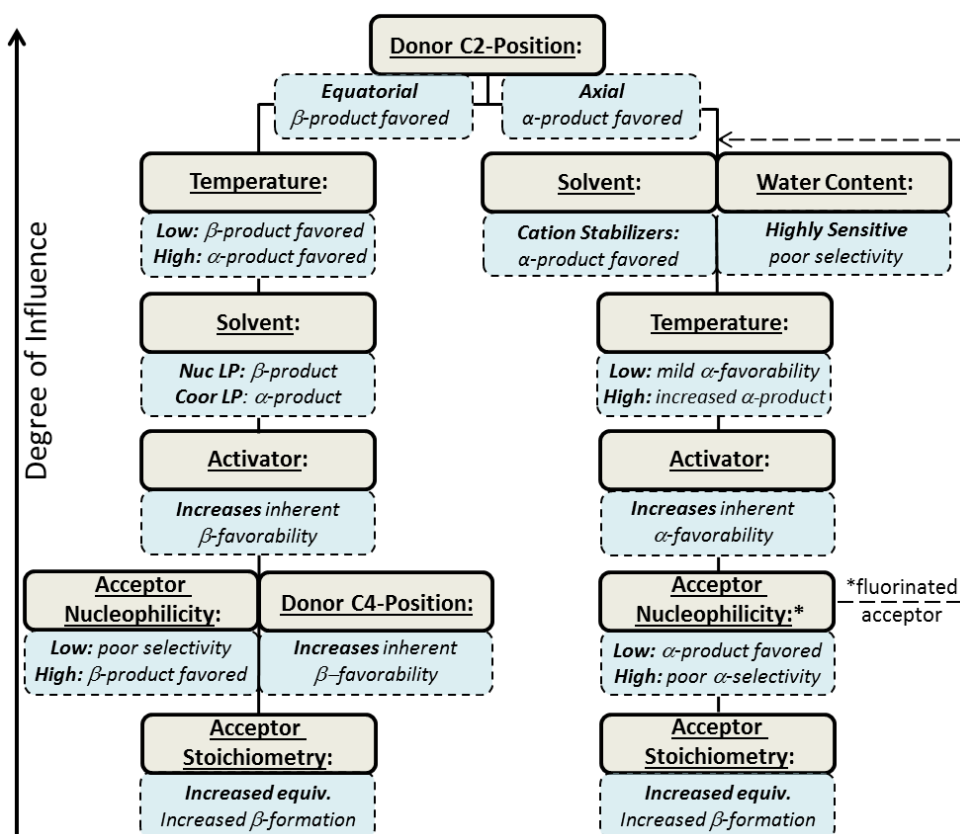


Figure 3.22: Degree of influence of environmental variables and permanent factors on the stereoselectivity of glycosylation.

Mannose, bearing a C2 axial ether, has a *strong* inherent preference for the formation of the α -product. Glucose and galactose donors both have equatorial, C2-ether, and form the β -anomer preferentially. Nevertheless, this β -selectivity has more sensitivity towards environmental variables and can be easily controlled and influenced, in contrast to couplings of mannose. The β -selectivity preference observed for glucosylation and galactosylation can be easily controlled by the temperature, giving β -product at lower temperatures. At higher temperature, it shows a weak preference for alpha. The second most important factor to control the stereochemical outcome is solvent. Solvents having non-halogen lone pair electrons influences the stereoselectivity and with acetonitrile, β -selectivity is increased for gluco- and galactosylation. Similarly, α -selectivity is increased by using coordinating solvents such as MTBE.

The activator also influences and enhances the β -product formation for gluco- and galactosylation, which is the inherent selectivity preference of the donor. When the C4 ether position is axial as is in the case of galactose, β -selectivity increases moderately. The result is comparable to the stepwise increase in the acceptor's nucleophilicity. A further systematic decrease of the nucleophilicity of acceptor nucleophiles, such as fluorinated alcohols, the α -

stereoisomer is weakly favored. Additionally, with increased equivalents of acceptor, the selectivity towards β -product increases for both gluco- and galactosylations. In addition, the branch representing the glucose/galactose in the Figure 3.22 is less water sensitive when compared to the branch representing mannosylations.

Though the initial preference for dictating the stereochemical outcome for a typical glycosylation reaction is guided by the choice of the glycosyl partners, judicious choice of environmental conditions can be used to control the final stereochemical outcome significantly. The nature of the intermediates formed during and after the activation of the glycosyl donor plays a huge role in guiding the selectivity of the reaction towards a particular anomer. The nature of these unexplored, formidable intermediates can be controlled both by permanent factors such as choice of donor/acceptor and manipulations of environmental conditions. The reaction can also be made to follow a particular mechanistic pathway (S_N1 -type or S_N2 -type) by the choice and control of environmental variables.

The reproducible systematic interrogation of the influence of various environmental variables on the stereochemical outcome in this work can be used to control the α/β -stereoselectivity for a model glycosylation reaction (Figure 3.23). The glycosylation between benzylated glucosyl α -trichloroacetimidate and isopropanol highlights this stereoselective control. This reaction can be used as a showcase the approach. Near complete stereoselective control was achieved for this glycosylation in DCM using Tf_2NH , 11:1 selectivity favoring the β -diastereomer. Upon facile change of solvent to MTBE and activator to $TfOH$ and precise control of temperature at $-30\text{ }^\circ\text{C}$, the selectivity was completely reversed giving a 9:1 ratio favoring the α -diastereomer.

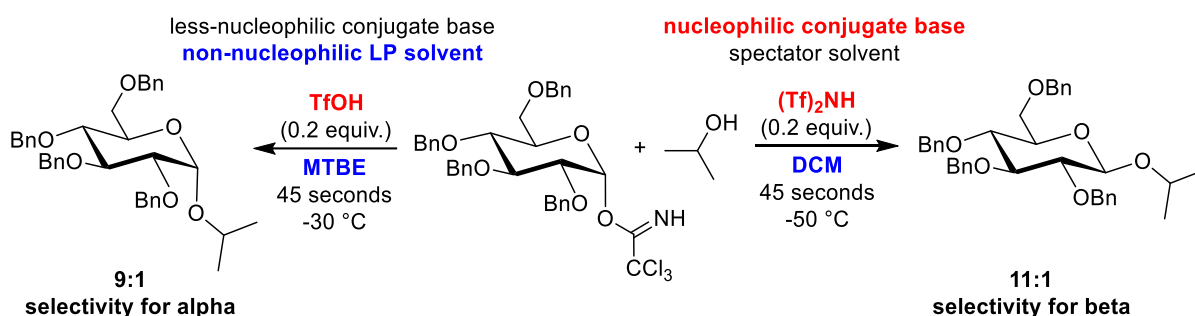


Figure 3.23: Tunable stereoselectivity ratios of a given glycosylation coupling pair based on variation of environmental conditions.

Chapter 4 Machine learning approach to glycosylation

4.1 Introduction

The results described in the previous chapters of this thesis clearly indicate the problems associated with predicting the stereochemical outcome of chemical glycosylations. Controlling and predicting glycosylation stereoselectivity is one of the most challenging problems in organic chemistry due to sheer number of factors dictating the reaction outcome. Therefore, gaining a detailed mechanistic understanding is a formidable challenge. There is a lack of systematic studies of numerous influencing factors affecting glycosylation in the literature. *Chapter 3* details how this thesis addressed these challenges by reporting more than 270 reproducible experiments on a fully automated platform for model glycosylation reaction, intercepting several factors affecting glycosylation such as temperature, reaction stoichiometry, equivalents, influence of donor, acceptor, activator and solvent without human intervention.¹⁴

Machine learning is a powerful tool to analyze large datasets to extract correlations and identify underlying processes and mechanisms behind the data.⁹⁵⁻¹⁰³ With an empirical understanding of glycosylation in hand, along with the data generated in this research, it is a perfect opportunity to apply machine learning algorithms to create a model capable of predicting stereochemical selectivity of the model chemical glycosylation reactions.

However, the majority of machine learning applications in the chemical literature utilize a “classification” rather than “regression” based approach.¹⁰⁴ The former approach uses classification based algorithms to categorize data into various distinct classes. This approach is limited in its ability to predict continuous numeric parameters such as stereoselectivity or yield of a chemical reaction as well as generating plausible mechanistic hypothesis. Recent paper published,⁹⁸ shows good prediction of yield using a regression based approach.

4.2 Numeric quantification of permanent factors

A range of different potential descriptors were obtained using SPARTAN software (Table 4.1) to quantify the molecular property of donor, acceptor, activator and solvent, with density functional theory (DFT) calculations. Descriptors for donor, acceptor, activator and solvent were chosen based on the empirical understanding of the glycosylation mechanism (Figure 3.22 in Chapter 3) gained in this research work (Figure 4.1).

Table 4.1: the potential descriptors.

Donor		Acceptor	Activator	Solvent
Area	HOMO	(O-H) IR Peak	HOMO	Area
C1 Electrostatic charge	LUMO	(O-H) Lowdin Bond Order	LUMO	Dipole Moment
C1 exposed Area	Max EIPot	(O-H) Mulliken Bond Order	Area	HOMO
C1 Mulliken charge	Min EIPot	α C chem shift	Dipole Moment	Log P
C1 Natural charge	O2O3	α C electrostatic charge	Max EIPot	LUMO
C1 Shift	O3O4	α C exposed area	Min EIPot	Max EIPot
Dipole moment	O4C6	α C mulliken charge	O ⁻ /N ⁻ Electrostatic charge	Min EIPot
H1-H2 j	Ovality	α C natural charge	O ⁻ /N ⁻ Mulliken charge	Ovality
H2-H3 j	Polarizability	O chem shift	O ⁻ /N ⁻ Natural charge	Polarizability
H3-H4 j	PSA	O electrostatic charge	O ⁻ /N ⁻ NMR	PSA
H4-H5 j	Volume	O exposed area	O ⁻ /N ⁻ area	Volume
	X1O2	O mulliken charge	Ovality	
		O natural charge	Polarizability	
			PSA	
			Si NMR	
			Volume	

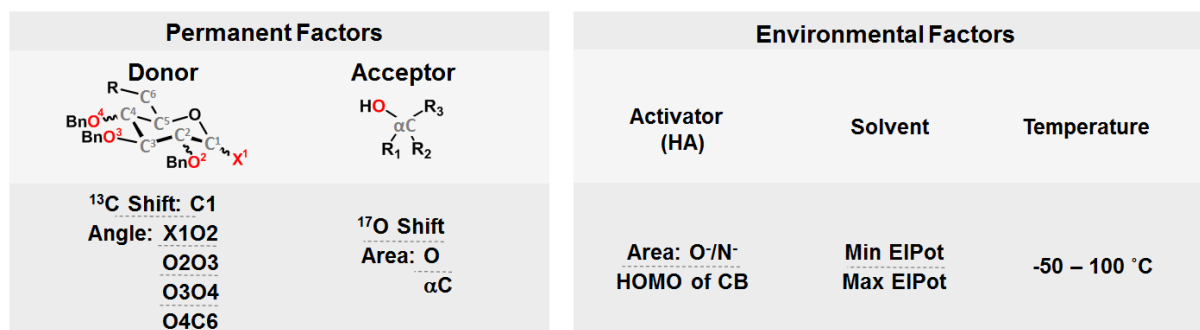


Figure 4.1: The selected descriptors.

4.2.1 Donor

Starting with the coupling partners, it was critical to identify and quantify their reactivity, capturing steric and electronic effects of both the nucleophile and electrophile. Following the screening of potential descriptors for the steric/electronic properties of the donor, five variables were identified (Figure 4.2). Numerical quantification of donor properties consists of the reactivity of the C1 position, which describes the electrophilicity, and the relative orientations of the substituents of the pyran ring, which describes the stereochemistry and sterics (Figure 4.2). With respect to the anomeric position (C1), it has

previously been revealed that the reactivity of the donor could be numerically quantified by using the ^1H NMR chemical shift.¹⁰⁵ Based on this work, we calculated (DFT calculation using basis set B3LYP 6-31G*) the anomeric ^{13}C NMR chemical shift, which is not only correlated to the reactivity of the donor but also allows for differentiation of leaving groups. Previously, three different leaving groups were investigated (trichloroacetimidate ($-\text{OC}(\text{CCl}_3)=\text{NH}$), ethylthioether ($-\text{SEt}$), phosphate ($-\text{OP}(\text{OnBu})_2=\text{O}$ and $-\text{OP}(\text{OPh})_2=\text{O}$). In the case of trichloroacetimidate, an oxygen is bonded to anomeric carbon, resulting in C1 ^{13}C NMR shifts between 98.3–103.0 ppm. The ethylthioether derivatives contain a C-S bond at C1 and exhibit an upfield shift in the NMR (81.4–86.1 ppm).

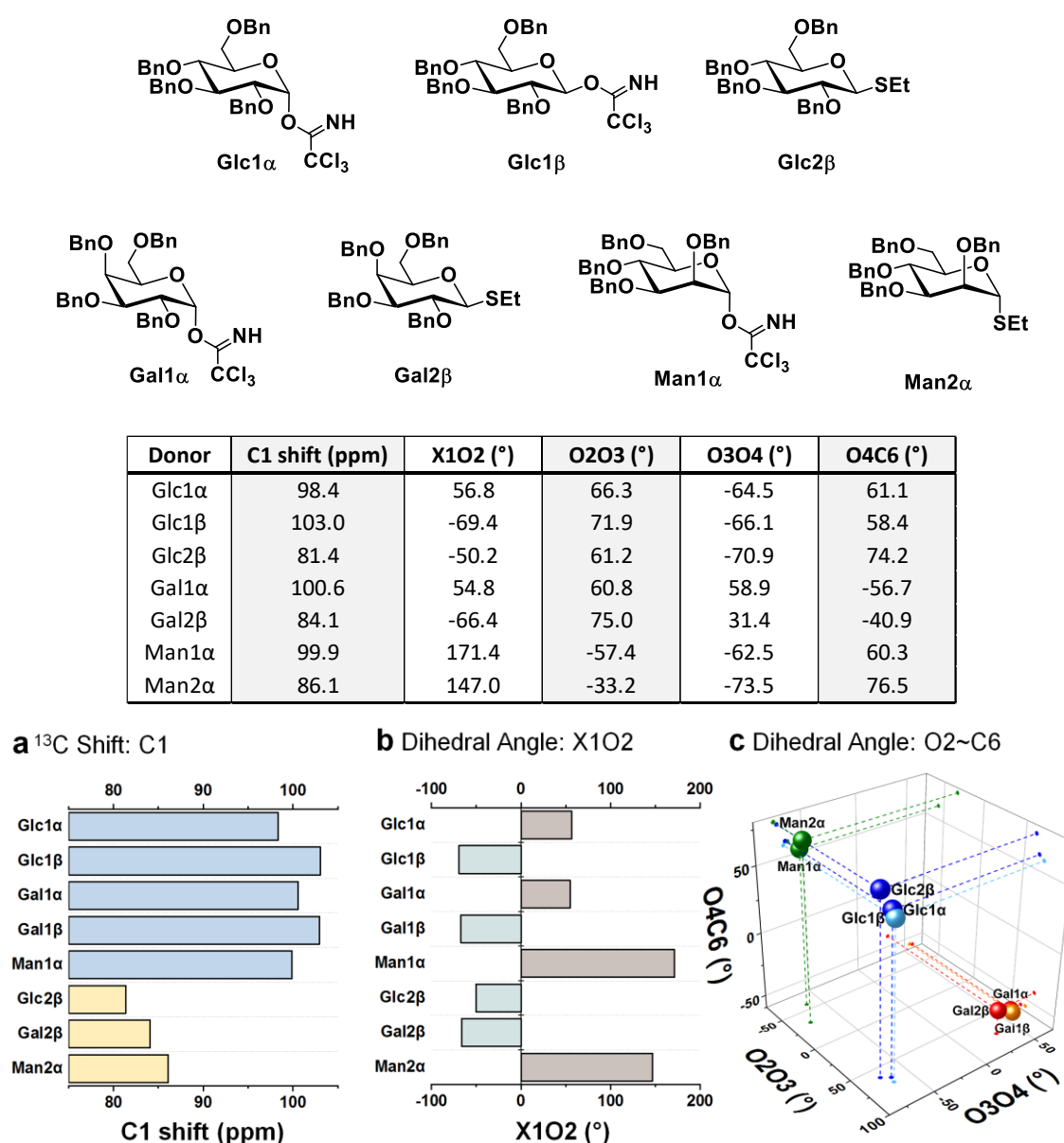


Figure 4.2: **a**, ^{13}C Carbon NMR chemical shift (ppm). **b**, Dihedral angle (°) of X1-C1-C2-O2. **c**, 3D map of donor chemical subspace (X: Dihedral angle (°) of O2-C2-C3-O3, Y: Dihedral angle (°) of O3-C3-C4-O4, Z: Dihedral angle (°) of O4-C4-C5-C6). Basis set: B3LYP 6-31G* level of theory.

To quantify the donor's stereochemical properties, the dihedral angles of substituents at positions C1, C2, C3, C4 of the pyranose ring were considered. First, dihedral angle (X1-C1-C2-O2) between oxygen/sulfur at the anomeric position and the C2 oxygen, providing information about the orientation of both the C2 position as well as the leaving group. Clockwise (+) values for this descriptor indicate that the leaving group is α (Figure 4.3a/c) while counterclockwise (-) is the β orientation (Figure 4.3b). The mannose α -donor is differentiated from the respective glucose and galactose donors with angles ranging from $+147.0$ to $+177.5^\circ$ (Figure 4.3c) as compared to -69.4 – $+60.7^\circ$ (Figure 4.3a/b). Dihedral angles with the respective sugars are given in the table of Figure 4.2.

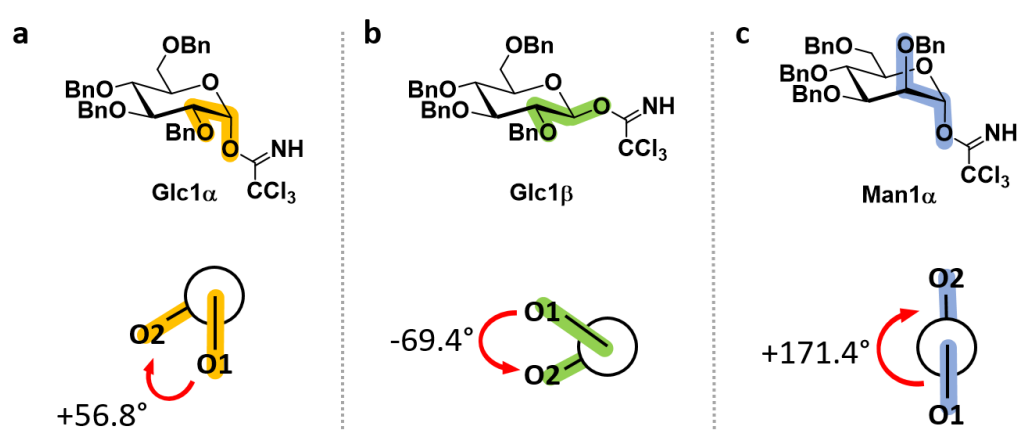


Figure 4.3: Comparison of dihedral angle of O1-C1-C2-O2 for **Glc1 α** , **Glc1 β** and **Man1 α** . For **Gal1 α** , **Gal1 β** , refer to the table of Figure 4.2.

Similarly, the remaining dihedral angles from the C2 to the C5 positions describe the orientation of the rest of the pyran ring. Mannose only has negative values for the O2-C2-C3-O3 dihedral (-33.2 – -60.5°) due to the axial orientation of C2 position, which results in a counterclockwise rotation to the C3 substituent (Figure 4.4c). However, glucose and galactose have positive values ranging from 61.2° to 75.0° due to the equatorial orientation of the C2 group (Figure 4.4a/b). These dihedral angles with the respective sugars are also given in the table of Figure 4.2.

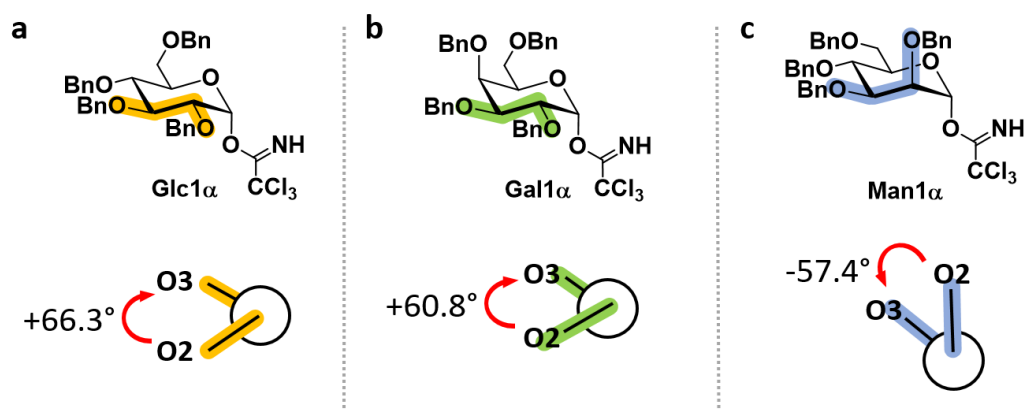


Figure 4.4: Comparison of dihedral angle of O2-C2-C3-O3 for **Glc1 α** , **Gal α** and **Man1 α** . For **Gal1 β** , refer to the table of Figure 4.2.

In the case of galactose, dihedral angle of O4-C4-C5-C6 is and (-) due to the axial O4 substituent on C4 position whereas glucose and mannose donor have (+) value (Figure 4.5). Change of the dihedral angles leads to the changing of the hyperconjugation and “through the space effects”⁵² which can subsequently alter and generate homoconjugation and remote double hyperconjugation effects. Quantifying these “through the space effects” can result in quantifying the steric and overall electronics of the molecule, which is an important parameter for the numerical quantification of donor.

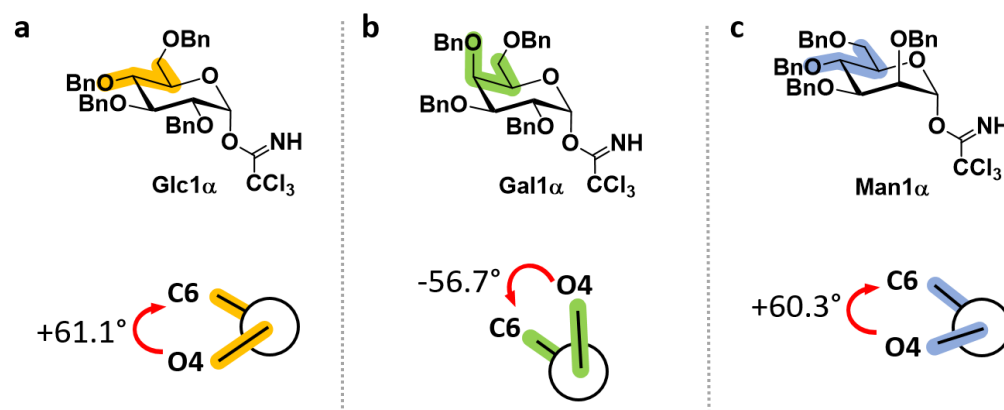


Figure 4.5: Comparison of dihedral angle of O4-C5-C6 for **Glc1 α** , **Gal α** and **Man1 α** . For **Gal1 β** , refer to the table of Figure 4.2.

4.2.2 Acceptor

The most important parameter to be considered in the acceptor (nucleophile) is the nature of the nucleophilic oxygen. In previous research by Codée,⁷⁴ Mayr’s nucleophilicity parameters and field inductive parameters were used for correlate stereochemistry outcome of the glycosylation reactions with a set of simple alcohols. However, these parameters are

an experimentally derived values, this limits the scope of the acceptor. In this study, nucleophilicity is characterized by the ^{17}O NMR chemical shift (B3LYP 6-311G*), which shows the electron distribution of the oxygen according to the local geometry (binding partners, bond lengths, angles between bonds, etc.). As the number of adjacent methyl groups is increased (methanol, ethanol, isopropanol to *tert*-butanol), the ^{17}O NMR shift decreases stepwise by about 31.2 ppm, ascribed to hyperconjugative donations of the $\sigma\text{-CC}$ and $\sigma\text{-CH}$ orbitals into the LP_{O}^* and the $\sigma^*\text{-CO}$ orbitals, respectively. In addition, when strong electron withdrawing substituents such as fluorine are bonded to the α -carbon on ethanol, the ^{17}O NMR chemical shift offsets hyperconjugation donations, as evidenced by di-, and trifluoroethanol have similar chemical shifts to methanol. To describe the steric hindrance of the acceptor, the exposed surface area of the oxygen and α -carbon, respectively, was calculated using a space-filling model (\AA^2) using basis set B3LYP 6-311G*. As the number of methyl groups increased, oxygen and α -carbon exposed surface areas decreased about 0.27 \AA^2 and 7.7 \AA^2 , respectively. However, when fluorine is bonded to the α -carbon of ethanol, the oxygen exposed area increased about 0.31 \AA^2 and α -carbon exposed area slightly decreased 0.51 \AA^2 (Figure 4.6).

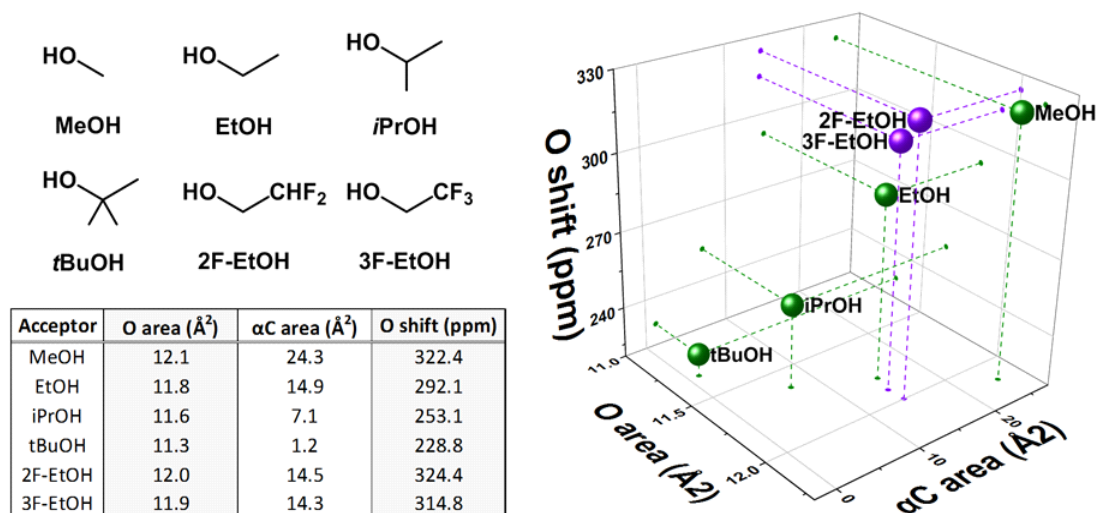


Figure 4.6: 3D map of acceptor chemical subspace (X: exposed surface area (\AA^2) of Oxygen in a space-filling model, Y: exposed surface area (\AA^2) of α -Carbon in a space-filling model, Z: ^{17}O Oxygen NMR chemical shift of hydroxyl group of acceptor). Basis set: B3LYP 6-311G* level of theory.

4.3 Numeric quantification of environmental factors

The influence of environmental parameters such as temperature, activators and solvents over the stereochemical outcome of glycosylation was discussed in *Chapter 3*. These parameters were influential in altering and even inverting stereoselectivity. An accurate description of their influential factors is critical to accurately predict the effect environmental conditions have on glycosylation stereoselectivity. Temperature is already a quantified numeric descriptor. A thorough screening of potential variables revealed a set of descriptors that quantify the relevant steric and electronic factors of both acid catalysts (activators) and solvents.

4.3.1 Activator

The activator changes the stereoselectivity by changing the mechanism^{14, 90-92} that arises from coordination of conjugate base to activated donor in reaction solution. The HOMO (highest occupied molecular orbital) energy value is correlated as to how easily the activators can deprotonate to form the conjugate base. Mechanistically, this conjugate base can interact both covalently and non-covalently with the activated donor and related intermediates, thereby strongly affecting the reaction outcome.⁸⁷ As such, the HOMO energy value was calculated (basis set B3LYP 6-311G*). Strong acids MsOH, FSO₃H, TfOH and Tf₂NH were used as activators, and HOMO energy values were -1.54, -2.36, -2.48 and -4.06 eV respectively. Akin to acceptors, steric hindrance parameters were calculated for the activator using either the oxygen (O⁻) or nitrogen anion (N⁻) exposed surface area, as determined from a space-filling model of the conjugate base. Tf₂NH is a nitrogen based activator and it had unique size of exposed surface area of 9.7 Å², while oxygen based activators had values ranging from 17.7 to 18.3 Å² (Figure 4.7).

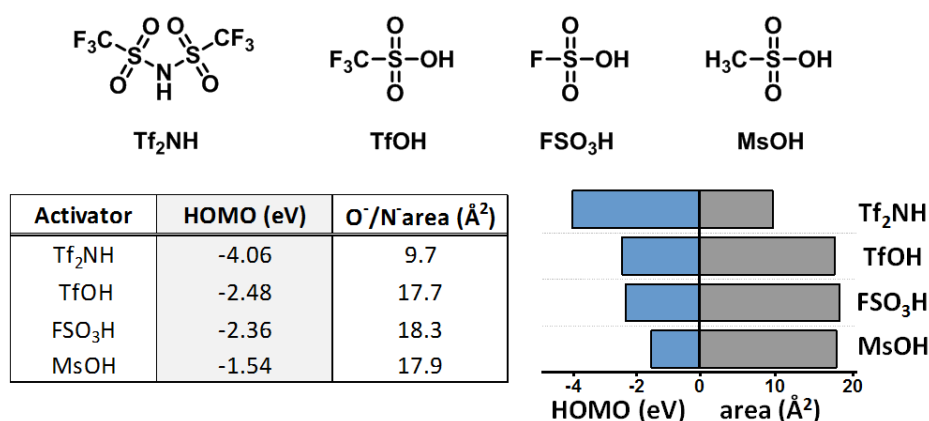


Figure 4.7: The numerical descriptors for activators.

4.3.2 Solvent

Solvents are of fundamental importance in organic chemistry, with their physical characteristics influencing a variety of reaction parameters *e.g.* a solvent's polarity affecting the separation and stabilization of the large number of intermediates formed in the glycosylation reaction.⁹³⁻⁹⁴ Upon decomposition of the activated donor, an oxocarbenium ion is formed. This ion – and the conformations thereof – can be stabilized by both through-space or covalently with lone pair electrons or π -systems of the solvent. With respect to glycosylations, solvents have previously been divided into four main categories: polar and non-coordinating, weakly polar and non-coordinating, polar and coordinating and weakly polar and coordinating solvents.⁹² I initially selected solvents in *Chapter 3* on those four distinct classes,¹⁴ by choosing four solvents namely dichloromethane(DCM), toluene, acetonitrile (ACN), and methyl *tert*-butyl ether (MTBE) respectively (Figure 4.8).

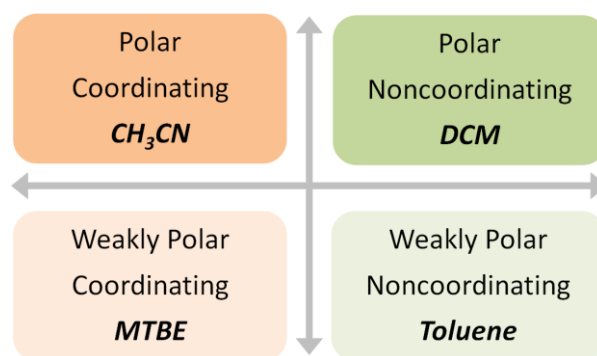


Figure 4.8: Four main categories for solvents.

However, Donicity is an experimentally derived value, and limits the scope of solvents, which can be included. To numerically quantify the solvent properties, DFT calculations were performed, and following screening the minimum value of the electrostatic potential (MinElPot) and maximum value of the electrostatic potential (MaxElPot) were identified as suitable descriptors. In the case of DCM, the two electron withdrawing chlorine atoms bonded to methylene group result in a MinElPot of -62.1 kJ/mol and MaxElPot of 146.6 kJ/mol. However, toluene has MinElPot and MaxElPot values as -95.2 and 69.3 kJ/mol respectively. This is because this molecule is composed of only carbon and hydrogen. If the molecule has an atom of high electronegativity, the intensity of MinElPot increases and lowers the MinElPot value. This trend is visible in ACN and MTBE. However, ACN has triple bond, which affects its overall electron density, and increases the magnitude of its MaxElPot. In contrast, MTBE has a lower MaxElPot value (Figure 4.9).

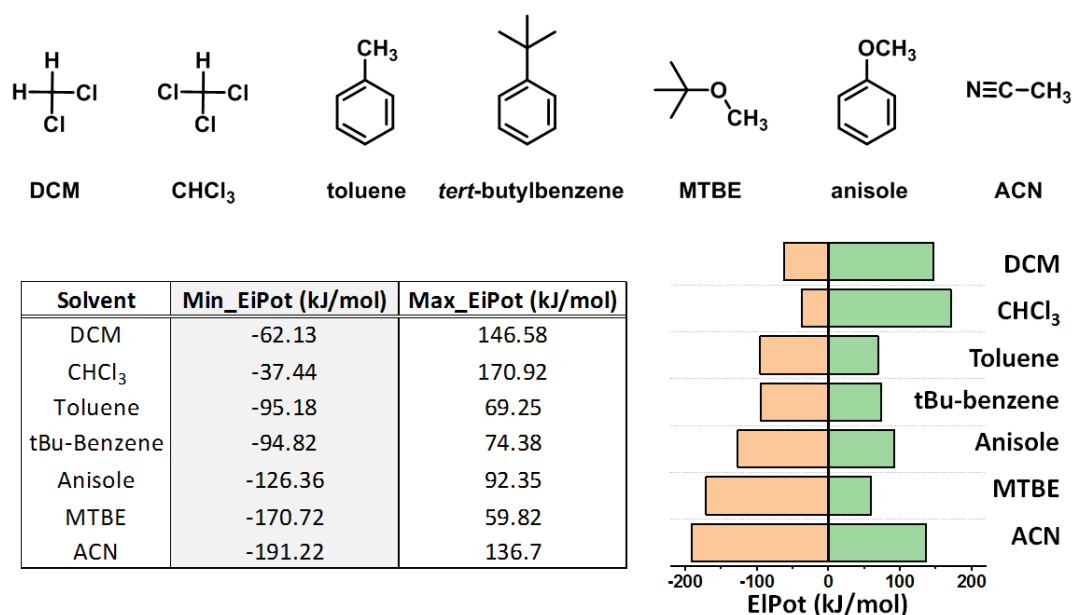


Figure 4.9: The numerical descriptors for solvents.

4.4 Machine learning software development

Many software development platforms exist for developing machine learning software based on machine learning algorithms. The popular choices include Python based TensorFlow, R studio, or MATLAB.

For my thesis work, statistical and machine learning toolbox in MATLAB was used for the development machine learning code. The core machine learning algorithm is based on Random Forest algorithm. Random Forest algorithm was used to train the data with the goal of predicting stereoselectivity. Random Forest algorithm generates several weak models (learners) in the form of binary decision trees. The nodes of each of these decision trees are generated by random shuffling of features (descriptors) in the training set. The final model outcome is generated by creating an “ensemble” by a combined weighted sum of these generated decision trees, representing a collective decision of all the individual trees, dictating the final output prediction of the model. Modeling the data with these ensemble learners generates good prediction and reduces over-fitting.¹⁰⁶

Random Forest algorithm was used by invoking the “fitrensemble” function in MATLAB. The general syntax for the function used is

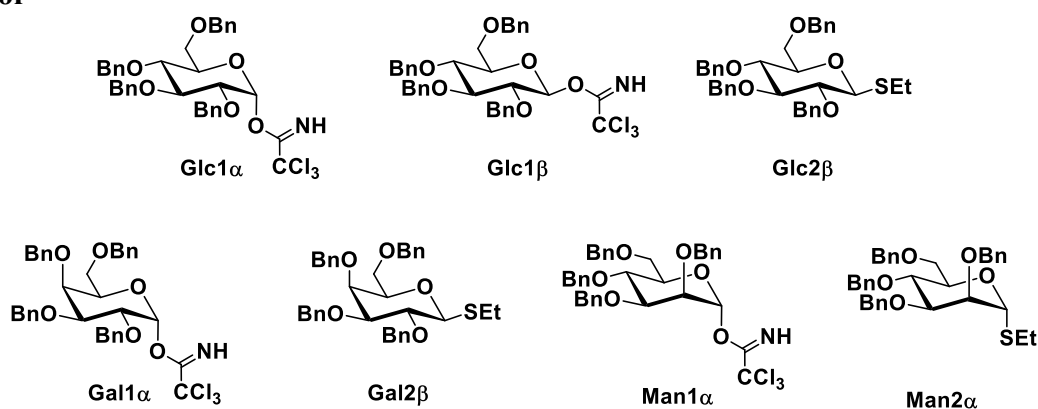
```
"Mdl" =
fitrensemble(X,Y,'Method','Learners','OptimizeHyperparameters',
            'HyperparameterOptimizationOptions')
```

Mdl is the model output as a “Regression Ensemble” which is a complex data structure consisting of the trained model along with compiled information on every parameter including function weights, fit info, and hyperparameter optimizations results. Mdl also contain the trained model that will be later used in the prediction section. X is the input variable, which contains experimental data along with the input descriptors. Y is the response variable containing the experimental observations. ‘Leaners’ is the specification for the type of decision tree or model.

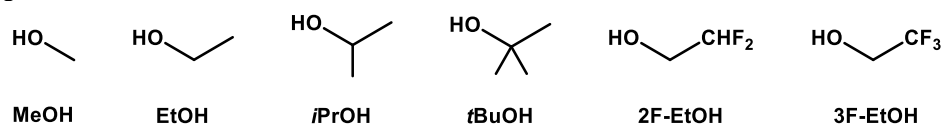
4.5 Generation of a training set for machine learning

Data points (268) in the training set dictate a maximum of thirteen descriptors, temperature, five for donor, three for acceptors, two for activator and two for solvents respectively to avoid any overfitting to get statistically meaningful results.¹⁰⁷ The donors, acceptors, activators and solvent, which were included in the training set are shown in Figure 4.10. The training set is comprised of experimental conditions (reaction conditions, yield, and stereoselectivity) as well as the numerical descriptors calculated for donors, acceptors, activators and solvents by using DFT calculation in SPARTAN software as described in the Sections 4.2 and 4.3. The reaction condition was kept constant, having previously been found to have no impact on stereoselectivity (Scheme 4.1). Entries 1-106, 116-134, 136-141, 143-196, 220-302 in Table 6.1 (Chapter 6) were included in 268 training data points set.

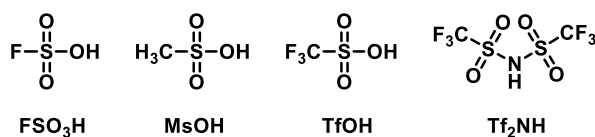
Donor



Acceptor



Activator



Solvent

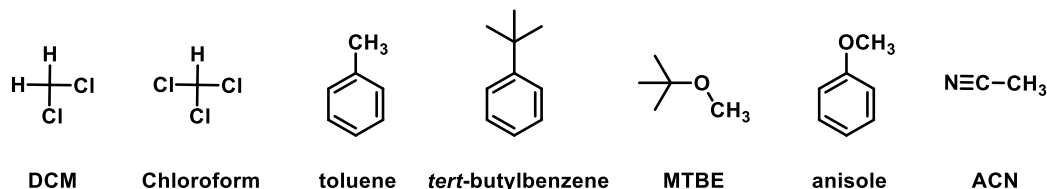


Figure 4.10: The compounds included in the training set.

4.6 Machine learning: ‘under the hood’

The machine learning methodology used in the research could be broadly categorized into five individual sections:

- 1) Data input and preconditioning section
- 2) Model input section
- 3) Machine learning and data processing section
- 4) Prediction section
- 5) Data output section

1) Data input and preconditioning section

Data input and preconditioning section consists of codes to import the training set data having both descriptor input data and response data into different arrays using the ‘xlsread’ function of MATLAB. Different arrays were also created for other functions, such as storing the model output data in the preconditioning section. Validation and experimental data were also stored into separate arrays to be used for prediction and validation purposes.

2) Model input section

After the import of the training data, the software generates the learner function, which is based on a template regression model tree. Model tree was generated using

the “`templatetree`” function in the MATLAB code. The template tree function could be invoked as shown below:

```
t = templateTree('NumPredictorsToSample',  
'PredictorSelection','Prune','Surrogate',);
```

The `templatetree` function generates decision trees and in this case, regression trees based on a number of nested functions including “`NumPredictorToSample`” which selects the appropriate number of predictors to the random sampling of data.

3) Machine learning and data processing section

The optimal template tree as described in the previous section is used in the Random Forest algorithm as learners. The trees were randomly selected and grown using algorithm based on “*Bagging*” and “*LSBoost*” type algorithm.

3.1) *Bagging algorithm*

Bagging algorithm is an ensemble learning technology called Bootstrap Aggregation. With this technology, random replica models or decision trees are grown on the all the samples in the training set. With this technique, many replica models could be generated from the same training set. For generating the splits in the decision tree, the predictor is randomly selected. This random selection of predictors leads to what is called Random Forest.

3.2) *LSBoost*

This algorithm is used here for regression based ensemble learning. The least square boosting is done to fit the regression trees with the observed data. At every iteration, the algorithm works by fitting a new learner with the observed difference between prediction from the model and observed data.¹⁰⁸ This fitting is achieved by minimization of the mean-square-error (MSE).

3.3) *Tuning of hyperparameters*

The learning performance of machine learning algorithms can be enhanced quite significantly by choosing proper hyper-parameters. However, this optimization is still empirical in nature and often depends on the dataset being optimized. As an alternative, automated hyperparameter tuning is becoming increasingly important.¹⁰⁶

Here we have used the algorithm. “Expected-improvement-plus” in MATLAB for automated tuning of hyperparameters.

4) Prediction section

Upon completion of the training, the model output is stored in a variable ‘Mdl’. The prediction algorithm ‘predict’ can now be used to along with the trained model stored in ‘Mdl’ to predict new experimental results based on the trained model. Once the prediction is completed, the predictor importance is calculated by summation of the variation of Mean square errors (MSE) which generates from split of each predictor and dividing this quantity by the total number of branch nodes. Separate arrays are created for storing the prediction results and the predictor importance.

5) Data output section

The arrays generated for storing the model output in the form of prediction data and predictor importance along with R^2 are exported and converted into table data types in this section. These tables are then written to Microsoft Excel datasheets using the ‘`xlswrite`’ function of MATLAB.

4.7 Quantifying of accuracy and benchmarking model with R^2 and RMSE

In all the results that follow, the quantification of accuracy and benchmarking of Machine Learning models are demonstrated by R^2 (coefficient of determination) and Root Mean Square Error (RMSE) values. The ideal value for the coefficient of determination is 1 and RMSE is 0. These are calculated with *Experimental* (X) and *Predicted* (Y) values by the equations given below and it is worth mentioning here that both of these values need to be taken into account when judging the prediction ability of the model. Utilizing only one of these values is not enough, as demonstrated in Figure 4.11. The dashed line and the solid line represents prediction values and experimental values simultaneously. Figure 4.11a represents a model for which the RMSE is 9.7, however the R^2 is 0.2 which is poor. Therefore, in this case the model performs poorly, compared to the model represented by Figure 4.11b. The increase in RMSE is negligible here compared to the model in Figure 4.11a and R^2 is 1 which is ideal. However, the model represented by Figure 4.11b always over predicts the experimental data. The model shown in Figure 4.11c represents an ideal

case scenario. Both the RMSE and R^2 values are ideal, however, this type of model accuracies are seldom observed in practical situations.

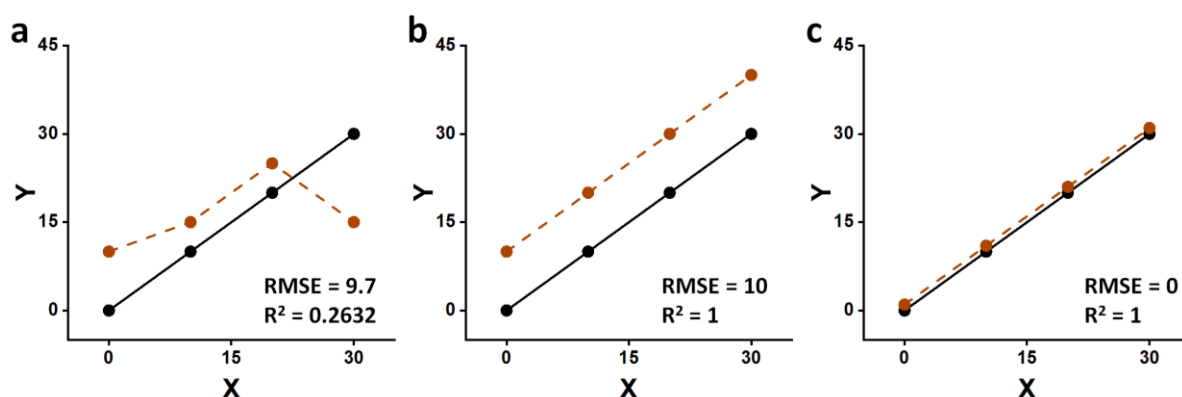
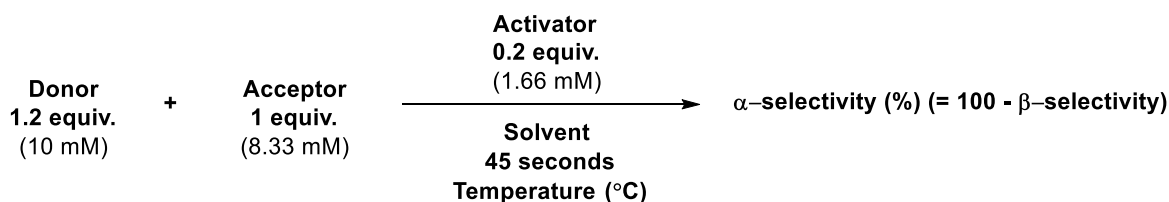


Figure 4.11: (a)-(c) represents three different models and quantifies the model performance with the help of RMSE and R^2 values.

4.8 Default glycosylation conditions

Glycosylations were performed in an automated microreactor flow platform, described in detail in *Chapter 2*. Compounds listed in the training set above were combined using the following stoichiometries (Scheme 4.1). The complete training dataset is provided in Table 6.1 of *Chapter 6*.



Scheme 4.1: A default glycosylation condition for machine learning in an automated microreactor flow platform.

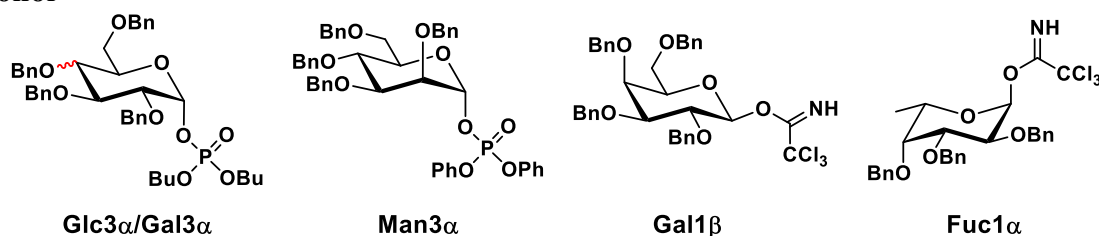
4.9 Training and prediction of glycosylation

The training set contains systematic combinations of seven electrophiles, six nucleophiles, four acid catalysts, and seven solvents over a solvent-dependent temperature range of -50 – 100 °C. Along with the experimental data, the descriptors described in the sections above were utilized to train the Random Forest algorithm in conjunction with hyperparameter tuning. After the initial training, the trained model was used to predict the stereoselectivities of a set of out-of-sample glycosylations, varying each of the four

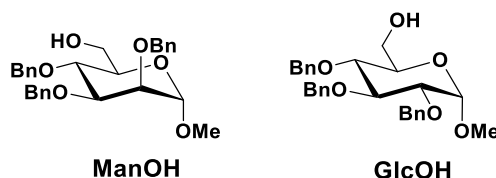
chemical species in the reaction over the accessible temperature range. Validation of the predicted results was performed using the automated microreactor platform as discussed in *Chapters 2 and 3* of this thesis.

As the descriptors were chosen based on chemical intuition and my current understanding of glycosylations, it becomes important to quantify the scope of the model in predicting newly discovered mechanistic rules by which stereoselectivity could be influenced. The compounds were organized by donor/ acceptor/ activator/ solvent, and were not included in the training set and used to quantify the scope of the model (Figure 4.12). Similarly, predictions were run using these molecules and were subsequently validated experimentally on the same microreactor platform.

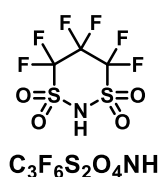
Donor



Acceptor



Activator



Solvent

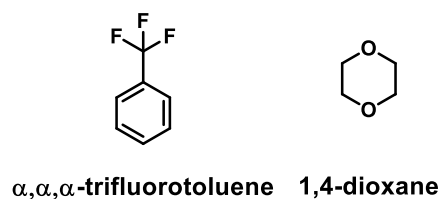


Figure 4.12: Out-of-sample reagents used to validate prediction accuracy of the model with variances for each chemical category: donors, acceptors, an activator, and solvents.

Accurate predictions were obtained for the selectivity of electrophiles bearing phosphate leaving groups, whose resultant selectivity was revealed to be similar to those of glycosyl imidates and thioethers for glucose, galactose, and mannose donors, with a combined root mean square error (RMSE) of 4.1 (Figure 4.13a). It was also revealed that

the model could be applied to other pyran cores such as L-fucose. The predicted stereoselectivity accurately matched the experimental data (RMSE: 7.2) for the coupling of fucose α -imidate donor with isopropanol, where β -anomer formation is favored at low temperatures and exhibits a decrease in stereoselectivity with increase in temperature (Figure 4.13b).

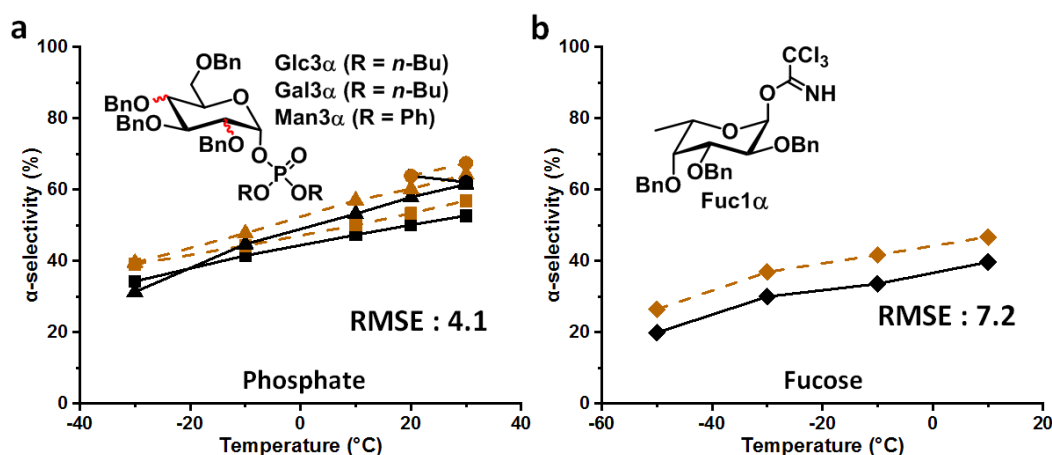


Figure 4.13: Prediction of stereoselectivity for glycosylations using different anomeric leaving groups and pyran core. **a**, Prediction of stereoselectivity for glycosylations involving a glycosylphosphate leaving group. **b**, Prediction of stereoselectivity using a fucose donor with *i*PrOH in DCM. For full experimental details, see entries 313-328 of Table 6.1 in Chapter 6. Figure code: Fucose (◆); Glucose (▲); Galactose (■); Mannose (●); Experimental (solid black line); Predicted (dashed colored line).

The model successfully predicted the stereoselectivities of disaccharide formation though the training set contains only simple alkyl alcohols as nucleophiles. Predictions were made for the coupling of α -galactose imidate with both glucose and mannose C6 alcohols, and the predictions match well with experimental data, albeit predicting a less α -selective process than observed (RMSE: 12.4 and 13.9, Figure 4.14a/b, respectively).

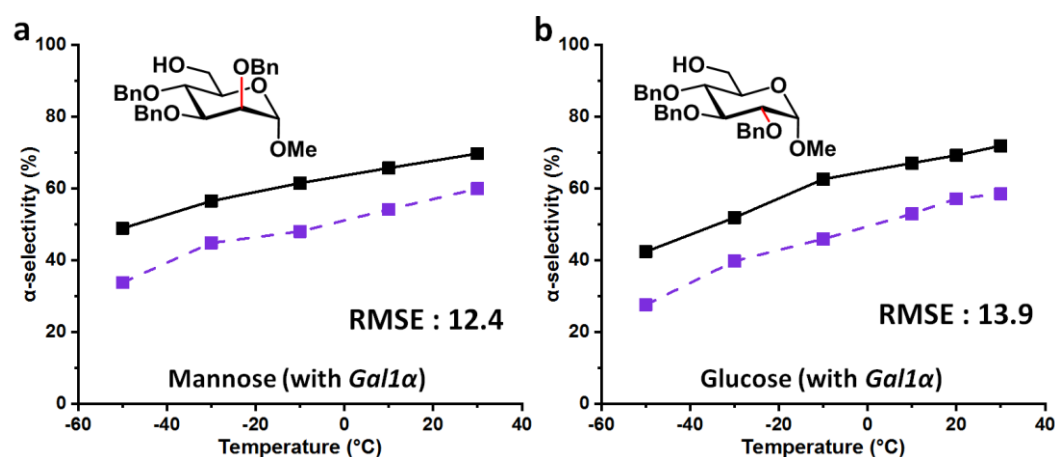


Figure 4.14: Prediction of mannose and glucose C6-acceptor with galactose imidate donor in DCM. For full experimental details, see entries 329-339 of Table 6.1 in Chapter 6. Figure code: Galactose (■); Experimental (solid black line); Predicted (dashed colored line).

A bit of over-prediction (values predicted are higher than obtained from experiments) in the model was observed towards α -selective processes than experimentally observed in glycosylations using superacid 4,4,5,5,6,6-hexafluoro-1,3,2-dithiazinane-1,1,3,3-tetraoxide ($C_3F_6S_2O_4NH$) as acid catalyst. The over-prediction mainly happens at higher temperatures with galactose, however the model is able to capture the trend properly and has a low RMSE of 7.2 (Figure 4.15a).

However, for $C_3F_6S_2O_4NH$ -catalyzed coupling of mannose with isopropanol in DCM, the model over-predicts the α -selectivity significantly (Figure 4.15b). The RMSE increases to almost 18.7%. The prediction of a stereoselective plateau at low temperatures with α -selectivity around 60% was observed experimentally for other activators with mannose (Figure 3.15). However, this finding of β -mannosylation product formation at low temperatures (-50 °C, 63% β -product) is rather unexpected due to the challenging nature of β -mannosylation which generally requires locked donor configurations.¹⁰ With $C_3F_6S_2O_4NH$, the perbenzylated donor ranges from a 63% β -selectivity at -50 °C to 98% α -selectivity at 30 °C (Figure 4.15b).

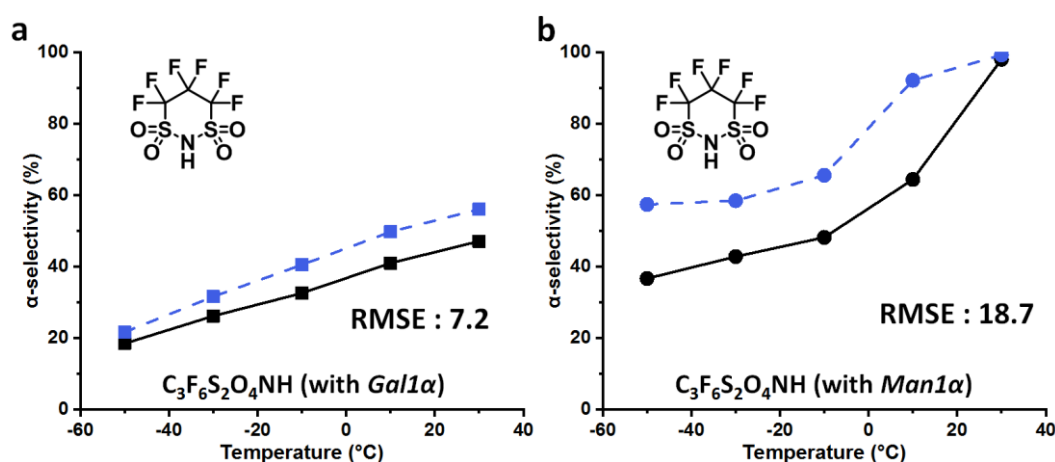


Figure 4.15: **a**, Prediction of 4,4,5,5,6,6-hexafluoro-1,3,2-dithiazinane 1,1,3,3-tetraoxide ($C_3F_6S_2O_4NH$) activator with galactose donor and *i*PrOH acceptor in DCM. **b**, Prediction of $C_3F_6S_2O_4NH$ with mannose donor and *i*PrOH in DCM. For full experimental details, see entries 340-349 of Table 6.1 in *Chapter 6*. Figure code: Galactose (■); Mannose (●); Experimental (solid black line); Predicted (dashed colored line)

As a final test of the model, two new solvents were employed and the stereoselectivity of glucose and galactose α -imidate donors with isopropanol were predicted (Figure 4.16). The strong influence of solvent⁹³ on the stereoselectivity of glycosylations is nicely captured by the descriptors chosen, and the model is accurate across a wide

temperature range for both α,α,α -trifluorotoluene (RMSE: 8.1) and 1,4-dioxane (RMSE: 4.2).

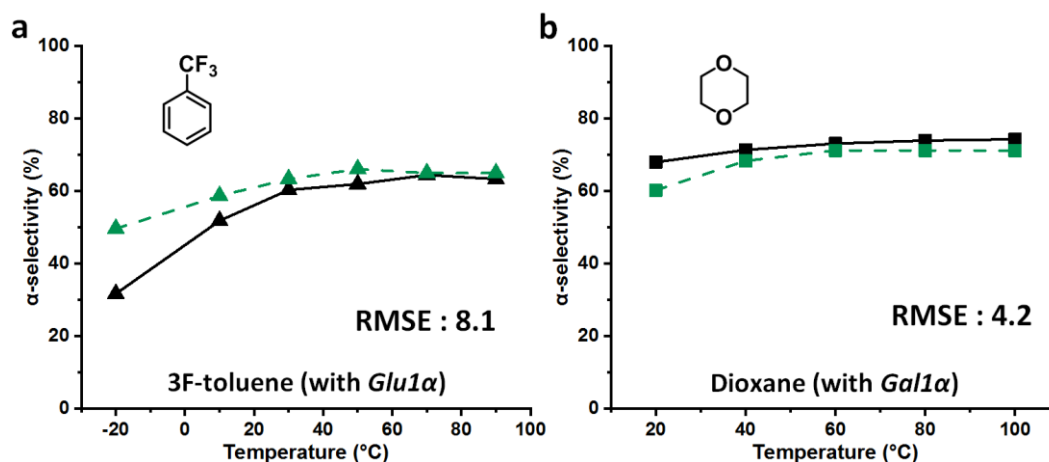


Figure 4.16: a, Prediction of α,α,α -trifluorotoluene (3F-toluene) solvent with glucose α -imidate donor and *i*PrOH in DCM. b, Prediction of 1,4-dioxane solvent with galactose α -imidate donor and *i*PrOH in DCM. For full experimental details, see entries 350-360 of Table 6.1 in Chapter 6. Figure code: Glucose (\blacktriangle); Galactose (\blacksquare); Experimental (solid black line); Predicted (dashed colored line)

4.10 Generation of validation set for benchmarking

During my thesis work, an intriguing result regarding the stereochemistry of the leaving group influencing stereoselectivity was revealed. This is traditionally not considered an exploitable factor to influence the stereoselectivity of glycosylations.^{14, 56} This assumption is not without experimental evidence. It was experimentally revealed that the α/β -orientation of the leaving group of glycosyl donor has no influence on stereoselectivity in dichloromethane. This was reported in Figure 3.4 of Chapter 3 and the subsequent publication.¹⁴ Divergences in stereoselectivity based on this factor have only sparingly been observed in the literature, *e.g.* when phenylsilicon trifluoride (PhSiF_3) is used as catalyst.¹⁰⁹

The influence of the leaving group orientation on stereoselectivity using solvent was revealed in this research work and has not previously been reported. While essentially identical behavior is observed in DCM and chloroform, a slight divergence in MTBE at low temperatures is observed, with an 11% difference at -50 °C where the β -donor reaches 96% α -selectivity. This variable becomes important in toluene. Glucose β -imidate donor yields almost unchanged stereoselectivity ($\sim 60\%$ α) over a 120 °C range! The orientation of the leaving group of the donor influences the stereoselectivity by more than 40% at -50 °C (Figure 4.17).

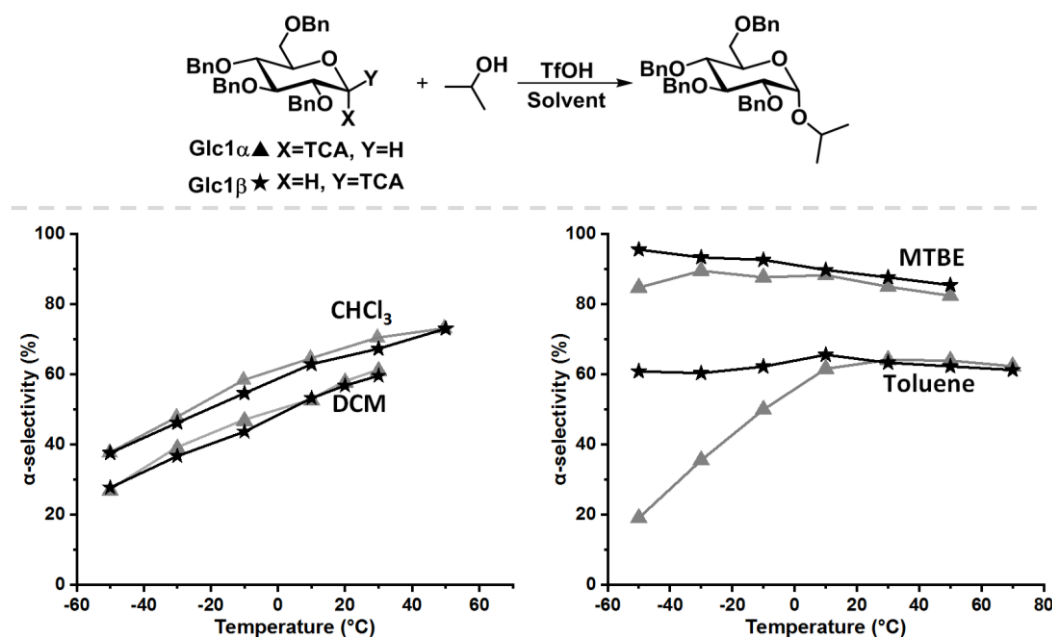


Figure 4.17: Experimental results of coupling α/β -glucose donors with *i*PrOH (Glc1 α and Glc1 β) in different four solvents DCM, CHCl₃, toluene, and MTBE. For full experimental details, see entries 13-34, 61-74, 95-106, 123-134 of Table 6.1 in *Chapter 6*.

After inclusion of this intriguing data in the training set, we tested the scope of and ability of the model to predict the influence of other factors on this to-date unreported phenomenon (Figure 4.18). The stereoselectivity of glucose α -imidate with ethanol as acceptor ranges from 10 – 54% α -product in toluene. The model predicts that the β -donor will behave differently, with a much less selective coupling overall (45%-55% α -product). This prediction matches well with the experimental results, with an RMSE of 7.7 over the 120 °C range, though the process is less α -selective than predicted at low temperatures. The model also accurately predicts the ~10% decrease in α -selectivity at low temperatures with *t*BuOH as acceptor and the overall similarity of the observed stereoselectivities of the α/β -donor under these conditions (RMSE:7.0).

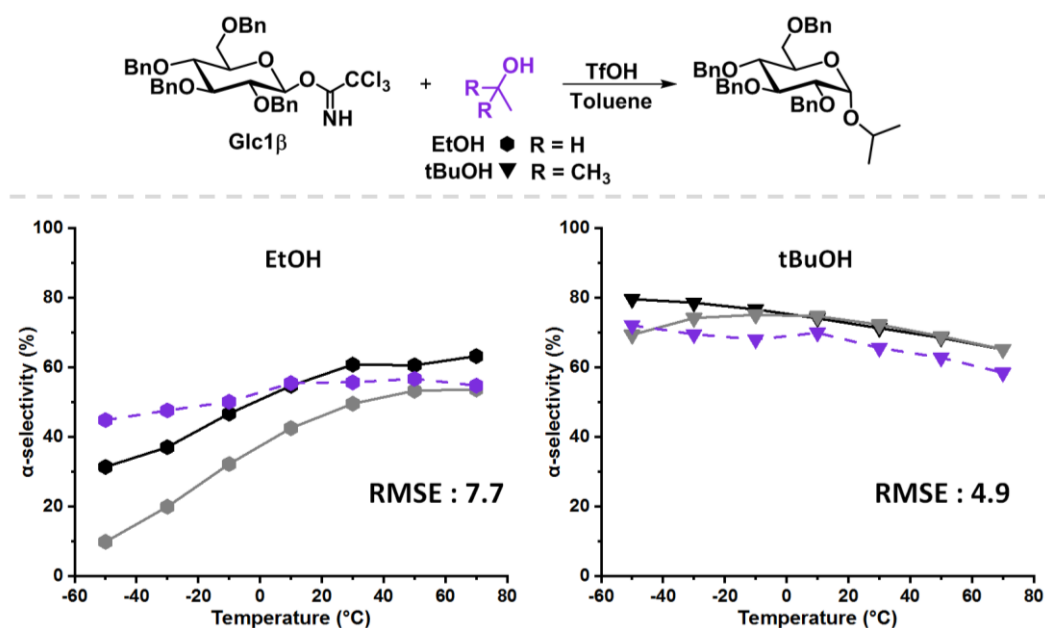


Figure 4.18: Prediction and experimental results of β-glucose donor (**Glc1β**) with EtOH and *t*BuOH in toluene. For full experimental details, see entries 75-88, 361-374 of Table 6.1 in *Chapter 6*. Figure code: EtOH (●); *t*BuOH (▼); Experimental data with α-donor (solid grey line); Experimental data with β-donor (solid black line); Predicted data in dashed, colored line.

Lastly, we sought to explore whether this additional mechanistic complexity exists for other electrophiles (Figure 4.19). The model predicts that the α/β-galactose donors, when coupling with isopropanol, will give similar α-selectivity in DCM over the 80 °C temperature range, matching experimental values (RMSE 2.9). In toluene, the model predicts a divergence in stereoselectivity at low temperatures, though not as large as what is observed with glucose. This prediction again aligns with experimental results (RMSE: 5.7). Overall, the model correctly predicts the previously unknown ability to turn on and off the influence of the donor leaving group's orientation using solvents under otherwise identical conditions.

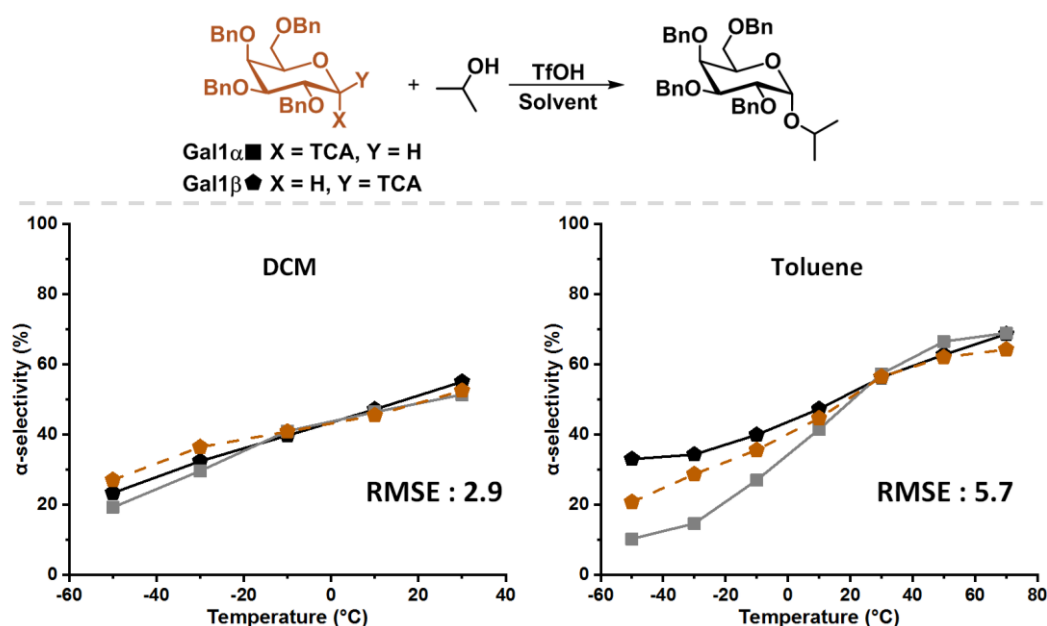


Figure 4.19: Prediction and experimental results of β -galactose donor (Gal1 β) with $i\text{PrOH}$ in DCM and toluene. For full experimental details, see entries 149-154, 375-386 of Table 6.1 in *Chapter 6*. Figure code: Gal1 α (■); Gal1 β (◆); Experimental data with α -donor (solid grey line); Experimental data with β -donor (solid black line); Predicted data in dashed, colored line.

Along with prediction, the machine learning software running Random Forest algorithm generates the degree of influence each variable has on the model outcome. This helps to numerically quantify the influence of the variables within the model (Figure 4.20). It was revealed that in the chemical subspaces covered by our model, 46% of the influence over a glycosylation's stereoselectivity is determined by the inherent properties of the coupling partners. The donor descriptors which influences the overall model outcome by 26% is more impactful than the acceptor which is 20%. Once the coupling partners are fixed, more than half of the stereoselectivity observed is controlled by the environmental conditions chosen. The most important environmental factors are the reaction temperature (21%) and the solvent (26%).

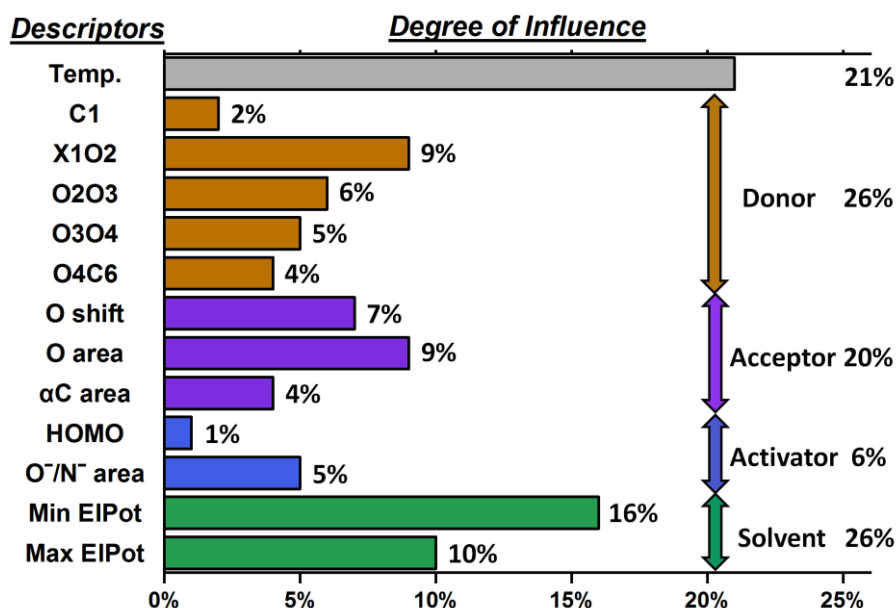


Figure 4.20: Degree of influence of the twelve chemical factors influencing the stereoselectivity of glycosylations, rounded to nearest whole number.

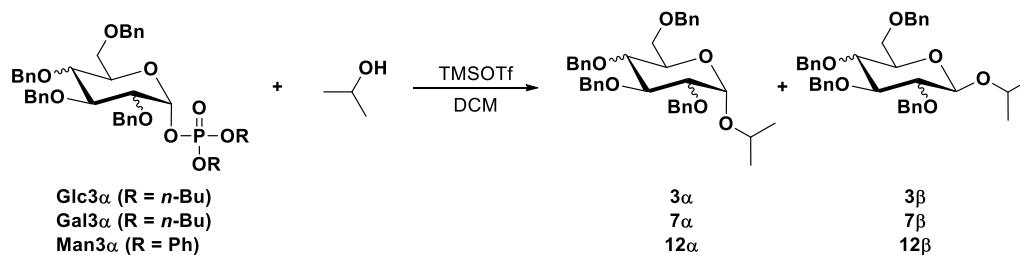
4.11 Comparison of four different algorithms

Along with regression based Random Forest (RF) algorithm, used as the core algorithm in this thesis, separate software was developed in order to screen other common regression based machine learning algorithms. These are Gaussian Process Regression (GPR), Regression Tree (RT) and regression based Support Vector Machine (SVM). For implementation of GPR, SVM and RT in MATLAB, ‘fitrgp’, ‘fitrsvm’ and ‘fitrtree’ functions were used respectively using similar methodology as described for the implementation of Random Forest in MATLAB, which was discussed in detail in *Section 4.4*. This additional study was performed in order to compare the prediction performance and benchmarking different algorithm compared to RF. Each of the four ML algorithms was trained using the training set and the models were compared with the experimental data as shown below. In nearly all the cases, RF was the superior model. The following experimental and validation data are reported as benchmarking references.

Prediction of phosphate leaving group

In the case of prediction of phosphate leaving group (**Glc3α**, **Gal3α**, **Man3α**), RF clearly out performs when compared to RT, SVM and GPR which is shown by corresponding RMSE and R^2 values (Figure 4.21). However, three other algorithms (RT,

SVM and GPR) also performed quite well and predict the experimental results with high accuracy (RMSE value less than 5.1).



Temp. (°C)	Experimental	RF	RT	GPR	SVM
-30	31.3	39.5	41.0	36.0	38.8
-10	44.7	47.8	49.6	45.6	47.1
10	53.2	57.0	54.4	54.5	53.5
20	57.9	60.2	57.5	58.4	57.3
30	61.5	64.3	60.1	62.1	61.1
-30	34.3	39.1	41.0	39.0	45.4
-10	41.5	44.3	49.6	47.1	49.4
10	47.3	50.0	49.9	54.3	51.7
20	50.1	53.4	49.9	57.4	52.4
30	52.7	56.9	53.8	60.1	53.2
20	63.9	63.9	68.9	61.4	58.4
30	62.1	67.5	68.9	63.3	59.1

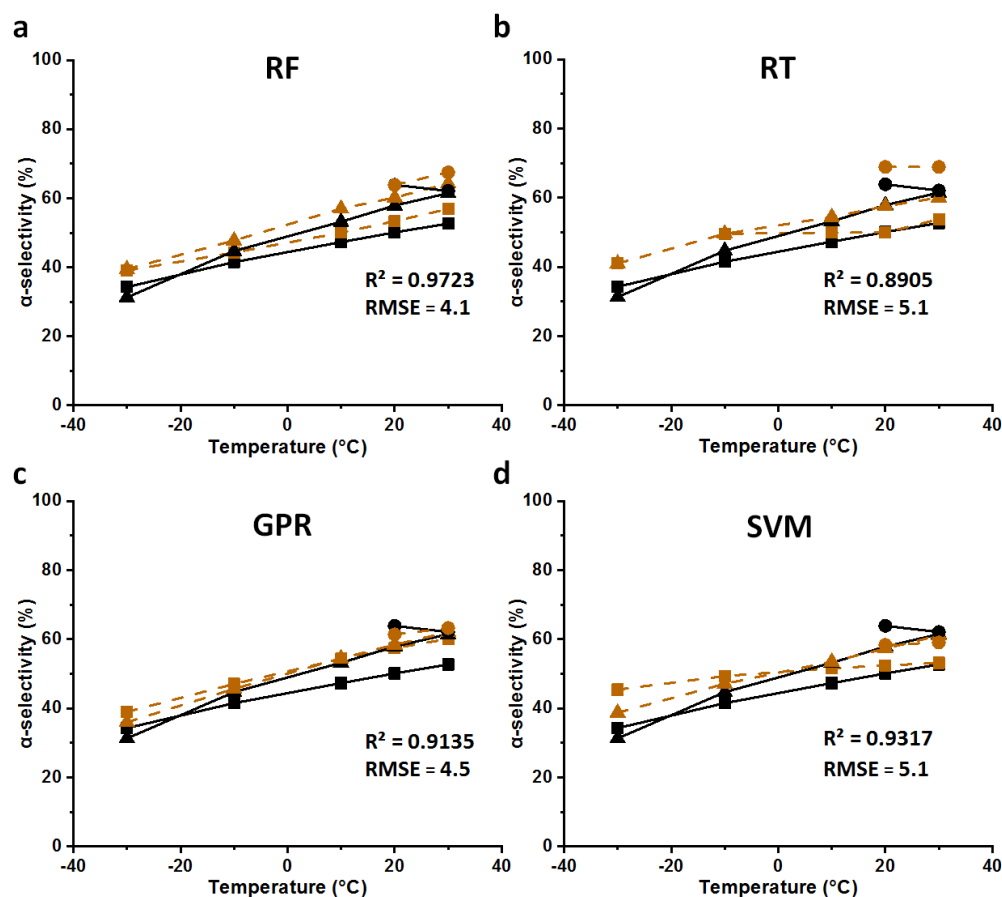
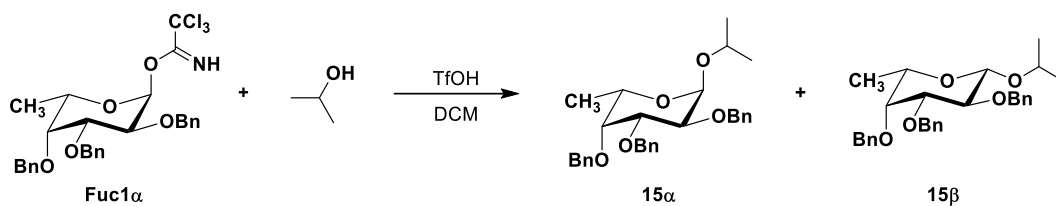


Figure 4.21: Validation data collected from the automated flow platform to predict phosphate leaving group with glucose, galactose and mannose. **a**, Prediction with Random Forest (RF). **b**, Prediction with Regression Tree (RT). **c**, Prediction with Gaussian Process Regression (GPR). **d**, Prediction with Support Vector Machine

(SVR). Experimental (solid black line); Predicted (dashed colored line). For full experimental details, see entries 313-324 of Table 6.1 in Chapter 6.

Prediction of Donor- Fucose

Prediction of **Fuc1 α** with RF algorithm gives better results when compared to RT, SVM and GPR which is shown by corresponding RMSE and R^2 values (Figure 4.22). In the case of RF, RMSE and R^2 were 7.2 and around 1 respectively which is higher than other algorithms. However, the accuracy of SVM model gives poorest prediction with 14.6 RMSE and 0.87 R^2 (Figure 4.22d).



Temp. (°C)	Experimental	RF	RT	GPR	SVM
-50	19.9	26.4	33.4	27.6	40.0
-30	30	36.9	41.0	35.9	41.9
-10	33.6	41.7	49.6	44.1	47.4
10	39.7	46.8	49.9	51.4	50.6

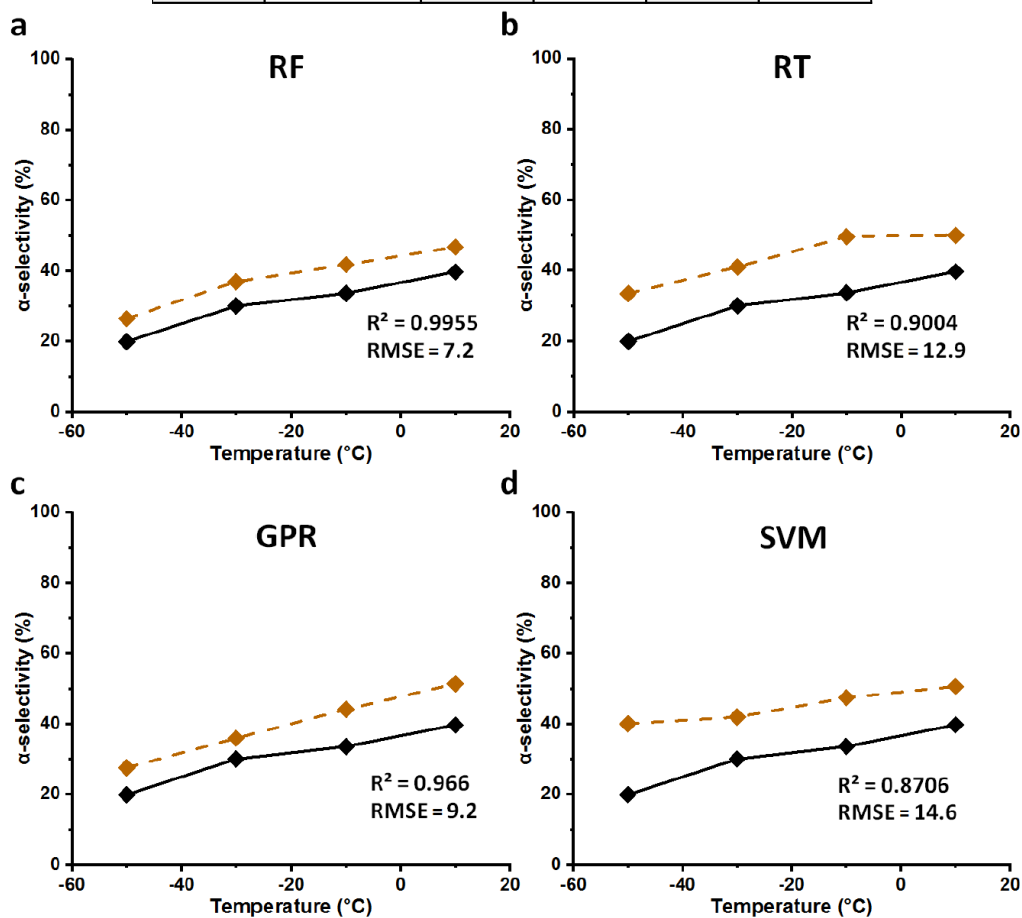
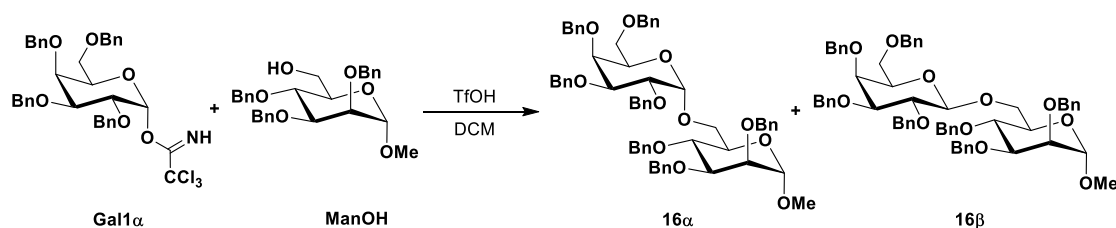


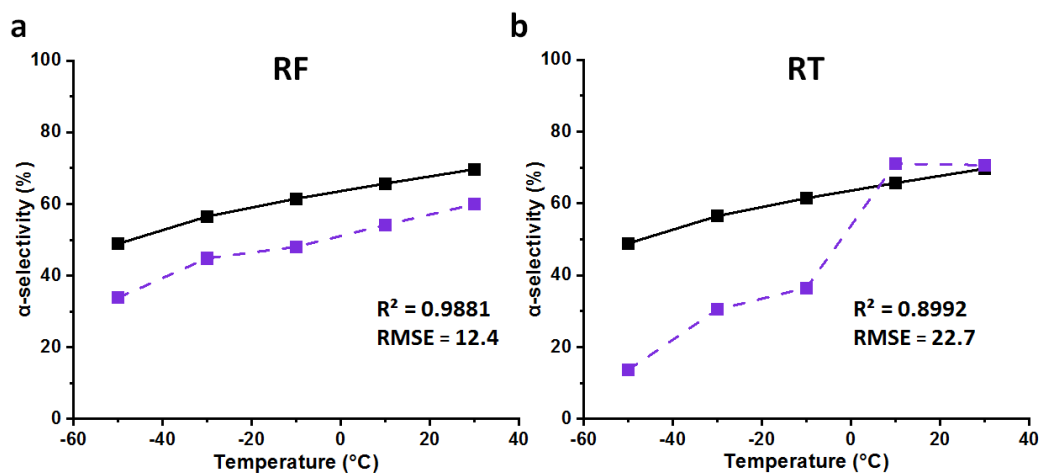
Figure 4.22: Validation data collected from the automated flow platform to predict **Fuc1 α** donor. **a**, Prediction with Random Forest (RF). **b**, Prediction with Regression Tree (RT). **c**, Prediction with Gaussian Process Regression (GPR). **d**, Prediction with Support Vector Machine (SVR). Experimental (solid black line); Predicted (dashed colored line). For full experimental details, see entries 325-328 of Table 6.1 in *Chapter 6*.

Prediction of Acceptor- Mannose

The experimental and prediction results for the out-of-sample glycosylations involving a C6 mannose glycosyl acceptors (Figure 4.23) reveal that GPR has the worst RMSE value (29.7, Figure 4.23c), however, it predicts the temperature trend well as shown by R^2 very close to 1. In the case of prediction by RT, it predicts poorly at lower temperatures and then gives a RMSE of 22.7 (Figure 4.23b).



Temp. (°C)	Experimental	RF	RT	GPR	SVR
-50	48.9	33.8	13.6	15.8	54.4
-30	56.5	44.8	30.4	25.4	54.4
-10	61.5	48.1	36.5	32.8	54.4
10	65.7	54.2	71.1	38.0	54.4
30	69.7	59.9	70.7	42.2	54.4



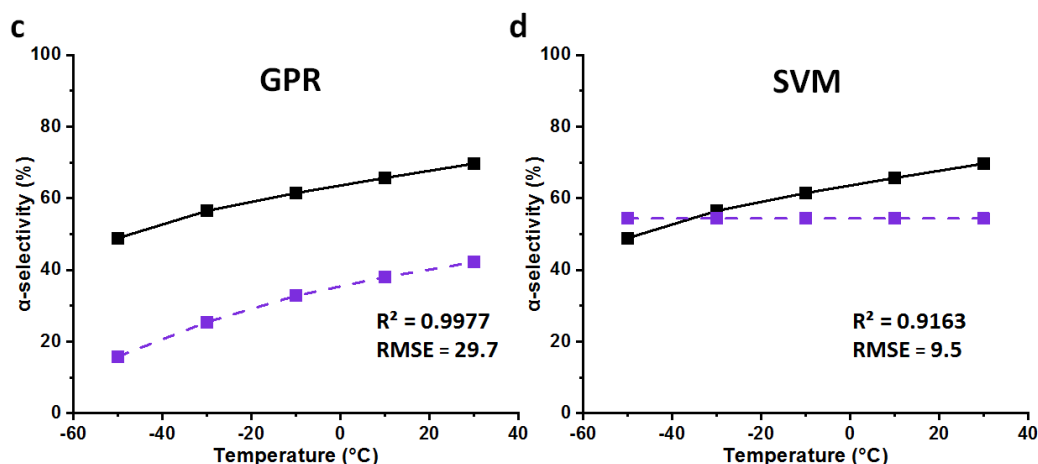
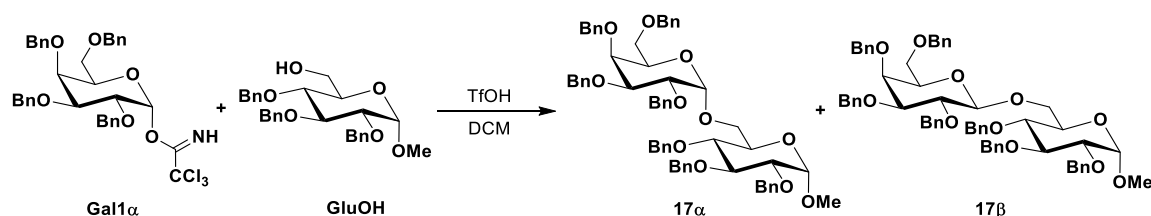


Figure 4.23: Validation data collected from the automated flow platform to predict **ManOH** acceptor. **a**, Prediction with Random Forest (RF). **b**, Prediction with Regression Tree (RT). **c**, Prediction with Gaussian Process Regression (GPR). **d**, Prediction with Support Vector Machine (SVR). Experimental (solid black line); Predicted (dashed colored line). For full experimental details, see entries 329-333 of Table 6.1 in Chapter 6.

Prediction of Acceptor- Glucose

Prediction of **GlcOH** with the GPR algorithm gives better results when compared to RT, SVM and RF as shown by corresponding RMSE and R^2 values of 10.7 and 0.995 respectively (Figure 4.24c). Interestingly, a prediction trend similar to **ManOH** was observed for RT giving a RMSE and R^2 of 18.2 and 0.88 respectively (Figures 4.23b and 4.24b).



Temp. (°C)	Experimental	RF	RT	GPR	SVM
-50	42.4	27.6	13.6	32.4	33.2
-30	51.9	39.8	30.4	42.4	34.0
-10	62.6	46.0	36.5	50.4	41.8
10	67.1	52.9	71.1	56.2	49.4
20	69.2	57.1	71.1	58.6	52.2
30	71.9	58.5	70.7	60.8	54.3

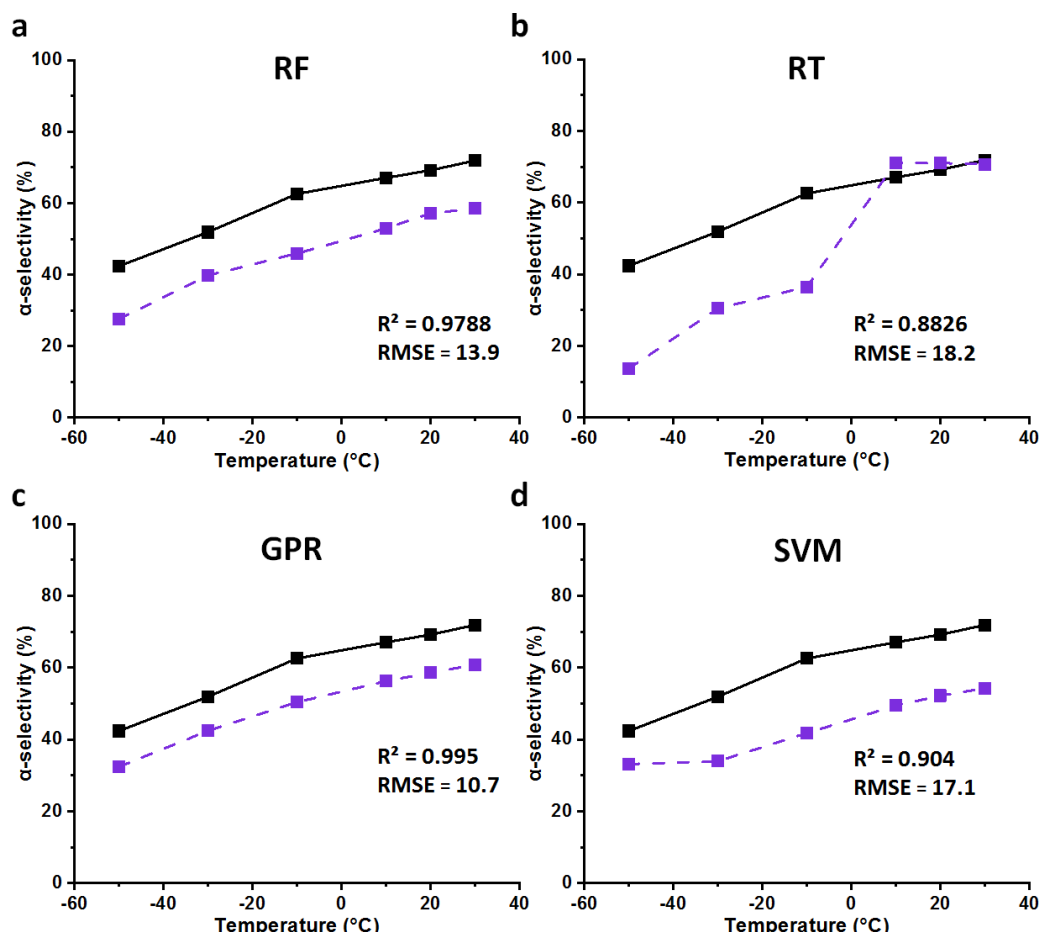
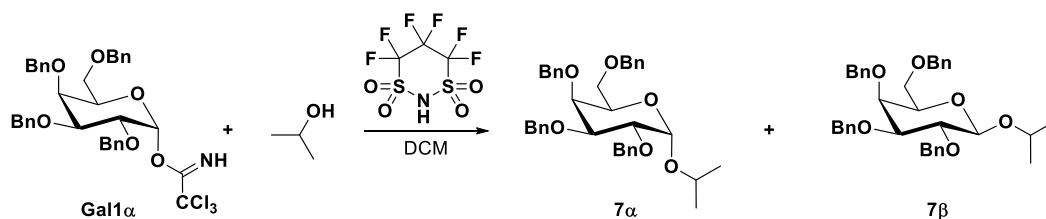


Figure 4.24: Validation data collected from the automated flow platform to predict **GlcOH** acceptor. **a**, Prediction with Random Forest (RF). **b**, Prediction with Regression Tree (RT). **c**, Prediction with Gaussian Process Regression (GPR). **d**, Prediction with Support Vector Machine (SVR). Experimental (solid black line); Predicted (dashed colored line). For full experimental details, see entries 334-339 of Table 6.1 in *Chapter 6*.

Prediction of Activator- $\text{C}_3\text{F}_6\text{S}_2\text{O}_4\text{NH}$ with **Gal1a**

The prediction of 4,4,5,5,6,6-hexafluoro-1,3,2-dithiazinane 1,1,3,3-tetraoxide ($\text{C}_3\text{F}_6\text{S}_2\text{O}_4\text{NH}$) as activator coupling a galactose imidate donor (**Gal1a**) and isopropanol as acceptor (Figure 4.25) reveal that GPR clearly out performs RT, SVM and RF as shown by corresponding RMSE and R^2 values (Figure 4.25c). The RF algorithm performs quite well and predicts the experimental results with high accuracy (RMSE is 7.2 and R^2 is close to 1, Figure 4.25a). However, SVM fails prediction of the temperature trend totally and gives high RMSE of 23.6 (Figure 4.25d).



Temp. (°C)	Experimental	RF	RT	GPR	SVM
-50	18.5	21.7	16.2	16.7	54.4
-30	26.2	31.6	16.2	25.8	54.4
-10	32.6	40.5	16.2	34.7	54.4
10	41	49.7	45.8	42.5	54.4
30	47.1	56.0	53.8	48.6	54.4

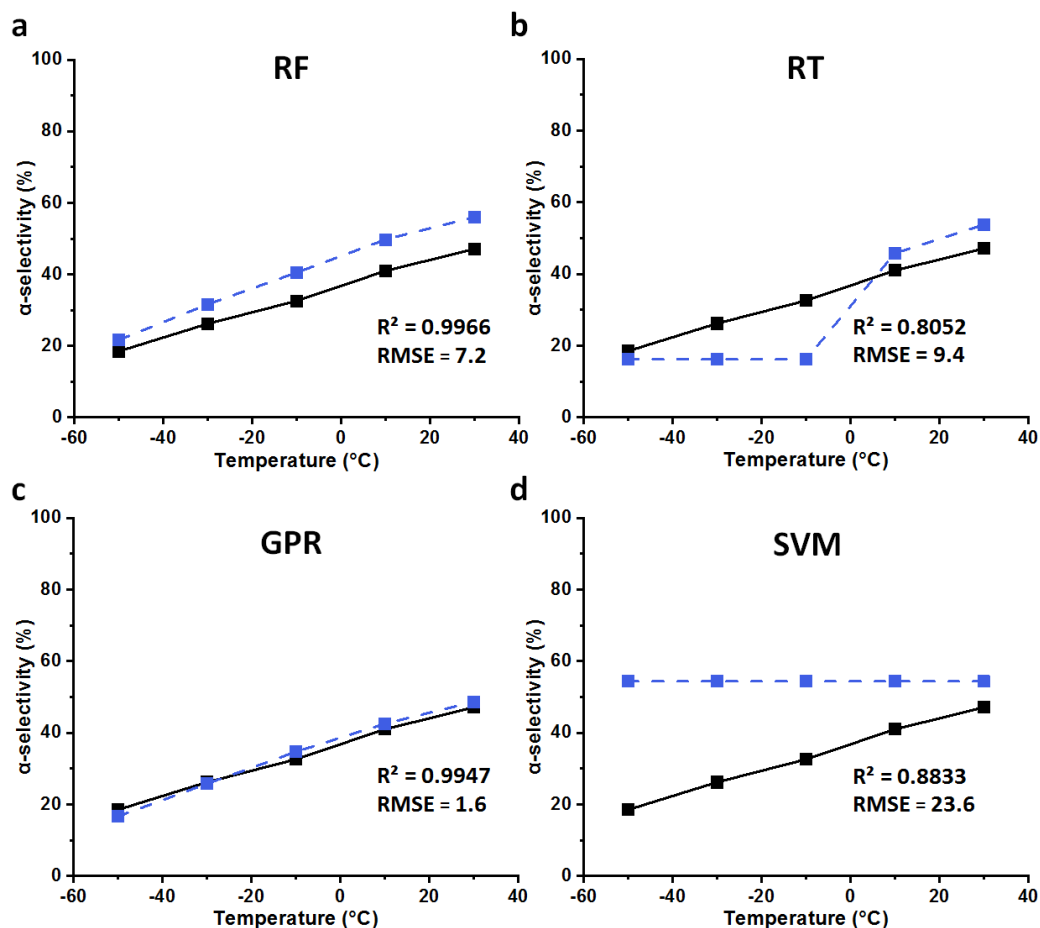
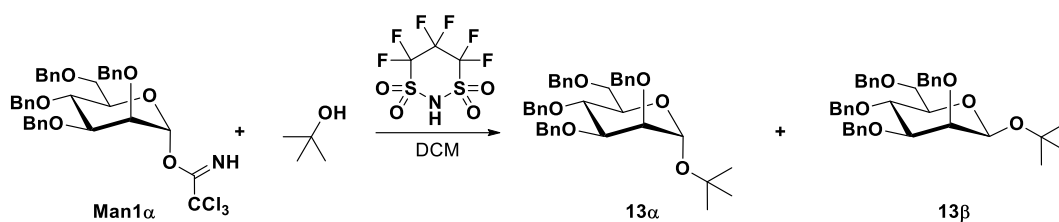


Figure 4.25: Validation data collected from the automated flow platform to predict $C_3F_6S_2O_4NH$ with **Gal1 α** . **a**, Prediction with Random Forest (RF). **b**, Prediction with Regression Tree (RT). **c**, Prediction with Gaussian Process Regression (GPR). **d**, Prediction with Support Vector Machine (SVR). Experimental (solid black line); Predicted (dashed colored line). For full experimental details, see entries 340-344 of Table 6.1 in Chapter 6.

Prediction of Activator- $C_3F_6S_2O_4NH$ with **Man1 α**

In the case of prediction of $C_3F_6S_2O_4NH$ with **Man1 α** , all four machine learning algorithms show similar RMSE values range from 16.2 to 18.7 (Figure 4.26). The prediction of a stereoselective plateau at lower temperatures with α -selectivity around 60% was observed, due to previous experimental results for Tf_2NH activator with **Man1 α** and *t*BuOH (Figure 3.15 in Chapter 3).



Temp. (°C)	Experimental	RF	RT	GPR	SVM
-50	36.7	57.4	56.7	54.2	56.3
-30	42.8	58.4	56.7	59.9	54.8
-10	48.2	65.6	59.3	71.4	64.8
10	64.4	92.1	91.5	85.4	86.1
30	98	99.2	91.5	95.3	92.4

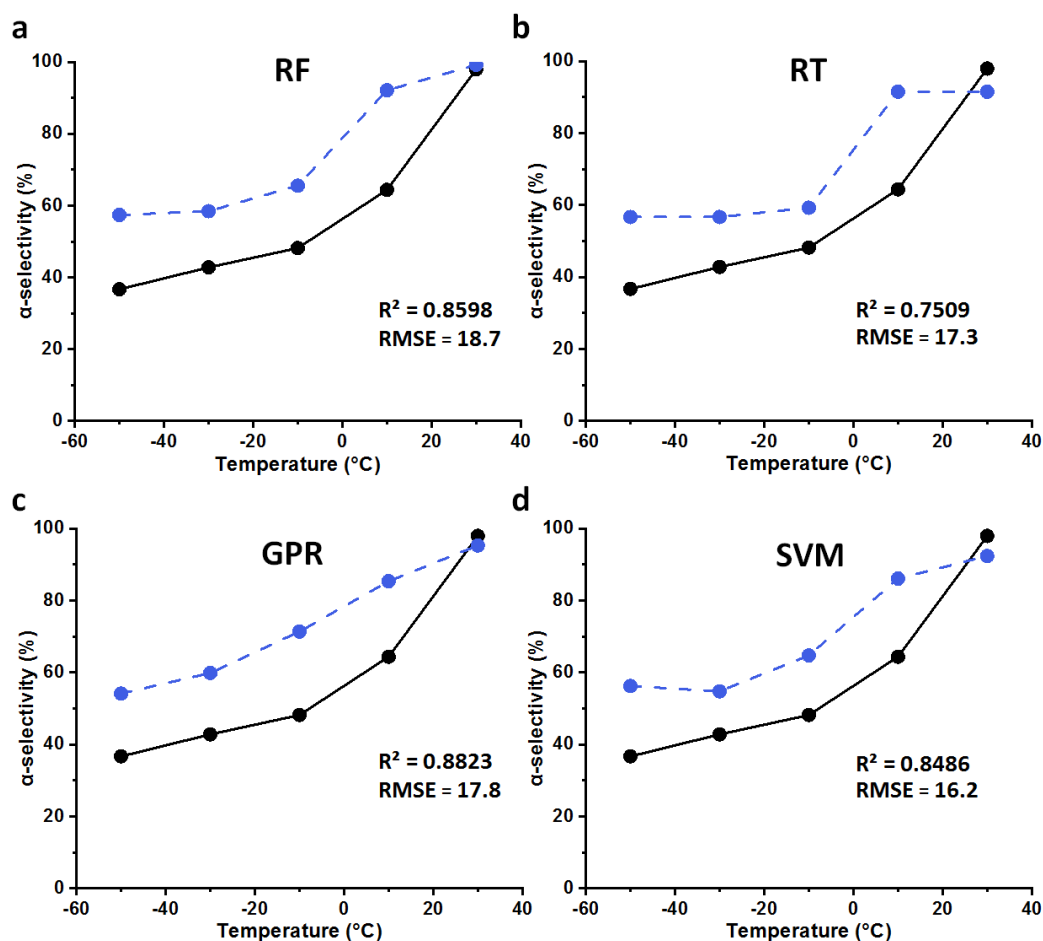
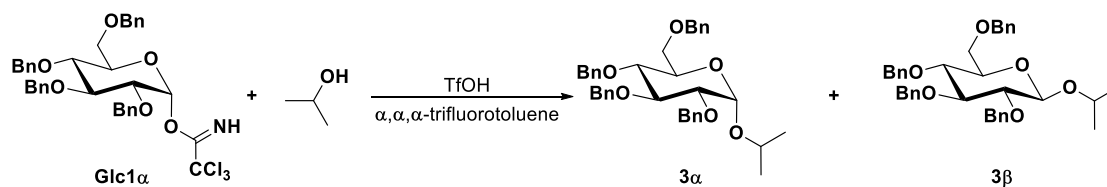


Figure 4.26: Validation data collected from the automated flow platform to predict $\text{C}_3\text{F}_6\text{S}_2\text{O}_4\text{NH}$ with Man1 α . **a**, Prediction with Random Forest (RF). **b**, Prediction with Regression Tree (RT). **c**, Prediction with Gaussian Process Regression (GPR). **d**, Prediction with Support Vector Machine (SVR). Experimental (solid black line); Predicted (dashed colored line). For full experimental details, see entries 345-349 of Table 6.1 in Chapter 6.

Prediction of Solvent- α,α,α -trifluorotoluene

The experimental and prediction results for the out-of-sample glycosylations involving α,α,α -trifluorotoluene as solvent coupling a glucose imidate donor and isopropanol as acceptor (Figure 4.27) reveal that RF clearly out performs RT, SVM and

GPR as shown by corresponding RMSE and R^2 values (Figure 4.27a). In the case of RF, RMSE and R^2 were 8.1 and 0.98 respectively which is better than other algorithms. However RT gives poorest prediction compared to RF, SVM and GPR, and fails to predict a temperature trend at lower temperature (Figure 4.27b).



Temp. (°C)	Experimental	RF	RT	GPR	SVM
-20	31.7	49.6	61.1	15.7	38.0
10	51.8	58.6	64.3	31.8	46.5
30	60.3	63.3	60.1	41.5	50.1
50	61.9	66.0	60.1	49.5	52.7
70	64.4	64.9	60.1	56.0	54.2
90	63.3	64.9	60.1	61.6	54.6

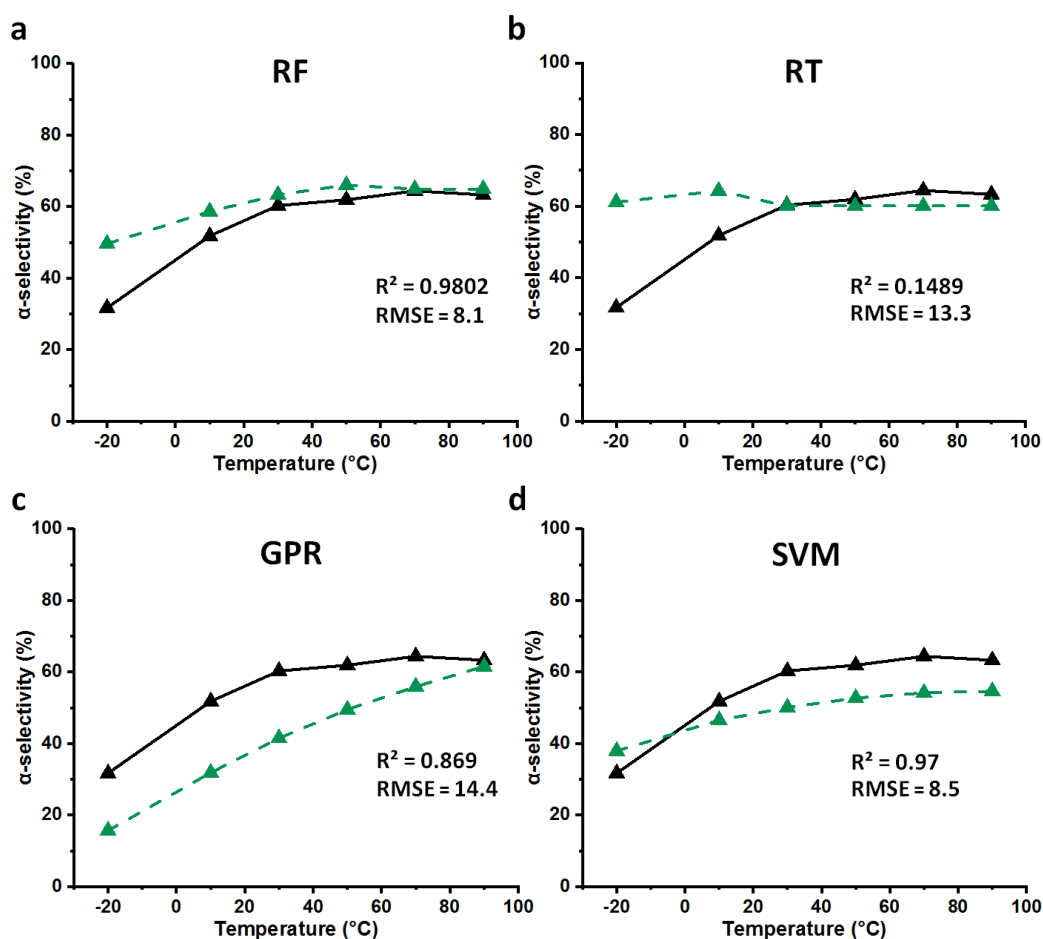
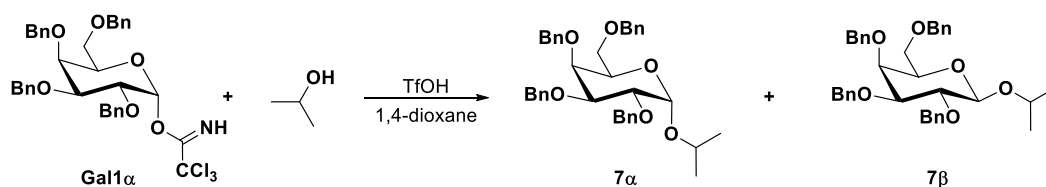


Figure 4.27: Validation data collected from the automated flow platform to predict α,α,α -trifluorotoluene. **a**, Prediction with Random Forest (RF). **b**, Prediction with Regression Tree (RT). **c**, Prediction with Gaussian Process Regression (GPR). **d**, Prediction with Support Vector Machine (SVR). Experimental (solid black line); Predicted (dashed colored line). For full experimental details, see entries 350-355 of Table 6.1 in Chapter 6.

Prediction of Solvent - 1,4-dioxane

In the case of prediction of 1,4-dioxane solvent, RF shows best prediction having RMSE and R^2 of 4.2 and 0.95 respectively (Figure 4.278). However, in the case of SVM, poor prediction was observed which gives an opposite trend to experimental data showing a decrease of α -product formation with temperature, and at 100 °C error was about 15% (Figure 4.278d).



Temp. (°C)	Experimental	RF	RT	GPR	SVM
20	67.9	60.2	49.9	71.5	71.4
40	71.3	68.3	68.3	73.5	74.9
60	73.1	71.2	68.3	74.5	74.3
80	73.9	71.2	68.3	73.6	67.3
100	74.2	71.2	68.3	71.4	59.6

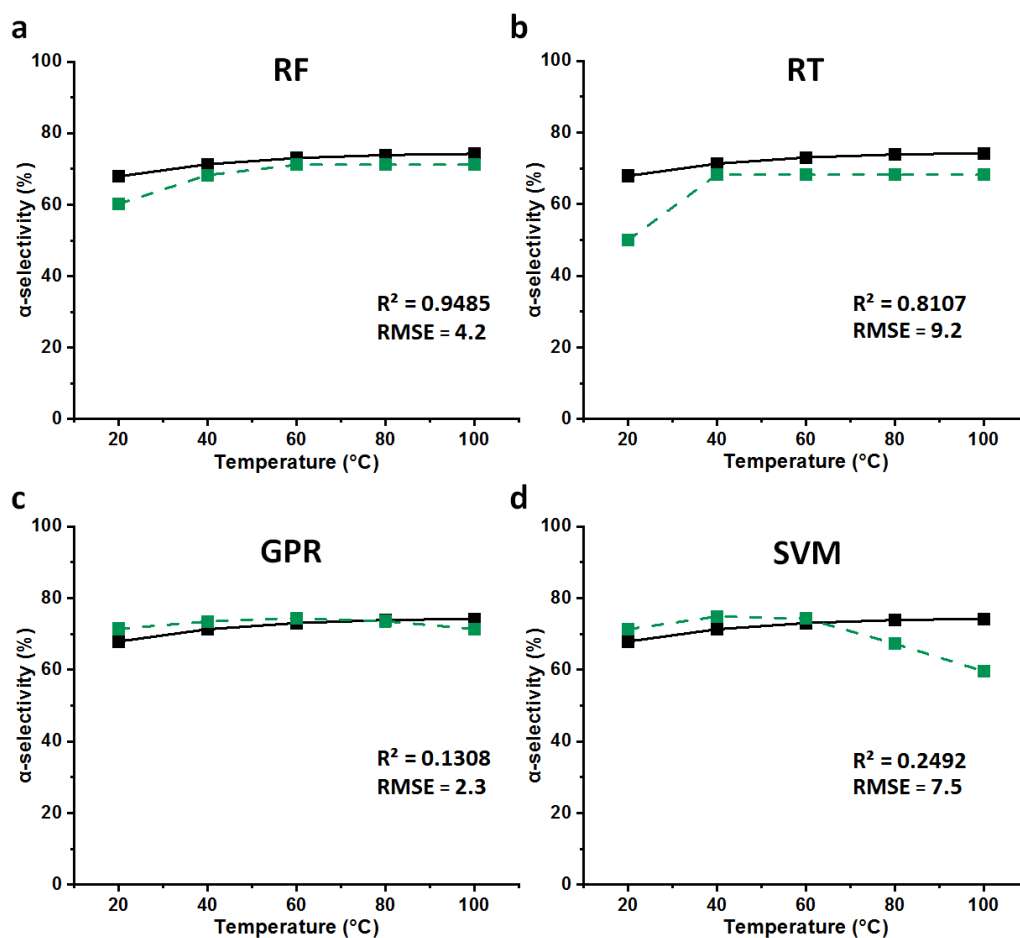
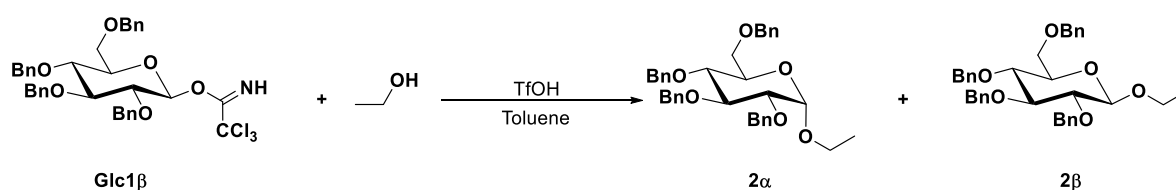


Figure 4.28: Validation data collected from the automated flow platform to predict 1,4-dioxane. **a**, Prediction with Random Forest (RF). **b**, Prediction with Regression Tree (RT). **c**, Prediction with Gaussian Process Regression (GPR). **d**, Prediction with Support Vector Machine (SVR). Experimental (solid black line); Predicted (dashed colored line). For full experimental details, see entries 356-360 of Table 6.1 in *Chapter 6*.

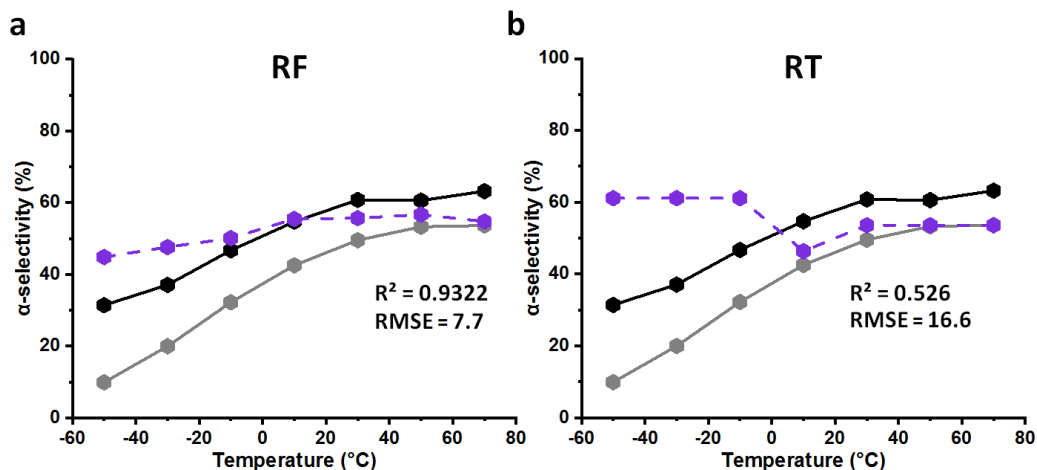
Prediction of leaving group stereochemistry

1) β -Glucose donor with ethanol in toluene

The experimental and prediction results for the out-of-sample glycosylations involving a glucose imidate donor with the leaving group as the beta anomer with ethanol as acceptor (Figure 4.29) reveal that RF gives best prediction having RMSE 7.2 and R^2 0.93 when compared to RT, SVM and GPR. Other three algorithms (RT, SVM and GPR) failed to predict the temperature trends of glycosylation with β -oriented leaving group donor and ethanol in toluene.



Temp. (°C)	Experimental	RF	RT	GPR	SVM
-50	31.4	44.8	61.1	60.3	53.4
-30	37.1	47.6	61.1	61.6	53.3
-10	46.7	50.1	61.1	64.0	53.8
10	54.7	55.5	46.4	66.1	54.2
30	60.8	55.7	53.6	66.8	54.4
50	60.6	56.7	53.6	66.4	54.5
70	63.2	54.8	53.6	66.7	54.5



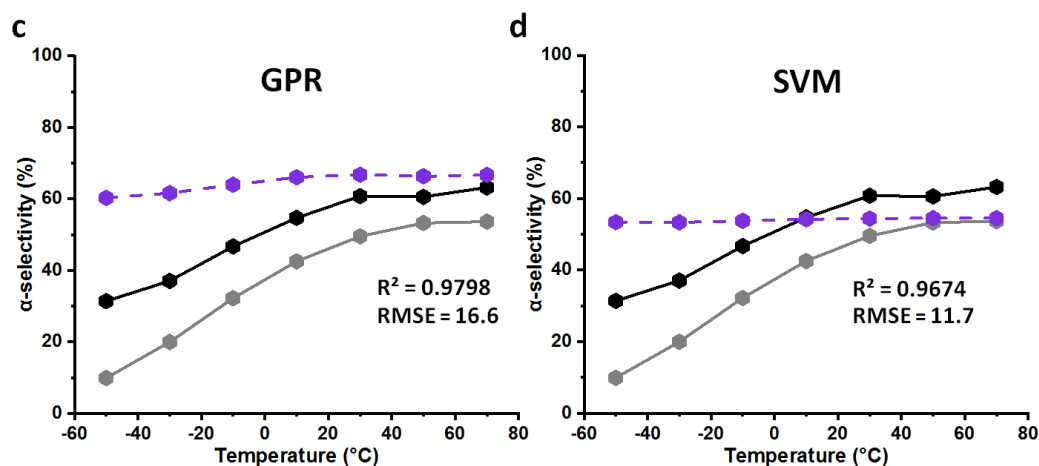
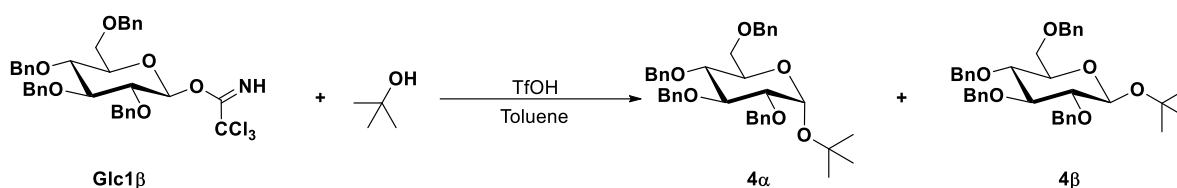


Figure 4.29: Validation data collected from the automated flow platform to predict β -glucose donor with ethanol in toluene. **a**, Prediction with Random Forest (RF). **b**, Prediction with Regression Tree (RT). **c**, Prediction with Gaussian Process Regression (GPR). **d**, Prediction with Support Vector Machine (SVR). Experimental (solid black line); Predicted (dashed colored line). For full experimental details, see entries 361-367 of Table 6.1 in Chapter 6.

2) β -Glucose donor with *tert*-butanol in toluene

The experimental and prediction results for the out-of-sample glycosylations involving a glucose imidate donor with the leaving group as the β -anomer with *tert*-butanol as acceptor (Figure 4.30) reveal that similar results were observed when compared to prediction of β -Glucose donor with ethanol in toluene (Figure 4.29). RF clearly outperforms RT, SVM and GPR which is shown by corresponding RMSE and R^2 values. In the case of RF, RMSE and R^2 were 7.0 and 0.90 respectively which is better than other algorithms. However, RT, GPR and SVM give poor prediction compared to RF and failed to predict the temperature trends.



Temp. (°C)	Experimental	RF	RT	GPR	SVM
-50	79.6	72.1	53.1	62.4	55.1
-30	78.6	69.5	53.1	63.0	55.3
-10	76.6	68.0	53.1	64.4	55.4
10	74.1	69.9	68.1	65.4	55.5
30	71.2	65.6	68.8	64.9	55.3
50	68.5	62.8	68.8	63.4	55.1
70	65.1	58.4	68.8	62.9	55.0

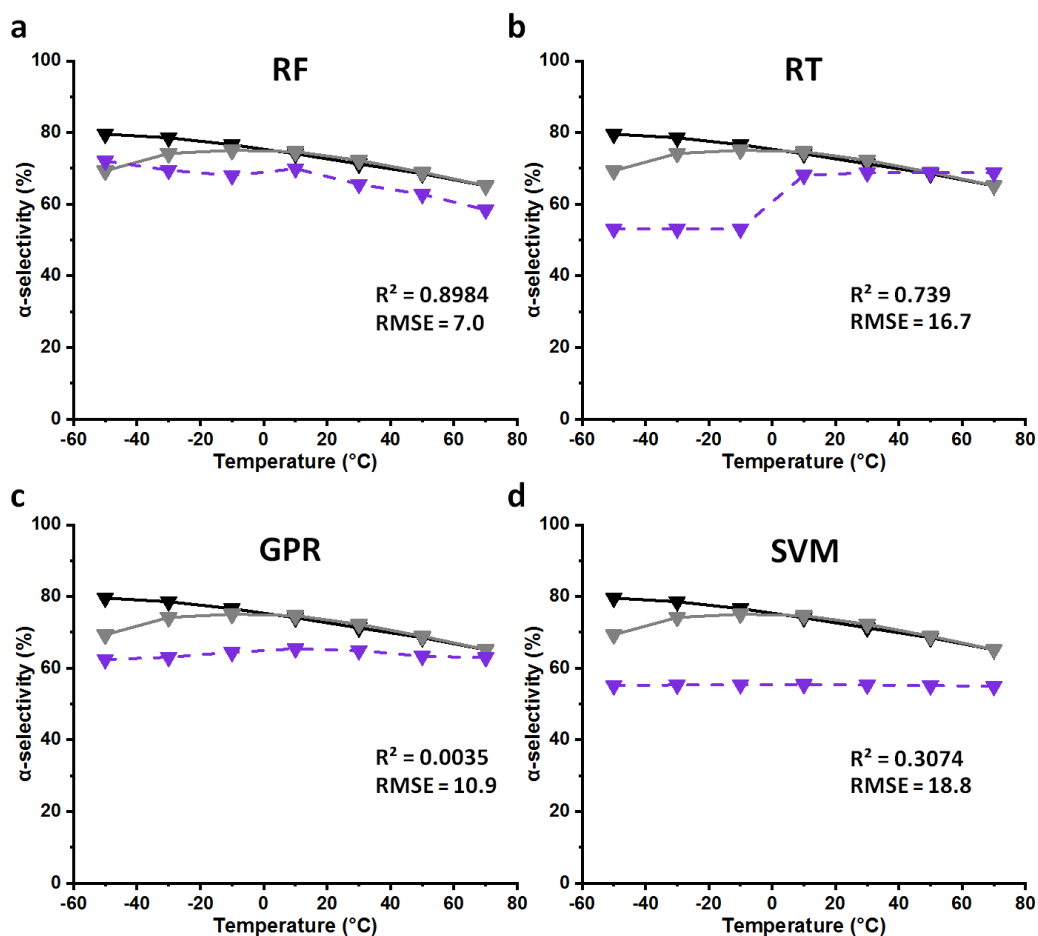
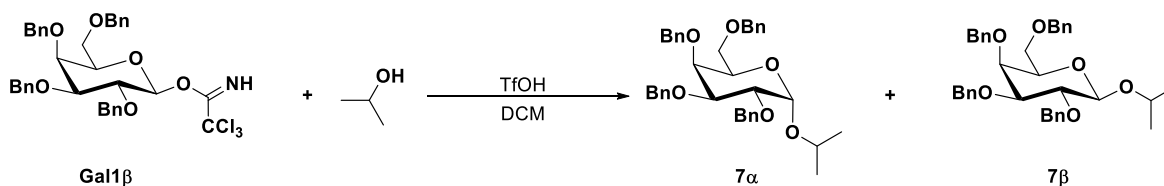


Figure 4.30: Validation data collected from the automated flow platform to predict β -glucose donor with *tert*-butanol in toluene. **a**, Prediction with Random Forest (RF). **b**, Prediction with Regression Tree (RT). **c**, Prediction with Gaussian Process Regression (GPR). **d**, Prediction with Support Vector Machine (SVR). Experimental (solid black line); Predicted (dashed colored line). For full experimental details, see entries 368-374 of Table 6.1 in Chapter 6.

3) β -Galactose donor with isopropanol in DCM

The prediction of β -galactose donor with isopropanol in DCM (Figure 4.31) reveal that RF out performs when compared to RT, SVM and GPR which is shown by corresponding RMSE 2.9 and R^2 0.99 values (Figure 4.31a). Also, RT and GPR algorithms perform quite well and predicts the experimental results with high accuracy (Figure 4.31b/c). However, SVM totally fails prediction of a temperature trend and gives highest RMSE of 16.6 (Figure 4.31d).



Temp. (°C)	Experimental	RF	RT	GPR	SVM
-50	23.4	27.1	33.4	25.4	51.4
-30	32.4	36.4	41.0	28.1	51.8
-10	39.7	40.8	49.6	31.5	52.9
10	47.2	45.5	49.9	36.2	53.6
30	55.0	52.5	53.8	41.8	54.0

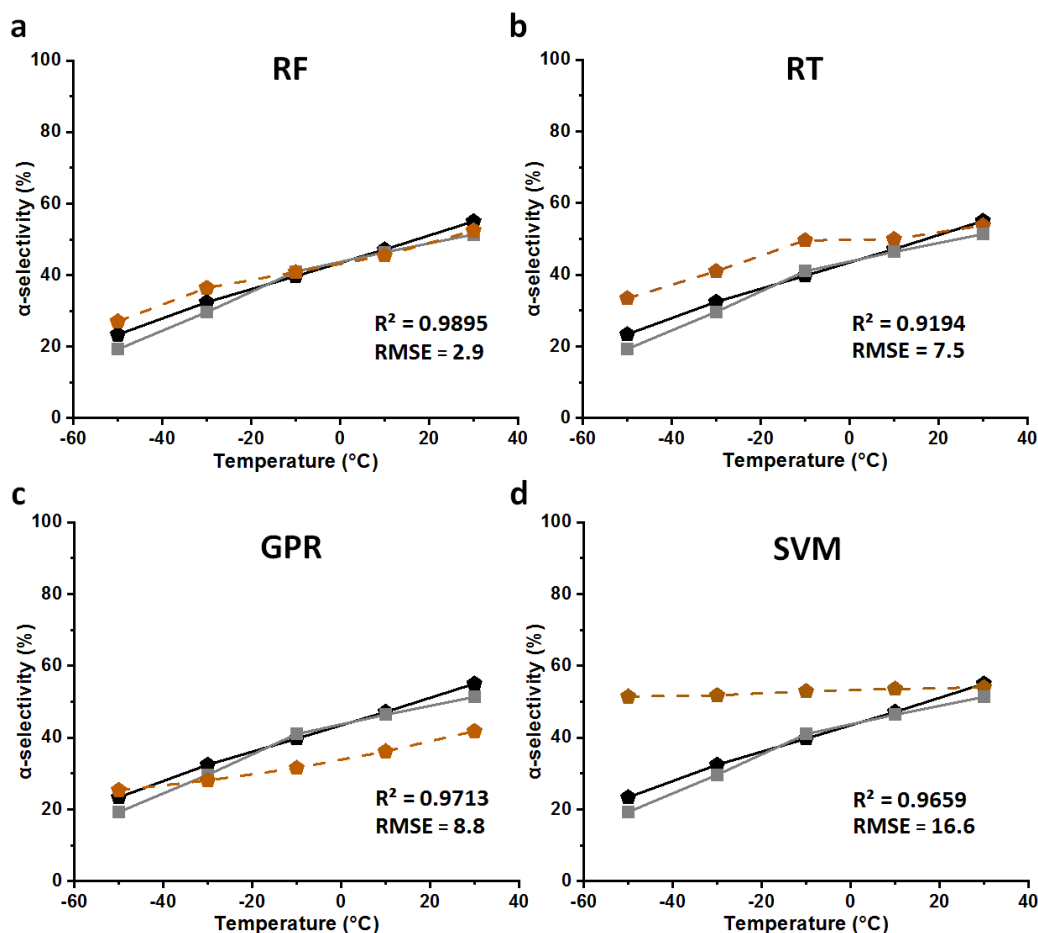
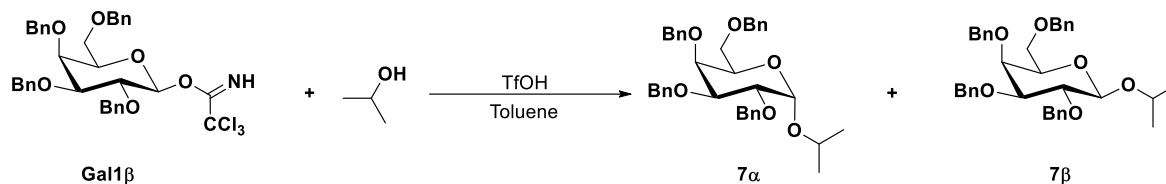


Figure 4.31: Validation data collected from the automated flow platform to predict β -galactose donor with isopropanol in DCM. **a**, Prediction with Random Forest (RF). **b**, Prediction with Regression Tree (RT). **c**, Prediction with Gaussian Process Regression (GPR). **d**, Prediction with Support Vector Machine (SVR). Experimental (solid black line); Predicted (dashed colored line). For full experimental details, see entries 375-379 of Table 6.1 in *Chapter 6*.

4) β -Galactose donor with isopropanol in toluene

The experimental and prediction results for the out-of-sample glycosylations involving a galactose imidate donor with the leaving group as the β -anomer with isopropanol as acceptor in toluene (Figure 4.32) reveal that the accuracy of RF and GPR algorithms were high (Figure 4.32a/c). In the case of RT, poorest prediction was observed (RMSE 17.1 and R^2 0.07, Figure 4.32b). The SVM totally failed to predict a temperature trend (Figure 4.32d).



Temp. (°C)	Experimental	RF	RT	GPR	SVM
-50	33.0	20.8	61.1	41.5	51.2
-30	34.3	28.7	61.1	44.7	50.8
-10	39.9	35.6	61.1	48.6	51.5
10	47.3	44.6	49.9	53.2	53.1
30	56.3	56.5	63.3	58.1	54.6
50	62.7	62.0	63.3	62.8	55.7
70	68.6	64.2	63.3	66.6	55.9

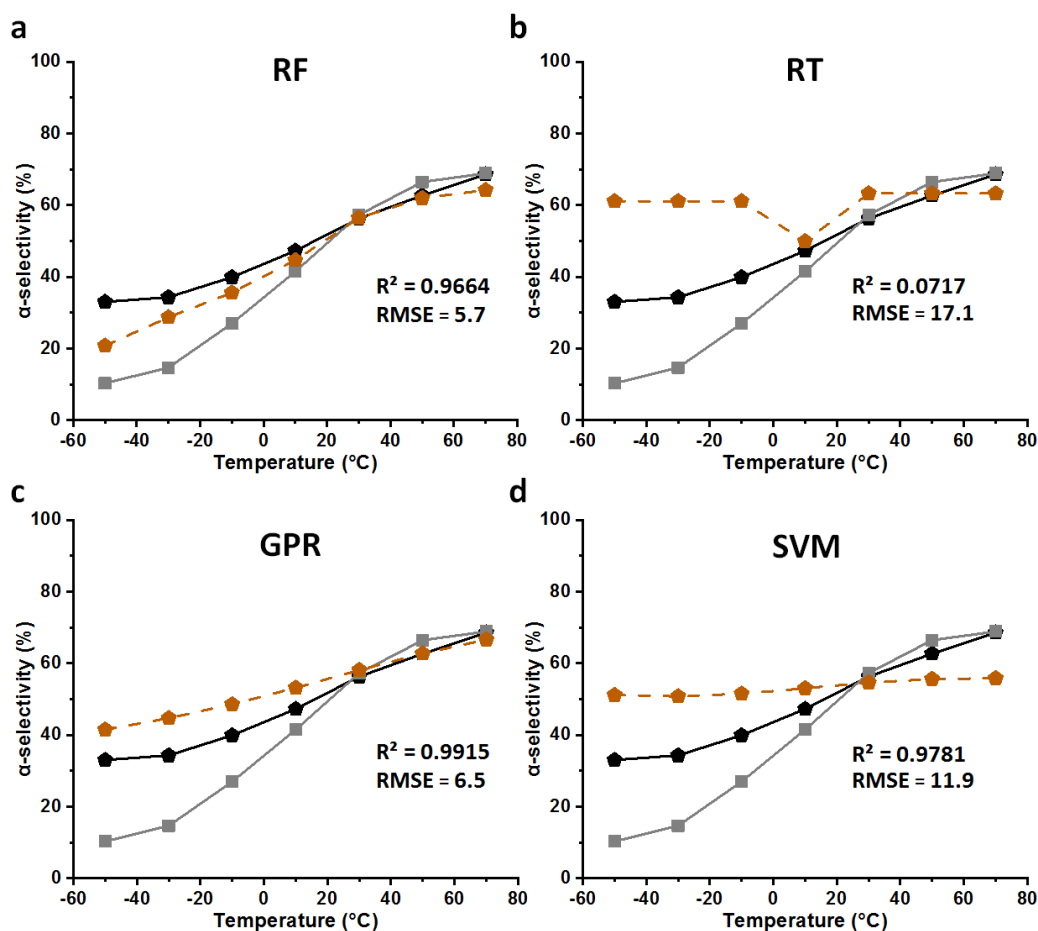


Figure 4.32: Validation data collected from the automated flow platform to predict β -galactose donor with isopropanol in toluene. **a**, Prediction with Random Forest (RF). **b**, Prediction with Regression Tree (RT). **c**, Prediction with Gaussian Process Regression (GPR). **d**, Prediction with Support Vector Machine (SVR). Experimental (solid black line); Predicted (dashed colored line). For full experimental details, see entries 380-386 of Table 6.1 in *Chapter 6*.

4.12 Conclusion

This chapter demonstrates the power of the machine learning in chemistry in general and for glycosylations in particular. A model was created utilizing a balanced dataset capable of accurately predicting one of the complex aspects of reaction outcomes – stereoselectivity – for one of the most complex reactions in organic chemistry – glycosylations. The fully reproducible dataset was generated on a continuous flow platform and utilized to train Random Forest algorithm. Chemical institution guided the identification of a set of variables to describe and quantify 13 individual factors influencing the stereoselectivity, describing steric and electronic factors of all four chemical species in the reaction: donor, acceptor, acid catalyst, solvent. The values were obtained through DFT calculations.

The model accurately predicts out-of-sample glycosylations – testing nucleophiles, electrophiles, catalysts, solvent, and temperature with an overall RMSE of only 8.9. All predictions were validated experimentally. Further, the model accurately predicts a previously unknown means of controlling glycosylation stereoselectivity. The approach will be applicable to better understand the stereoselectivity of other transformations based on reactions of nucleophiles and electrophiles.

Chapter 5 Conclusion and Recommendations

5.1 Conclusion

This thesis set out to address a variety of voids in our understanding of glycosylation chemistry. These gaps in the literature were presented as questions posed at the end of *Chapter 1, Section 1.9*. These are as follows:

- 1) Can an automated flow platform provide reproducible glycosylation data, which is scarce in the present literature?
- 2) Will I be able successfully identify, interrogate, and study various factors influencing the stereochemical output of glycosylation in an automated flow platform?
- 3) Can I generate a thorough understanding of the mechanism of glycosylation using such a platform?
- 4) Finally, can I predict the stereoselectivity of a glycosylation reaction by application of flow chemistry, automation, and machine learning techniques?

Through the systematic studies and research presented in *Chapters 2, 3 and 4*, answers to these questions were sought. An overview of the carbohydrate chemistry literature in *Chapter 1* revealed chemical glycosylation is an extremely sensitive reaction and controlling stereoselectivity of this reaction depends on a number of factors, namely those presented by the reagents (permanent) and the conditions of the coupling (environmental). Permanent factors dictate judicious choices of coupling partners, whereas environmental factors need to be controlled precisely to reproducibly obtain the expected selectivity in high yield. A canonical approach of controlling stereoselectivity of glycosylation reaction in batch can be significantly improved by running the reaction in continuous miniaturized reactors commonly known as microreactors. This continuous mode of operation, called flow chemistry, has several advantages compared to its batch counterparts, including better mixing and temperature control.

Taking advantage of this increased control, an automated microreactor-based flow platform was designed and built as part of this research project. The automated flow platform consists of a computerized temperature controlled silicon based microreactor. Computer controlled, high precision syringe pumps were used to deliver reagents into the reactor and automated reaction analysis were carried out using in-line HPLC analysis. The software for the whole system was programmed in LabVIEW as was described in detail in *Chapter 2* of this thesis.

In *Chapters 2* and *3*, I demonstrate that is possible to control and generate reproducible environmental conditions inside a microreactor based platform. By coupling such a platform with automation, human errors could be minimized, leading to the generation of glycosylation data without human intervention. The system generated highly reproducible chemical glycosylation data, which was generally not observed in the literature before. With such an automated flow platform in hand, it was possible to thoroughly interrogate various factors such as influence of the pyran core of donor, including three leaving groups of donor namely, trichloroimidates, thioethers and phosphase, donor concentration, choice of the acceptors interms of both sterics and electronics, chemical equivalence of acceptors, reaction temperature, choice of activator, solvent, chemical equivalence, and water content, which influences the stereoselectivity of glycosylation in systematic manner.

This thesis reveals that temperature plays a highly influential role in determining the stereoselectivity. As such, the other potential influencing factors were screened as a function of temperature, comparing judiciously chosen combinations of donors, acceptors, activators, and solvents. The 386 reproducible data points generated afforded an overall empirical understanding of the various factors influencing the stereoselectivity of glycosylations. These reproducible data points presented a perfect opportunity to apply machine learning algorithms to build a model capable of predicting the stereoselectivity of glycosylations.

Random Forest (RF) algorithm was chosen, owing its success in the literature for predicting chemistry data. However, to predict continuous parameters such as stereoselectivity, regression-based RF was chosen instead of classification based machine learning algorithm, as the latter is only capable of generating categorical outputs such as whether a reaction is fast or slow or the reaction will occur or not. Hence, the underlying chemical intuition, which was generated at the end of *Chapter 3*, was used to calculate

numerically relevant descriptors to combine with the 268 experimental data points to generate training set for training the machine learning algorithm, which was described in detail in *Chapter 4* of this thesis. For numerical descriptor generation, key properties such as reactivities, nucleophilicities, and sterics were calculated using density functional theory (DFT) calculations at B3LYP 6-31G* and B3LYP 6-311G* levels of theory. Donor properties were successfully represented by ^{13}C NMR chemical shift (ppm) on carbon 1 position, Dihedral angles ($^\circ$) of X1-C1-C2-O2, O2-C2-C3-O3, O3-C3-C4-O4, and O4-C4-C5-C6). Similarly for acceptor, exposed surface area (\AA^2) of oxygen and α -carbon in a space-filling model and ^{17}O NMR chemical shift of hydroxyl group were calculated. Activators were numerically explained by HOMO (highest occupied molecular orbital) energy value and the oxygen (O^-) or nitrogen anion (N^-) exposed surface area. Minimum value of the electrostatic potential (MinElPot) and maximum value of the electrostatic potential (MaxElPot) were used for Solvents. Experimental data obtained from the automated flow platform was combined with the DFT based numerical descriptors to generate the training set, which was used to train the Random Forest algorithm.

Different factors influencing the stereoselectivity of glycosylation reactions such as choice of acceptors, donors, activators, solvent choice and temperature were trained with Random Forest algorithm. With the model in hand, the stereoselectivity of glycosylation with the combination of new donor, acceptor, activator, solvent and temperature were predicted and subsequently validated experimentally. In the end, the model could successfully predict out-of-sample glycosylations with an overall accuracy of 91%. Furthermore, during this study, the effect of the influence of donor's leaving groups on the stereoselectivity in specific solvents was revealed. This previously unknown effect could be successfully predicted with the model in hand and was subsequently validated the prediction and validation, the RF model predicts the influence of the donor leaving group's orientation in different solvents which is a previously unknown means of controlling glycosylation stereoselectivity.

5.2 Recommendations

A systematic study was carried to study a model glycosylation reaction that involved model perbenzylated donors and model acceptors. Owing to the fact that consistent and reproducible data was obtained for this model reaction in the automated flow platform, the study needs to be expanded to include other important factors given below:

1) Influence of protecting groups:

The importance of protecting groups in influencing the stereochemical outcome of glycosylation is well known in the literature. Chapter 3 was given a brief account of effects by different protecting group on 4- and/or 6-position using acetyl group (OAc). This study can be easily expanded by systematic study of influence of various protecting groups including non-/participating, electron withdrawing/donating and their positions in the pyran ring for dictating the stereochemical outcome of the reaction.

2) Complex glycosyl nucleophiles:

To study glycosyations in this thesis, simple nucleophiles were used such as methanol, ethanol, isopropanol, *tert*-butanol and perbenbnzylated primary sugar nucleophiles. However, glycosylations with secondary hydroxyl groups on sugar acceptors were not possible. Hence, the scope for acceptors needs to be expanded and glycosyl nucleophiles having more complexity which have various stereochemical and primary/secondary hydroxyl group, which needs to be taken into account.

3) Longer residence time:

The maximum residence time that can be currently attained in the automated flow platform is 270 seconds. However, less reactive coupling partners, may need more residence time in the reactor, hence implementation of longer residence time by redesigning the microchip or implementing tubular reactor is recommended in the future for this system.

4) Faster analysis:

Finding a proper HPLC method to separate diastereomers (α/β -products) is one of the most difficult tasks of the work flow. For this study, the longest HPLC method used in the automated flow platform is around 20 minutes, which is a major bottleneck. Implementation of a faster analysis platform other than conventional HPLC such as inline flow NMR or UHPLC can lead to faster and more data acquisition.

5) Implementation of active learning:

The machine learning algorithm, implemented in *Chapter 4* of this thesis, can be coupled with the LabVIEW control software of the automated flow platform. By doing so, predictions generated by the machine learning model can be directly fed back to the control algorithm. This will implement active learning and automated prediction in the flow platform. In order to make such machine a reality, a reagent and solvent delivery system capable of simultaneously incorporating multiple donors, acceptors, activators and solvents with automated inline dilution similar to the system described elsewhere needs to be implemented in the automated flow-chemical platform.¹¹⁰ The data coming from this modified system needs to be fed back to the Random Forest based machine-learning algorithm. Once a new optimized data point is predicted, it needs to go through an automated experimental validation process guided by an accuracy parameter. This automated process could then be repeated using several combinations of reagents and temperatures guided by a DOE (Design of Experiments) algorithm until the desired accuracy between the prediction and experimental data is obtained. In the hand of a glycochemist, this autonomous machine can learn and perform glycosylation eventually generating a very broad training set. In the near future such machine can guide the synthesis of complex oligosaccharides, thus becoming a must have toolbox, for any glycochemist.

Chapter 6 Experimental section

6.1 Total experimental data collected from the automated flow platform.

Table 6.1: Total experimental data collected from the automated flow platform

Donor (mM) + Acceptor (mM)		Activator (mM)			Solvent			Residence Time (sec)			Temperature (°C)			α -selectivity (%) (= 100 - β -selectivity)	
Entry	Temp. (°C)	Donor	Acceptor	Activator	Solvent	Donor Equiv.	Acceptor Equiv.	Activator Equiv.	Donor Conc.	T _{res} (sec)	Yield (%)	α ratio (%)	Product		
1	-50	Glc1 α	MeOH	TfOH	DCM	1.2	1	0.2	10	45	92.4	29.6	1 $\alpha\beta$		
2	-30	Glc1 α	MeOH	TfOH	DCM	1.2	1	0.2	10	45	95.7	32.5	1 $\alpha\beta$		
3	-10	Glc1 α	MeOH	TfOH	DCM	1.2	1	0.2	10	45	98.7	38.7	1 $\alpha\beta$		
4	10	Glc1 α	MeOH	TfOH	DCM	1.2	1	0.2	10	45	98.1	46.5	1 $\alpha\beta$		
5	20	Glc1 α	MeOH	TfOH	DCM	1.2	1	0.2	10	45	94.1	48.7	1 $\alpha\beta$		
6	30	Glc1 α	MeOH	TfOH	DCM	1.2	1	0.2	10	45	93.7	52.6	1 $\alpha\beta$		
7	-50	Glc1 α	EtOH	TfOH	DCM	1.2	1	0.2	10	45	83.2	15.5	2 $\alpha\beta$		
8	-30	Glc1 α	EtOH	TfOH	DCM	1.2	1	0.2	10	45	83.5	29.4	2 $\alpha\beta$		
9	-10	Glc1 α	EtOH	TfOH	DCM	1.2	1	0.2	10	45	100.0	36.0	2 $\alpha\beta$		
10	10	Glc1 α	EtOH	TfOH	DCM	1.2	1	0.2	10	45	87.0	46.2	2 $\alpha\beta$		
11	20	Glc1 α	EtOH	TfOH	DCM	1.2	1	0.2	10	45	90.7	50.2	2 $\alpha\beta$		
12	30	Glc1 α	EtOH	TfOH	DCM	1.2	1	0.2	10	45	83.5	55.5	2 $\alpha\beta$		
13	-50	Glc1 α	iPrOH	TfOH	DCM	1.2	1	0.2	10	45	98.3	26.9	3 $\alpha\beta$		
14	-30	Glc1 α	iPrOH	TfOH	DCM	1.2	1	0.2	10	45	88.5	38.8	3 $\alpha\beta$		
15	-10	Glc1 α	iPrOH	TfOH	DCM	1.2	1	0.2	10	45	90.1	46.7	3 $\alpha\beta$		
16	10	Glc1 α	iPrOH	TfOH	DCM	1.2	1	0.2	10	45	99.2	52.6	3 $\alpha\beta$		
17	20	Glc1 α	iPrOH	TfOH	DCM	1.2	1	0.2	10	45	84.0	57.7	3 $\alpha\beta$		
18	30	Glc1 α	iPrOH	TfOH	DCM	1.2	1	0.2	10	45	82.1	61.0	3 $\alpha\beta$		
19	-50	Glc1 β	iPrOH	TfOH	DCM	1.2	1	0.2	10	45	88.6	27.7	3 $\alpha\beta$		
20	-45	Glc1 β	iPrOH	TfOH	DCM	1.2	1	0.2	10	45	79.4	30.6	3 $\alpha\beta$		
21	-40	Glc1 β	iPrOH	TfOH	DCM	1.2	1	0.2	10	45	70.6	32.7	3 $\alpha\beta$		
22	-35	Glc1 β	iPrOH	TfOH	DCM	1.2	1	0.2	10	45	65.0	34.4	3 $\alpha\beta$		
23	-30	Glc1 β	iPrOH	TfOH	DCM	1.2	1	0.2	10	45	77.9	36.7	3 $\alpha\beta$		
24	-25	Glc1 β	iPrOH	TfOH	DCM	1.2	1	0.2	10	45	72.4	37.4	3 $\alpha\beta$		
25	-20	Glc1 β	iPrOH	TfOH	DCM	1.2	1	0.2	10	45	71.2	38.6	3 $\alpha\beta$		
26	-15	Glc1 β	iPrOH	TfOH	DCM	1.2	1	0.2	10	45	94.7	41.9	3 $\alpha\beta$		
27	-10	Glc1 β	iPrOH	TfOH	DCM	1.2	1	0.2	10	45	94.7	43.7	3 $\alpha\beta$		
28	-5	Glc1 β	iPrOH	TfOH	DCM	1.2	1	0.2	10	45	95.9	45.6	3 $\alpha\beta$		
29	5	Glc1 β	iPrOH	TfOH	DCM	1.2	1	0.2	10	45	93.5	50.5	3 $\alpha\beta$		
30	10	Glc1 β	iPrOH	TfOH	DCM	1.2	1	0.2	10	45	94.8	53.2	3 $\alpha\beta$		
31	15	Glc1 β	iPrOH	TfOH	DCM	1.2	1	0.2	10	45	87.1	55.0	3 $\alpha\beta$		
32	20	Glc1 β	iPrOH	TfOH	DCM	1.2	1	0.2	10	45	89.4	56.8	3 $\alpha\beta$		
33	25	Glc1 β	iPrOH	TfOH	DCM	1.2	1	0.2	10	45	88.7	58.3	3 $\alpha\beta$		
34	30	Glc1 β	iPrOH	TfOH	DCM	1.2	1	0.2	10	45	79.1	59.6	3 $\alpha\beta$		

Entry	Temp. (°C)	Donor	Acceptor	Activator	Solvent	Donor Equiv.	Acceptor Equiv.	Activator Equiv.	Donor Conc.	T _{res} (sec)	Yield (%)	α ratio (%)	Product
35	-50	Glc1α	tBuOH	TfOH	DCM	1.2	1	0.2	10	45	77.9	38.1	4αβ
36	-30	Glc1α	tBuOH	TfOH	DCM	1.2	1	0.2	10	45	87.7	44.8	4αβ
37	-10	Glc1α	tBuOH	TfOH	DCM	1.2	1	0.2	10	45	88.3	54.5	4αβ
38	10	Glc1α	tBuOH	TfOH	DCM	1.2	1	0.2	10	45	88.3	62.8	4αβ
39	20	Glc1α	tBuOH	TfOH	DCM	1.2	1	0.2	10	45	91.5	66.8	4αβ
40	30	Glc1α	tBuOH	TfOH	DCM	1.2	1	0.2	10	45	80.7	71.0	4αβ
41	-10	Glc2β	iPrOH	TfOH ^d	DCM	1.2	1	0.2	10	45	44.6	38.0	3αβ
42	10	Glc2β	iPrOH	TfOH ^d	DCM	1.2	1	0.2	10	45	88.1	54.5	3αβ
43	20	Glc2β	iPrOH	TfOH ^d	DCM	1.2	1	0.2	10	45	89.5	57.5	3αβ
44	30	Glc2β	iPrOH	TfOH ^d	DCM	1.2	1	0.2	10	45	90.4	63.8	3αβ
45	-50	Glc1α	tBuOH	Tf2NH	DCM	1.2	1	0.2	10	45	67.2	6.1	4αβ
46	-30	Glc1α	tBuOH	Tf2NH	DCM	1.2	1	0.2	10	45	62.1	16.8	4αβ
47	-10	Glc1α	tBuOH	Tf2NH	DCM	1.2	1	0.2	10	45	55.2	35.2	4αβ
48	20	Glc1α	tBuOH	Tf2NH	DCM	1.2	1	0.2	10	45	59.5	47.9	4αβ
49	-50	Glc1α	iPrOH	Tf2NH	DCM	1.2	1	0.2	10	45	95.5	8.7	3αβ
50	-30	Glc1α	iPrOH	Tf2NH	DCM	1.2	1	0.2	10	45	89.3	16.4	3αβ
51	-10	Glc1α	iPrOH	Tf2NH	DCM	1.2	1	0.2	10	45	82.2	26.8	3αβ
52	10	Glc1α	iPrOH	Tf2NH	DCM	1.2	1	0.2	10	45	79.2	42.1	3αβ
53	20	Glc1α	iPrOH	Tf2NH	DCM	1.2	1	0.2	10	45	76.7	47.5	3αβ
54	30	Glc1α	iPrOH	Tf2NH	DCM	1.2	1	0.2	10	45	76.0	55.0	3αβ
55	-50	Glc1α	EtOH	Tf2NH	DCM	1.2	1	0.2	10	45	64.2	5.8	2αβ
56	-30	Glc1α	EtOH	Tf2NH	DCM	1.2	1	0.2	10	45	64.1	10.4	2αβ
57	-10	Glc1α	EtOH	Tf2NH	DCM	1.2	1	0.2	10	45	62.6	19.6	2αβ
58	10	Glc1α	EtOH	Tf2NH	DCM	1.2	1	0.2	10	45	65.5	33.6	2αβ
59	20	Glc1α	EtOH	Tf2NH	DCM	1.2	1	0.2	10	45	57.4	39.0	2αβ
60	30	Glc1α	EtOH	Tf2NH	DCM	1.2	1	0.2	10	45	53.8	45.0	2αβ
61	-50	Glc1α	iPrOH	TfOH	Toluene	1.2	1	0.2	10	45	65.7	19.1	3αβ
62	-30	Glc1α	iPrOH	TfOH	Toluene	1.2	1	0.2	10	45	84.0	35.5	3αβ
63	-10	Glc1α	iPrOH	TfOH	Toluene	1.2	1	0.2	10	45	86.2	49.9	3αβ
64	10	Glc1α	iPrOH	TfOH	Toluene	1.2	1	0.2	10	45	85.0	61.6	3αβ
65	30	Glc1α	iPrOH	TfOH	Toluene	1.2	1	0.2	10	45	84.5	64.1	3αβ
66	50	Glc1α	iPrOH	TfOH	Toluene	1.2	1	0.2	10	45	81.3	63.9	3αβ
67	70	Glc1α	iPrOH	TfOH	Toluene	1.2	1	0.2	10	45	70.2	62.3	3αβ
68	-50	Glc1β	iPrOH	TfOH	Toluene	1.2	1	0.2	10	45	84.8	60.8	3αβ
69	-30	Glc1β	iPrOH	TfOH	Toluene	1.2	1	0.2	10	45	85.4	60.3	3αβ
70	-10	Glc1β	iPrOH	TfOH	Toluene	1.2	1	0.2	10	45	90.9	62.2	3αβ
71	10	Glc1β	iPrOH	TfOH	Toluene	1.2	1	0.2	10	45	86.1	65.6	3αβ
72	30	Glc1β	iPrOH	TfOH	Toluene	1.2	1	0.2	10	45	85.3	63.3	3αβ
73	50	Glc1β	iPrOH	TfOH	Toluene	1.2	1	0.2	10	45	68.6	62.2	3αβ
74	70	Glc1β	iPrOH	TfOH	Toluene	1.2	1	0.2	10	45	56.9	61.2	3αβ
75	-50	Glc1α	EtOH	TfOH	Toluene	1.2	1	0.2	10	45	90.4	9.9	2αβ
76	-30	Glc1α	EtOH	TfOH	Toluene	1.2	1	0.2	10	45	91.5	20.0	2αβ
77	-10	Glc1α	EtOH	TfOH	Toluene	1.2	1	0.2	10	45	89.7	32.2	2αβ
78	10	Glc1α	EtOH	TfOH	Toluene	1.2	1	0.2	10	45	85.8	42.5	2αβ
79	30	Glc1α	EtOH	TfOH	Toluene	1.2	1	0.2	10	45	82.2	49.6	2αβ
80	50	Glc1α	EtOH	TfOH	Toluene	1.2	1	0.2	10	45	75.6	53.3	2αβ
81	70	Glc1α	EtOH	TfOH	Toluene	1.2	1	0.2	10	45	68.4	53.7	2αβ
82	-50	Glc1α	tBuOH	TfOH	Toluene	1.2	1	0.2	10	45	43.0	69.3	4αβ
83	-30	Glc1α	tBuOH	TfOH	Toluene	1.2	1	0.2	10	45	64.7	74.2	4αβ
84	-10	Glc1α	tBuOH	TfOH	Toluene	1.2	1	0.2	10	45	83.7	75.1	4αβ
85	10	Glc1α	tBuOH	TfOH	Toluene	1.2	1	0.2	10	45	82.8	74.7	4αβ
86	30	Glc1α	tBuOH	TfOH	Toluene	1.2	1	0.2	10	45	78.5	72.3	4αβ
87	50	Glc1α	tBuOH	TfOH	Toluene	1.2	1	0.2	10	45	75.7	68.9	4αβ
88	70	Glc1α	tBuOH	TfOH	Toluene	1.2	1	0.2	10	45	67.5	65.2	4αβ

Entry	Temp. (°C)	Donor	Acceptor	Activator	Solvent	Donor Equiv.	Acceptor Equiv.	Activator Equiv.	Donor Conc.	T _{res} (sec)	Yield (%)	α ratio (%)	Product
89	-30	Glc1α	iPrOH	TfOH	ACN	1.2	1	0.2	10	45	79.7	9.5	3αβ
90	-10	Glc1α	iPrOH	TfOH	ACN	1.2	1	0.2	10	45	74.1	14.0	3αβ
91	10	Glc1α	iPrOH	TfOH	ACN	1.2	1	0.2	10	45	71.4	21.7	3αβ
92	30	Glc1α	iPrOH	TfOH	ACN	1.2	1	0.2	10	45	75.9	25.1	3αβ
93	50	Glc1α	iPrOH	TfOH	ACN	1.2	1	0.2	10	45	78.4	31.0	3αβ
94	70	Glc1α	iPrOH	TfOH	ACN	1.2	1	0.2	10	45	76.9	41.8	3αβ
95	-50	Glc1α	iPrOH	TfOH	MTBE	1.2	1	0.2	10	45	70.5	84.7	3αβ
96	-30	Glc1α	iPrOH	TfOH	MTBE	1.2	1	0.2	10	45	72.4	89.5	3αβ
97	-10	Glc1α	iPrOH	TfOH	MTBE	1.2	1	0.2	10	45	67.7	87.6	3αβ
98	10	Glc1α	iPrOH	TfOH	MTBE	1.2	1	0.2	10	45	80.6	88.2	3αβ
99	30	Glc1α	iPrOH	TfOH	MTBE	1.2	1	0.2	10	45	65.2	85.0	3αβ
100	50	Glc1α	iPrOH	TfOH	MTBE	1.2	1	0.2	10	45	57.3	82.4	3αβ
101	-50	Glc1β	iPrOH	TfOH	MTBE	1.2	1	0.2	10	45	14.5	95.5	3αβ
102	-30	Glc1β	iPrOH	TfOH	MTBE	1.2	1	0.2	10	45	55.6	93.3	3αβ
103	-10	Glc1β	iPrOH	TfOH	MTBE	1.2	1	0.2	10	45	54.6	92.6	3αβ
104	10	Glc1β	iPrOH	TfOH	MTBE	1.2	1	0.2	10	45	60.0	89.7	3αβ
105	30	Glc1β	iPrOH	TfOH	MTBE	1.2	1	0.2	10	45	56.9	87.6	3αβ
106	50	Glc1β	iPrOH	TfOH	MTBE	1.2	1	0.2	10	45	47.5	85.4	3αβ
107 ^c	-50	Glc1α	iPrOH	TfOH	DCM	1.2	1	0.2	10	45	68.2	29.6	3αβ
108 ^c	30	Glc1α	iPrOH	TfOH	DCM	1.2	1	0.2	10	45	74.0	61.1	3αβ
109	-40	Glc1α	iPrOH	TfOH	DCM	1.2	1	0.2	4.8	45	61.0	32.6	3αβ
110	-10	Glc1α	iPrOH	TfOH	DCM	1.2	1	0.2	4.8	45	99.3	41.5	3αβ
111	20	Glc1α	iPrOH	TfOH	DCM	1.2	1	0.2	4.8	45	78.4	57.8	3αβ
112	30	Glc1α	iPrOH	TfOH	DCM	1.2	1	0.2	4.8	45	74.7	58.9	3αβ
113	20	Glc1α	tBuOH	TfOH	DCM	1.2	1	0.2	4.8	45	73.6	65.2	4αβ
114	20	Glc1α	tBuOH	TfOH	DCM	1.2	1	0.2	15	45	97.8	67.0	4αβ
115	20	Glc1α	tBuOH	TfOH	DCM	1.2	1	0.2	20	45	97.6	67.0	4αβ
116	-50	Glc1α	iPrOH	TfOH	tBu-Benzene	1.2	1	0.2	10	45	59.5	17.4	3αβ
117	-30	Glc1α	iPrOH	TfOH	tBu-Benzene	1.2	1	0.2	10	45	67.7	25.9	3αβ
118	-10	Glc1α	iPrOH	TfOH	tBu-Benzene	1.2	1	0.2	10	45	98.9	39.6	3αβ
119	10	Glc1α	iPrOH	TfOH	tBu-Benzene	1.2	1	0.2	10	45	96.9	47.2	3αβ
120	30	Glc1α	iPrOH	TfOH	tBu-Benzene	1.2	1	0.2	10	45	95.3	54.0	3αβ
121	50	Glc1α	iPrOH	TfOH	tBu-Benzene	1.2	1	0.2	10	45	79.0	58.2	3αβ
122	70	Glc1α	iPrOH	TfOH	tBu-Benzene	1.2	1	0.2	10	45	77.0	60.1	3αβ
123	-50	Glc1α	iPrOH	TfOH	Chloroform	1.2	1	0.2	10	45	67.1	37.4	3αβ
124	-30	Glc1α	iPrOH	TfOH	Chloroform	1.2	1	0.2	10	45	86.6	47.5	3αβ
125	-10	Glc1α	iPrOH	TfOH	Chloroform	1.2	1	0.2	10	45	89.5	58.1	3αβ
126	10	Glc1α	iPrOH	TfOH	Chloroform	1.2	1	0.2	10	45	97.9	64.3	3αβ
127	30	Glc1α	iPrOH	TfOH	Chloroform	1.2	1	0.2	10	45	96.3	70.2	3αβ
128	50	Glc1α	iPrOH	TfOH	Chloroform	1.2	1	0.2	10	45	93.1	72.9	3αβ
129	-50	Glc1β	iPrOH	TfOH	Chloroform	1.2	1	0.2	10	45	72.7	37.6	3αβ
130	-30	Glc1β	iPrOH	TfOH	Chloroform	1.2	1	0.2	10	45	81.2	46.2	3αβ
131	-10	Glc1β	iPrOH	TfOH	Chloroform	1.2	1	0.2	10	45	88.6	54.6	3αβ
132	10	Glc1β	iPrOH	TfOH	Chloroform	1.2	1	0.2	10	45	84.3	62.9	3αβ
133	30	Glc1β	iPrOH	TfOH	Chloroform	1.2	1	0.2	10	45	88.3	67.3	3αβ
134	50	Glc1β	iPrOH	TfOH	Chloroform	1.2	1	0.2	10	45	89.1	73.0	3αβ
135	30	Glc1α	iPrOH	TfOH	DCM	1.2	1	0.2	10	240	77.4	61.5	3αβ
136	-50	Gal1α	MeOH	TfOH	DCM	1.2	1	0.2	10	45	98.0	14.3	5αβ
137	-30	Gal1α	MeOH	TfOH	DCM	1.2	1	0.2	10	45	92.4	30.4	5αβ
138	-10	Gal1α	MeOH	TfOH	DCM	1.2	1	0.2	10	45	96.5	42.1	5αβ
139	10	Gal1α	MeOH	TfOH	DCM	1.2	1	0.2	10	45	96.8	52.7	5αβ
140	20	Gal1α	MeOH	TfOH	DCM	1.2	1	0.2	10	45	94.1	55.6	5αβ
141	30	Gal1α	MeOH	TfOH	DCM	1.2	1	0.2	10	45	95.2	59.5	5αβ
142	30	Gal1α	MeOH	TfOH	DCM	1	10	0.2	10	45	89.8	33.4	5αβ

Entry	Temp. (°C)	Donor	Acceptor	Activator	Solvent	Donor Equiv.	Acceptor Equiv.	Activator Equiv.	Donor Conc.	T _{res} (sec)	Yield (%)	α ratio (%)	Product
143	-50	Gal1α	EtOH	TfOH	DCM	1.2	1	0.2	10	45	92.4	10.7	6αβ
144	-30	Gal1α	EtOH	TfOH	DCM	1.2	1	0.2	10	45	98.3	21.9	6αβ
145	-10	Gal1α	EtOH	TfOH	DCM	1.2	1	0.2	10	45	99.0	34.5	6αβ
146	10	Gal1α	EtOH	TfOH	DCM	1.2	1	0.2	10	45	96.6	44.0	6αβ
147	20	Gal1α	EtOH	TfOH	DCM	1.2	1	0.2	10	45	98.2	47.9	6αβ
148	30	Gal1α	EtOH	TfOH	DCM	1.2	1	0.2	10	45	98.2	50.9	6αβ
149	-50	Gal1α	iPrOH	TfOH	DCM	1.2	1	0.2	10	45	98.2	19.3	7αβ
150	-30	Gal1α	iPrOH	TfOH	DCM	1.2	1	0.2	10	45	99.7	29.6	7αβ
151	-10	Gal1α	iPrOH	TfOH	DCM	1.2	1	0.2	10	45	96.4	41.0	7αβ
152	10	Gal1α	iPrOH	TfOH	DCM	1.2	1	0.2	10	45	96.9	46.4	7αβ
153	20	Gal1α	iPrOH	TfOH	DCM	1.2	1	0.2	10	45	95.0	49.3	7αβ
154	30	Gal1α	iPrOH	TfOH	DCM	1.2	1	0.2	10	45	78.0	51.4	7αβ
155	-50	Gal1α	tBuOH	TfOH	DCM	1.2	1	0.2	10	45	51.7	36.1	8αβ
156	-30	Gal1α	tBuOH	TfOH	DCM	1.2	1	0.2	10	45	99.4	40.3	8αβ
157	-10	Gal1α	tBuOH	TfOH	DCM	1.2	1	0.2	10	45	100.0	45.6	8αβ
158	10	Gal1α	tBuOH	TfOH	DCM	1.2	1	0.2	10	45	82.5	50.2	8αβ
159	20	Gal1α	tBuOH	TfOH	DCM	1.2	1	0.2	10	45	77.9	54.7	8αβ
160	30	Gal1α	tBuOH	TfOH	DCM	1.2	1	0.2	10	45	74.1	57.2	8αβ
161	-30	Gal2β	iPrOH	TfOH ^d	DCM	1.2	1	0.2	10	45	15.9	38.6	7αβ
162	-10	Gal2β	iPrOH	TfOH ^d	DCM	1.2	1	0.2	10	45	87.1	42.1	7αβ
163	10	Gal2β	iPrOH	TfOH ^d	DCM	1.2	1	0.2	10	45	75.3	45.6	7αβ
164	20	Gal2β	iPrOH	TfOH ^d	DCM	1.2	1	0.2	10	45	76.6	50.2	7αβ
165	30	Gal2β	iPrOH	TfOH ^d	DCM	1.2	1	0.2	10	45	78.6	52.8	7αβ
166	-50	Gal1α	2F-EtOH	TfOH	DCM	1.2	1	0.2	10	45	76.8	62.6	9αβ
167	-30	Gal1α	2F-EtOH	TfOH	DCM	1.2	1	0.2	10	45	78.3	72.7	9αβ
168	-10	Gal1α	2F-EtOH	TfOH	DCM	1.2	1	0.2	10	45	83.3	70.6	9αβ
169	10	Gal1α	2F-EtOH	TfOH	DCM	1.2	1	0.2	10	45	84.1	71.3	9αβ
170	20	Gal1α	2F-EtOH	TfOH	DCM	1.2	1	0.2	10	45	93.5	70.8	9αβ
171	30	Gal1α	2F-EtOH	TfOH	DCM	1.2	1	0.2	10	45	86.0	70.7	9αβ
172	-50	Gal1α	iPrOH	TfOH	Toluene	1.2	1	0.2	10	45	96.7	10.3	7αβ
173	-30	Gal1α	iPrOH	TfOH	Toluene	1.2	1	0.2	10	45	93.1	14.7	7αβ
174	-10	Gal1α	iPrOH	TfOH	Toluene	1.2	1	0.2	10	45	95.6	27.0	7αβ
175	10	Gal1α	iPrOH	TfOH	Toluene	1.2	1	0.2	10	45	96.7	41.5	7αβ
176	30	Gal1α	iPrOH	TfOH	Toluene	1.2	1	0.2	10	45	90.6	57.3	7αβ
177	50	Gal1α	iPrOH	TfOH	Toluene	1.2	1	0.2	10	45	85.6	66.5	7αβ
178	70	Gal1α	iPrOH	TfOH	Toluene	1.2	1	0.2	10	45	77.0	68.9	7αβ
179	-50	Gal1α	iPrOH	TfOH	MTBE	1.2	1	0.2	10	45	39.6	43.6	7αβ
180	-30	Gal1α	iPrOH	TfOH	MTBE	1.2	1	0.2	10	45	63.5	55.9	7αβ
181	-10	Gal1α	iPrOH	TfOH	MTBE	1.2	1	0.2	10	45	85.3	67.1	7αβ
182	10	Gal1α	iPrOH	TfOH	MTBE	1.2	1	0.2	10	45	86.2	72.0	7αβ
183	30	Gal1α	iPrOH	TfOH	MTBE	1.2	1	0.2	10	45	81.5	76.0	7αβ
184	50	Gal1α	iPrOH	TfOH	MTBE	1.2	1	0.2	10	45	79.9	77.8	7αβ
185	-30	Gal1α	iPrOH	TfOH	ACN	1.2	1	0.2	10	45	29.8	16.1	7αβ
186	-10	Gal1α	iPrOH	TfOH	ACN	1.2	1	0.2	10	45	73.1	22.0	7αβ
187	10	Gal1α	iPrOH	TfOH	ACN	1.2	1	0.2	10	45	73.4	24.9	7αβ
188	30	Gal1α	iPrOH	TfOH	ACN	1.2	1	0.2	10	45	74.7	29.1	7αβ
189	50	Gal1α	iPrOH	TfOH	ACN	1.2	1	0.2	10	45	69.8	34.6	7αβ
190	70	Gal1α	iPrOH	TfOH	ACN	1.2	1	0.2	10	45	63.9	38.6	7αβ
191	-30	Gal1α	iPrOH	TfOH	Anisole	1.2	1	0.2	10	45	61.9	65.4	7αβ
192	-10	Gal1α	iPrOH	TfOH	Anisole	1.2	1	0.2	10	45	68.0	58.2	7αβ
193	10	Gal1α	iPrOH	TfOH	Anisole	1.2	1	0.2	10	45	65.9	61.6	7αβ
194	30	Gal1α	iPrOH	TfOH	Anisole	1.2	1	0.2	10	45	62.5	65.5	7αβ
195	50	Gal1α	iPrOH	TfOH	Anisole	1.2	1	0.2	10	45	52.2	69.1	7αβ
196	70	Gal1α	iPrOH	TfOH	Anisole	1.2	1	0.2	10	45	43.5	70.2	7αβ

Entry	Temp. (°C)	Donor	Acceptor	Activator	Solvent	Donor Equiv.	Acceptor Equiv.	Activator Equiv.	Donor Conc.	T _{res} (sec)	Yield (%)	α ratio (%)	Product
197	-50	Gal1α	tBuOH	TfOH	DCM	1	1	0.2	8.33	45	81.1	33.6	8αβ
198	-50	Gal1α	tBuOH	TfOH	DCM	1	5	0.2	8.33	45	37.5	35.7	8αβ
199	-50	Gal1α	tBuOH	TfOH	DCM	1.2	1	0.2	10	180	70.0	35.0	8αβ
200	-50	Gal1α	tBuOH	TfOH	DCM	1.2	1	0.2	10	270	74.7	33.5	8αβ
201	-50	Gal1α	2F-EtOH	TfOH	DCM	1	10	0.2	8.33	45	79.1	49.8	9αβ
202	-30	Gal1α	2F-EtOH	TfOH	DCM	1	10	0.2	8.33	45	81.0	56.5	9αβ
203	-10	Gal1α	2F-EtOH	TfOH	DCM	1	10	0.2	8.33	45	84.7	62.8	9αβ
204	10	Gal1α	2F-EtOH	TfOH	DCM	1	10	0.2	8.33	45	87.4	63.9	9αβ
205	20	Gal1α	2F-EtOH	TfOH	DCM	1	10	0.2	8.33	45	92.1	66.4	9αβ
206	30	Gal1α	2F-EtOH	TfOH	DCM	1	10	0.2	8.33	45	87.4	68.5	9αβ
207	-50	Gal1α	2F-EtOH	TfOH	DCM	1	5	0.2	8.33	45	83.1	57.7	9αβ
208	-30	Gal1α	2F-EtOH	TfOH	DCM	1	5	0.2	8.33	45	78.7	61.8	9αβ
209	-10	Gal1α	2F-EtOH	TfOH	DCM	1	5	0.2	8.33	45	84.0	66.7	9αβ
210	10	Gal1α	2F-EtOH	TfOH	DCM	1	5	0.2	8.33	45	89.1	67.9	9αβ
211	20	Gal1α	2F-EtOH	TfOH	DCM	1	5	0.2	8.33	45	90.1	69.6	9αβ
212	30	Gal1α	2F-EtOH	TfOH	DCM	1	5	0.2	8.33	45	91.7	69.6	9αβ
213	-50	Gal1α	2F-EtOH	TfOH	DCM	1	1	0.2	8.33	45	76.2	70.3	9αβ
214	-10	Gal1α	2F-EtOH	TfOH	DCM	1	1	0.2	8.33	45	75.6	73.1	9αβ
215	10	Gal1α	2F-EtOH	TfOH	DCM	1	1	0.2	8.33	45	79.7	73.5	9αβ
216	20	Gal1α	2F-EtOH	TfOH	DCM	1	1	0.2	8.33	45	79.6	73.4	9αβ
217	30	Gal1α	2F-EtOH	TfOH	DCM	1	1	0.2	8.33	45	76.1	72.5	9αβ
218	-50	Gal1α	2F-EtOH	TfOH	DCM	1	2.5	0.2	8.33	45	78.4	63.3	9αβ
219	-50	Gal1α	2F-EtOH	TfOH	DCM	1	7.5	0.2	8.33	45	79.6	54.5	9αβ
220	-50	Man1α	MeOH	TfOH	DCM	1.2	1	0.2	10	45	96.8	50.6	10αβ
221	-30	Man1α	MeOH	TfOH	DCM	1.2	1	0.2	10	45	96.0	54.1	10αβ
222	-10	Man1α	MeOH	TfOH	DCM	1.2	1	0.2	10	45	97.5	57.4	10αβ
223	10	Man1α	MeOH	TfOH	DCM	1.2	1	0.2	10	45	92.1	59.6	10αβ
224	20	Man1α	MeOH	TfOH	DCM	1.2	1	0.2	10	45	75.5	64.1	10αβ
225	30	Man1α	MeOH	TfOH	DCM	1.2	1	0.2	10	45	86.7	64.7	10αβ
226	-50	Man1α	EtOH	TfOH	DCM	1.2	1	0.2	10	45	99.8	47.9	11αβ
227	-30	Man1α	EtOH	TfOH	DCM	1.2	1	0.2	10	45	97.3	53.1	11αβ
228	-10	Man1α	EtOH	TfOH	DCM	1.2	1	0.2	10	45	93.8	56.5	11αβ
229	10	Man1α	EtOH	TfOH	DCM	1.2	1	0.2	10	45	91.9	59.4	11αβ
230	20	Man1α	EtOH	TfOH	DCM	1.2	1	0.2	10	45	92.1	59.5	11αβ
231	30	Man1α	EtOH	TfOH	DCM	1.2	1	0.2	10	45	90.0	59.3	11αβ
232	-50	Man1α	iPrOH	TfOH	DCM	1.2	1	0.2	10	45	98.1	49.9	12αβ
233	-30	Man1α	iPrOH	TfOH	DCM	1.2	1	0.2	10	45	95.8	53.1	12αβ
234	-10	Man1α	iPrOH	TfOH	DCM	1.2	1	0.2	10	45	99.1	56.5	12αβ
235	10	Man1α	iPrOH	TfOH	DCM	1.2	1	0.2	10	45	99.0	59.4	12αβ
236	20	Man1α	iPrOH	TfOH	DCM	1.2	1	0.2	10	45	98.7	59.5	12αβ
237	30	Man1α	iPrOH	TfOH	DCM	1.2	1	0.2	10	45	93.9	64.9	12αβ
238	-50	Man1α	tBuOH	TfOH	DCM	1.2	1	0.2	10	45	99.4	55.3	13αβ
239	-30	Man1α	tBuOH	TfOH	DCM	1.2	1	0.2	10	45	92.7	57.6	13αβ
240	-10	Man1α	tBuOH	TfOH	DCM	1.2	1	0.2	10	45	81.0	61.5	13αβ
241	10	Man1α	tBuOH	TfOH	DCM	1.2	1	0.2	10	45	78.6	66.1	13αβ
242	20	Man1α	tBuOH	TfOH	DCM	1.2	1	0.2	10	45	78.3	74.9	13αβ
243	30	Man1α	tBuOH	TfOH	DCM	1.2	1	0.2	10	45	74.9	94.6	13αβ
244	-50	Man1α	tBuOH	FSO ₃ H	DCM	1.2	1	0.2	10	45	96.4	55.0	13αβ
245	-30	Man1α	tBuOH	FSO ₃ H	DCM	1.2	1	0.2	10	45	96.5	57.4	13αβ
246	-10	Man1α	tBuOH	FSO ₃ H	DCM	1.2	1	0.2	10	45	94.6	57.8	13αβ
247	10	Man1α	tBuOH	FSO ₃ H	DCM	1.2	1	0.2	10	45	90.7	59.2	13αβ
248	30	Man1α	tBuOH	FSO ₃ H	DCM	1.2	1	0.2	10	45	100.0	61.3	13αβ

Entry	Temp. (°C)	Donor	Acceptor	Activator	Solvent	Donor Equiv.	Acceptor Equiv.	Activator Equiv.	Donor Conc.	T _{res} (sec)	Yield (%)	α ratio (%)	Product
249	-50	Man1α	tBuOH	MsOH	DCM	1.2	1	0.2	10	45	50.2	57.5	13αβ
250	-30	Man1α	tBuOH	MsOH	DCM	1.2	1	0.2	10	45	50.4	60.2	13αβ
251	-10	Man1α	tBuOH	MsOH	DCM	1.2	1	0.2	10	45	50.1	61.2	13αβ
252	10	Man1α	tBuOH	MsOH	DCM	1.2	1	0.2	10	45	51.6	63.3	13αβ
253	30	Man1α	tBuOH	MsOH	DCM	1.2	1	0.2	10	45	49.7	63.6	13αβ
254	-40	Man1α	tBuOH	Tf2NH	DCM	1.2	1	0.2	10	45	67.7	55.5	13αβ
255	-30	Man1α	tBuOH	Tf2NH	DCM	1.2	1	0.2	10	45	81.4	55.1	13αβ
256	-10	Man1α	tBuOH	Tf2NH	DCM	1.2	1	0.2	10	45	65.3	62.3	13αβ
257	-5	Man1α	tBuOH	Tf2NH	DCM	1.2	1	0.2	10	45	65.4	71.4	13αβ
258	5	Man1α	tBuOH	Tf2NH	DCM	1.2	1	0.2	10	45	61.8	93.7	13αβ
259	10	Man1α	tBuOH	Tf2NH	DCM	1.2	1	0.2	10	45	61.3	97.7	13αβ
260	20	Man1α	tBuOH	Tf2NH	DCM	1.2	1	0.2	10	45	56.8	97.3	13αβ
261	30	Man1α	tBuOH	Tf2NH	DCM	1.2	1	0.2	10	45	45.9	97.6	13αβ
262	-50	Man1α	EtOH	Tf2NH	DCM	1.2	1	0.2	10	45	74.3	54.8	11αβ
263	-30	Man1α	EtOH	Tf2NH	DCM	1.2	1	0.2	10	45	70.5	57.0	11αβ
264	-10	Man1α	EtOH	Tf2NH	DCM	1.2	1	0.2	10	45	69.1	57.0	11αβ
265	10	Man1α	EtOH	Tf2NH	DCM	1.2	1	0.2	10	45	66.7	61.7	11αβ
266	30	Man1α	EtOH	Tf2NH	DCM	1.2	1	0.2	10	45	45.4	62.3	11αβ
267	-10	Man2α	iPrOH	TfOH ^d	DCM	1.2	1	0.2	10	45	21.7	53.8	12αβ
268	10	Man2α	iPrOH	TfOH ^d	DCM	1.2	1	0.2	10	45	67.9	57.0	12αβ
269	20	Man2α	iPrOH	TfOH ^d	DCM	1.2	1	0.2	10	45	73.6	57.5	12αβ
270	30	Man2α	iPrOH	TfOH ^d	DCM	1.2	1	0.2	10	45	76.0	58.0	12αβ
271	-50	Man1α	iPrOH	TfOH	Toluene	1.2	1	0.2	10	45	67.8	61.2	12αβ
272	-30	Man1α	iPrOH	TfOH	Toluene	1.2	1	0.2	10	45	98.1	63.8	12αβ
273	-10	Man1α	iPrOH	TfOH	Toluene	1.2	1	0.2	10	45	100.0	66.7	12αβ
274	10	Man1α	iPrOH	TfOH	Toluene	1.2	1	0.2	10	45	95.2	70.2	12αβ
275	30	Man1α	iPrOH	TfOH	Toluene	1.2	1	0.2	10	45	94.7	74.4	12αβ
276	50	Man1α	iPrOH	TfOH	Toluene	1.2	1	0.2	10	45	90.5	78.5	12αβ
277	70	Man1α	iPrOH	TfOH	Toluene	1.2	1	0.2	10	45	77.7	87.1	12αβ
278	-30	Man1α	iPrOH	TfOH	ACN	1.2	1	0.2	10	45	70.8	64.9	12αβ
279	-10	Man1α	iPrOH	TfOH	ACN	1.2	1	0.2	10	45	70.5	65.9	12αβ
280	10	Man1α	iPrOH	TfOH	ACN	1.2	1	0.2	10	45	69.4	74.4	12αβ
281	20	Man1α	iPrOH	TfOH	ACN	1.2	1	0.2	10	45	68.5	91.3	12αβ
282	30	Man1α	iPrOH	TfOH	ACN	1.2	1	0.2	10	45	79.1	97.1	12αβ
283	50	Man1α	iPrOH	TfOH	ACN	1.2	1	0.2	10	45	75.5	98.6	12αβ
284	70	Man1α	iPrOH	TfOH	ACN	1.2	1	0.2	10	45	70.7	98.2	12αβ
285	-50	Man1α	iPrOH	TfOH	MTBE	1.2	1	0.2	10	45	44.6	72.0	12αβ
286	-30	Man1α	iPrOH	TfOH	MTBE	1.2	1	0.2	10	45	46.7	75.1	12αβ
287	-10	Man1α	iPrOH	TfOH	MTBE	1.2	1	0.2	10	45	65.9	76.4	12αβ
288	10	Man1α	iPrOH	TfOH	MTBE	1.2	1	0.2	10	45	55.2	79.6	12αβ
289	30	Man1α	iPrOH	TfOH	MTBE	1.2	1	0.2	10	45	54.6	81.6	12αβ
290	50	Man1α	iPrOH	TfOH	MTBE	1.2	1	0.2	10	45	51.7	83.9	12αβ
291	-50	Man1α	3F-EtOH	TfOH	DCM	1.2	1	0.2	10	45	95.5	100.0	14α
292	-30	Man1α	3F-EtOH	TfOH	DCM	1.2	1	0.2	10	45	99.4	100.0	14α
293	-10	Man1α	3F-EtOH	TfOH	DCM	1.2	1	0.2	10	45	91.1	100.0	14α
294	10	Man1α	3F-EtOH	TfOH	DCM	1.2	1	0.2	10	45	91.8	100.0	14α
295	20	Man1α	3F-EtOH	TfOH	DCM	1.2	1	0.2	10	45	93.1	100.0	14α
296	30	Man1α	3F-EtOH	TfOH	DCM	1.2	1	0.2	10	45	92.7	100.0	14α
297	-30	Man1α	iPrOH	TfOH	Anisole	1.2	1	0.2	10	45	94.5	57.8	12αβ
298	-10	Man1α	iPrOH	TfOH	Anisole	1.2	1	0.2	10	45	85.3	61.3	12αβ
299	10	Man1α	iPrOH	TfOH	Anisole	1.2	1	0.2	10	45	71.9	64.5	12αβ
300	30	Man1α	iPrOH	TfOH	Anisole	1.2	1	0.2	10	45	54.4	66.3	12αβ
301	50	Man1α	iPrOH	TfOH	Anisole	1.2	1	0.2	10	45	51.0	66.2	12αβ
302	70	Man1α	iPrOH	TfOH	Anisole	1.2	1	0.2	10	45	60.3	49.1	12αβ

Entry	Temp. (°C)	Donor	Acceptor	Activator	Solvent	Donor Equiv.	Acceptor Equiv.	Activator Equiv.	Donor Conc.	T _{res} (sec)	Yield (%)	α ratio (%)	Product
303 ^c	-50	Man1α	tBuOH	TfOH	DCM	1.2	1	0.2	10	45	77.4	56.0	13αβ
304 ^c	-30	Man1α	tBuOH	TfOH	DCM	1.2	1	0.2	10	45	93.0	58.1	13αβ
305 ^c	-10	Man1α	tBuOH	TfOH	DCM	1.2	1	0.2	10	45	96.1	60.3	13αβ
306 ^c	10	Man1α	tBuOH	TfOH	DCM	1.2	1	0.2	10	45	97.0	61.7	13αβ
307 ^c	20	Man1α	tBuOH	TfOH	DCM	1.2	1	0.2	10	45	95.1	63.3	13αβ
308 ^c	30	Man1α	tBuOH	TfOH	DCM	1.2	1	0.2	10	45	89.6	64.9	13αβ
309	20	Man1α	MeOH	TfOH	DCM	1	10	0.2	10	45	81.1	60.9	10αβ
310	-50	Man1α	iPrOH	TfOH	Toluene	1	5	0.2	10	45	68.2	61.7	12αβ
311	10	Man1α	iPrOH	TfOH	Toluene	1	5	0.2	10	45	94.3	71.3	12αβ
312	70	Man1α	iPrOH	TfOH	Toluene	1	5	0.2	10	45	69.6	82.7	12αβ
313	-30	Glc3α	iPrOH	TMSOTf	DCM	1.2	1	1.2	10	45	29.5	31.3	3αβ
314	-10	Glc3α	iPrOH	TMSOTf	DCM	1.2	1	1.2	10	45	60.1	44.7	3αβ
315	10	Glc3α	iPrOH	TMSOTf	DCM	1.2	1	1.2	10	45	79.1	53.2	3αβ
316	20	Glc3α	iPrOH	TMSOTf	DCM	1.2	1	1.2	10	45	90.4	57.9	3αβ
317	30	Glc3α	iPrOH	TMSOTf	DCM	1.2	1	1.2	10	45	98.6	61.5	3αβ
318	-30	Gal3α	iPrOH	TMSOTf	DCM	1.2	1	1.2	10	45	33.9	34.3	7αβ
319	-10	Gal3α	iPrOH	TMSOTf	DCM	1.2	1	1.2	10	45	49.2	41.5	7αβ
320	10	Gal3α	iPrOH	TMSOTf	DCM	1.2	1	1.2	10	45	79.2	47.3	7αβ
321	20	Gal3α	iPrOH	TMSOTf	DCM	1.2	1	1.2	10	45	93.1	50.1	7αβ
322	30	Gal3α	iPrOH	TMSOTf	DCM	1.2	1	1.2	10	45	98.1	52.7	7αβ
323	20	Man3α	iPrOH	TMSOTf	DCM	1.2	1	1.2	10	45	37.5	63.9	12αβ
324	30	Man3α	iPrOH	TMSOTf	DCM	1.2	1	1.2	10	45	81.1	62.1	12αβ
325	-50	Fuc1α	iPrOH	TfOH	DCM	1.2	1	0.2	10	45	71.7	19.9	15αβ
326	-30	Fuc1α	iPrOH	TfOH	DCM	1.2	1	0.2	10	45	69.4	30.0	15αβ
327	-10	Fuc1α	iPrOH	TfOH	DCM	1.2	1	0.2	10	45	71.8	33.6	15αβ
328	10	Fuc1α	iPrOH	TfOH	DCM	1.2	1	0.2	10	45	56.3	39.7	15αβ
329	-50	Gal1α	ManOH	TfOH	DCM	1.2	1	0.2	10	45	95.4	48.9	16αβ
330	-30	Gal1α	ManOH	TfOH	DCM	1.2	1	0.2	10	45	92.0	56.5	16αβ
331	-10	Gal1α	ManOH	TfOH	DCM	1.2	1	0.2	10	45	84.1	61.5	16αβ
332	10	Gal1α	ManOH	TfOH	DCM	1.2	1	0.2	10	45	82.9	65.7	16αβ
333	30	Gal1α	ManOH	TfOH	DCM	1.2	1	0.2	10	45	76.2	69.7	16αβ
334	-50	Gal1α	GlcOH	TfOH	DCM	1.2	1	0.2	10	45	98.1	42.4	17αβ
335	-30	Gal1α	GlcOH	TfOH	DCM	1.2	1	0.2	10	45	93.6	51.9	17αβ
336	-10	Gal1α	GlcOH	TfOH	DCM	1.2	1	0.2	10	45	94.1	62.6	17αβ
337	10	Gal1α	GlcOH	TfOH	DCM	1.2	1	0.2	10	45	93.2	67.1	17αβ
338	20	Gal1α	GlcOH	TfOH	DCM	1.2	1	0.2	10	45	88.1	69.2	17αβ
339	30	Gal1α	GlcOH	TfOH	DCM	1.2	1	0.2	10	45	93.2	71.9	17αβ
340	-50	Gal1α	iPrOH	C ₃ F ₆ S ₂ O ₄ NH	DCM	1.2	1	0.2	10	45	33.0	18.5	7αβ
341	-30	Gal1α	iPrOH	C ₃ F ₆ S ₂ O ₄ NH	DCM	1.2	1	0.2	10	45	37.4	26.2	7αβ
342	-10	Gal1α	iPrOH	C ₃ F ₆ S ₂ O ₄ NH	DCM	1.2	1	0.2	10	45	36.0	32.6	7αβ
343	10	Gal1α	iPrOH	C ₃ F ₆ S ₂ O ₄ NH	DCM	1.2	1	0.2	10	45	45.0	41.0	7αβ
344	30	Gal1α	iPrOH	C ₃ F ₆ S ₂ O ₄ NH	DCM	1.2	1	0.2	10	45	59.6	47.1	7αβ
345	-50	Man1α	tBuOH	C ₃ F ₆ S ₂ O ₄ NH	DCM	1.2	1	0.2	10	45	71.9	36.7	13αβ
346	-30	Man1α	tBuOH	C ₃ F ₆ S ₂ O ₄ NH	DCM	1.2	1	0.2	10	45	69.6	42.8	13αβ
347	-10	Man1α	tBuOH	C ₃ F ₆ S ₂ O ₄ NH	DCM	1.2	1	0.2	10	45	86.3	48.2	13αβ
348	10	Man1α	tBuOH	C ₃ F ₆ S ₂ O ₄ NH	DCM	1.2	1	0.2	10	45	87.5	64.4	13αβ
349	30	Man1α	tBuOH	C ₃ F ₆ S ₂ O ₄ NH	DCM	1.2	1	0.2	10	45	91.7	98.0	13αβ
350	-20	Glc1α	iPrOH	TfOH	3F-Toluene	1.2	1	0.2	10	45	85.5	31.7	3αβ
351	10	Glc1α	iPrOH	TfOH	3F-Toluene	1.2	1	0.2	10	45	96.8	51.8	3αβ
352	30	Glc1α	iPrOH	TfOH	3F-Toluene	1.2	1	0.2	10	45	97.5	60.3	3αβ
353	50	Glc1α	iPrOH	TfOH	3F-Toluene	1.2	1	0.2	10	45	85.5	61.9	3αβ
354	70	Glc1α	iPrOH	TfOH	3F-Toluene	1.2	1	0.2	10	45	82.2	64.4	3αβ
355	90	Glc1α	iPrOH	TfOH	3F-Toluene	1.2	1	0.2	10	45	60.2	63.3	3αβ

Entry	Temp. (°C)	Donor	Acceptor	Activator	Solvent	Donor Equiv.	Acceptor Equiv.	Activator Equiv.	Donor Conc.	T _{res} (sec)	Yield (%)	α ratio (%)	Product
356	20	Gal1 α	iPrOH	TfOH	1,4-Dioxane	1.2	1	0.2	10	45	99.2	67.9	7 α β
357	40	Gal1 α	iPrOH	TfOH	1,4-Dioxane	1.2	1	0.2	10	45	96.0	71.3	7 α β
358	60	Gal1 α	iPrOH	TfOH	1,4-Dioxane	1.2	1	0.2	10	45	89.6	73.1	7 α β
359	80	Gal1 α	iPrOH	TfOH	1,4-Dioxane	1.2	1	0.2	10	45	82.3	73.9	7 α β
360	100	Gal1 α	iPrOH	TfOH	1,4-Dioxane	1.2	1	0.2	10	45	80.3	74.2	7 α β
361	-50	Glc1 β	EtOH	TfOH	Toluene	1.2	1	0.2	10	45	83.2	31.4	2 α β
362	-30	Glc1 β	EtOH	TfOH	Toluene	1.2	1	0.2	10	45	86.6	37.1	2 α β
363	-10	Glc1 β	EtOH	TfOH	Toluene	1.2	1	0.2	10	45	85.5	46.7	2 α β
364	10	Glc1 β	EtOH	TfOH	Toluene	1.2	1	0.2	10	45	82.7	54.7	2 α β
365	30	Glc1 β	EtOH	TfOH	Toluene	1.2	1	0.2	10	45	78.2	60.8	2 α β
366	50	Glc1 β	EtOH	TfOH	Toluene	1.2	1	0.2	10	45	76.0	60.6	2 α β
367	70	Glc1 β	EtOH	TfOH	Toluene	1.2	1	0.2	10	45	73.8	63.2	2 α β
368	-50	Glc1 β	tBuOH	TfOH	Toluene	1.2	1	0.2	10	45	68.6	79.6	4 α β
369	-30	Glc1 β	tBuOH	TfOH	Toluene	1.2	1	0.2	10	45	89.1	78.6	4 α β
370	-10	Glc1 β	tBuOH	TfOH	Toluene	1.2	1	0.2	10	45	99.1	76.6	4 α β
371	10	Glc1 β	tBuOH	TfOH	Toluene	1.2	1	0.2	10	45	95.0	74.1	4 α β
372	30	Glc1 β	tBuOH	TfOH	Toluene	1.2	1	0.2	10	45	90.1	71.2	4 α β
373	50	Glc1 β	tBuOH	TfOH	Toluene	1.2	1	0.2	10	45	84.6	68.5	4 α β
374	70	Glc1 β	tBuOH	TfOH	Toluene	1.2	1	0.2	10	45	74.3	65.1	4 α β
375	-50	Gal1 β	iPrOH	TfOH	DCM	1.2	1	0.2	10	45	99.4	23.4	7 α β
376	-30	Gal1 β	iPrOH	TfOH	DCM	1.2	1	0.2	10	45	99.9	32.4	7 α β
377	-10	Gal1 β	iPrOH	TfOH	DCM	1.2	1	0.2	10	45	93.8	39.7	7 α β
378	10	Gal1 β	iPrOH	TfOH	DCM	1.2	1	0.2	10	45	81.6	47.2	7 α β
379	30	Gal1 β	iPrOH	TfOH	DCM	1.2	1	0.2	10	45	75.6	55.0	7 α β
380	-50	Gal1 β	iPrOH	TfOH	Toluene	1.2	1	0.2	10	45	80.6	33.0	7 α β
381	-30	Gal1 β	iPrOH	TfOH	Toluene	1.2	1	0.2	10	45	96.4	34.3	7 α β
382	-10	Gal1 β	iPrOH	TfOH	Toluene	1.2	1	0.2	10	45	96.8	39.9	7 α β
383	10	Gal1 β	iPrOH	TfOH	Toluene	1.2	1	0.2	10	45	93.2	47.3	7 α β
384	30	Gal1 β	iPrOH	TfOH	Toluene	1.2	1	0.2	10	45	94.1	56.3	7 α β
385	50	Gal1 β	iPrOH	TfOH	Toluene	1.2	1	0.2	10	45	90.8	62.7	7 α β
386	70	Gal1 β	iPrOH	TfOH	Toluene	1.2	1	0.2	10	45	87.3	68.6	7 α β

^aAll experiments were carried out following by the procedure of general automation platform and all the reactions were quenched with pyridine using twice of the activator equivalents. ^b α/β ratio determined by HPLC. ^c0.25 equiv. of water added. ^d1.44 equiv. of NIS was used with TfOH.

6.2 Calibration curve for products

For calculating the product yield, an external method of calibration was chosen and calibration curve for all the products were prepared which are shown below.

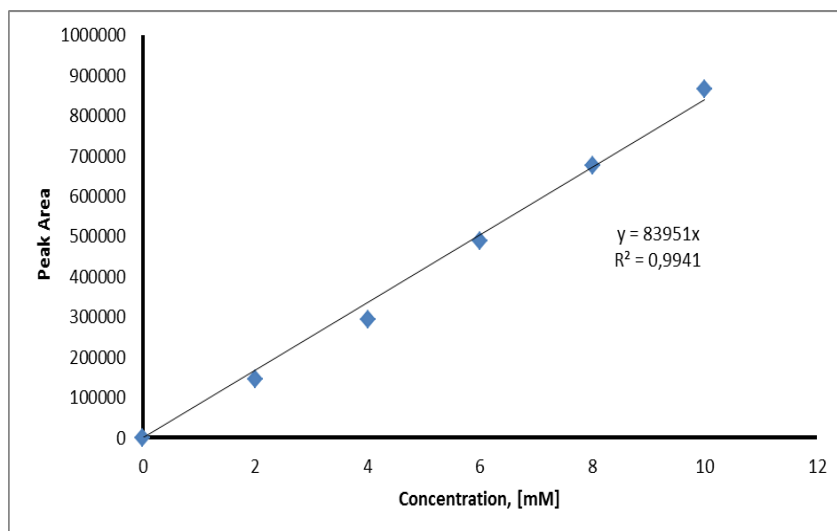


Figure 6.1: HPLC calibration curve of Glc_OBn_OMe (**1α**).

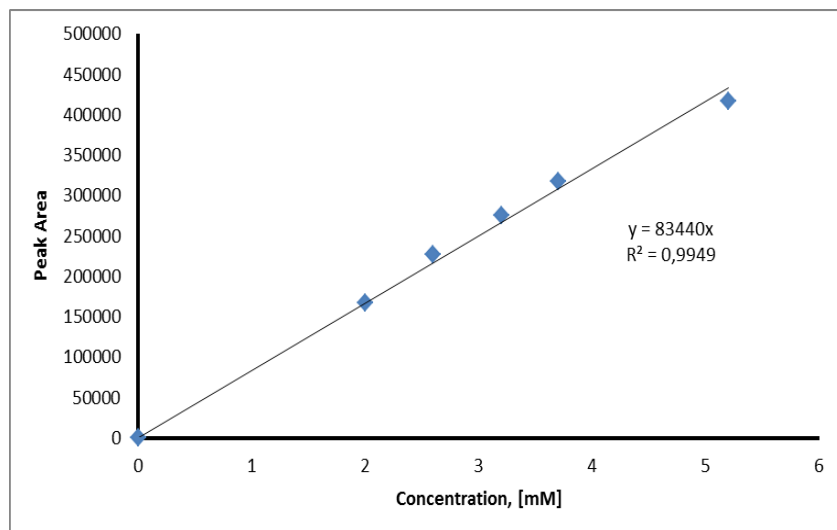


Figure 6.2: HPLC calibration curve of **2β**.

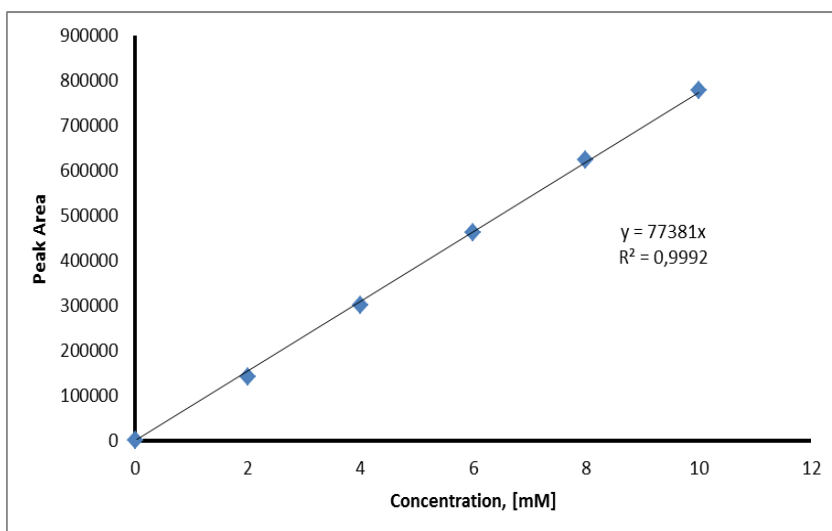


Figure 6.3: HPLC calibration curve of **3αβ**.

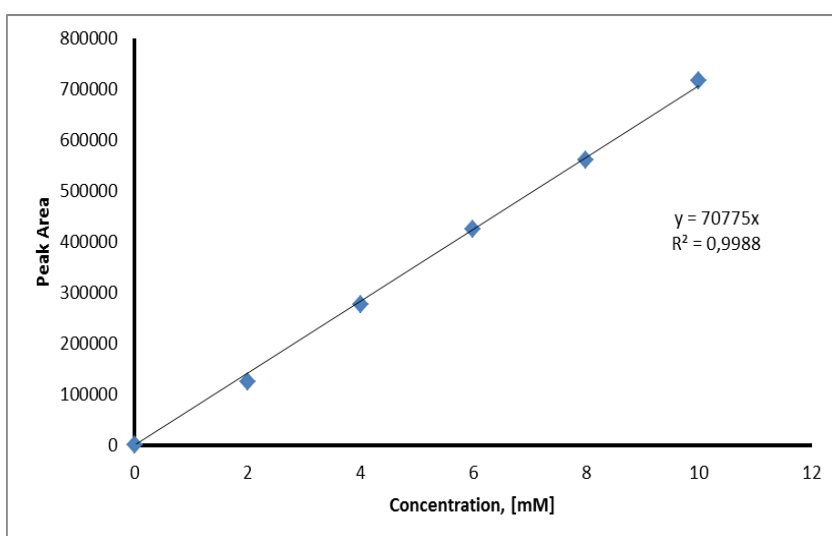


Figure 6.4: HPLC calibration curve of **4αβ**.

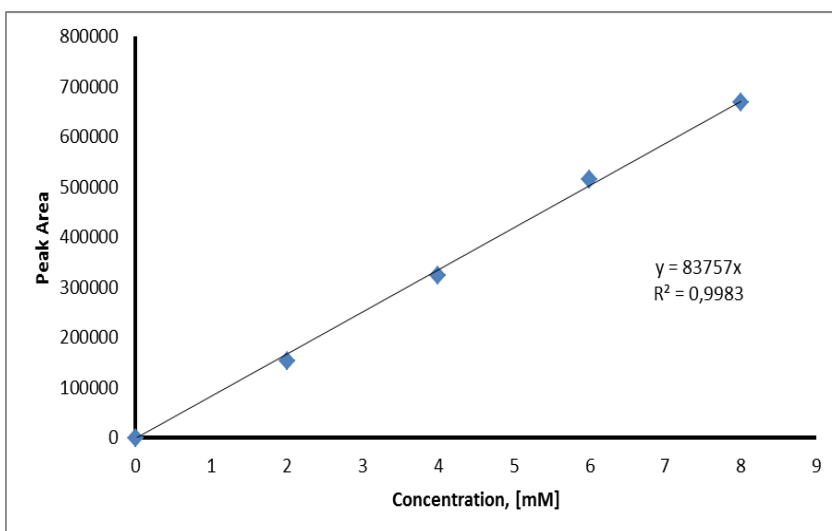


Figure 6.5: HPLC calibration curve of Gal_OBn_OCH₂CF₂H (**9αβ**).

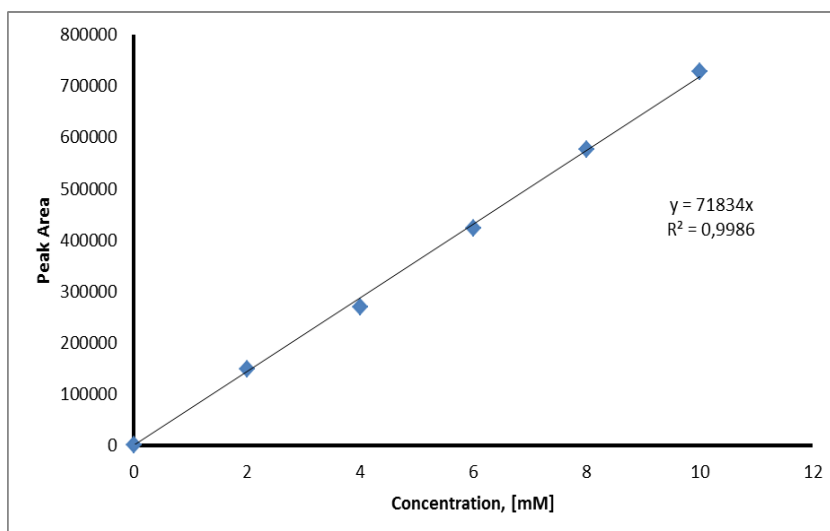


Figure 6.6: HPLC calibration curve of **13aβ**.

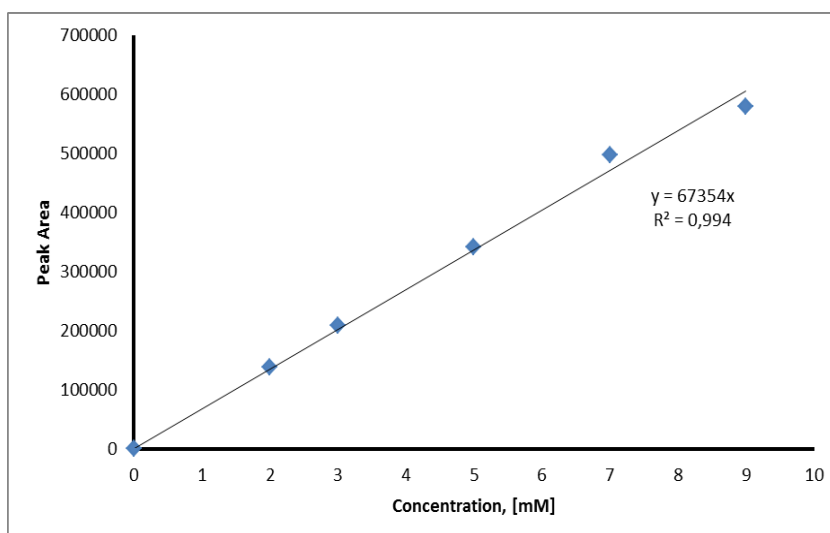


Figure 6.7: HPLC calibration curve of **14a**.

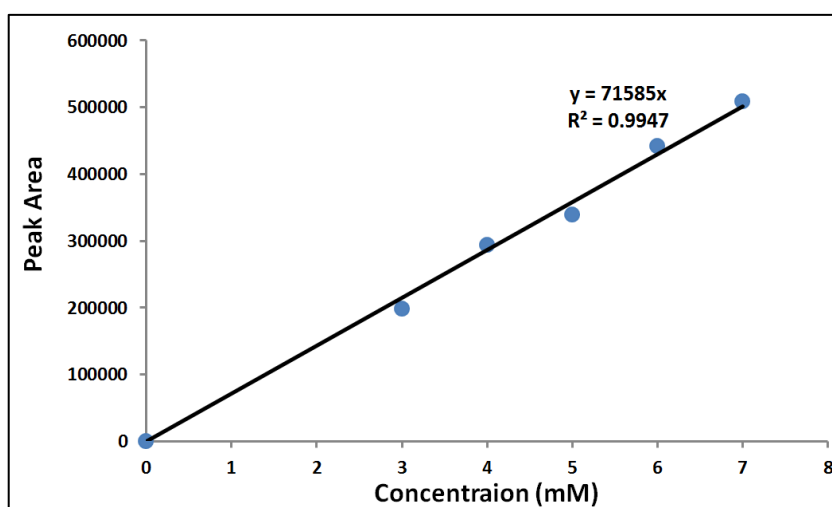


Figure 6.8: HPLC calibration curve of **15aβ**.

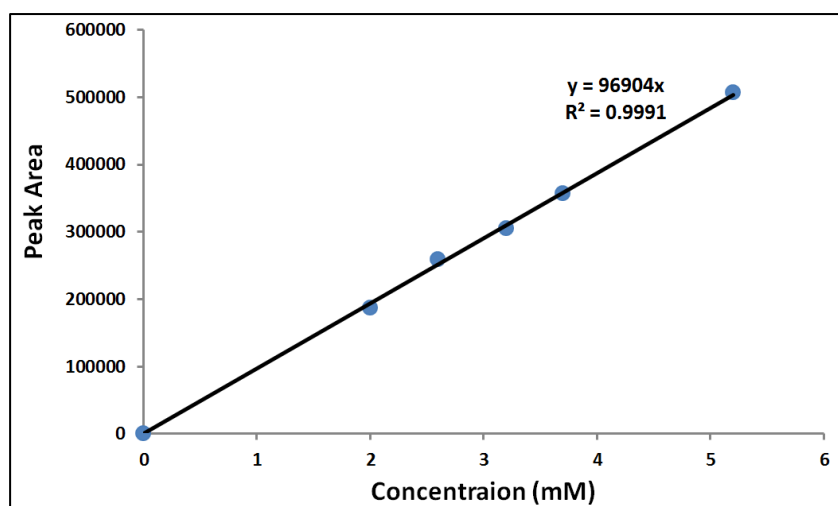


Figure 6.9: HPLC calibration curve of **16a β** .

6.3 General procedure for performing glycosylations in the automated flow platform

The requisite benzyl protected donors were prepared following or adapting literature procedures, described in later sections. Donors were stored at $-20\text{ }^{\circ}\text{C}$, azeotroped three times with 1 mL of toluene and dried under high vacuum overnight prior to use. All solvents, activators, and acceptors were dried to less than 3 ppm water using 3 Å molecular sieves (see section below for drying procedure). The donor, acceptor, and the activator were loaded into airtight Hamilton glass syringes at the desired high concentration, in the ranges of 50-110 mM, 60-110 mM, and 22.6-120 mM respectively. The reactants were brought into appropriate concentrations and stoichiometries with the help of respective dilution pumps. The reaction temperature, concentration of reagents, stoichiometry, and residence time were all set with the aid of the graphical user interface. After reaction completion and inline quenching with pyridine (two equivalents with respect to activator), the outcome of the reaction was monitored by an automated injection of 1 μL reactor solution into inline HPLC. After the completion of HPLC, the HPLC sends feedback to the software and the next reaction is run automatically. The automation system terminated after completion of all the runs given in the data input VI.

Table 6.2: HPLC Methods A, B and C.

Method A				Method B			
Time (min)	Flow (ml/min)	EtOAc (%)	Hexane (%)	Time (min)	Flow (ml/min)	EtOAc (%)	Hexane (%)
0	1	2	98	0	1	10	90
5	1	30	70	3.5	1	20	80
10	1	30	70	4.5	1	30	70
16	1	70	30	8.5	1	30	70
18	1	70	30	9	1	70	30
19	1	30	70	12	1	70	30
20	1	10	90	13	1	30	70
				15	1	10	90
				18	1	10	90

Method C			
Time (min)	Flow (ml/min)	EtOAc (%)	Hexane (%)
0	1	2	98
14	1	25	75
16	1	70	30
18	1	70	30
19	1	2	98
22	1	2	98

6.4 Procedure for drying solvents

Solvents used in this study such as toluene, dichloromethane (DCM), Acetonitrile (ACN), and Methyl *tert*-butyl ether (MTBE) were dried using 3 Å molecular sieves, activated by heating under microwave radiation of 500 W for nine mins and subsequent cooling to ambient temperature under high vacuum. This procedure was repeated five times. The activated molecular sieves were added to the solvents and the solvents were kept under argon atmosphere for two days. The water content of the solvents was determined using Karl Fischer titration.

6.5 General experimental details for preparing building blocks

Commercial grade solvents and reagents were used unless stated otherwise. Anhydrous solvents were obtained from a dry solvent system (Waters, Milford, USA). Unless otherwise noted, all other reagents and solvents were purchased from commercial suppliers and used without further purification. All reactions were carried out under an argon

atmosphere. Analytical thin layer chromatography (TLC) was performed on Macherey-Nagel Pre-coated TLC-sheets, ALUGRAM Xtra SIL G/UV254 sheets and visualized with 254 nm light, 2,5-dinitrophenylhydrazine (DNPH) staining solutions followed by heating. Purification of the reaction products was carried out by flash chromatography using Macherey-Nagel Silica 60 M (0.04-0.063 mm) silica gel. Proton (^1H) NMR spectra were recorded using Agilent 400 (400 MHz) or Agilent 600 (600 MHz) in CDCl_3 and are reported in ppm relative to the residual solvent peaks (CDCl_3 at 7.26 ppm) Peaks are reported as: s = singlet, d = doublet, t = triplet, q = quartet, quint = quintet, m = multiplet. Carbon (^{13}C) NMR spectra were recorded with ^1H -decoupling on Agilent 400 (101 MHz) or Agilent 600 (151 MHz) in CDCl_3 and reported in ppm relative to the residual solvent peak (CDCl_3 at 77.16 ppm). Phosphorous (^{31}P) NMR spectra were recorded on Agilent 600 (243 MHz). Fluorine (^{19}F) NMR spectra were recorded on Agilent 400 (376 MHz) or Agilent 600 (564 MHz). High-resolution mass spectral data were obtained using a Waters XEVO G2-XS 4K spectrometer (#186008532) with the XEVO G2-XS QTOF capability kit (#1860083535). Samples were prepared in LC-MS CHROMASOLV water and acetonitrile, and analyzed in the respective mixtures.

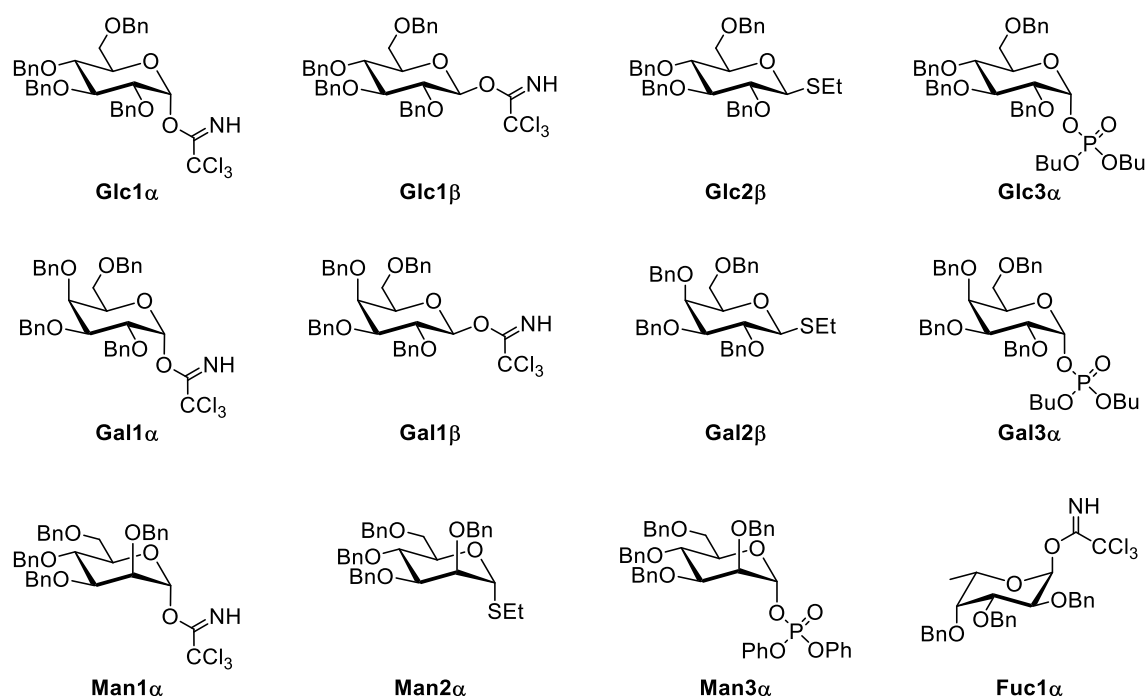
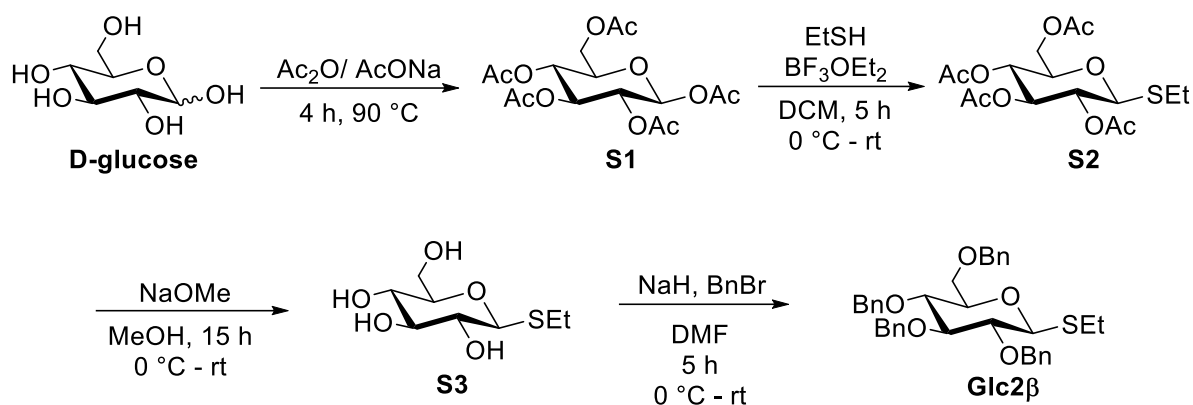


Figure 6.10: A Chart of all glycosyl donor building blocks.

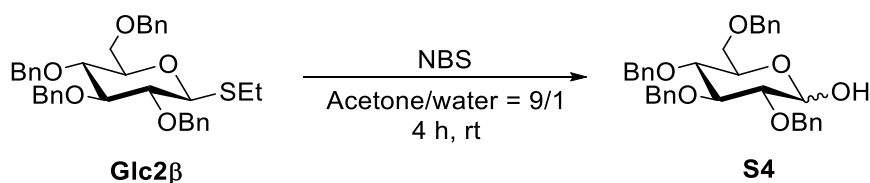
Preparation of Ethyl 2,3,4,6-tetra-*O*-benzyl-1-thio- β -D-glucopyranoside (**Glc2 β**)¹¹¹⁻¹¹²



To a gently refluxed Ac_2O (9.4 mL, 100 mmol) containing NaOAc (1.0 g, 13 mmol) was slowly added D-glucose (1.8g, 10 mmol) over a period of 15 min. After the mixture was heated to $90\text{ }^\circ\text{C}$ for 4h, the mixture was cooled to room temperature. When TLC showed complete disappearance of the starting material and the formation of **S1** (Rf: 0.38 in *n*-Hexane/ EtOAc = 3/2), the reaction was quenched by addition of ice under sonication. The precipitation was filtered and washed with H_2O until the acetic acid disappeared and recrystallized using EtOH (0.5 mL) by adding *n*-hexane (50 mL) to get **S1** (89%, 3.5 g, 8.9 mmol) as white solid. A mixture of **S1** (1.95 g, 5 mmol), EtSH (0.4 mL, 5.6 mmol) and BF_3OEt_2 (0.7 mL, 5.6 mmol) in anhydrous CH_2Cl_2 (20 mL) was cooled to $0\text{ }^\circ\text{C}$. The mixture was warmed to room temperature and stirred during 5 h. When TLC showed complete disappearance of **S1** and the formation of **S2** (Rf: 0.50 in *n*-Hexane/ EtOAc = 3/2), the reaction mixture was quenched with sat. aq. NaHCO_3 solution (10 mL), diluted with CH_2Cl_2 (20 mL) was extracted with CH_2Cl_2 (2x20 mL) and the combined organic layer was washed with brine (2x15 mL). The organic layer was dried over anhydrous Na_2SO_4 , filtered and evaporated under reduced pressure to get **S2** as yellow oil.¹¹¹ Without further purification, the reaction mixture of **S2** was used for next step. To the stirred solution of **S2** in methanol (50 mL) was added NaOMe (30% in MeOH, 3 mL) dropwise at room temperature. The reaction mixture was allowed to stir for 17 h at room temperature until all starting material was consumed as monitored by TLC (**S2** Rf: 0.96, **S3** Rf: 0.21 in CH_2Cl_2 / MeOH = 9/1). The reaction mixture was neutralized by the addition of Amberlite 120 (pH paper used for checking neutralization) and stirred for 2 h before filtration. Evaporation of the filtrate yielded brown colored gummy residue which was dried under vacuum to obtain **S3**.¹¹² The obtained **S3** was used in the next step without further purification. **S3** was dissolved in dry DMF (50 mL) and cooled to $-10\text{ }^\circ\text{C}$. Sodium hydride (60% in mineral oil, 1.00 g, 25 mmol)

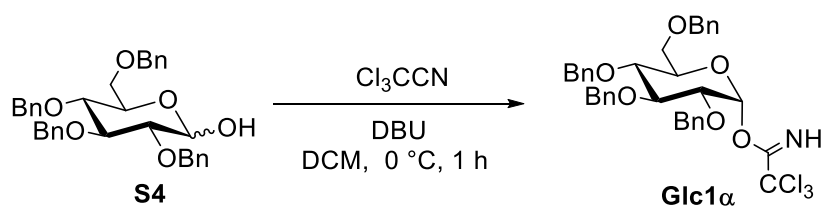
was added slowly and the mixture was stirred for 5 h while warming up to room temperature. Benzyl bromide (2.97 mL, 25 mmol) was added and the mixture was stirred for 15 h. The reaction was cooled down to 0 °C and water (2 mL) was added slowly. The solution was extracted with CH₂Cl₂ (3 × 100 mL) and the combined organic layers were washed with brine (3 × 200 mL). After silica gel column chromatography (Elution: *n*-Hexane/ EtOAc = 10/1), **Glc2β** (1.17 g, 2 mmol) was obtained with 40% yield over 3 steps as a white solid (**Glc2β** Rf: 0.82 in *n*-Hexane/ EtOAc = 5/1); ¹H NMR (400 MHz, Chloroform-*d*) δ 7.40 – 7.22 (m, 18H), 7.19 – 7.12 (m, 2H), 4.91 (d, *J* = 10.8, 1H), 4.92 (d, *J* = 10.0 Hz, 2H), 4.87 – 4.79 (m, 2H), 4.74 (d, *J* = 10.1 Hz, 1H), 4.63 – 4.52 (m, 3H), 4.46 (d, *J* = 9.7 Hz, 1H), 3.77–3.72 (m, 1H), 3.71–3.64 (m, 2H), 3.61 (t, *J* = 9.4 Hz, 1H), 3.50–3.41 (m, 2H), 2.84–2.69 (m, 2H), 1.33 (t, *J* = 7.4 Hz, 3H). This data is in accordance with those previously published.¹¹²

Preparation of 2,3,4,6-tetra-*O*-benzyl-glucopyranose (**S4**)



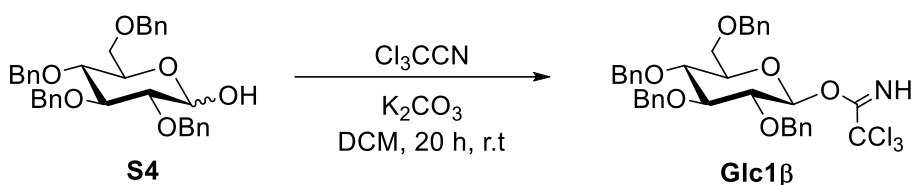
To a solution **Glc2β** (596 mg, 1.02 mmol) in Acetone (7.2 mL) and water (0.8 mL) was added *N*-Bromosuccinimide (548 mg, 3.08 mmol) and stirred for 4 h at room temperature. Then, the reaction mixture was cooled in an ice-bath and then quenched with triethylamine (0.7 mL, 5.0 mmol). The mixture was concentrated to remove acetone, diluted with sat. aq. NaHCO₃ solution (10 mL) and EtOAc (10 mL). The organic layer was extracted with CH₂Cl₂ (2 × 10 mL) and washed with brine (10 mL). The organic layer was dried over anhydrous Na₂SO₄, filtered and evaporated under reduced pressure for column chromatography purification (Elution: *n*-hexane/EtOAc = 5/1 to 2/1) and obtained as an inseparable α/β mixture as a white solid **S4** (510 mg, 0.938 mmol) with 92% yield; ¹H NMR (400 MHz, Chloroform-*d*) δ 7.39 – 7.24 (m, 18H), 7.16 – 7.10 (m, 2H), 5.23 (d, *J* = 3.5 Hz, 1H), 4.97 – 4.91 (m, 2H), 4.86 – 4.77 (m, 2H), 4.62 – 4.45 (m, 4H), 4.03 (ddd, *J* = 10.2, 4.0, 2.1 Hz, 1H, H5), 3.96 (t, *J* = 9.3 Hz, 1H), 3.74–3.69 (m, 1H), 3.68 – 3.62 (m, 2H), 3.62 – 3.56 (m, 1H). This data is in accordance with those previously published.¹¹²

Preparation of 2,3,4,6-tetra-*O*-benzyl- α -D-glucopyranosyl trichloroacetimidate (**Glc1 α**)⁸⁶

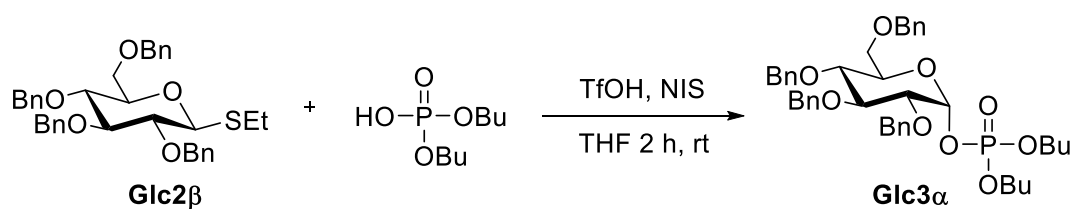


To a solution **S4** (556 mg, 1.03 mmol) in CH_2Cl_2 (10 mL) was added CCl_3CN (1.0 mL, 9.97 mmol) and DBU (0.08 mL, 0.52 mmol) at 0 °C. The solution was stirred at room temperature for 1 h, and then the reaction mixture was concentrated. The residue was purified by silica gel column chromatography (Elution: *n*-hexane/EtOAc = 4/1 containing 1% Et_3N) to give **Glc1 α** (564 mg, 0.82 mmol) as a colorless oil with 80% yield; ^1H NMR (400 MHz, Chloroform-*d*) δ 8.60 (s, 1H), 7.40 – 7.23 (m, 18H), 7.17 (d, J = 6.4 Hz, 2H), 6.55 (d, J = 3.4 Hz, 1H), 4.98 (d, J = 11.0 Hz, 1H), 4.86 (t, J = 10.6 Hz, 2H), 4.80 – 4.67 (m, 2H), 4.63 (d, J = 12.1 Hz, 1H), 4.51 (dd, J = 21.1, 11.4 Hz, 2H), 4.07 (t, J = 9.3 Hz, 1H), 4.01 (d, J = 10.2 Hz, 1H), 3.81 (m, 3H), 3.69 (d, J = 11.0 Hz, 1H). This data is in accordance with those previously published.⁸⁶

Preparation of 2,3,4,6-tetra-*O*-benzyl- β -D-glucopyranosyl trichloroacetimidate (**Glc1 β**)¹¹³

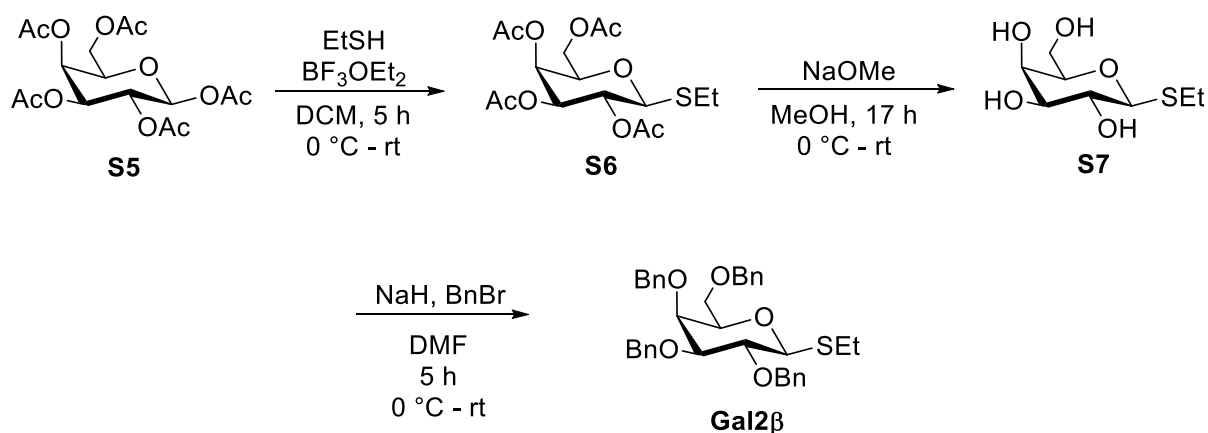


To a solution **S4** (641 mg, 1.19 mmol) in CH_2Cl_2 (10 mL) was added CCl_3CN (1.0 mL, 9.97 mmol) and K_2CO_3 (713 mg, 5.16 mmol) at room temperature. The solution was stirred at room temperature for 20 h, and then the reaction mixture was concentrated. The residue was purified by silica gel column chromatography (Elution: *n*-hexane/EtOAc = 4/1 containing 1% Et_3N) to give **Glc1 β** (560 mg, 0.82 mmol) as a colorless oil with 69% yield; ^1H NMR (400 MHz, Chloroform-*d*) δ 8.71 (s, 1H), 7.37 – 7.25 (m, 18H), 7.19 – 7.13 (m, 2H), 5.80 (m, 1H), 4.95 (d, J = 10.8 Hz, 1H), 4.91 (d, J = 10.9 Hz, 1H), 4.82 (d, J = 10.8 Hz, 2H), 4.76 (d, J = 10.8 Hz, 1H), 4.63 (d, J = 12.2 Hz, 1H), 4.60 – 4.52 (m, 2H), 3.75 (m, 5H), 3.64 (m, 1H). This data is in accordance with those previously published.¹¹³

Preparation of 2,3,4,6-tetra-*O*-benzyl- α -D-glucopyranosyl di-*n*-butyl phosphate (**Glc3 α**)

5.1 g of dry powder 3 Å molecular sieves were added to 60 ml dry DCM. Dibutyl hydrogen phosphate (1.43 ml, 7.21 mmol) were added and left stirring for 1.5 h. After stirring, the molecular sieves were allowed to settle and the supernatant (51 mL, 5.97 mmol) was added to a solution of **Glc2 β** (1.40 g, 2.39 mmol) in CH₂Cl₂ (10 mL), cooled to 0 °C when *N*-Iodosuccinimide (0.70 g, 3.11 mmol) and TfOH (0.063 ml, 0.718 mmol) were added. After stirred for 2 h at room temperature, the reaction mixture was diluted with sat. aq. NaHCO₃ solution (50 mL), sat. aq. Na₂S₂O₃ solution (50 mL) and EtOAc (100 mL). The organic layer was extracted with EtOAc (2 × 100 mL) and washed with brine (100 mL). The organic layer was dried over anhydrous Na₂SO₄, filtered and evaporated under reduced pressure for silica gel column chromatography purification (Elution: *n*-hexane/EtOAc = 5/1 to 1/1) and obtained as a white solid **Glc3 α** (1.42 g, 1.94 mmol) with 81% yield. (**Glc2 β** Rf: 0.82, **Glc3 α** Rf: 0.35 in *n*-Hexane/ EtOAc = 5/1); ¹H NMR (600 MHz, Chloroform-*d*) δ 7.36 (d, *J* = 7.3 Hz, 2H), 7.33 – 7.23 (m, 19H), 7.14 (d, *J* = 7.0 Hz, 2H), 5.88 (dd, *J* = 7.2, 3.1 Hz, 1H), 4.94 (d, *J* = 10.9 Hz, 1H), 4.80 (dt, *J* = 20.5, 10.6 Hz, 3H), 4.66 (d, *J* = 11.4 Hz, 1H), 4.58 (d, *J* = 12.1 Hz, 1H), 4.47 (dd, *J* = 18.7, 11.3 Hz, 2H), 3.98 (ddq, *J* = 38.2, 18.7, 9.6 Hz, 7H), 3.77 – 3.68 (m, 2H), 3.68 – 3.59 (m, 2H), 1.65 – 1.49 (m, 4H), 1.31 (dq, *J* = 28.9, 7.5 Hz, 4H), 0.86 (dt, *J* = 19.0, 7.4 Hz, 6H); ¹³C NMR (151 MHz, Chloroform-*d*) δ 138.7, 138.2, 138.0, 137.8, 128.52, 128.50, 128.47, 128.2, 128.1, 128.01, 127.99, 127.92, 127.88, 127.85, 127.78, 95.2 (d, *J* = 5.9 Hz), 81.3 (d, *J* = 7.0 Hz), 79.5, 77.0, 75.8, 75.3, 73.6, 73.0, 72.5, 68.2, 67.9 (d, *J* = 5.9 Hz), 67.6 (d, *J* = 5.8 Hz), 32.4 (d, *J* = 7.0 Hz), 32.2 (d, *J* = 6.9 Hz), 18.8, 18.7, 13.72, 13.70; ³¹P NMR (243 MHz, Chloroform-*d*) δ -2.04; HRMS (ESI): [M+Na]⁺ calcd for C₄₂H₅₃O₉PNa⁺ 755.3319, found 755.3326.

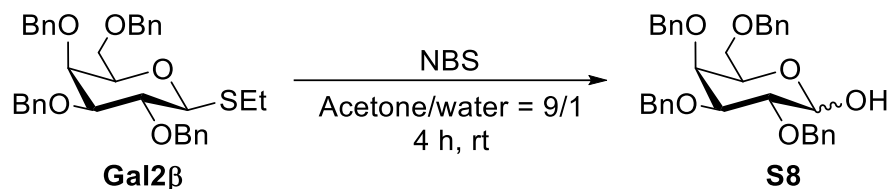
Preparation of Ethyl 2,3,4,6-tetra-*O*-benzyl-1-thio- β -D-galactopyranoside (**Gal2 β**)^{112, 114}



A mixture of **S5** (1.95 g, 5 mmol), EtSH (0.4 mL, 5.6 mmol) and BF₃OEt₂ (0.7 mL, 5.6 mmol) in anhydrous CH₂Cl₂ (20 mL) was cooled to 0 °C. The mixture was warmed to room temperature and stirred during 5 h. When TLC showed complete disappearance of **S5** (Rf: 0.32 in *n*-Hexane/ EtOAc = 3/2) and the formation of **S6** (Rf: 0.5 in *n*-Hexane/ EtOAc = 3/2), the reaction mixture was quenched with sat. aq. NaHCO₃ solution (10 mL), diluted with CH₂Cl₂ (20 mL) was extracted with CH₂Cl₂ (2 × 20 mL) and the combined organic layer was washed with brine (2 × 15 mL). The organic layer was dried over anhydrous Na₂SO₄, filtered and evaporated under reduced pressure to get **S6** as yellow oil.¹¹⁴ Without further purification, the reaction mixture of **S2** was used for next step. To the stirred solution of **S6** in methanol (50 mL) was added NaOMe (30% in MeOH, 3 mL) dropwise at room temperature. The reaction mixture was allowed to stir for 17 h at room temperature until all starting material was consumed as monitored by TLC (**S7** Rf: 0.00 in *n*-Hexane/ EtOAc = 3/2). The reaction mixture was neutralized by the addition of Amberlite 120 (pH paper used for checking neutralization) and stirred for 2 h before filtration. Evaporation of the filtrate yielded brown colored gummy residue which was dried under vacuum to obtain **S7**. The obtained **S7** was used in the next step without further purification. **S7** was dissolved in dry DMF (50 mL) and cooled to –10 °C. Sodium hydride (60% in mineral oil, 1.00 g, 25 mmol) was added slowly and the mixture was stirred for 5 h while warming up to room temperature. Benzyl bromide (2.97 mL, 25 mmol) was added and the mixture was stirred for 17 h. The reaction was cooled down to 0 °C and water (2 mL) was added slowly. The solution was extracted with CH₂Cl₂ (3 × 100 mL) and the combined organic layers were washed with brine (3 × 200 mL). After silica gel column chromatography (Elution: *n*-Hexane/ EtOAc = 10/1), **Gal2 β** (1.02 g, 1.75 mmol) was obtained with 35% yield over 3 steps as a white solid. (**Gal2 β** Rf: 0.28 in *n*-Hexane/ EtOAc = 10/1). ¹H NMR (400 MHz, Chloroform-*d*) δ

7.42 – 7.24 (m, 20H), 4.95 (d, $J = 11.6$ Hz, 1H), 4.88 (d, $J = 10.2$ Hz, 1H), 4.80 (d, $J = 10.2$ Hz, 1H), 4.73 (s, 2H), 4.62 (d, $J = 11.6$ Hz, 1H), 4.42 (t, $J = 10.6$ Hz, 3H), 3.96 (s, 1H), 3.83 (t, $J = 9.4$ Hz, 1H), 3.64 – 3.52 (m, 4H), 2.83 – 2.65 (m, 2H), 1.30 (t, $J = 7.1$ Hz, 3H). This data is in accordance with those previously published.¹¹²

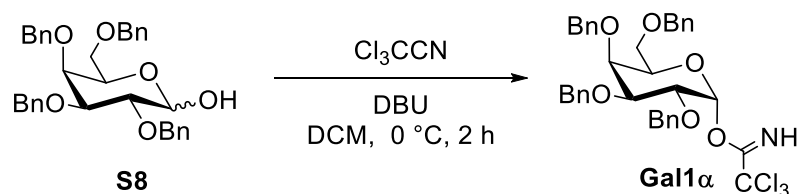
Preparation of 2,3,4,6-tetra-*O*-benzyl-galactopyranose (**S8**)



To a solution **Gal2β** (605 mg, 1.03 mmol) in Acetone (7.2 mL) and water (0.8 mL) was added *N*-Bromosuccinimide (548 mg, 3.08 mmol) and stirred for 4 h at room temperature. Then, the reaction mixture was cooled in an ice-bath and then quenched with triethylamine (0.7 mL, 5.0 mmol). The mixture was concentrated to remove acetone, diluted with sat. aq. NaHCO₃ solution (10 mL) and EtOAc (10 mL). The organic layer was extracted with CH₂Cl₂ (2 × 10 mL) and washed with brine (10 mL). The organic layer was dried over anhydrous Na₂SO₄, filtered and evaporated under reduced pressure for column chromatography purification (Elution: *n*-hexane/EtOAc = 4/1 to 2/1) and obtained as an inseparable α/β mixture as a colorless oil **S8** (479 mg, 0.886 mmol) with 86% yield. (**Gal2β** Rf: 0.75, **S8** Rf: 0.26 in *n*-Hexane/ EtOAc = 3/1); ¹H NMR (400 MHz, Chloroform-*d*) δ 7.40 – 7.22 (m, 20H), 5.28 (d, $J = 3.6$ Hz, 1H), 4.96 – 4.39 (m, 10H), 4.16 (t, $J = 6.5$ Hz, 1H), 4.04 (dd, $J = 9.8, 3.7$ Hz, 1H), 3.92 – 3.88 (m, 1H), 3.58 – 3.47 (m, 3H). This data is in accordance with those previously published.¹¹⁵

Preparation of 2,3,4,6-tetra-*O*-benzyl-α-D-galactopyranosyl trichloroacetimidate

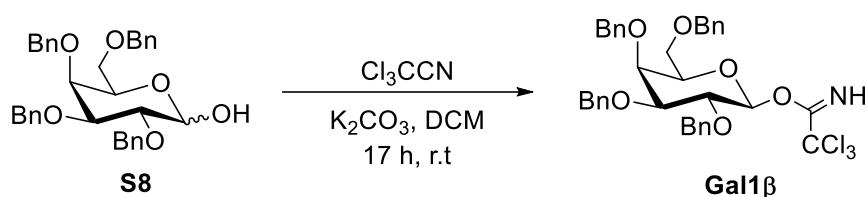
(**Gal1α**)¹¹⁶



To a solution of **S8** (479 mg, 0.886 mmol) in CH₂Cl₂ (10 mL) were added CCl₃CN (1.0 mL, 9.97 mmol) and DBU (0.08 mL, 0.52 mmol) at 0 °C. The dark solution was stirred at room temperature for 2 h, and then the reaction mixture was concentrated. The residue

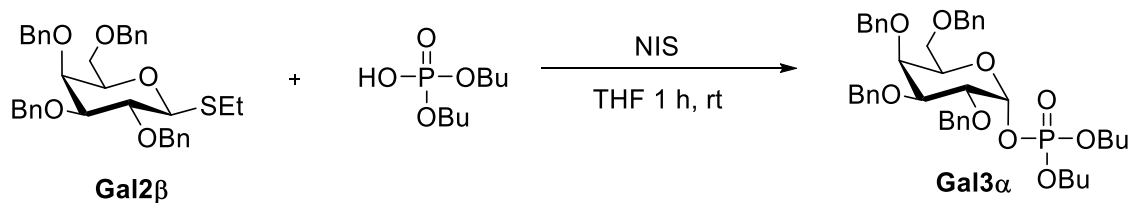
was purified by silica gel column chromatography (Elution: *n*-hexane–EtOAc, 4:1 containing 1% Et₃N) to give **Gal1a** (516 mg, 0.753 mmol) as a colorless oil with 85% yield; ¹H NMR (600 MHz, Chloroform-*d*) δ 8.51 (s, 1H), 7.38 – 7.23 (m, 20H), 6.52 (d, *J* = 3.5 Hz, 1H), 4.97 (d, *J* = 11.3 Hz, 1H), 4.82 (d, *J* = 11.9 Hz, 1H), 4.78 – 4.71 (m, 3H), 4.60 (d, *J* = 11.3 Hz, 1H), 4.46 (d, *J* = 11.7 Hz, 1H), 4.40 (d, *J* = 11.6 Hz, 1H), 4.24 (dd, *J* = 10.0, 3.5 Hz, 1H), 4.16 (t, *J* = 6.6 Hz, 1H), 4.06 (s, 1H), 4.02 (dd, *J* = 10.1, 2.8 Hz, 1H), 3.61 (dd, *J* = 9.4, 7.6 Hz, 1H), 3.55 (dd, *J* = 9.3, 5.5 Hz, 1H). This data is in accordance with those previously published.¹¹⁶

Preparation of 2,3,4,6-tetra-O-benzyl-β-D-galactopyranosyl trichloroacetimidate (**Gal1β**)



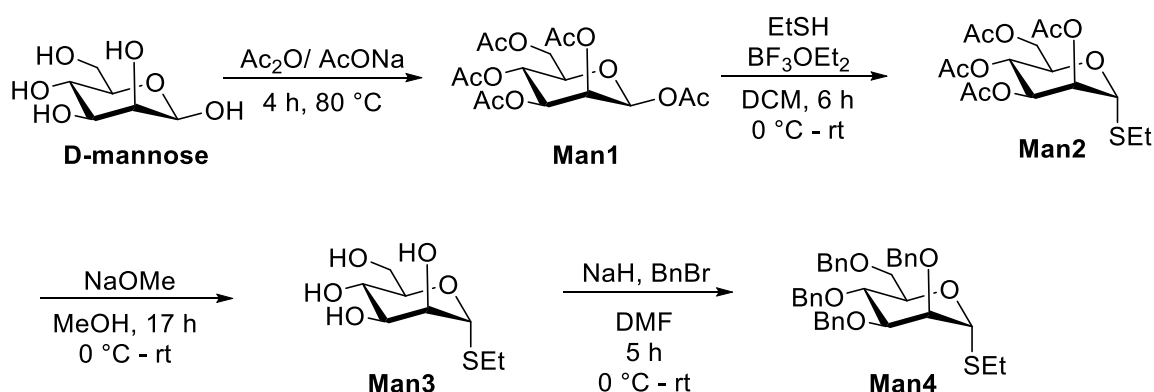
To compound **S8** in dry DCM (10 mL) were added CCl₃CN (0.1 mL, 1 mmol) and K₂CO₃ (138 mg, 1 mmol) at room temperature. The solution was stirred for 17 h at room temperature, and then the reaction mixture was concentrated. The residue was purified by silica gel column chromatography (Elution: *n*-hexane/EtOAc = 10/1 containing 1% Et₃N) to give **Gal1β** (67.1 mg, 0.11 mmol) as white solid (R_f: 0.49 in *n*-Hexane/ EtOAc = 3/1). with 57% yield; ¹H NMR (600 MHz, Chloroform-*d*) δ 8.62 (s, 1H), 7.36 – 7.26 (m, 20H), 5.75 (d, H-1β, *J* = 8.0 Hz, 1H), 4.95 (d, *J* = 11.5 Hz, 1H), 4.91 (d, *J* = 10.8 Hz, 1H), 4.81 (d, *J* = 10.8 Hz, 1H), 4.73 (d, *J* = 2.0 Hz, 2H), 4.64 (d, *J* = 11.5 Hz, 1H), 4.47 (d, *J* = 11.7 Hz, 1H), 4.43 (d, *J* = 11.8 Hz, 1H), 4.09 (dd, *J* = 9.7, 8.0 Hz, 1H), 3.99 (d, *J* = 3.1 Hz, 1H), 3.75 (t, *J* = 6.5 Hz, 1H), 3.68 – 3.59 (m, 3H). This data is in accordance with those previously published.⁸³

Preparation of 2,3,4,6-tetra-O-benzyl-α-D-galactopyranosyl di-*n*-butyl phosphate (**Gal3α**)



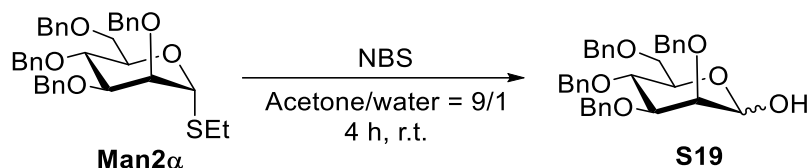
5.1 g of dry powder 3 Å molecular sieves were added to 60 ml dry DCM. Dibutyl hydrogen phosphate (1.43 ml, 7.21 mmol) were added and left stirring for 1.5 h. After stirring, the molecular sieves were allowed to settle and the supernatant (51 mL, 5.97 mmol) was added to a solution of **Gal2β** (1.00 g, 1.71 mmol) in CH₂Cl₂ (10 mL), cooled to 0 °C when *N*-Iodosuccinimide (0.70 g, 3.11 mmol) and TfOH (0.063 ml, 0.718 mmol) were added. After stirred for 2 h at room temperature, the reaction mixture was diluted with sat. aq. NaHCO₃ solution (50 mL), sat. aq. Na₂S₂O₃ solution (50 mL) and EtOAc (100 mL). The organic layer was extracted with EtOAc (2 × 100 mL) and washed with brine (100 mL). The organic layer was dried over anhydrous Na₂SO₄, filtered and evaporated under reduced pressure for silica gel column chromatography purification (Elution: *n*-hexane/EtOAc = 5/1 to 1/1) and obtained as a white solid **Gal3α** (1.10 g, 1.50 mmol) with 88% yield. (**Gal2β** Rf: 0.58, **Gal3α** Rf: 0.25 in *n*-Hexane/ EtOAc = 5/1); ¹H NMR (600 MHz, Chloroform-*d*) δ 7.41 – 7.24 (m, 20H), 5.88 (dd, *J* = 6.8, 3.4 Hz, 1H), 4.96 (d, *J* = 11.4 Hz, 1H), 4.83 – 4.73 (m, 4H), 4.58 (d, *J* = 11.4 Hz, 1H), 4.43 (q, *J* = 11.7 Hz, 2H), 4.15 – 4.09 (m, 2H), 4.05 – 3.95 (m, 5H), 3.91 (dd, *J* = 10.0, 2.8 Hz, 1H), 3.59 – 3.50 (m, 2H), 1.59 – 1.49 (m, 4H), 1.29 (ddq, *J* = 32.4, 14.8, 7.4 Hz, 4H), 0.86 (dt, *J* = 16.0, 7.4 Hz, 6H); ¹³C NMR (151 MHz, Chloroform-*d*) δ 138.7, 138.6, 138.3, 138.0, 128.52, 128.50, 128.40, 128.36, 128.3, 128.1, 127.94, 127.89, 127.78, 127.71, 127.69, 127.6, 96.2 (d, *J* = 6.3 Hz), 78.2, 76.0 (d, *J* = 7.3 Hz), 75.0, 74.8, 73.6, 73.3, 73.1, 71.5, 68.7, 67.8 (d, *J* = 5.8 Hz), 67.5 (d, *J* = 5.7 Hz), 32.3 (d, *J* = 7.0 Hz), 32.2 (d, *J* = 7.0 Hz), 18.75, 18.69, 13.7; ³¹P NMR (243 MHz, Chloroform-*d*) δ -1.87; HRMS (ESI): [M+Na]⁺ calcd for C₄₂H₅₃O₉PNa⁺ 755.3319, found 755.3325.

Preparation of ethyl 2,3,4,6-tetra-*O*-benzyl-1-thio- α -D-mannopyranoside (**Man2a**)¹¹⁷⁻¹¹⁸

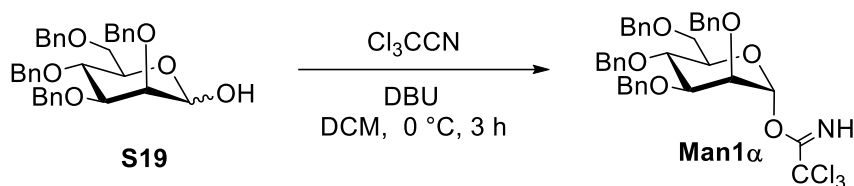


To a gently refluxed Ac₂O (9.4 mL, 100 mmol) containing NaOAc (1.0 g, 13 mmol) was slowly added D-mannose (1.8g, 10 mmol) over a period of 15 min. After the mixture was heated to 80 °C for 4h, the mixture was cooled to room temperature. When TLC showed

complete disappearance of the starting material and the formation of **S16** (Rf: 0.30 in *n*-Hexane/ EtOAc = 3/2), the reaction was quenched by addition of ice under sonication. The precipitation was filtered and washed with H₂O until the acetic acid disappeared and recrystallized using EtOH (0.5 mL) by adding *n*-hexane (50 mL) to get **S16** (81%, 3.1 g, 8.1 mmol) as white solid.¹¹⁷ A mixture of **S16** (1.95 g, 5 mmol), EtSH (0.4 mL, 5.6 mmol) and BF₃OEt₂ (0.7 mL, 5.6 mmol) in anhydrous CH₂Cl₂ (20 mL) was cooled to 0 °C. The mixture was warmed to room temperature and stirred during 6 h. When TLC showed complete disappearance of **S16** and the formation of **S17** (Rf: 0.42 in *n*-Hexane/ EtOAc = 3/2), the reaction mixture was quenched with sat. aq. NaHCO₃ solution (10 mL), diluted with CH₂Cl₂ (20 mL) was extracted with CH₂Cl₂ (2 × 20 mL) and the combined organic layer was washed with brine (2 × 15 mL). The organic layer was dried over anhydrous Na₂SO₄, filtered and evaporated under reduced pressure to get **S17** as yellow oil. Without further purification, the reaction mixture of **S17** was used for next step. To the stirred solution of **S17** in methanol (50 mL) was added NaOMe (30% in MeOH, 3 mL) dropwise at room temperature. The reaction mixture was allowed to stir for 17 h at room temperature until all starting material was consumed as monitored by TLC (**S18** Rf: 0.00 in *n*-Hexane/ EtOAc = 3/2). The reaction mixture was neutralized by the addition of Amberlite 120 (pH paper used for checking neutralization) and stirred for 2 h before filtration. Evaporation of the filtrate yielded brown colored gummy residue which was dried under vacuum to obtain **S18**. The obtained **S18** was used in the next step without further purification. **S18** was dissolved in dry DMF (50 mL) and cooled to -10 °C. Sodium hydride (60% in mineral oil, 1.00 g, 25 mmol) was added slowly and the mixture was stirred for 5 h while warming up to room temperature. Benzyl bromide (2.97 mL, 25 mmol) was added and the mixture was stirred for 15 h. The reaction was cooled down to 0 °C and water (2 mL) was added slowly. The solution was extracted with CH₂Cl₂ (3 × 100 mL) and the combined organic layers were washed with brine (3 × 200 mL). After silica gel column chromatography (Elution: *n*-Hexane/ EtOAc = 10/1), **Man2a** (884 mg, 1.51 mmol) was obtained with 30% yield over 3 steps as a pale yellow oil (**Man2a** Rf: 0.35 in *n*-Hexane/ EtOAc = 3/1); ¹H NMR (400 MHz, Chloroform-*d*) δ 7.43 – 7.14 (m, 20H), 5.40 (s, 1H), 4.88 (d, *J* = 10.8 Hz, 1H), 4.76 – 4.63 (m, 3H), 4.57 (d, *J* = 2.1 Hz, 2H), 4.54 – 4.48 (m, 2H), 4.13 (ddd, *J* = 9.8, 4.8, 1.9 Hz, 1H), 4.03 (t, *J* = 9.6 Hz, 1H), 3.87 – 3.79 (m, 3H), 3.71 (dd, *J* = 10.8, 2.0 Hz, 1H), 2.70 – 2.49 (m, 2H), 1.25 (t, *J* = 7.4 Hz, 3H). This data is in accordance with those previously published.¹¹⁸

Preparation of 2,3,4,6-tetra-*O*-benzyl-D-mannopyranoside (**S19**)

To a solution **Man2α** (621 mg, 1.06 mmol) in Acetone (7.2 mL) and water (0.8 mL) was added *N*-Bromosuccinimide (548 mg, 3.08 mmol) and stirred for 4 h at room temperature. Then, the reaction mixture was cooled in an ice-bath and then quenched with triethylamine (0.7 mL, 5.0 mmol). The mixture was concentrated to remove acetone, diluted with sat. aq. NaHCO_3 solution (10 mL) and EtOAc (10 mL). The organic layer was extracted with CH_2Cl_2 (2×10 mL) and washed with brine (10 mL). The organic layer was dried over anhydrous Na_2SO_4 , filtered and evaporated under reduced pressure for column chromatography purification (Elution: *n*-hexane/EtOAc = 4/1 to 2/1) and obtained as an inseparable α/β mixture as a colorless oil **S19** (470 mg, 0.862 mmol) with 82% yield. (**S19** Rf: 0.17 in *n*-Hexane/ EtOAc = 4/1); ^1H NMR (400 MHz, Chloroform-*d*) δ 7.41 – 7.25 (m, 18H), 7.20 – 7.09 (m, 2H), 5.26 (s, 1H), 4.88 (d, J = 11.0 Hz, 1H), 4.74 (d, J = 4.0 Hz, 2H), 4.62 (s, 2H), 4.56 (d, J = 7.7 Hz, 2H), 4.49 (d, J = 10.9 Hz, 1H), 4.03 (dd, J = 8.9, 6.1 Hz, 1H), 3.99 – 3.93 (m, 1H), 3.91 – 3.83 (m, 1H), 3.81 (dd, J = 3.0, 1.9 Hz, 1H), 3.76 – 3.67 (m, 2H), 3.08 (s, 1H). This data is in accordance with those previously published.¹¹⁵

Preparation of 2,3,4,6-tetra-*O*-benzyl- α -D-mannopyranosyl trichloroacetimidate (**Man1α**)¹¹⁹

To a solution of **S19** (470 mg, 0.862 mmol) in CH_2Cl_2 (10 mL) were added CCl_3CN (1.0 mL, 9.97 mmol) and DBU (0.06 mL, 0.40 mmol) at 0 °C. The dark solution was stirred at room temperature for 3 h, and then the reaction mixture was concentrated. The residue was purified by silica gel column chromatography (Elution: *n*-hexane/EtOAc = 4/1 containing 1% Et_3N) to give **Man1α** (516 mg, 0.753 mmol) as colorless oil with 85% yield; ^1H NMR (400 MHz, Chloroform-*d*) δ 8.54 (s, 1H), 7.46 – 7.19 (m, 20H), 6.39 (d, J = 2.0 Hz, 1H), 4.92 (d, J = 10.7 Hz, 1H), 4.79 (d, J = 2.2 Hz, 2H), 4.72 – 4.52 (m, 5H), 4.17 (t, J

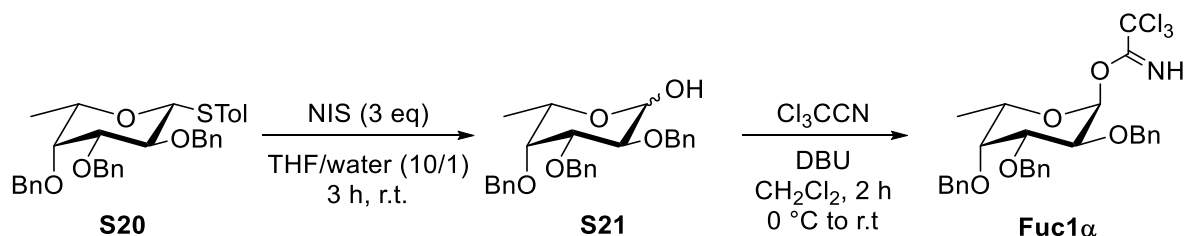
= 9.7 Hz, 1H), 4.01 – 3.92 (m, 2H), 3.89 (t, $J = 2.6$ Hz, 1H), 3.84 (dd, $J = 11.2, 4.4$ Hz, 1H), 3.75 (dd, $J = 11.2, 1.9$ Hz, 1H). This data is in accordance with those previously published.¹¹⁹

Preparation of 2,3,4,6-Tetra-O-benzyl- α -D-mannopyranosyl diphenyl phosphate (**Man3 α**)¹²⁰



To a solution of **S19** (500 mg, 0.925 mmol) in CH_2Cl_2 (10 mL) were added diphenylphosphoryl chloride (0.25 mL, 1.20 mmol) and DMAP (283 mg, 2.31 mmol) at 0 °C. After stirred for 30 min at 0 °C, and then the reaction mixture was quenched with crushed ice, followed by stirring at room temperature for 15 min. The reaction mixture was diluted with sat. aq. NaHCO_3 solution (15 mL) and Et_2O (10 mL), and then the organic layer was extracted with EtOAc (2×30 mL) and washed with brine (20 mL). The organic layer was dried over anhydrous Na_2SO_4 , filtered and evaporated under reduced pressure for silica gel column chromatography purification (Elution: n -hexane/ EtOAc = 8/1 to 3/1) and obtained as a colorless oil **Man3 α** (515 mg, 0.666 mmol) with 72% yield. (Rf: 0.19 in n -Hexane/ EtOAc = 3/1) ^1H NMR (600 MHz, $\text{Chloroform-}d$) δ 7.39 – 7.07 (m, 30H), 5.99 (d, $J = 6.2$ Hz, 1H), 4.85 (d, $J = 10.6$ Hz, 1H), 4.69 (s, 2H), 4.63 (d, $J = 12.0$ Hz, 1H), 4.46 (td, $J = 27.9, 26.6, 11.2$ Hz, 4H), 4.09 (t, $J = 9.8$ Hz, 1H), 3.91 – 3.78 (m, 2H), 3.77 – 3.68 (m, 2H), 3.52 (d, $J = 11.2$ Hz, 1H). This data is in accordance with those previously published.¹²⁰

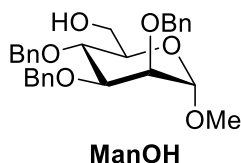
Preparation of 2,3,4-tri-O-benzyl- α -L-fucopyranosyl trichloroacetimidate (**Fuc1 α**)¹²¹



To a solution **S20**¹²² (279 mg, 0.52 mmol) in THF (20 mL) and water (2 mL) were added N -Iodosuccinimide (232 mg 1.03 mmol), and then stirred for 1 h at room temperature. The reaction mixture was quenched with sat. aq. NaHCO_3 solution (10 mL) and DCM (10

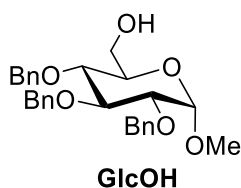
mL). The organic layer was extracted with DCM (2×10 mL) and washed with brine (10 mL). The organic layer was dried over anhydrous Na_2SO_4 , filtered and evaporated under reduced pressure for column chromatography purification (Elution: *n*-hexane/EtOAc = 6/1 to 2/1) and obtained as an inseparable α/β mixture **S21** (Rf: 0.1 in *n*-Hexane/ EtOAc = 3/1). To compound **S21** in dry DCM (15 mL) were added CCl_3CN (0.2 mL, 1.99 mmol) and DBU (0.05 mL, 0.33 mmol) at 0 °C. The dark solution was stirred at room temperature for 2 h, and then the reaction mixture was concentrated. The residue was purified by silica gel column chromatography (Elution: Toluene/EtOAc = 20/1 containing 1% to give **Fuc1a** (153 mg, 0.26 mmol) as a white solid (Rf: 0.21 in Toluene/EtOAc = 3/1) with 51% yield; ^1H NMR (400 MHz, Chloroform-*d*) δ 8.50 (s, 1H), 7.53 – 7.11 (m, 15H), 6.52 (d, $J = 3.5$ Hz, 1H), 5.01 (d, $J = 11.5$ Hz, 1H), 4.95 – 4.61 (m, 5H), 4.24 (dd, $J = 10.2, 3.4$ Hz, 1H), 4.09 (d, $J = 6.6$ Hz, 1H), 4.06 – 3.96 (m, 1H), 3.71 (s, 1H), 1.16 (d, $J = 6.5$ Hz, 3H). This data is in accordance with those previously published.¹²³

Methyl 2,3,4-tri-O-benzyl- α -D-mannopyranoside (**ManOH**)



ManOH was synthesized as described in ref 7. ^1H NMR (400 MHz, Chloroform-*d*) δ 7.35 – 7.25 (m, 15H), 4.93 (d, $J = 10.9$ Hz, 1H), 4.77 (d, $J = 12.3$ Hz, 1H), 4.71 – 4.68 (m, 2H), 4.66 (d, $J = 6.0$ Hz, 1H), 4.62 (s, 2H), 3.95 (t, $J = 9.4$ Hz, 1H), 3.89 (dd, $J = 9.4, 2.9$ Hz, 1H), 3.84 (dd, $J = 11.7, 2.9$ Hz, 1H), 3.80 – 3.72 (m, 2H), 3.61 (ddd, $J = 9.4, 4.7, 3.0$ Hz, 1H), 3.29 (s, 3H), 1.79 (bs, 1H). This data is in accordance with those previously published.¹²⁴

Methyl 2,3,4-tri-O-benzyl- α -D-glucopyranoside (**GlcOH**)



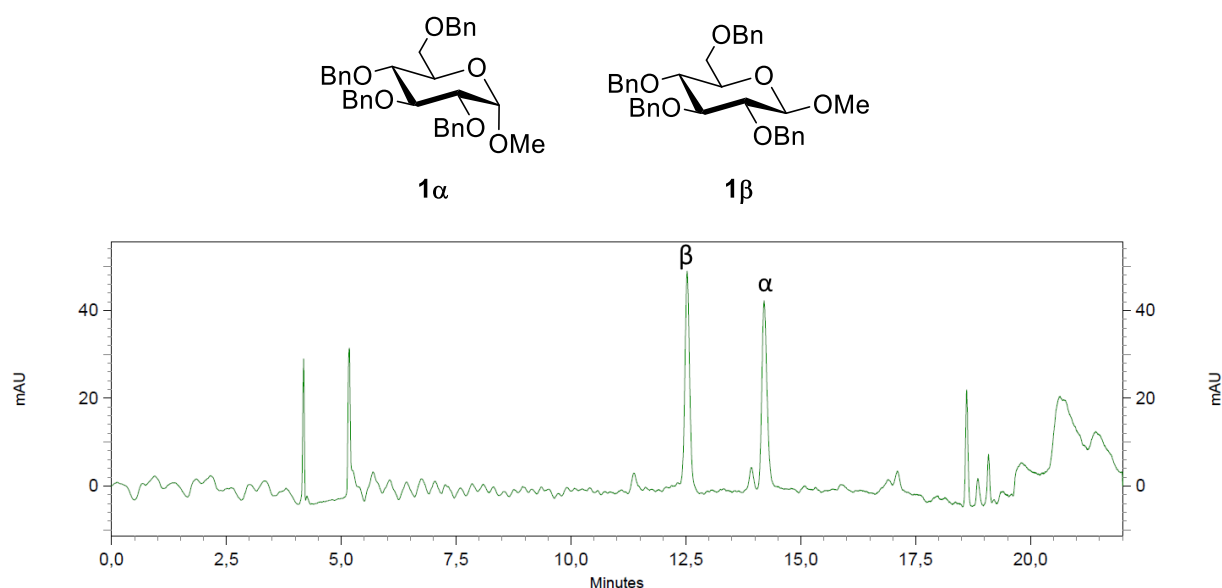


Figure 6.12: a HPLC spectrum of **1 α** , **1 β** (Method A)

Methyl 2,3,4,6-tetra-*O*-benzyl- α / β -D-glucopyranoside (**1 α**) ^1H NMR (400 MHz, Chloroform-*d*) δ 7.32 – 7.22 (m, 18H), 7.13 (dd, J = 7.1, 2.4 Hz, 2H), 4.98 (d, J = 10.9 Hz, 1H), 4.87 – 4.77 (m, 3H), 4.70 – 4.57 (m, 3H), 4.47 (dd, J = 11.4, 4.4 Hz, 2H), 3.98 (t, J = 9.3 Hz, 1H), 3.79 – 3.69 (m, 2H), 3.67 – 3.59 (m, 2H), 3.56 (dd, J = 9.6, 3.6 Hz, 1H), 3.38 (s, 3H).

(**1 β**) ^1H NMR (400 MHz, Chloroform-*d*) δ 7.37 – 7.19 (m, 18H), 7.12 (dd, J = 6.8, 2.7 Hz, 2H), 4.89 (dd, J = 11.0, 2.1 Hz, 2H), 4.77 (t, J = 11.1 Hz, 2H), 4.67 (d, J = 11.0 Hz, 1H), 4.63 – 4.46 (m, 3H), 4.28 (d, J = 7.7 Hz, 1H), 3.72 (dd, J = 10.7, 2.0 Hz, 1H), 3.69 – 3.56 (m, 3H), 3.56 (s, 3H), 3.47 – 3.37 (m, 2H). These data are in accordance with those previously published.¹²⁵

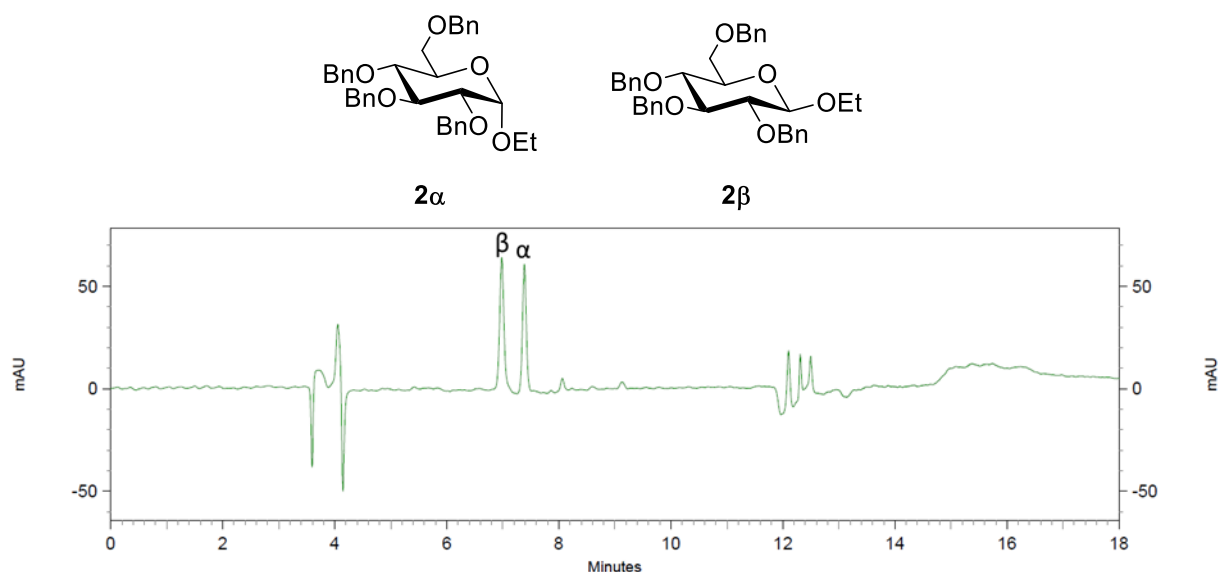


Figure 6.13: a HPLC spectrum of **2 α** , **2 β** (Method B)

Ethyl 2,3,4,6-tetra-*O*-benzyl- α/β -D-glucopyranoside (**2a**) ^1H NMR (400 MHz, Chloroform-*d*) δ 7.40 – 7.26 (m, 18H), 7.15 – 7.09 (m, 2H), 5.00 (d, J = 10.8 Hz, 1H), 4.86 – 4.77 (m, 3H), 4.75 (d, J = 3.6 Hz, 1H), 4.68 – 4.58 (m, 2H), 4.46 (dd, J = 11.4, 4.0 Hz, 2H), 4.00 (t, J = 9.3 Hz, 1H), 3.78 (ddd, J = 10.0, 3.6, 2.0 Hz, 1H), 3.74 – 3.59 (m, 4H), 3.58 – 3.46 (m, 2H), 1.23 (d, J = 7.1 Hz, 3H).

(**2b**) ^1H NMR (400 MHz, Chloroform-*d*) δ 7.37 – 7.26 (m, 18H), 7.15 (dd, J = 7.1, 2.5 Hz, 2H), 4.95 (t, J = 10.9 Hz, 2H), 4.80 (dd, J = 12.3, 10.8 Hz, 2H), 4.72 (d, J = 10.9 Hz, 1H), 4.58 (q, J = 12.2 Hz, 2H), 4.52 (d, J = 10.8 Hz, 1H), 4.41 (d, J = 7.8 Hz, 1H), 4.02 (dq, J = 9.6, 7.1 Hz, 1H), 3.75 (dd, J = 10.7, 2.0 Hz, 1H), 3.71 – 3.53 (m, 4H), 3.49 – 3.42 (m, 2H), 1.30 (t, J = 7.0 Hz, 3H). These data are in accordance with those previously published.¹²⁶

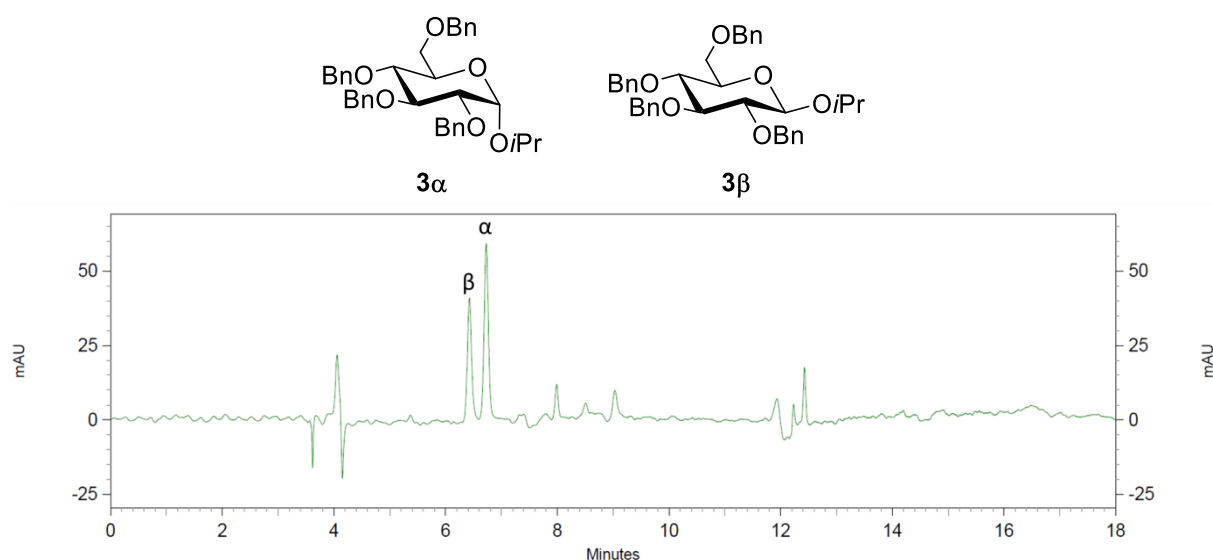


Figure 6.14: a HPLC spectrum of **3a**, **3b** (Method B)

Isopropyl 2,3,4,6-tetra-*O*-benzyl- α/β -D-glucopyranoside (**3a**) ^1H NMR (400 MHz, Chloroform-*d*) δ 7.41 – 7.08 (m, 20H), 5.00 (d, J = 10.9, 1H), 4.90 – 4.74 (m, 4H), 4.63 (t, J = 12.8, 2H), 4.46 (d, J = 11.5, 2H), 3.99 (t, J = 9.3, 1H), 3.94 – 3.79 (m, 2H), 3.74 (d, J = 11.0, 1H), 3.68 – 3.58 (m, 2H), 3.55 (d, J = 9.3, 1H), 1.22 (d, J = 6.3, 3H), 1.18 (d, J = 6.0, 3H).

(**3b**) ^1H NMR (400 MHz, Chloroform-*d*) δ 7.39 – 7.06 (m, 20H), 4.97 – 4.85 (m, 2H), 4.83 – 4.71 (m, 2H), 4.67 (d, J = 10.9, 1H), 4.61 – 4.47 (m, 3H), 4.43 (d, J = 7.9, 1H), 3.99 (q, J = 6.3, 1H), 3.74 – 3.66 (m, 1H), 3.65 – 3.56 (m, 2H), 3.51 (t, J = 9.0, 1H), 3.46 – 3.35 (m, 2H), 1.28 (d, J = 5.8, 3H), 1.21 (d, J = 5.9, 3H). These data are in accordance with those previously published.⁹⁰

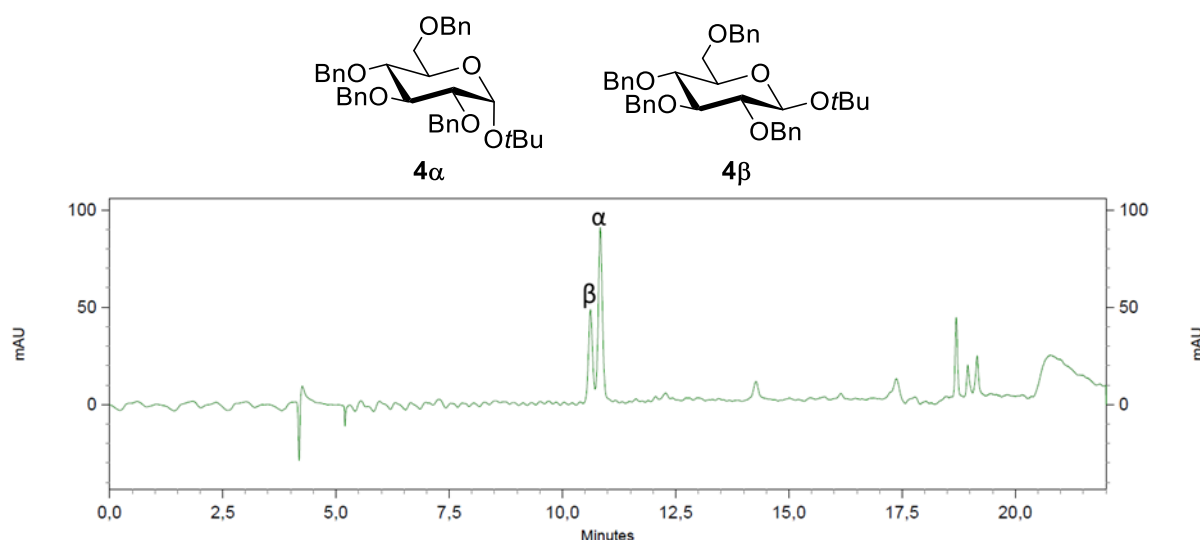


Figure 6.15: a HPLC spectrum of **4α**, **4β** (Method A)

tert-Butyl 2,3,4,6-tetra-*O*-benzyl- α/β -D-glucopyranoside (**4α**) ^1H NMR (400 MHz, Chloroform-*d*) δ 7.34 (d, $J = 7.6$ Hz, 18H), 7.16 – 7.10 (m, 2H), 5.14 (d, $J = 3.6$ Hz, 1H), 4.99 (d, $J = 10.8$ Hz, 1H), 4.83 (dd, $J = 10.7, 7.1$ Hz, 2H), 4.76 – 4.61 (m, 3H), 4.46 (d, $J = 10.4$ Hz, 1H), 4.45 (d, $J = 12.1$ Hz, 1H), 4.04 – 3.92 (m, 2H), 3.77 (dd, $J = 10.4, 3.4$ Hz, 1H), 3.68 (dd, $J = 10.0, 8.9$ Hz, 1H), 3.59 (dd, $J = 10.4, 2.1$ Hz, 1H), 3.54 (dd, $J = 9.7, 3.7$ Hz, 1H), 1.27 (s, 9H).

(**4β**) ^1H NMR (400 MHz, Chloroform-*d*) δ 7.35 – 7.19 (m, 18H), 7.18 – 7.12 (m, 2H), 4.95 (d, $J = 10.9$ Hz, 1H), 4.89 (d, $J = 10.9$ Hz, 1H), 4.79 (d, $J = 10.9$ Hz, 1H), 4.75 (d, $J = 10.9$ Hz, 1H), 4.69 (d, $J = 10.9$ Hz, 1H), 4.59 – 4.48 (m, 4H), 3.68 (dd, $J = 10.7, 1.9$ Hz, 1H), 3.66 – 3.57 (m, 2H), 3.50 (t, $J = 9.2$ Hz, 1H), 3.46 – 3.36 (m, 2H), 1.30 (s, 9H). These data are in accordance with those previously published.¹²⁶

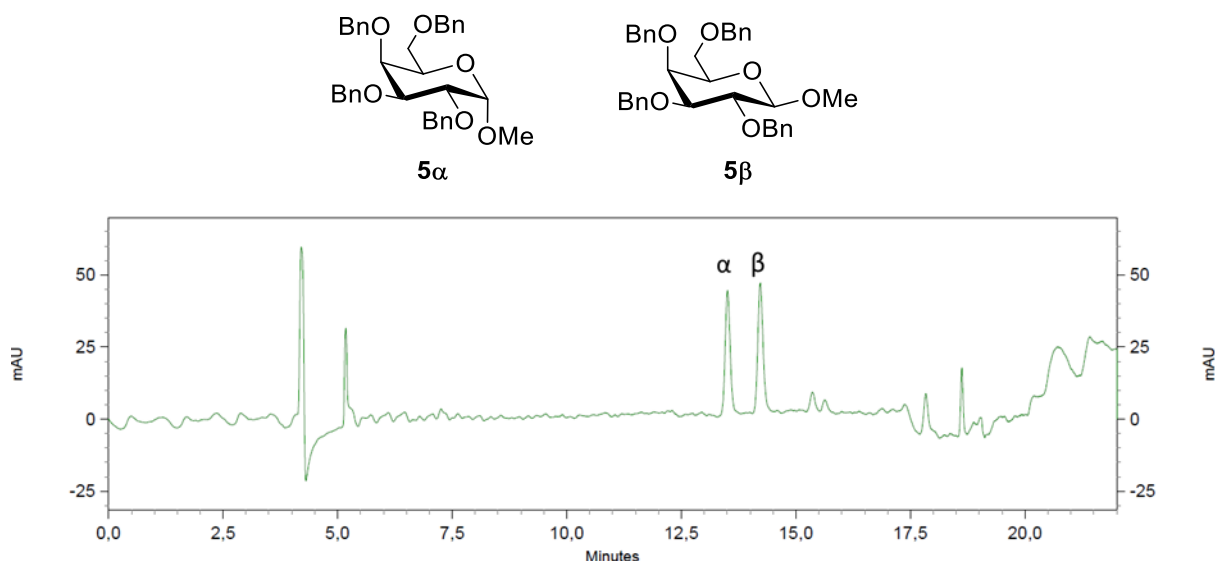


Figure 6.16: a HPLC spectrum of **5α**, **5β** (Method A)

Methyl 2,3,4,6-tetra-*O*-benzyl- α/β -D-galactopyranoside (**5a**) ^1H NMR (400 MHz, Chloroform-*d*) δ 7.41 – 7.26 (m, 20H), 4.95 (d, J = 11.5 Hz, 1H), 4.85 (dd, J = 11.9, 4.7 Hz, 2H), 4.78 – 4.66 (m, 3H), 4.58 (d, J = 11.5 Hz, 1H), 4.48 (d, J = 11.8 Hz, 1H), 4.39 (d, J = 11.8 Hz, 1H), 4.04 (ddd, J = 11.0, 3.6, 1.4 Hz, 1H), 3.98 – 3.86 (m, 3H), 3.52 (d, J = 6.5 Hz, 2H), 3.37 (s, 3H).

(**5 β**) ^1H NMR (400 MHz, Chloroform-*d*) δ 7.39 – 7.25 (m, 20H), 4.94 (d, J = 11.7 Hz, 1H), 4.90 (d, J = 10.9 Hz, 1H), 4.78 – 4.69 (m, 3H), 4.62 (d, J = 11.7 Hz, 1H), 4.45 (d, J = 11.7 Hz, 1H), 4.40 (d, J = 11.7 Hz, 1H), 4.27 (d, J = 7.6 Hz, 1H), 3.89 (d, J = 2.8 Hz, 1H), 3.80 (dd, J = 9.8, 7.7 Hz, 1H), 3.59 (dd, J = 6.3, 2.8 Hz, 2H), 3.55 (s, 3H), 3.54 – 3.49 (m, 2H).

These data are in accordance with those previously published.¹²⁵

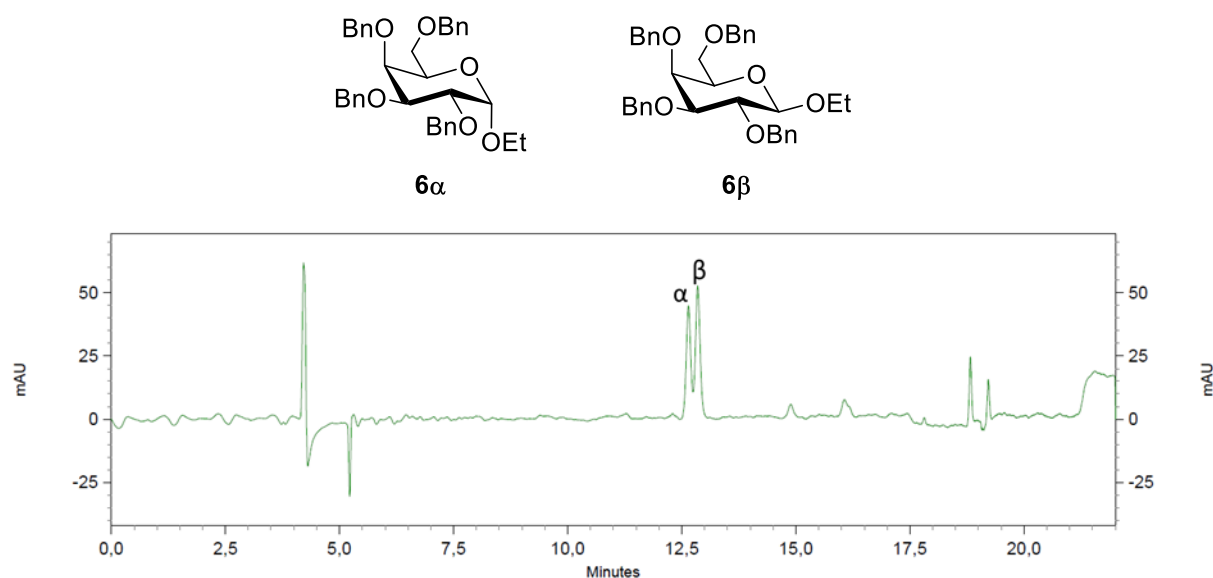


Figure 6.17: a HPLC spectrum of **6 α** , **6 β** (Method A)

Ethyl 2,3,4,6-tetra-*O*-benzyl- α/β -D-galactopyranoside (**6 α**) ^1H NMR (600 MHz, Chloroform-*d*) δ 7.45 – 7.15 (m, 20H), 4.93 (d, J = 11.4 Hz, 1H), 4.84 (d, J = 11.7 Hz, 1H), 4.81 (dd, J = 7.9, 4.2 Hz, 2H), 4.72 (d, J = 11.7 Hz, 1H), 4.66 (d, J = 12.1 Hz, 1H), 4.55 (d, J = 11.4 Hz, 1H), 4.46 (d, J = 11.8 Hz, 1H), 4.38 (d, J = 11.8 Hz, 1H), 4.01 (dd, J = 9.4, 3.7 Hz, 1H), 3.97 – 3.92 (m, 3H), 3.68 (dq, J = 10.1, 7.1 Hz, 1H), 3.55 – 3.47 (m, 3H), 1.22 (t, J = 7.1 Hz, 3H); ^{13}C NMR (151 MHz, Chloroform-*d*) δ 139.1, 138.9, 138.8, 138.2, 128.52, 128.47, 128.43, 128.36, 128.3, 128.2, 127.9, 127.8, 127.75, 127.66, 127.59, 127.57, 97.3, 79.3, 76.7, 75.4, 74.9, 73.6, 73.5, 73.4, 69.4, 69.2, 63.5, 15.1; HRMS (ESI): $[\text{M}+\text{Na}]^+$ calcd for $\text{C}_{36}\text{H}_{40}\text{O}_6\text{Na}^+$ 591.2717, found 591.2733.

(**6 β**) ^1H NMR (400 MHz, Chloroform-*d*) δ 7.40 – 7.26 (m, 20H), 4.93 (dd, J = 11.3, 2.5 Hz, 2H), 4.78 – 4.67 (m, 3H), 4.61 (d, J = 11.7 Hz, 1H), 4.48 – 4.32 (m, 3H), 4.03 – 3.93 (m,

1H), 3.88 (d, $J = 2.8$ Hz, 1H), 3.81 (dd, $J = 9.8, 7.7$ Hz, 1H), 3.63 – 3.55 (m, 3H), 3.55 – 3.48 (m, 2H), 1.25 (d, $J = 7.0$ Hz, 3H). These data are in accordance with those previously published.⁷⁵

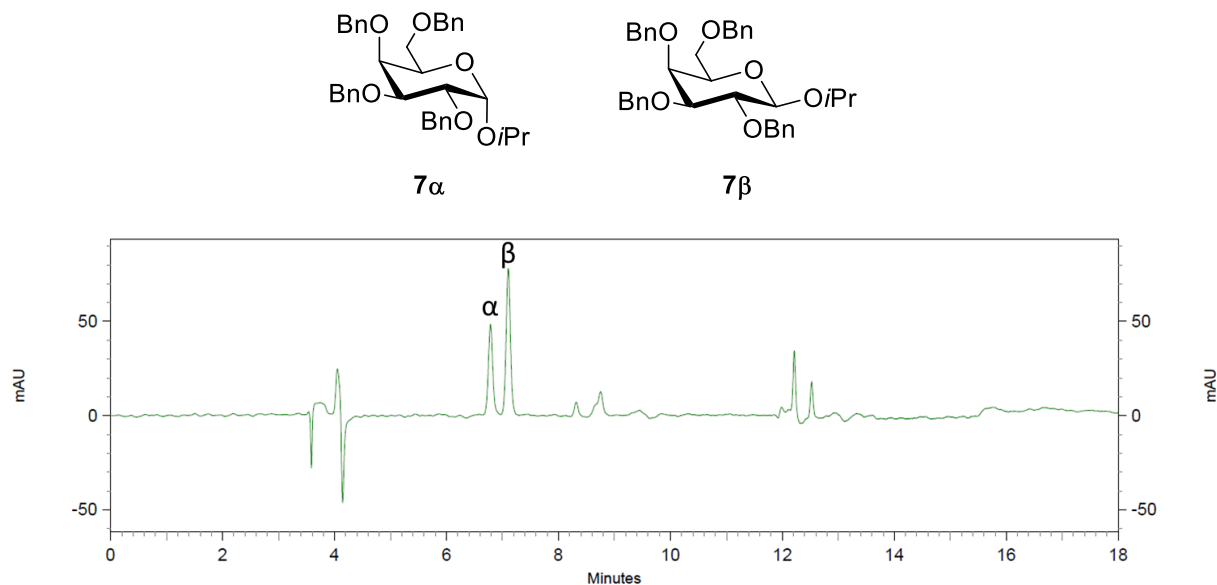
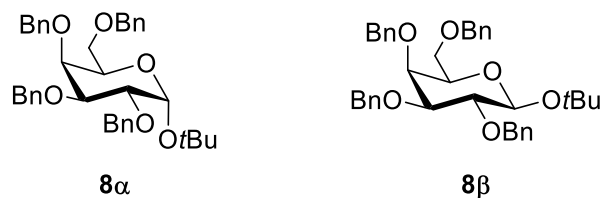


Figure 6.18: a HPLC spectrum of **7 α** , **7 β** (Method B)

Isopropyl 2,3,4,6-tetra-*O*-benzyl- α/β -D-galactopyranoside (**7 α**) ^1H NMR (400 MHz, Chloroform-*d*) δ 7.42 – 7.22 (m, 20H), 5.01 – 4.90 (m, 2H), 4.83 (dd, $J = 18.0, 11.8$ Hz, 2H), 4.73 (d, $J = 11.6$ Hz, 1H), 4.67 (d, $J = 12.0$ Hz, 1H), 4.57 (d, $J = 11.5$ Hz, 1H), 4.51 – 4.36 (m, 2H), 4.08 – 3.82 (m, 5H), 3.52 (m, 2H), 1.23 (d, $J = 6.3$ Hz, 3H), 1.18 (d, $J = 6.1$ Hz, 3H). These data are in accordance with those previously published.¹²⁷

(**7 β**) ^1H NMR (400 MHz, Chloroform-*d*) δ 7.31 (m, 20H), 4.94 (dd, $J = 11.2, 4.0$ Hz, 2H), 4.80 – 4.68 (m, 3H), 4.63 (d, $J = 11.7$ Hz, 1H), 4.47 – 4.38 (m, 3H), 3.99 (hept, $J = 6.2$ Hz, 1H), 3.88 (d, $J = 2.9$ Hz, 1H), 3.79 (dd, $J = 9.8, 7.7$ Hz, 1H), 3.61 – 3.47 (m, 4H), 1.28 (d, $J = 6.2$ Hz, 3H), 1.22 (d, $J = 6.1$ Hz, 3H). These data are in accordance with those previously published.⁹⁰



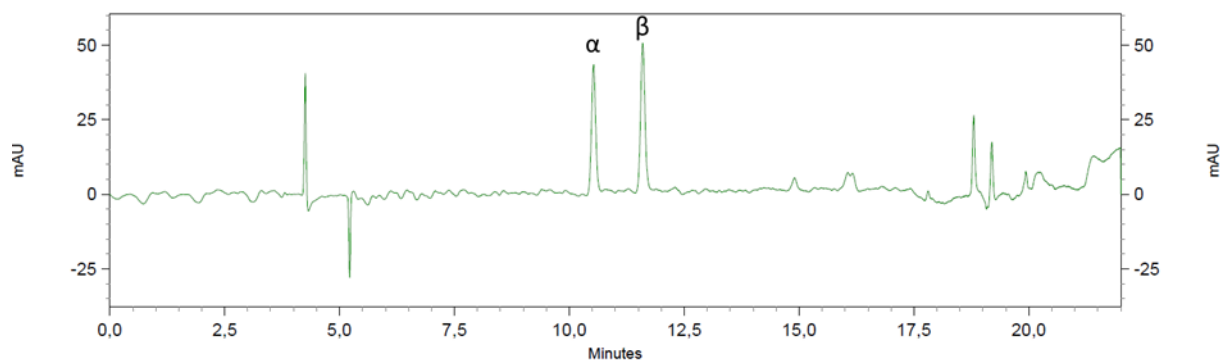
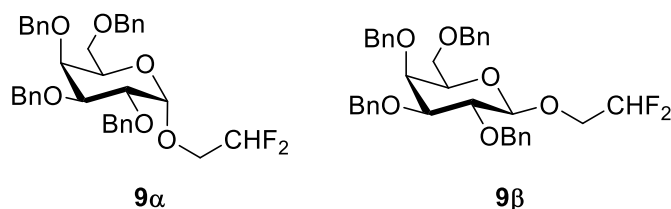


Figure 6.19: a HPLC spectrum of **8α**, **8β** (Method A)

tert-Butyl 2,3,4,6-tetra-*O*-benzyl- α/β -D-galactopyranoside (**8α**) ^1H NMR (600 MHz, Chloroform-*d*) δ 7.42 – 7.20 (m, 20H), 5.16 (d, $J = 3.7$ Hz, 1H), 4.95 (d, $J = 11.4$ Hz, 1H), 4.82 (d, $J = 11.6$ Hz, 1H), 4.77 (d, $J = 11.9$ Hz, 1H), 4.73 (d, $J = 11.6$ Hz, 1H), 4.68 (d, $J = 11.9$ Hz, 1H), 4.55 (d, $J = 11.4$ Hz, 1H), 4.46 (d, $J = 11.7$ Hz, 1H), 4.40 (d, $J = 11.7$ Hz, 1H), 4.13 (t, $J = 6.6$ Hz, 1H), 4.03 – 3.99 (m, 2H), 3.95 (dd, $J = 10.2, 2.8$ Hz, 1H), 3.57 (dd, $J = 9.2, 7.7$ Hz, 1H), 3.47 (dd, $J = 9.1, 5.7$ Hz, 1H), 1.25 (s, 9H); ^{13}C NMR (151 MHz, Chloroform-*d*) δ 139.1, 139.0, 138.9, 138.2, 128.5, 128.42, 128.40, 128.3, 128.2, 128.1, 127.85, 127.79, 127.6, 127.54, 127.50, 127.47, 92.3, 79.4, 76.7, 75.2, 75.1, 74.9, 73.6, 73.4, 73.0, 69.1, 68.7, 28.8; HRMS (ESI): $[\text{M}+\text{Na}]^+$ calcd for $\text{C}_{38}\text{H}_{44}\text{O}_6\text{Na}^+$ 619.3030, found 619.3040.

(**8β**) ^1H NMR (600 MHz, Chloroform-*d*) δ 7.40 – 7.23 (m, 20H), 4.93 (dd, $J = 11.2, 9.3$ Hz, 2H), 4.75 (d, $J = 9.3$ Hz, 2H), 4.70 (d, $J = 11.8$ Hz, 1H), 4.61 (d, $J = 11.7$ Hz, 1H), 4.52 (d, $J = 7.7$ Hz, 1H), 4.44 (d, $J = 11.7$ Hz, 1H), 4.40 (d, $J = 11.7$ Hz, 1H), 3.87 (d, $J = 2.9$ Hz, 1H), 3.80 – 3.75 (m, 1H), 3.60 – 3.48 (m, 4H), 1.29 (s, 9H); ^{13}C NMR (151 MHz, Chloroform-*d*) δ 139.0, 138.9, 138.8, 138.2, 128.6, 128.57, 128.52, 128.4, 128.38, 128.33, 127.9, 127.8, 127.7, 127.63, 127.59, 98.3, 82.9, 79.8, 75.9, 75.4, 74.6, 73.8, 73.7, 73.4, 73.3, 69.4, 29.0; HRMS (ESI): $[\text{M}+\text{Na}]^+$ calcd for $\text{C}_{38}\text{H}_{44}\text{O}_6\text{Na}^+$ 619.3030, found 619.3042.



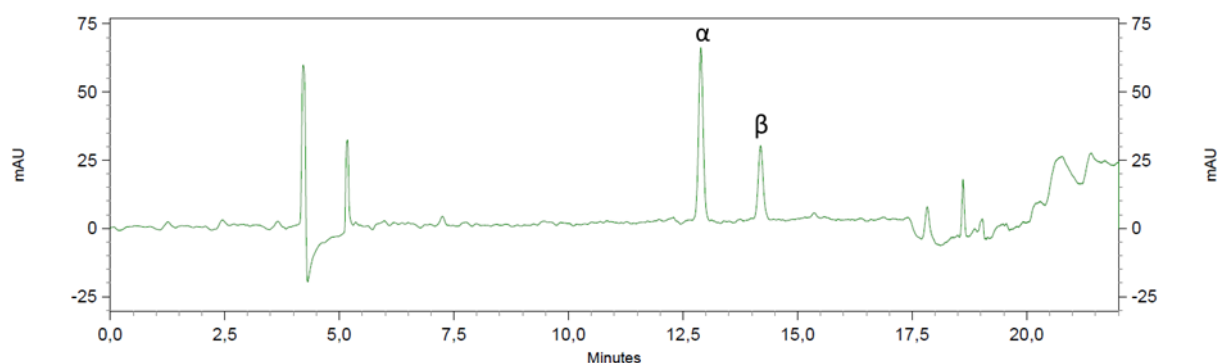
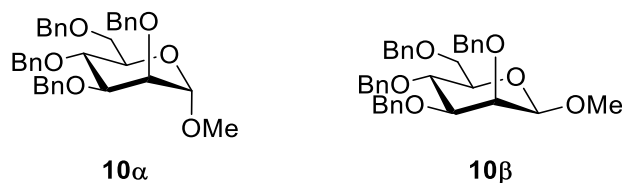


Figure 6.20: a HPLC spectrum of **9α**, **9β** (Method A)

2,2-Difluoroethyl 2,3,4,6-tetra-*O*-benzyl- α/β -D-galactopyranoside (**9α**) ^1H NMR (600 MHz, Chloroform-*d*) δ 7.42 – 7.20 (m, 20H), 5.98 (tt, $J = 55.7, 4.4$ Hz, 1H), 4.95 (d, $J = 11.4$ Hz, 1H), 4.88 – 4.80 (m, 3H), 4.74 (d, $J = 11.6$ Hz, 1H), 4.66 (d, $J = 11.9$ Hz, 1H), 4.57 (d, $J = 11.4$ Hz, 1H), 4.47 (d, $J = 11.9$ Hz, 1H), 4.41 (d, $J = 11.9$ Hz, 1H), 4.06 (dd, $J = 10.0, 3.7$ Hz, 1H), 3.99 – 3.90 (m, 3H), 3.79 – 3.68 (m, 2H), 3.51 (qd, $J = 9.5, 6.3$ Hz, 2H). ^{13}C NMR (151 MHz, Chloroform-*d*) δ 138.8, 138.6, 138.5, 138.0, 128.535, 128.528, 128.518, 128.378, 128.372, 128.2, 127.93, 127.86, 127.83, 127.77, 127.7, 127.6, 114.3 (t, $J = 241.3$ Hz), 98.9, 78.9, 76.5, 75.1, 74.9, 73.8, 73.6, 73.4, 69.9, 69.1, 67.5 (t, $J = 28.9$ Hz); ^{19}F NMR (376 MHz, Chloroform-*d*) δ -124.8 (ddt, $J = 55.5, 40.4, 13.5$ Hz). HRMS (ESI): $[\text{M}+\text{Na}]^+$ calcd for $\text{C}_{36}\text{H}_{38}\text{F}_2\text{O}_6\text{Na}^+$ 627.2528, found 627.2538;

(**9β**) ^1H NMR (600 MHz, Chloroform-*d*) δ 7.40 – 7.20 (m, 20H), 6.04 – 5.80 (m, 1H), 4.94 (d, $J = 11.7$ Hz, 1H), 4.88 (d, $J = 10.7$ Hz, 1H), 4.76 (q, $J = 5.7, 5.2$ Hz, 2H), 4.71 (d, $J = 11.8$ Hz, 1H), 4.62 (d, $J = 11.6$ Hz, 1H), 4.42 (d, $J = 5.5$ Hz, 2H), 4.40 (d, $J = 7.6$ Hz, 1H), 4.06 – 3.97 (m, 1H), 3.88 (d, $J = 2.9$ Hz, 1H), 3.84 (dd, $J = 9.8, 7.6$ Hz, 1H), 3.77 (dtd, $J = 13.1, 11.3, 5.3$ Hz, 1H), 3.59 – 3.49 (m, 4H); ^{13}C NMR (151 MHz, Chloroform-*d*) δ 138.60, 138.59, 138.5, 137.9, 128.6, 128.54, 128.53, 128.46, 128.44, 128.37, 128.03, 128.00, 127.82, 127.79, 127.7, 114.4 (dd, $J = 242.3, 239.5$ Hz), 104.4, 82.1, 79.4, 75.5, 74.7, 73.8, 73.7, 73.5, 73.3, 68.9, 68.7 (dd, $J = 30.7, 26.6$ Hz); ^{19}F NMR (564 MHz, Chloroform-*d*) δ -124.5 (dddd, $J = 294.1, 56.3, 21.5, 13.1$ Hz), -125.8 (dddd, $J = 294.1, 54.8, 11.0, 9.4$ Hz); HRMS (ESI): $[\text{M}+\text{Na}]^+$ calcd for $\text{C}_{36}\text{H}_{38}\text{F}_2\text{O}_6\text{Na}^+$ 627.2528, found 627.2534.



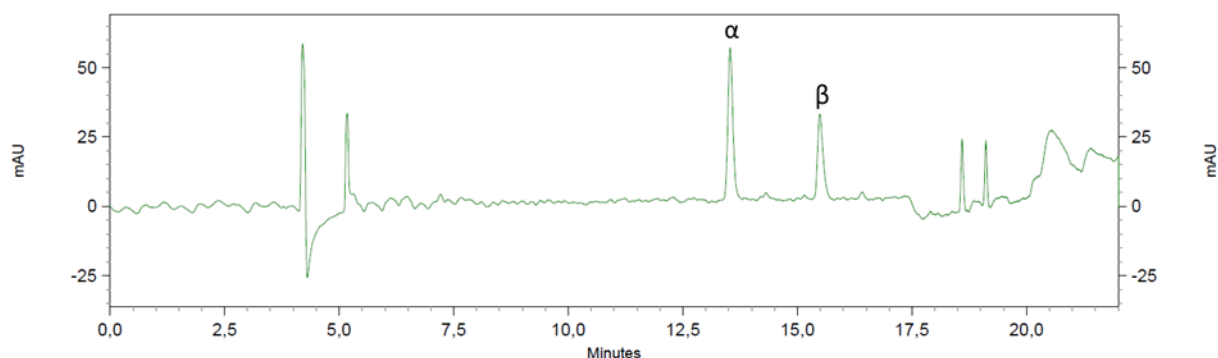


Figure 6.21: a HPLC spectrum of **10α**, **10β** (Method A)

Methyl 2,3,4,6-tetra-*O*-benzyl- α/β -D-mannopyranoside (**10α**) ^1H NMR (400 MHz, Chloroform-*d*) δ 7.40 – 7.25 (m, 18H), 7.16 (m, 2H), 4.89 (d, $J = 10.7$ Hz, 1H), 4.81 – 4.72 (m, 3H), 4.67 (d, $J = 12.1$ Hz, 1H), 4.61 (s, 2H), 4.56 (d, $J = 12.1$ Hz, 1H), 4.50 (d, $J = 10.8$ Hz, 1H), 3.98 (t, $J = 9.2$ Hz, 1H), 3.88 (dd, $J = 9.3, 3.1$ Hz, 1H), 3.83 – 3.71 (m, 4H), 3.33 (s, 3H).

(**10β**) ^1H NMR (400 MHz, Chloroform-*d*) δ 7.49 – 7.41 (m, 2H), 7.37 – 7.24 (m, 16H), 7.20 – 7.15 (m, 2H), 4.97 (d, $J = 12.4$ Hz, 1H), 4.90 (d, $J = 10.7$ Hz, 1H), 4.84 (d, $J = 12.4$ Hz, 1H), 4.64 (d, $J = 12.1$ Hz, 1H), 4.59 (d, $J = 12.1$ Hz, 1H), 4.55 – 4.42 (m, 3H), 4.30 (s, 1H), 3.90 (d, $J = 3.1$ Hz, 1H), 3.87 (d, $J = 9.5$ Hz, 1H), 3.82 (dd, $J = 10.8, 2.0$ Hz, 1H), 3.76 (dd, $J = 10.8, 5.8$ Hz, 1H), 3.54 (s, 3H), 3.51 (dd, $J = 9.3, 3.0$ Hz, 1H), 3.49 – 3.44 (m, 1H).

These data are in accordance with those previously published.¹²⁵

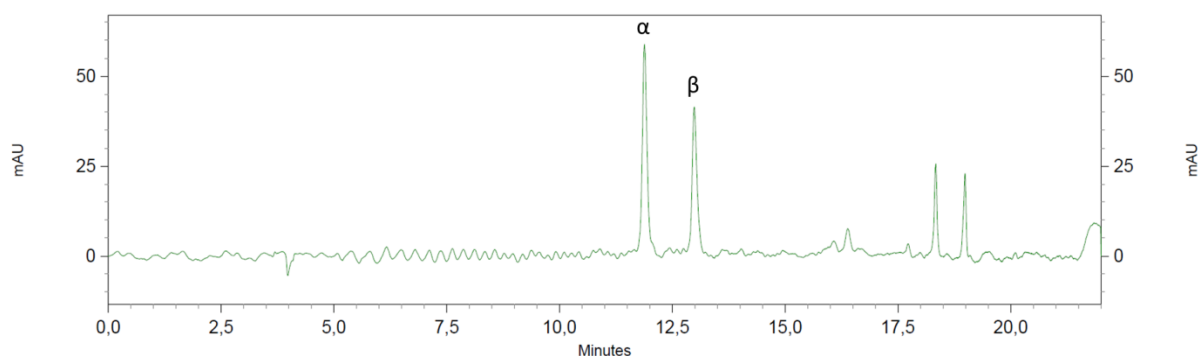
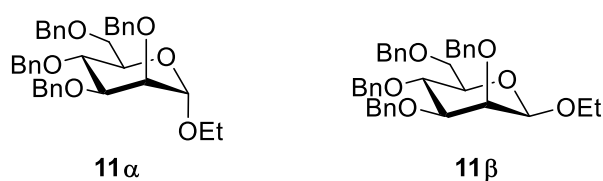


Figure 6.22: a HPLC spectrum of **11α**, **11β** (Method A)

Ethyl 2,3,4,6-tetra-*O*-benzyl- α/β -D-mannopyranoside (**11α**) ^1H NMR (400 MHz, Chloroform-*d*) δ 7.40 – 7.22 (m, 18H), 7.18 – 7.11 (m, 2H), , 4.87 (d, $J = 11.3$ Hz, 2H), 4.78

– 4.44 (m, 7H), 4.03 – 3.87 (m, 2H), 3.83 – 3.64 (m, 5H), 3.42 (dq, $J = 9.8, 7.1$ Hz, 1H), 1.14 (t, $J = 7.0$ Hz, 3H). These data are in accordance with those previously published.¹²⁸

(11 β) ^1H NMR (600 MHz, Chloroform- d) δ 7.49 – 7.46 (m, 2H), 7.37 – 7.23 (m, 18H), 7.18 (dd, $J = 7.4, 2.0$ Hz, 2H), 4.99 (d, $J = 12.5$ Hz, 1H), 4.90 (dd, $J = 11.6, 9.7$ Hz, 2H), 4.64 – 4.57 (m, 2H), 4.55 – 4.49 (m, 2H), 4.44 (d, $J = 11.8$ Hz, 1H), 4.39 (s, 1H), 4.02 (dq, $J = 9.3, 7.1$ Hz, 1H), 3.89 (d, $J = 3.0$ Hz, 1H), 3.86 (t, $J = 9.5$ Hz, 1H), 3.81 (dd, $J = 10.7, 1.8$ Hz, 1H), 3.74 (dd, $J = 10.7, 6.1$ Hz, 1H), 3.53 – 3.49 (m, 2H), 3.48 – 3.44 (m, 1H), 1.27 (t, $J = 7.0$ Hz, 3H); ^{13}C NMR (151 MHz, Chloroform- d) δ 138.9, 138.6, 138.5, 138.3, 128.6, 128.5, 128.4, 128.21, 128.19, 128.0, 127.8, 127.71, 127.70, 127.6, 127.5, 101.6, 82.5, 76.0, 75.3, 75.1, 73.9, 73.7, 73.6, 71.5, 69.9, 65.5, 15.4; HRMS (ESI): $[\text{M}+\text{Na}]^+$ calcd for $\text{C}_{36}\text{H}_{40}\text{O}_6\text{Na}^+$ 591.2717, found 591.2725.

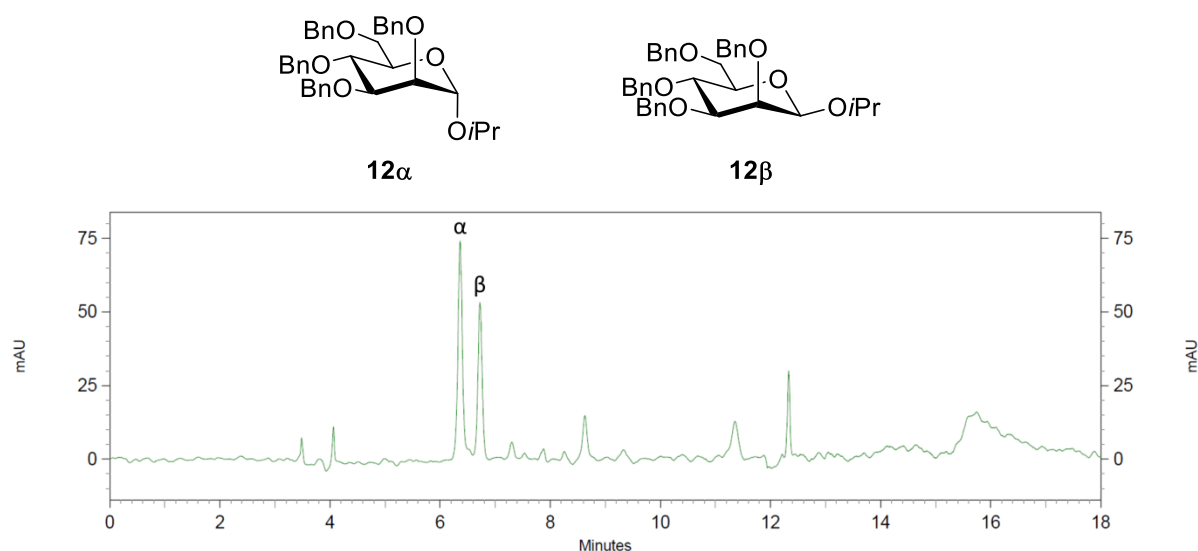


Figure 6.23: a HPLC spectrum of **12 α** , **12 β** (Method B)

Isopropyl 2,3,4,6-tetra-*O*-benzyl- α/β -D-mannopyranoside (**12 α**) ^1H NMR (400 MHz, Chloroform- d) δ 7.42 – 7.13 (m, 20H), 4.96 (s, 1H), 4.87 (d, $J = 10.7$ Hz, 1H), 4.81 – 4.61 (m, 5H), 4.56 – 4.47 (m, 2H), 4.02 – 3.68 (m, 7H), 1.16 (d, $J = 6.3$ Hz, 3H), 1.06 (d, $J = 5.9$ Hz, 3H).

(12 β) ^1H NMR (400 MHz, Chloroform- d) δ 7.50 – 7.16 (m, 20H), 4.98 (d, $J = 12.5$ Hz, 1H), 4.92 – 4.85 (m, 2H), 4.64 – 4.39 (m, 6H), 3.99 (septet, $J = 6.3$ Hz, 1H), 3.86 – 3.68 (m, 4H), 3.48 (d, $J = 12.5$ Hz, 1H), 3.43 (dd, $J = 8.8, 6.2$ Hz, 1H), 1.28 (d, $J = 6.0$ Hz, 3H), 1.14 (d, $J = 6.0$ Hz, 3H). These data are in accordance with those previously published.¹²⁹

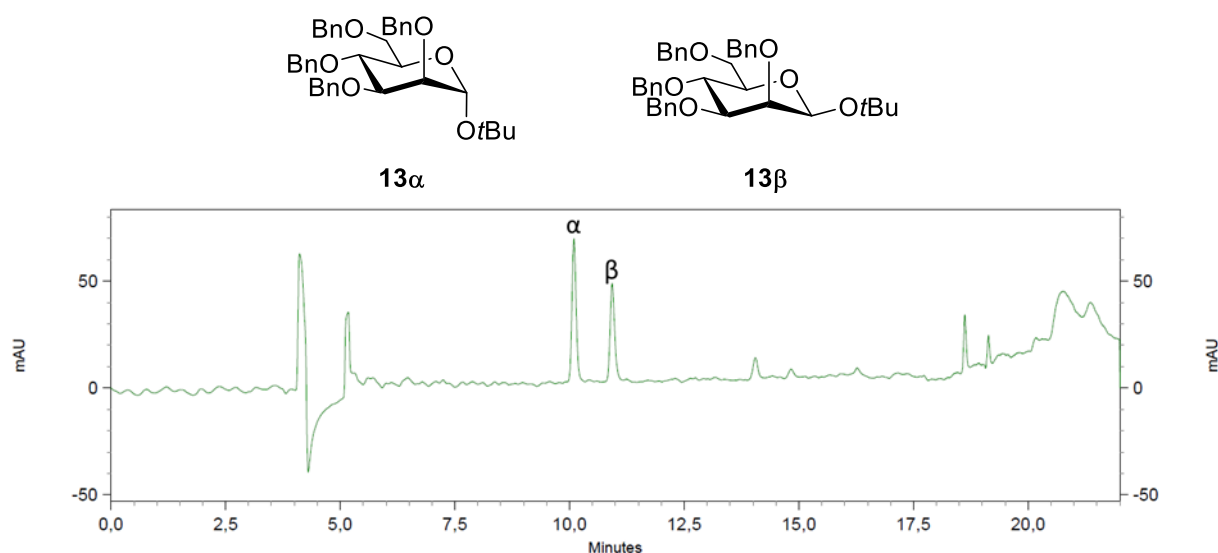
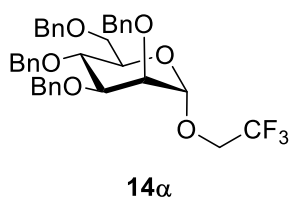


Figure 6.24: a HPLC spectrum of **13α**, **13β** (Method A)

tert-Butyl 2,3,4,6-tetra-*O*-benzyl- α/β -D-mannopyranoside (**13α**) ^1H NMR (400 MHz, Chloroform-*d*) δ 7.44 – 7.21 (m, 18H), 7.21 – 7.12 (m, 2H), 5.12 (s, 1H), 4.89 (d, J = 10.6 Hz, 1H), 4.79 (d, J = 12.5 Hz, 1H), 4.75 – 4.67 (m, 2H), 4.64 (d, J = 2.3 Hz, 2H), 4.52 (d, J = 4.3 Hz, 1H), 4.49 (d, J = 2.8 Hz, 1H), 4.06 – 3.90 (m, 3H), 3.81 (dd, J = 10.5, 4.2 Hz, 1H), 3.70 (d, J = 10.4 Hz, 1H), 3.59 (s, 1H), 1.16 (s, 9H); ^{13}C NMR (101 MHz, Chloroform-*d*) δ 138.6, 138.52, 138.50, 138.48, 128.28, 128.27, 128.19, 128.1, 127.9, 127.71, 127.67, 127.54, 127.52, 127.46, 127.3, 92.5, 80.2, 75.8, 75.23, 75.17, 75.1, 73.3, 72.4, 72.1, 71.2, 69.3, 28.4; HRMS (ESI): $[\text{M}+\text{Na}]^+$ calcd for $\text{C}_{38}\text{H}_{44}\text{O}_6\text{Na}^+$ 619.3030, found 619.3035.

(**13β**) ^1H NMR (400 MHz, Chloroform-*d*) δ 7.53 – 7.46 (m, 2H), 7.30 (d, J = 13.0 Hz, 16H), 7.22 – 7.16 (m, 2H), 5.02 (d, J = 12.7 Hz, 1H), 4.97 – 4.89 (m, 2H), 4.65 – 4.52 (m, 4H), 4.50 (d, J = 11.8 Hz, 1H), 4.43 (d, J = 11.8 Hz, 1H), 3.86 – 3.75 (m, 3H), 3.71 (dd, J = 10.7, 6.4 Hz, 1H), 3.51 (dd, J = 9.4, 3.1 Hz, 1H), 3.43 (ddd, J = 9.8, 6.4, 2.0 Hz, 1H), 1.29 (s, 9H); ^{13}C NMR (101 MHz, Chloroform-*d*) δ 139.0, 138.7, 138.6, 138.4, 128.7, 128.5, 128.45, 128.44, 128.2, 128.1, 127.9, 127.7, 127.6, 127.50, 127.47, 96.2, 83.1, 75.9, 75.7, 75.2, 75.1, 74.7, 73.8, 73.5, 71.5, 70.1, 28.8; HRMS (ESI): $[\text{M}+\text{Na}]^+$ calcd for $\text{C}_{38}\text{H}_{44}\text{O}_6\text{Na}^+$ 619.3030, found 619.3040.



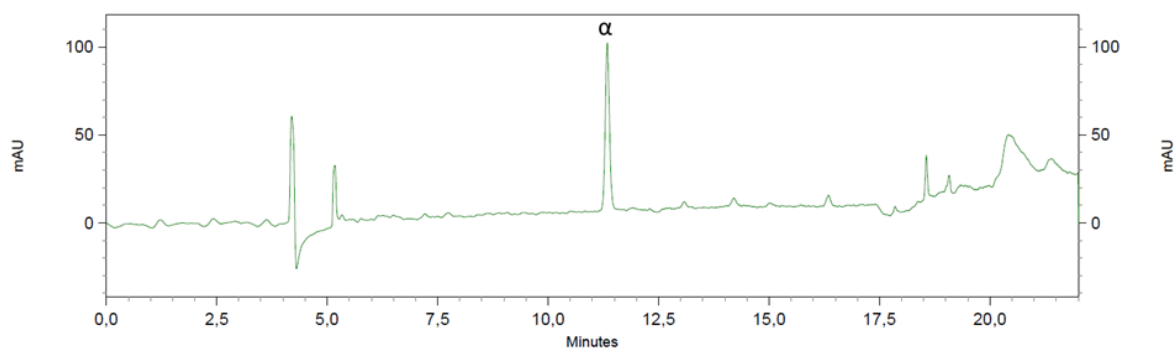


Figure 6.25: a HPLC spectrum of **14a** (Method A)

2,2,2-Trifluoro 2,3,4,6-tetra-*O*-benzyl- α -D-mannopyranoside (**14a**) ^1H NMR (600 MHz, Chloroform-*d*) δ 7.40 – 7.24 (m, 18H), 7.19 – 7.12 (m, 2H), 4.94 (d, $J = 1.9$ Hz, 1H), 4.86 (d, $J = 10.7$ Hz, 1H), 4.76 (d, $J = 12.3$ Hz, 1H), 4.69 (d, $J = 12.3$ Hz, 1H), 4.67 – 4.61 (m, 3H), 4.53 (d, $J = 12.1$ Hz, 1H), 4.50 (d, $J = 10.7$ Hz, 1H), 3.98 (s, 1H), 3.96 – 3.80 (m, 4H), 3.78 – 3.69 (m, 3H); ^{13}C NMR (101 MHz, Chloroform-*d*) δ 138.3, 138.2, 138.1, 138.0, 128.35, 128.34, 128.32, 128.30, 128.0, 127.8, 127.72, 127.69, 127.66, 127.63, 127.61, 127.5, 123.7 (q, $J = 278.2$ Hz), 98.5, 79.7, 75.1, 74.4, 74.2, 73.3, 72.9, 72.5, 72.4, 68.9, 63.9 (q, $J = 34.9$ Hz); ^{19}F NMR (564 MHz, Chloroform-*d*) δ -74.1 (t, $J = 8.6$ Hz); HRMS (ESI): $[\text{M}+\text{Na}]^+$ calcd for $\text{C}_{36}\text{H}_{37}\text{F}_3\text{O}_6\text{Na}^+$ 645.2434, found 645.2446.

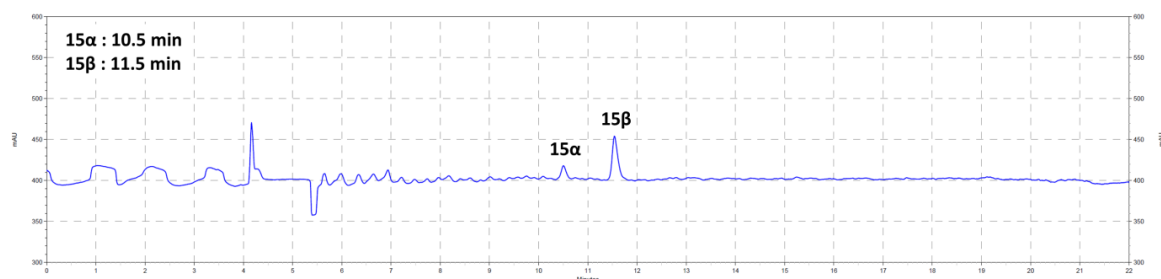
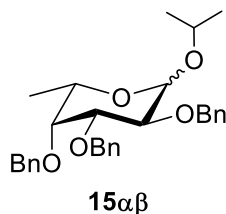


Figure 6.26: a HPLC spectrum of **15a**, **15β** (Method A)

Isopropyl 2,3,4-tri-*O*-benzyl- α -L-fucopyranoside (**15a β**) ^1H NMR (600 MHz, Chloroform-*d*) δ 7.52 – 7.11 (m, 57H), 5.01 – 4.94 (m, 7H), 4.90 (d, H-1 α , $J_{1,2} = 3.8$ Hz, 1H), 4.88 (d, $J = 11.7$ Hz, 1H), 4.80 (dd, $J = 11.9, 2.8$ Hz, 4H), 4.77 – 4.63 (m, 13H), 4.38 (d, H-1 β , $J_{1,2} = 7.7$ Hz, 3H), 4.03 – 3.91 (m, 6H), 3.87 (hept, $J = 6.2$ Hz, 1H), 3.78 (dd, $J = 9.7, 7.7$ Hz, 3H), 3.67 (dd, $J = 2.9, 1.2$ Hz, 1H), 3.54 (dd, $J = 3.1, 1.1$ Hz, 3H), 3.50 (dd, $J = 9.7, 3.0$ Hz, 3H),

3.43 (q, $J = 6.5, 1.1$ Hz, 3H), 1.27 (d, Me- β , $J = 6.2$ Hz, 9H), 1.21 (d, Me- β , $J = 6.1$, 9H), 1.21 (d, Me- α , $J = 6.2$, 3H), 1.18 (d, Me- α , $J = 6.1$ Hz, 3H), 1.16 (d, Me- β , $J = 6.4$ Hz, 9H), 1.09 (d, Me- α , $J = 6.6$ Hz, 3H). This data is in accordance with those previously published.¹³⁰

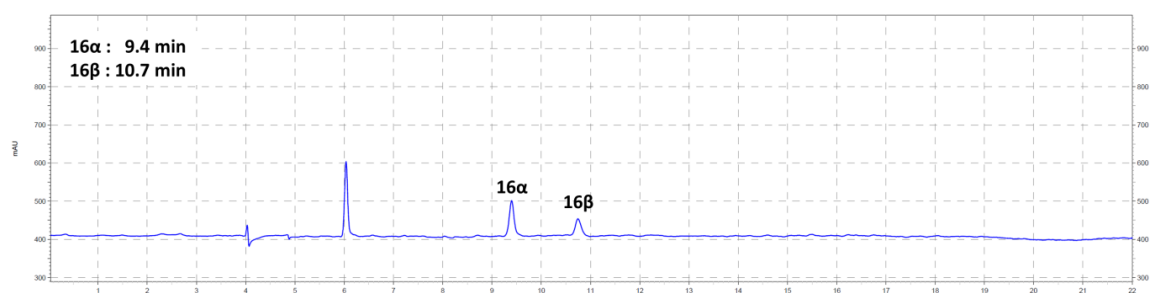
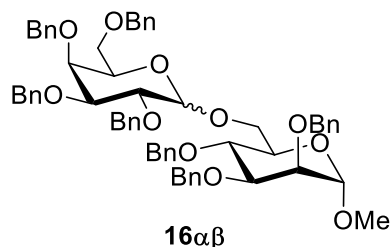


Figure 6.27: a HPLC spectrum of **16 α** , **16 β** (Method C)

Methyl 2,3,4,6-tetra-O-benzyl- α/β -D-galactopyranosyl-(1 \rightarrow 6)-2,3,4-tri-O-benzyl- α -D-mannopyranoside (**16 α**) ^1H NMR (600 MHz, Chloroform- d) δ 7.50 – 7.08 (m, 35H), 5.11 (d, $J = 3.5$ Hz, 1H), 4.96 (d, $J = 11.5$ Hz, 1H), 4.87 (d, $J = 11.0$ Hz, 1H), 4.80 (d, $J = 11.9$ Hz, 1H), 4.74 – 4.65 (m, 6H), 4.63 – 4.57 (m, 4H), 4.46 (d, $J = 11.8$ Hz, 1H), 4.40 (d, $J = 11.8$ Hz, 1H), 4.09 – 4.03 (m, 2H), 3.99 – 3.95 (m, 2H), 3.94 (d, $J = 9.6$ Hz, 1H), 3.89 (dd, $J = 9.3, 3.1$ Hz, 1H), 3.85 (d, $J = 4.0$ Hz, 2H), 3.80 – 3.76 (m, 2H), 3.59 (dd, $J = 9.3, 7.4$ Hz, 1H), 3.54 (dd, $J = 9.3, 5.7$ Hz, 1H), 3.22 (s, 3H). (**16 β**) ^1H NMR (600 MHz, Chloroform- d) δ 7.29 (m, 35H), 5.00 (d, $J = 10.8$ Hz, 1H), 4.94 (d, $J = 11.6$ Hz, 1H), 4.81 – 4.74 (m, 2H), 4.74 – 4.52 (m, 8H), 4.49 (d, $J = 11.2$ Hz, 1H), 4.41 (dt, $J = 22.2, 10.2$ Hz, 3H), 4.23 (d, $J = 10.6$ Hz, 1H), 3.93 – 3.75 (m, 6H), 3.70 (dd, $J = 10.7, 6.3$ Hz, 1H), 3.59 (dt, $J = 24.2, 8.6$ Hz, 2H), 3.54 – 3.46 (m, 2H), 3.21 (s, 3H). This data is in accordance with those previously published.¹³¹

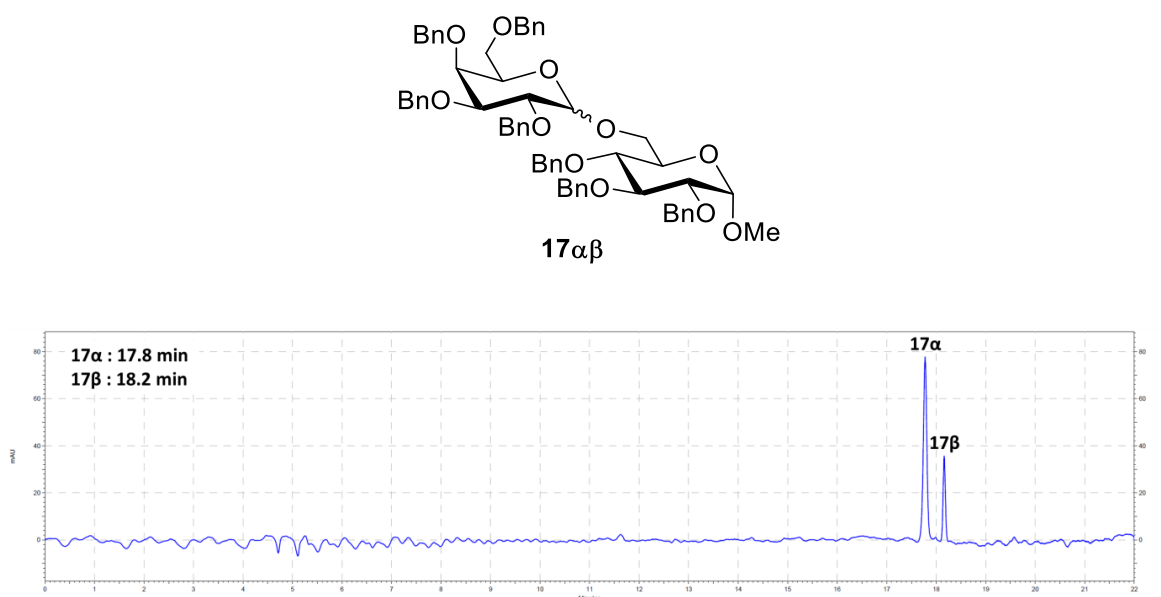


Figure 6.28: a HPLC spectrum of **17α**, **17β** (Method A)

Methyl 2,3,4,6-tetra-O-benzyl- α/β -D-galactopyranosyl-(1 \rightarrow 6)-2,3,4-tri-O-benzyl- α -D-glucopyranoside (**17α**) ^1H NMR (400 MHz, Chloroform-*d*) δ 7.41 – 7.11 (m, 35H), 4.99 (s, 1H), 4.94 (t, J = 9.3 Hz, 2H), 4.84 (d, J = 10.9 Hz, 1H), 4.82 – 4.76 (m, 2H), 4.76 – 4.65 (m, 4H), 4.61 – 4.55 (m, 2H), 4.55 – 4.49 (m, 2H), 4.43 (d, J = 11.8 Hz, 1H), 4.36 (d, J = 11.9 Hz, 1H), 4.03 (d, J = 9.8 Hz, 1H), 3.99 – 3.87 (m, 4H), 3.83 – 3.74 (m, 2H), 3.72 (d, J = 12.3 Hz, 1H), 3.58 (t, J = 9.4 Hz, 1H), 3.54 – 3.46 (m, 2H), 3.41 (d, J = 8.8 Hz, 1H), 3.29 (s, 3H). (**17β**) ^1H NMR (400 MHz, Chloroform-*d*) δ 7.41 – 7.09 (m, 35H), 5.01 – 4.87 (m, 3H), 4.86 – 4.33 (m, 12H), 4.30 (d, J = 7.7 Hz, 1H), 4.13 (d, J = 10.8 Hz, 1H), 3.97 (t, J = 9.2 Hz, 1H), 3.92 – 3.73 (m, 3H), 3.65 – 3.42 (m, 7H), 3.29 (s, 3H). This data is in accordance with those previously published.¹³²⁻¹³³

6.6 XYZ Coordinates

Donor

Glc1 α

N	0.797797	-3.866059	2.237765
C	0.823887	-2.617078	2.423338
C	0.650994	-2.027420	3.836995
Cl	2.114927	-1.055263	4.250686
Cl	-0.800808	-0.941707	3.824682
Cl	0.419698	-3.293013	5.063734
O	0.984897	-1.599334	1.540935
C	1.306992	-1.925777	0.179156
C	1.762229	-0.633913	-0.505343
O	2.844804	-0.090498	0.216032
C	3.910689	0.416971	-0.584008
C	4.893168	1.164952	0.288847
C	5.949816	1.857404	-0.318041
C	6.880987	2.549863	0.453895
C	6.764487	2.562993	1.846602
C	5.712775	1.878489	2.455136
C	4.780343	1.181498	1.682219
C	0.595871	0.357434	-0.625772
O	1.056814	1.428506	-1.430102
C	0.466031	2.714025	-1.181367
C	1.392489	3.776930	-1.714100
C	2.613119	4.027329	-1.072305
C	3.487691	4.993597	-1.565176
C	3.147794	5.727730	-2.705438
C	1.932896	5.488362	-3.348663
C	1.061749	4.514457	-2.854766
C	-0.625170	-0.338960	-1.261208
O	-1.757409	0.522563	-1.358826
C	-2.475699	0.813880	-0.156963
C	-3.357065	2.022678	-0.379460
C	-3.697267	2.837107	0.706808
C	-4.548666	3.929359	0.537626
C	-5.064662	4.223733	-0.725668
C	-4.725431	3.418101	-1.814251
C	-3.879441	2.321135	-1.643347
C	-0.962265	-1.680702	-0.575502
C	-2.022998	-2.468828	-1.351457
O	-2.853128	-3.278097	-0.544412
C	-2.223891	-4.440235	-0.009113
C	-3.264106	-5.340839	0.612507
C	-2.980052	-6.016255	1.804342
C	-3.913713	-6.891524	2.362472
C	-5.146457	-7.089306	1.739234
C	-5.439668	-6.409365	0.554559

C	-4.502762	-5.543181	-0.007591
O	0.225797	-2.507411	-0.490705
H	0.878464	-4.113107	1.250217
H	2.111546	-2.668049	0.176329
H	2.074330	-0.924606	-1.518934
H	3.513004	1.082235	-1.359038
H	4.420414	-0.420120	-1.092418
H	6.041686	1.856439	-1.402578
H	7.695671	3.080924	-0.031813
H	7.487608	3.105089	2.450232
H	5.613883	1.884121	3.537795
H	3.959587	0.651637	2.152720
H	0.357561	0.719077	0.384155
H	0.328196	2.840007	-0.096239
H	-0.519168	2.776611	-1.656035
H	2.879030	3.459258	-0.184021
H	4.432124	5.172465	-1.057970
H	3.827095	6.484878	-3.088509
H	1.662898	6.055501	-4.235943
H	0.116365	4.324906	-3.358328
H	-0.360686	-0.543321	-2.306358
H	-1.791545	1.007213	0.679929
H	-3.093668	-0.052380	0.124162
H	-3.291496	2.617090	1.692381
H	-4.800436	4.554347	1.390411
H	-5.723463	5.077378	-0.861537
H	-5.121124	3.642760	-2.801493
H	-3.610278	1.697365	-2.489529
H	-1.334854	-1.503680	0.439914
H	-1.516997	-3.062768	-2.130107
H	-2.692581	-1.755044	-1.838894
H	-1.475965	-4.168869	0.747020
H	-1.689452	-4.966144	-0.820161
H	-2.025565	-5.851668	2.300378
H	-3.680640	-7.409147	3.289350
H	-5.877829	-7.764188	2.176359
H	-6.401030	-6.554011	0.068046
H	-4.730767	-5.006530	-0.923476

Glc1 β

N	0.671274	-4.452114	1.121546
C	1.761251	-3.922271	0.778582
C	3.099255	-4.648156	1.010921
Cl	4.021134	-3.728197	2.273197
Cl	2.852383	-6.320257	1.568852
Cl	4.054081	-4.668494	-0.522032
O	2.008917	-2.708089	0.202578
C	0.996591	-1.724283	0.286816
C	1.537876	-0.428185	-0.315953
O	2.542198	0.128716	0.503964

C	3.876764	0.051631	-0.025220	H	3.489766	6.502150	-3.850511
C	4.785315	0.866141	0.857362	H	3.363501	4.121529	-4.553274
C	4.811751	2.262893	0.747957	H	2.071721	2.490571	-3.194852
C	5.646076	3.019979	1.569750	H	-0.704945	-0.176417	-2.099524
C	6.461653	2.386832	2.511509	H	-1.789938	1.500216	0.971188
C	6.436154	0.996717	2.630617	H	-3.188276	0.505748	0.551322
C	5.598685	0.241755	1.807925	H	-3.338760	3.056333	2.125762
C	0.416342	0.616795	-0.457485	H	-4.762788	5.065748	1.904283
O	0.930909	1.637562	-1.293531	H	-5.615387	5.750997	-0.331403
C	0.657352	2.973618	-0.893032	H	-5.026488	4.406429	-2.337710
C	1.471676	3.937293	-1.727456	H	-3.599780	2.386599	-2.107561
C	1.549984	5.280031	-1.335898	H	-1.453352	-1.121328	0.725217
C	2.268771	6.200365	-2.096581	H	-2.154729	-2.407677	-1.939240
C	2.925140	5.787333	-3.258378	H	-3.274563	-1.333834	-1.063339
C	2.853687	4.451427	-3.651414	H	-3.425073	-4.345516	-1.554016
C	2.129303	3.530174	-2.892143	H	-4.692445	-3.425008	-0.721457
C	-0.887322	0.032940	-1.039743	H	-1.858208	-5.655376	0.444253
O	-1.953673	0.979369	-1.052151	H	-2.179531	-7.534803	2.011121
C	-2.549381	1.330035	0.194730	H	-4.455136	-8.078625	2.863656
C	-3.381435	2.582561	0.020749	H	-6.401557	-6.708359	2.141701
C	-3.713396	3.347132	1.145967	H	-6.071154	-4.807526	0.586487
C	-4.517278	4.479995	1.022493				
C	-4.993868	4.865606	-0.231954	Glc2β			
C	-4.662789	4.110161	-1.357233	C	-6.716277	-1.204385	1.468287
C	-3.863137	2.972017	-1.233401	C	-5.255131	-0.854908	1.187057
C	-1.242691	-1.294136	-0.342212	S	-4.568764	-2.044924	-0.039960
C	-2.428645	-2.027755	-0.941570	C	-2.795581	-1.614615	-0.030699
O	-2.748100	-3.085568	-0.060578	C	-2.472787	-0.116792	-0.221270
C	-3.746188	-3.967627	-0.568629	O	-3.113566	0.502264	-1.328357
C	-3.946079	-5.106759	0.400553	C	-2.984104	-0.118090	-2.607816
C	-2.854821	-5.885282	0.810159	C	-3.426294	0.857132	-3.675981
C	-3.036679	-6.945740	1.695992	C	-4.422366	1.806243	-3.418441
C	-4.313739	-7.249465	2.175351	C	-4.842458	2.678283	-4.423162
C	-5.405615	-6.481625	1.769895	C	-4.279029	2.607392	-5.698820
C	-5.219252	-5.411769	0.891302	C	-3.288375	1.660338	-5.963620
O	-0.117365	-2.173091	-0.455886	C	-2.862665	0.794263	-4.955360
H	-0.134314	-3.875564	0.868598	C	-0.941699	0.084659	-0.226149
H	0.720576	-1.586388	1.345356	O	-0.592687	1.459213	-0.150297
H	1.916637	-0.666952	-1.318704	C	-0.467590	2.150805	-1.389074
H	3.876088	0.451011	-1.048928	C	0.168291	3.502169	-1.155127
H	4.206577	-0.994604	-0.061705	C	0.897613	4.110630	-2.183851
H	4.178011	2.753049	0.011782	C	1.450691	5.379556	-2.011307
H	5.665487	4.102061	1.471019	C	1.287151	6.053700	-0.800525
H	7.117257	2.976171	3.147910	C	0.564871	5.452071	0.231369
H	7.070368	0.499875	3.360255	C	0.005346	4.186129	0.055377
H	5.577897	-0.841680	1.898633	C	-0.260740	-0.595418	0.975114
H	0.229428	1.014590	0.551100	O	1.137552	-0.624467	0.729511
H	0.910234	3.101950	0.170390	C	1.925762	0.215844	1.589321
H	-0.415671	3.189612	-1.005875	C	3.297797	0.371513	0.984824
H	1.044145	5.606428	-0.428878	C	4.384436	-0.373895	1.453290
H	2.321328	7.238371	-1.779342	C	5.645929	-0.229295	0.871450

C	5.829934	0.661598	-0.186466	H	6.424860	-4.733189	4.512198
C	4.748812	1.409308	-0.661150	H	4.456048	-4.048294	5.867128
C	3.491315	1.263912	-0.078150	H	2.310152	-3.482532	4.745504
C	-0.780232	-2.026277	1.185384				
C	-0.410211	-2.648178	2.543856	Glc3a			
O	0.964797	-2.667756	2.860897	O	3.685392	0.618087	-0.961597
C	1.747574	-3.553437	2.070648	P	2.801164	-0.562625	-0.811993
C	3.059229	-3.841949	2.766551	O	3.090601	-1.782985	-1.823177
C	4.176079	-4.216526	2.009733	C	3.193204	-1.490206	-3.239817
C	5.380657	-4.542999	2.633272	C	3.503871	-2.787784	-3.969886
C	5.485788	-4.485578	4.024314	C	3.647263	-2.583044	-5.485055
C	4.379696	-4.101142	4.784000	C	3.969214	-3.882808	-6.228861
C	3.171619	-3.785621	4.160117	O	2.771955	-1.321439	0.588807
O	-2.212052	-2.041516	1.194010	C	3.958416	-1.391039	1.422457
H	-7.137787	-0.492081	2.185751	C	3.514665	-1.465019	2.874241
H	-7.318502	-1.157587	0.555156	C	4.706777	-1.531822	3.837292
H	-6.812456	-2.210204	1.888936	C	4.275178	-1.558899	5.307161
H	-4.655968	-0.921707	2.099950	O	1.229776	-0.284245	-1.062355
H	-5.174911	0.158047	0.781645	C	0.682599	1.050979	-1.135717
H	-2.378210	-2.203203	-0.863043	C	0.101476	1.457216	0.221863
H	-2.860050	0.423628	0.647989	O	1.138272	1.438364	1.185064
H	-3.609473	-1.022364	-2.639932	C	1.158527	2.553484	2.080285
H	-1.946693	-0.425366	-2.800749	C	2.453296	2.548111	2.855579
H	-4.852445	1.863656	-2.424321	C	2.444804	2.701873	4.245444
H	-5.611321	3.415891	-4.208038	C	3.642116	2.751291	4.963479
H	-4.605259	3.288769	-6.479687	C	4.861211	2.642254	4.294548
H	-2.838962	1.601350	-6.952052	C	4.876942	2.478147	2.905819
H	-2.082819	0.064597	-5.164042	C	3.682022	2.431590	2.188245
H	-0.504308	-0.359946	-1.134087	C	-1.054007	0.533342	0.618681
H	-1.455362	2.270150	-1.852050	O	-1.665896	1.094905	1.775080
H	0.153207	1.565226	-2.084209	C	-2.001125	0.165676	2.803241
H	1.033174	3.586785	-3.128164	C	-2.591149	0.915770	3.974594
H	2.015428	5.836424	-2.819726	C	-2.282778	0.536522	5.284059
H	1.722183	7.039015	-0.660553	C	-2.859040	1.194902	6.371730
H	0.435832	5.969750	1.178592	C	-3.745145	2.250712	6.159044
H	-0.553113	3.716145	0.857509	C	-4.054490	2.641525	4.853122
H	-0.490997	-0.005625	1.873708	C	-3.484524	1.976471	3.767901
H	1.984032	-0.239813	2.585168	C	-2.070337	0.432541	-0.532958
H	1.440680	1.195325	1.670512	O	-3.122390	-0.498663	-0.265676
H	4.244235	-1.070909	2.275186	C	-2.802268	-1.883573	-0.262855
H	6.482475	-0.813027	1.246572	C	-3.846827	-2.658284	0.514839
H	6.812259	0.777320	-0.637592	C	-3.643478	-4.024874	0.751695
H	4.888037	2.110012	-1.480429	C	-4.590204	-4.774000	1.447905
H	2.649141	1.850405	-0.437611	C	-5.755507	-4.163953	1.920452
H	-0.410537	-2.655449	0.358850	C	-5.962506	-2.804824	1.688300
H	-0.835134	-3.663878	2.576638	C	-5.015206	-2.054803	0.986725
H	-0.892693	-2.056325	3.328968	C	-1.400203	0.171569	-1.899966
H	1.935943	-3.114469	1.081515	C	-2.356979	0.364378	-3.066350
H	1.189843	-4.494931	1.918905	O	-2.914789	1.664842	-2.993367
H	4.102537	-4.247818	0.924718	C	-3.716631	2.012048	-4.109774
H	6.238607	-4.833031	2.032385	C	-2.922328	2.320606	-5.367747

C	-1.623304	2.836324	-5.278829	H	-1.802748	0.225013	-4.005172
C	-0.914987	3.167056	-6.434743	H	-4.269906	2.903828	-3.789431
C	-1.497581	2.993681	-7.691555	H	-4.459139	1.223485	-4.316153
C	-2.791277	2.477185	-7.787154	H	-1.168698	2.956704	-4.299486
C	-3.495381	2.137658	-6.630582	H	0.094985	3.560886	-6.353003
O	-0.298136	1.071462	-2.121755	H	-0.945458	3.254458	-8.590967
H	3.983379	-0.746469	-3.391708	H	-3.249541	2.329186	-8.761827
H	2.241585	-1.060806	-3.581543	H	-4.500589	1.726729	-6.711460
H	2.705886	-3.512479	-3.761341				
H	4.430063	-3.210719	-3.557149	Galla			
H	4.436644	-1.844800	-5.679886	N	-1.290125	-1.382621	4.670030
H	2.718962	-2.151307	-5.886725	C	-0.789584	-0.239439	4.489237
H	4.912029	-4.316493	-5.874703	C	-0.567927	0.719863	5.674156
H	3.183146	-4.631866	-6.077224	Cl	1.203024	1.052536	5.832645
H	4.063771	-3.711663	-7.306690	Cl	-1.433532	2.275464	5.333906
H	4.574139	-0.504607	1.244102	Cl	-1.175141	0.038964	7.200671
H	4.524946	-2.281880	1.126237	O	-0.369799	0.367550	3.344992
H	2.871065	-2.344112	3.009281	C	-0.165832	-0.466095	2.190113
H	2.904018	-0.580323	3.088114	C	0.493679	0.404151	1.110453
H	5.356508	-0.663303	3.665978	O	1.670088	0.997718	1.625630
H	5.312164	-2.422109	3.615671	C	2.840990	0.778917	0.840967
H	3.730907	-0.644602	5.569563	C	4.016157	1.475454	1.486317
H	3.616450	-2.412494	5.513140	C	5.087243	1.906877	0.694291
H	5.141548	-1.637427	5.974239	C	6.202227	2.511527	1.276597
H	1.470592	1.738648	-1.446452	C	6.252984	2.699773	2.658849
H	-0.293229	2.476463	0.101805	C	5.184383	2.278495	3.452551
H	0.294808	2.514679	2.754211	C	4.072823	1.666451	2.871839
H	1.077885	3.484168	1.493943	C	-0.499185	1.460180	0.605607
H	1.494923	2.784820	4.769694	O	0.080500	2.224967	-0.442590
H	3.620036	2.875110	6.043303	C	0.576031	3.512136	-0.037680
H	5.794386	2.684542	4.849879	C	1.286259	4.141431	-1.209192
H	5.823761	2.392280	2.378217	C	2.657433	4.411118	-1.150453
H	3.697482	2.283448	1.111955	C	3.314082	4.990666	-2.238835
H	-0.622160	-0.445806	0.858734	C	2.605146	5.297419	-3.400001
H	-1.103149	-0.384436	3.121611	C	1.235247	5.026869	-3.468878
H	-2.724969	-0.569463	2.421870	C	0.580942	4.456143	-2.378923
H	-1.583341	-0.279263	5.454037	C	-1.768812	0.743310	0.103585
H	-2.604466	0.889027	7.384664	O	-1.508809	-0.121307	-0.989638
H	-4.188796	2.768879	7.004825	C	-1.517574	0.466850	-2.302385
H	-4.740860	3.466190	4.680619	C	-1.531611	-0.661994	-3.301383
H	-3.718492	2.279923	2.751546	C	-2.733906	-1.108903	-3.861917
H	-2.583535	1.395564	-0.593410	C	-2.751849	-2.196812	-4.735990
H	-1.812709	-2.062918	0.179330	C	-1.561383	-2.852522	-5.057071
H	-2.760430	-2.266786	-1.296128	C	-0.355307	-2.412539	-4.505475
H	-2.736161	-4.505686	0.390611	C	-0.342324	-1.322108	-3.635811
H	-4.416876	-5.832233	1.625709	C	-2.339831	-0.105862	1.252484
H	-6.493008	-4.745323	2.467351	C	-3.624484	-0.917531	0.886517
H	-6.864763	-2.320505	2.053738	O	-3.484652	-2.314718	0.918433
H	-5.173282	-0.997668	0.804173	C	-2.867772	-2.895761	-0.223384
H	-1.017986	-0.855909	-1.940248	C	-2.821687	-4.400193	-0.077086
H	-3.152046	-0.396258	-3.013327	C	-2.341717	-5.168754	-1.146515

C	-2.256740	-6.555996	-1.041599	C	0.720068	0.238222	0.549605
C	-2.652710	-7.196011	0.136100	O	1.721130	0.920675	1.283517
C	-3.134416	-6.436314	1.201157	C	3.046792	0.799426	0.759948
C	-3.217832	-5.045384	1.097272	C	3.989431	1.616924	1.609927
O	-1.358187	-1.038825	1.736179	C	5.063977	2.291586	1.018791
H	-1.434296	-1.881027	3.788896	C	5.965674	3.017140	1.799729
H	0.479474	-1.301945	2.479089	C	5.794208	3.086004	3.182853
H	0.722887	-0.264960	0.272669	C	4.719971	2.421279	3.778945
H	2.689246	1.155101	-0.179617	C	3.825613	1.688352	2.999135
H	3.034308	-0.304904	0.766017	C	-0.492478	1.172190	0.391270
H	5.047017	1.771551	-0.384685	O	-0.152109	2.281828	-0.425022
H	7.026559	2.841982	0.649654	C	0.203010	3.480927	0.285125
H	7.117629	3.176073	3.113599	C	0.657895	4.509308	-0.718894
H	5.214453	2.427727	4.528692	C	1.998112	4.906408	-0.775109
H	3.235539	1.349020	3.484567	C	2.420330	5.849527	-1.714814
H	-0.775749	2.114497	1.443727	C	1.505538	6.397066	-2.614635
H	1.254460	3.400450	0.814537	C	0.165228	6.003783	-2.567945
H	-0.273664	4.136671	0.282784	C	-0.254431	5.069271	-1.623312
H	3.214440	4.163503	-0.250431	C	-1.684361	0.422463	-0.242694
H	4.378853	5.198466	-2.178332	O	-1.396111	0.036532	-1.576182
H	3.114812	5.746717	-4.248312	C	-1.855679	0.940546	-2.595503
H	0.677464	5.265716	-4.370965	C	-1.071787	0.678942	-3.855337
H	-0.485047	4.246182	-2.432519	C	-1.627240	-0.029961	-4.923816
H	-2.520028	1.498956	-0.181387	C	-0.880981	-0.274407	-6.078907
H	-0.638998	1.105790	-2.429421	C	0.432357	0.186962	-6.169725
H	-2.415203	1.094344	-2.414455	C	0.996376	0.894133	-5.104066
H	-3.662792	-0.602000	-3.609339	C	0.248749	1.138809	-3.953954
H	-3.692631	-2.532368	-5.164839	C	-1.960238	-0.844280	0.577320
H	-1.572380	-3.699543	-5.737930	C	-3.061884	-1.724279	0.012201
H	0.574246	-2.916283	-4.756721	O	-3.347016	-2.715991	0.978910
H	0.596728	-0.980109	-3.206047	C	-4.219917	-3.733613	0.499840
H	-2.591895	0.586650	2.067363	C	-4.357708	-4.807321	1.551052
H	-3.989530	-0.581836	-0.096587	C	-3.217505	-5.436495	2.069973
H	-4.396897	-0.691257	1.627983	C	-3.339305	-6.431555	3.038397
H	-1.855517	-2.498396	-0.354076	C	-4.603102	-6.817751	3.493598
H	-3.432362	-2.620951	-1.129558	C	-5.742533	-6.200959	2.977683
H	-2.033543	-4.674660	-2.066762	C	-5.617371	-5.196534	2.014823
H	-1.880281	-7.138258	-1.878575	O	-0.785531	-1.660530	0.625032
H	-2.586779	-8.277755	0.220111	H	-0.618986	-3.177562	2.174347
H	-3.445864	-6.925715	2.120862	H	0.034595	-0.820252	2.329612
H	-3.591170	-4.452573	1.924238	H	1.070620	-0.041085	-0.450186
Gal1β				H	3.068671	1.157989	-0.279162
N	0.240212	-3.656398	2.456076	H	3.344870	-0.257459	0.755626
C	1.266674	-3.093909	1.990583	H	5.198487	2.246876	-0.060293
C	2.669910	-3.691766	2.205480	H	6.795901	3.534733	1.325840
Cl	3.670431	-2.500792	3.133271	H	6.490773	3.655876	3.792440
Cl	2.604418	-5.225465	3.104934	H	4.577904	2.473648	4.855452
Cl	3.436944	-3.978183	0.593491	H	2.987412	1.175248	3.459440
O	1.386971	-1.943281	1.265085	H	-0.796827	1.518795	1.391689
C	0.294702	-1.042318	1.279821	H	0.995954	3.266486	1.006954
				H	-0.678913	3.843494	0.838113

H	2.713556	4.475293	-0.078356	C	0.667600	1.214736	3.974956
H	3.463433	6.152809	-1.744345	C	0.789499	1.876212	5.198558
H	1.832737	7.129017	-3.348212	C	-0.213192	2.741581	5.636411
H	-0.551587	6.429627	-3.265461	C	-1.340549	2.948916	4.838562
H	-1.299055	4.769304	-1.584010	C	-1.458901	2.293677	3.613515
H	-2.572128	1.071855	-0.206127	C	0.176514	-2.129395	0.663987
H	-1.702130	1.971158	-2.263362	C	0.597744	-2.627697	2.050645
H	-2.931694	0.781905	-2.767244	O	2.006862	-2.715050	2.167103
H	-2.650622	-0.392169	-4.852750	C	2.566512	-3.944229	1.727976
H	-1.324792	-0.824813	-6.904318	C	4.040968	-3.979531	2.064061
H	1.015317	-0.001252	-7.067731	C	4.544638	-3.286743	3.170969
H	2.018287	1.257975	-5.173157	C	5.899353	-3.365633	3.493022
H	0.678202	1.691749	-3.122335	C	6.763935	-4.144287	2.722541
H	-2.241893	-0.548891	1.602099	C	6.267025	-4.838132	1.617556
H	-2.716385	-2.168892	-0.931802	C	4.914224	-4.750083	1.287889
H	-3.954632	-1.112254	-0.201441	O	-1.250943	-2.204865	0.617202
H	-3.806537	-4.153817	-0.433010	H	-6.105424	-1.037249	1.629275
H	-5.206382	-3.307728	0.255446	H	-6.238239	-1.355353	-0.110156
H	-2.231972	-5.139542	1.722060	H	-5.920079	-2.689015	1.013736
H	-2.446244	-6.904747	3.437264	H	-3.674625	-1.671113	1.584556
H	-4.696637	-7.593492	4.248240	H	-4.005515	-0.336205	0.463522
H	-6.728991	-6.493328	3.328453	H	-1.314843	-2.691303	-1.403808
H	-6.507743	-4.709066	1.623727	H	-2.055358	0.154127	-0.577060
Gal2β				H	-1.801642	1.609909	-2.643727
C	-5.704275	-1.636518	0.803668	H	-3.379488	0.831417	-2.393515
C	-4.200284	-1.394355	0.667215	H	-2.003952	2.771578	-4.692159
S	-3.545007	-2.423567	-0.712821	H	-2.453431	2.795118	-7.130086
C	-1.767648	-1.986296	-0.688163	H	-3.337755	0.758021	-8.251887
C	-1.454692	-0.553544	-1.160065	H	-3.768218	-1.295982	-6.915518
O	-1.775698	-0.466700	-2.537024	H	-3.326260	-1.304821	-4.471419
C	-2.417550	0.749339	-2.927949	H	0.562310	-0.718982	-1.806826
C	-2.648358	0.734813	-4.419030	H	1.866085	1.283595	-2.279773
C	-2.400582	1.882840	-5.178729	H	2.117033	1.394568	-0.518588
C	-2.652700	1.895358	-6.552189	H	1.374100	3.290971	-3.563416
C	-3.146060	0.752786	-7.181553	H	1.158648	5.761854	-3.652638
C	-3.387738	-0.401189	-6.430984	H	1.029125	7.073485	-1.543493
C	-3.144171	-0.408851	-5.057779	H	1.117497	5.902369	0.648650
C	0.039979	-0.213531	-0.976543	H	1.332787	3.429038	0.727914
O	0.138886	1.193478	-1.126010	H	1.770523	-0.810945	0.179879
C	1.459748	1.697551	-1.343517	H	-1.338695	-0.162601	2.006351
C	1.371459	3.199671	-1.411800	H	-1.078655	1.348772	1.111875
C	1.317112	3.865661	-2.641053	H	1.449131	0.546510	3.629059
C	1.195374	5.255324	-2.691249	H	1.674286	1.714033	5.810449
C	1.122478	5.990652	-1.507594	H	-0.115918	3.254709	6.589233
C	1.171950	5.333308	-0.274917	H	-2.124515	3.626248	5.166056
C	1.296775	3.944771	-0.229032	H	-2.336274	2.466534	2.992113
C	0.691754	-0.715367	0.341050	H	0.588109	-2.811088	-0.101271
O	0.624042	0.205222	1.418270	H	0.115503	-3.597085	2.240409
C	-0.644339	0.676985	1.863734	H	0.265781	-1.919344	2.812902
C	-0.460351	1.416669	3.172272	H	2.428552	-4.086237	0.643234
				H	2.043053	-4.779787	2.225427

H	3.868273	-2.679567	3.763310	C	-1.398211	0.687148	-4.325057
H	6.279723	-2.817502	4.351732	C	-0.899850	0.251372	-5.683686
H	7.818409	-4.206816	2.977071	C	0.196871	0.897596	-6.265448
H	6.933446	-5.440781	1.005526	C	0.637227	0.544334	-7.542072
H	4.535121	-5.285070	0.419900	C	-0.008952	-0.471574	-8.248553
Gal3α				C	-1.098447	-1.127323	-7.670631
O	3.370989	0.037613	-0.893012	C	-1.543692	-0.766405	-6.398596
P	2.536444	-1.168174	-0.672434	O	-0.565992	0.639646	-1.354835
O	2.552939	-2.276864	-1.833744	H	2.812922	-1.046789	-3.495603
C	2.194521	-1.898975	-3.189475	H	1.141431	-1.591352	-3.201426
C	2.428065	-3.105830	-4.084736	H	1.843860	-3.950133	-3.694485
C	2.045183	-2.832832	-5.544597	H	3.485624	-3.394829	-4.015565
C	2.302894	-4.034691	-6.457395	H	2.606160	-1.965598	-5.917519
O	2.835681	-2.061460	0.613398	H	0.986025	-2.554385	-5.601087
C	4.199950	-2.281875	1.055733	H	3.364056	-4.310481	-6.465549
C	4.158533	-2.672831	2.523895	H	1.735790	-4.912479	-6.125684
C	5.561401	-2.886390	3.105203	H	2.005830	-3.815213	-7.489490
C	5.535281	-3.237977	4.596019	H	4.776106	-1.363240	0.904960
O	0.957364	-0.867829	-0.490219	H	4.636416	-3.076470	0.438679
C	0.448211	0.471954	-0.407146	H	3.560880	-3.587342	2.633104
C	-0.075914	0.728299	1.011579	H	3.639461	-1.880954	3.075893
O	0.983626	0.436105	1.898355	H	6.154206	-1.972833	2.960570
C	1.068782	1.233452	3.079245	H	6.077415	-3.681549	2.548299
C	2.473211	1.152031	3.631521	H	5.070971	-2.432494	5.178130
C	2.681170	1.020763	5.008357	H	4.964494	-4.156806	4.779521
C	3.974406	0.994015	5.535479	H	6.548968	-3.392414	4.985074
C	5.076044	1.092451	4.684626	H	1.242963	1.175516	-0.659264
C	4.876244	1.215315	3.306265	H	-0.328976	1.795208	1.070727
C	3.584622	1.245476	2.780586	H	0.334333	0.901463	3.822267
C	-1.329897	-0.108599	1.310247	H	0.823185	2.279458	2.828346
O	-1.883765	0.410469	2.507607	H	1.824615	0.936626	5.673329
C	-2.863366	-0.424963	3.132315	H	4.119045	0.890994	6.607732
C	-3.370356	0.280834	4.363597	H	6.084244	1.071160	5.090476
C	-2.994186	-0.138484	5.642756	H	5.730044	1.290368	2.637011
C	-3.457220	0.533855	6.775610	H	3.436502	1.318122	1.706573
C	-4.296086	1.639349	6.635309	H	-0.981990	-1.142097	1.467011
C	-4.673611	2.068146	5.359773	H	-2.412179	-1.394915	3.393287
C	-4.214124	1.391833	4.231217	H	-3.693444	-0.609364	2.436657
C	-2.366824	-0.147692	0.144956	H	-2.335165	-0.997723	5.753529
O	-3.346188	0.883333	0.183573	H	-3.160245	0.195281	7.764683
C	-2.925088	2.244264	0.198729	H	-4.657253	2.164217	7.515262
C	-4.128604	3.147212	0.021975	H	-5.328829	2.928478	5.244629
C	-5.428816	2.645212	-0.083075	H	-4.506763	1.723194	3.237909
C	-6.510939	3.517448	-0.230165	H	-2.973142	-1.052250	0.273178
C	-6.305547	4.896177	-0.273968	H	-2.197191	2.435117	-0.600781
C	-5.007415	5.403537	-0.170400	H	-2.440893	2.468481	1.158817
C	-3.928611	4.534124	-0.024203	H	-5.583518	1.572001	-0.054335
C	-1.651818	-0.298164	-1.209453	H	-7.517270	3.114425	-0.312117
C	-2.581601	-0.118367	-2.406575	H	-7.148704	5.572226	-0.387984
O	-1.937354	-0.433999	-3.629957	H	-4.836617	6.476920	-0.202833
				H	-2.919670	4.935136	0.056540

H	-1.232253	-1.309991	-1.259252	C	-3.051846	-4.704504	1.778485
H	-2.993905	0.897965	-2.426638	C	-2.782668	-5.343134	2.994012
H	-3.420867	-0.815133	-2.295202	C	-3.756956	-6.127923	3.613694
H	-0.585231	1.146316	-3.750771	C	-5.015948	-6.270593	3.028902
H	-2.187589	1.450224	-4.443120	C	-5.294113	-5.625906	1.821265
H	0.712744	1.682748	-5.715646	C	-4.316834	-4.850963	1.197199
H	1.490703	1.056781	-7.979177	O	0.580740	-2.098338	0.524086
H	0.335908	-0.751973	-9.240084	H	1.200000	-3.671208	2.272673
H	-1.605114	-1.921643	-8.212871	H	2.479415	-2.272840	1.109714
H	-2.385275	-1.280040	-5.944205	H	2.969571	0.209735	1.023285
Man1α				H	4.590893	-0.119908	-0.665764
N	1.151120	-3.401222	3.256559	H	3.538338	1.132281	-1.356248
C	1.235435	-2.151795	3.416428	H	3.175307	-2.384375	-2.460597
C	1.114833	-1.526777	4.820796	H	3.785209	-3.186157	-4.730337
Cl	2.608717	-0.568122	5.168103	H	5.008477	-1.689789	-6.293594
Cl	-0.315501	-0.413492	4.824017	H	5.611426	0.615564	-5.574544
Cl	0.899080	-2.758078	6.082293	H	4.987229	1.411636	-3.314241
O	1.423173	-1.157589	2.511696	H	0.730547	1.103246	1.349688
C	1.686500	-1.519578	1.139054	H	1.111767	3.393003	0.921483
C	2.150737	-0.235642	0.443194	H	-0.182602	3.115465	-0.264743
O	2.596169	-0.645775	-0.837236	H	1.787381	5.637429	0.509996
C	3.735390	0.055988	-1.341266	H	2.711895	7.365178	-1.004308
C	4.055656	-0.442029	-2.730998	H	2.996892	6.876220	-3.426464
C	3.718640	-1.736777	-3.141198	H	2.340786	4.647927	-4.319176
C	4.058316	-2.180765	-4.419697	H	1.400688	2.927630	-2.797725
C	4.745100	-1.341161	-5.298470	H	0.070823	-0.150765	-1.353564
C	5.084480	-0.048680	-4.894616	H	-1.446164	1.413435	1.586022
C	4.735414	0.398398	-3.620371	H	-2.733485	0.360406	0.987820
C	0.987671	0.767333	0.334798	H	-3.147994	2.889737	2.587118
O	1.457277	1.857066	-0.441485	H	-4.634100	4.837796	2.250040
C	0.905828	3.138674	-0.130331	H	-5.304959	5.512726	-0.050465
C	1.522698	4.169829	-1.045019	H	-4.474136	4.217310	-2.003403
C	1.900919	5.421999	-0.550343	H	-2.988291	2.258585	-1.656971
C	2.423345	6.396172	-1.403646	H	-0.961431	-1.030000	1.400990
C	2.584883	6.121415	-2.761698	H	-1.151251	-2.701032	-1.085226
C	2.216912	4.869756	-3.262176	H	-2.280182	-1.331843	-0.917577
C	1.684750	3.901908	-2.411225	H	-1.204837	-3.619807	1.827695
C	-0.220533	0.075590	-0.322977	H	-1.464049	-4.516834	0.324163
O	-1.351100	0.936470	-0.452114	H	-1.807122	-5.220901	3.460585
C	-2.104710	1.225068	0.726346	H	-3.534549	-6.617763	4.558373
C	-2.975507	2.438737	0.484390	H	-5.778138	-6.874954	3.513894
C	-3.443527	3.175620	1.579236	H	-6.275138	-5.726916	1.363859
C	-4.282043	4.273791	1.390517	H	-4.532133	-4.341495	0.262812
C	-4.657293	4.653063	0.099928	Man2α			
C	-4.190437	3.925459	-0.995398	C	-3.205153	-4.860745	-3.295568
C	-3.356961	2.821360	-0.806214	C	-3.379859	-3.820021	-2.190885
C	-0.582276	-1.245734	0.394995	S	-2.624626	-2.219702	-2.700509
C	-1.653964	-2.036667	-0.364381	C	-2.873959	-1.280971	-1.113691
O	-2.538357	-2.755582	0.472765	C	-2.455595	0.192701	-1.300507
C	-1.969291	-3.905585	1.092837	O	-3.247202	1.073509	-0.516516

C	-3.113130	1.042651	0.906122	H	-1.847146	2.699462	-2.162790
C	-4.108525	2.008774	1.506445	H	-0.300177	2.218052	-2.895259
C	-4.774062	1.687504	2.693782	H	0.946414	4.152173	-3.443979
C	-5.655632	2.594852	3.284206	H	1.868552	6.376754	-2.862443
C	-5.888581	3.833033	2.685060	H	1.277296	7.443614	-0.695794
C	-5.232806	4.158806	1.495570	H	-0.249162	6.269437	0.880375
C	-4.346645	3.254340	0.911831	H	-1.174743	4.047720	0.288288
C	-0.918726	0.361939	-1.139459	H	-0.426195	0.001192	0.940801
O	-0.542729	1.707340	-0.893518	H	2.047894	-0.321258	1.535496
C	-0.767014	2.608034	-1.977326	H	1.530553	1.188850	0.733355
C	-0.181582	3.952628	-1.619406	H	4.289597	-1.137126	1.174184
C	0.679737	4.617550	-2.497545	H	6.506137	-0.892976	0.095558
C	1.199843	5.872280	-2.170051	H	6.813959	0.725902	-1.768012
C	0.869458	6.469987	-0.954269	H	4.890381	2.101248	-2.539993
C	0.012925	5.809732	-0.068844	H	2.672258	1.855132	-1.444929
C	-0.511030	4.561787	-0.400786	H	-0.464511	-2.442444	-0.875398
C	-0.259136	-0.478676	-0.031488	H	-0.926179	-3.688007	1.210190
O	1.132547	-0.556658	-0.313421	H	-0.989820	-2.173978	2.136113
C	1.975478	0.199493	0.571745	H	1.857846	-3.050333	-0.158597
C	3.334344	0.343942	-0.064968	H	1.114177	-4.493440	0.565802
C	4.420601	-0.425935	0.362574	H	3.992859	-4.290886	-0.384494
C	5.670036	-0.289224	-0.247568	H	6.125335	-4.937905	0.692300
C	5.841647	0.617321	-1.293824	H	6.336530	-4.885209	3.173127
C	4.760237	1.389552	-1.728413	H	4.393576	-4.184973	4.558822
C	3.515641	1.252509	-1.116633	H	2.249436	-3.558498	3.467671
C	-0.827029	-1.904679	0.010125	Man3a			
C	-0.494153	-2.677730	1.299230	O	4.229743	0.144155	-0.464573
O	0.872040	-2.744435	1.642530	P	3.699425	-1.124110	-1.014955
C	1.665208	-3.563157	0.792952	O	4.310050	-1.624067	-2.415859
C	2.973615	-3.896648	1.474943	C	5.688854	-1.715848	-2.668101
C	4.076054	-4.280408	0.700703	C	6.161354	-2.938294	-3.138586
C	5.279104	-4.641512	1.306991	C	7.511978	-3.058722	-3.466879
C	5.398346	-4.610388	2.698556	C	8.371731	-1.967826	-3.324429
C	4.307047	-4.217602	3.475255	C	7.875787	-0.750535	-2.853797
C	3.099500	-3.867136	2.868357	C	6.526012	-0.611050	-2.526210
O	-2.262049	-1.888262	0.004987	O	3.906432	-2.458217	-0.120260
H	-3.662617	-5.808969	-2.990827	C	3.379318	-2.590750	1.167835
H	-3.684162	-4.538327	-4.226461	C	3.597155	-1.629080	2.154906
H	-2.146150	-5.045893	-3.504429	C	3.073682	-1.848328	3.431375
H	-2.896171	-4.141087	-1.263863	C	2.362747	-3.015136	3.720575
H	-4.442345	-3.652817	-1.980199	C	2.170650	-3.973408	2.721662
H	-3.944309	-1.304068	-0.892657	C	2.673896	-3.762831	1.437019
H	-2.724281	0.483860	-2.321103	O	2.129481	-1.158847	-1.312000
H	-2.092999	1.342401	1.181578	C	1.371568	0.064332	-1.638143
H	-3.284021	0.031435	1.295680	C	0.967379	0.757397	-0.332629
H	-4.603604	0.719236	3.159607	O	0.297713	1.948802	-0.720809
H	-6.166432	2.329762	4.206240	C	0.589135	3.113932	0.068461
H	-6.579364	4.538473	3.139367	C	-0.564617	4.074955	-0.063980
H	-5.412484	5.119796	1.020626	C	-0.472405	5.214041	-0.868998
H	-3.845317	3.502525	-0.018296	C	-1.560518	6.081065	-0.999073
H	-0.464793	0.014797	-2.082424				

C	-2.753139	5.809264	-0.327372	H	0.592756	-1.047112	0.777099
C	-2.854558	4.669677	0.476556	H	-0.091452	-1.055535	2.873015
C	-1.766934	3.807952	0.606801	H	-1.782365	-0.587223	2.609962
C	0.030659	-0.151203	0.477316	H	-2.679859	0.121466	4.681921
O	-0.357131	0.580407	1.632383	H	-2.558382	1.487690	6.746915
C	-0.771359	-0.193997	2.761608	H	-0.526881	2.839889	7.227235
C	-0.713791	0.670991	3.997720	H	1.381202	2.809264	5.631539
C	-1.785563	0.703215	4.894968	H	1.256775	1.423655	3.576212
C	-1.717875	1.474445	6.057747	H	-1.734039	0.391105	-0.559217
C	-0.578826	2.233182	6.327094	H	-0.681630	-2.813921	0.858702
C	0.493399	2.214525	5.430621	H	-1.768266	-3.340554	-0.432003
C	0.427250	1.435052	4.277465	H	-1.094802	-4.259023	2.679418
C	-1.167310	-0.528151	-0.409369	H	-2.645004	-5.275839	4.325082
O	-2.104166	-1.398299	0.234372	H	-5.095424	-4.910227	4.116787
C	-1.715453	-2.749746	0.495588	H	-5.981483	-3.521189	2.252650
C	-2.658081	-3.331626	1.523642	H	-4.423258	-2.511252	0.606707
C	-2.167329	-4.106924	2.579295	H	-0.287973	-2.095090	-1.606370
C	-3.040289	-4.677389	3.508152	H	-2.771012	-1.532018	-2.247678
C	-4.414800	-4.470103	3.392941	H	-1.611080	-2.068934	-3.488120
C	-4.911963	-3.690097	2.345409	H	-1.807819	1.553523	-2.470442
C	-4.039966	-3.126702	1.415281	H	-3.389727	0.757904	-2.305504
C	-0.713370	-1.097554	-1.779150	H	-2.606929	3.745652	-3.031069
C	-1.860664	-1.252855	-2.803342	H	-3.606307	5.272905	-4.702828
O	-2.088463	-0.145502	-3.643323	H	-4.718061	4.349395	-6.729957
C	-2.597879	1.031989	-3.026343	H	-4.817197	1.887241	-7.064420
C	-3.164971	1.950271	-4.085476	H	-3.817878	0.362419	-5.375028
C	-3.102464	3.336958	-3.908862				
C	-3.664405	4.197836	-4.852666	Fuc1α			
C	-4.286220	3.680296	-5.989979	C	-3.932972	-2.355837	-0.355763
C	-4.342358	2.297363	-6.176398	C	-2.426409	-2.232676	-0.513800
C	-3.788693	1.437178	-5.228227	C	-1.955226	-0.811231	-0.882622
O	0.294287	-0.293405	-2.412580	O	-2.678614	0.243337	-0.266256
H	5.472507	-3.770206	-3.243061	C	-2.472078	0.512369	1.128800
H	7.890248	-4.009169	-3.832980	C	-3.468087	1.562502	1.547142
H	9.422879	-2.065840	-3.579839	C	-4.622032	1.218482	2.257750
H	8.539363	0.102550	-2.742504	C	-5.549730	2.194863	2.626507
H	6.126470	0.325831	-2.155530	C	-5.329933	3.529433	2.283278
H	4.163916	-0.734759	1.921013	C	-4.179244	3.882621	1.573481
H	3.231495	-1.102423	4.205391	C	-3.255165	2.905052	1.208439
H	1.968075	-3.179557	4.718924	C	-0.404692	-0.694847	-0.761371
H	1.632286	-4.891492	2.940447	O	0.038138	0.651533	-0.761159
H	2.536830	-4.492065	0.645100	C	-0.157306	1.349052	-1.995131
H	1.993381	0.721342	-2.248052	C	0.546646	2.679776	-1.908828
H	1.868985	0.983477	0.246869	C	-0.181249	3.873616	-1.892147
H	1.523292	3.572509	-0.287627	C	0.473265	5.104345	-1.797686
H	0.720207	2.819967	1.114607	C	1.865277	5.149839	-1.712816
H	0.454963	5.423487	-1.397587	C	2.600648	3.961779	-1.727757
H	-1.475614	6.966366	-1.624129	C	1.945027	2.735829	-1.828538
H	-3.600637	6.482518	-0.427866	C	0.164328	-1.361128	0.500546
H	-3.780749	4.455995	1.003672	O	1.576579	-1.512254	0.444383
H	-1.835923	2.918600	1.228119	C	2.324885	-0.420208	0.999205

C	3.796471	-0.629600	0.738400
C	4.739734	-0.121503	1.639782
C	6.105931	-0.250957	1.386526
C	6.544614	-0.902585	0.233043
C	5.609457	-1.419396	-0.665383
C	4.243288	-1.279292	-0.418948
C	-0.443826	-2.757012	0.697796
O	-0.038151	-3.643104	-0.372827
C	0.930371	-4.573453	-0.152698
C	0.583692	-5.861146	-0.922720
Cl	1.862780	-7.090149	-0.780424
Cl	-0.963807	-6.524178	-0.259454
Cl	0.345811	-5.451167	-2.671495
N	1.976325	-4.493509	0.544948
O	-1.829923	-2.702946	0.723351
H	-4.305983	-1.697220	0.432509
H	-4.429062	-2.076201	-1.291012
H	-4.197006	-3.389457	-0.113401
H	-2.090879	-2.905420	-1.312915
H	-2.210029	-0.683567	-1.942194
H	-1.452403	0.887936	1.273981
H	-2.602916	-0.398747	1.724966
H	-4.792881	0.178449	2.527795
H	-6.440817	1.912915	3.182619
H	-6.047900	4.292540	2.571451
H	-4.001865	4.921723	1.308926
H	-2.356595	3.179279	0.660125
H	0.029238	-1.232982	-1.620132
H	-1.228044	1.497164	-2.179682
H	0.254237	0.741735	-2.817824
H	-1.266984	3.838528	-1.954256
H	-0.104540	6.024203	-1.787518
H	2.377234	6.105647	-1.636704
H	3.685782	3.991685	-1.663716
H	2.520837	1.813453	-1.838937
H	-0.105478	-0.777188	1.388697
H	2.136358	-0.353198	2.081476
H	1.976836	0.513395	0.543187
H	4.403484	0.376537	2.546451
H	6.825789	0.147592	2.096581
H	7.607487	-1.012497	0.040142
H	5.943146	-1.936169	-1.561587
H	3.516640	-1.691197	-1.111355
H	-0.115255	-3.188827	1.647694
H	2.086744	-3.546362	0.919081

Acceptor

MeOH

C	-0.123460	0.000000	0.337185
O	-0.192115	0.000000	-1.080034

H	-1.150831	0.000000	0.702318
H	0.380344	-0.892068	0.734004
H	0.380344	0.892068	0.734004
H	0.705719	0.000000	-1.427477

EtOH

C	-0.375357	0.000000	-0.947460
C	0.431171	0.000000	0.336500
O	-0.486171	0.000000	1.427114
H	0.282413	0.000000	-1.821036
H	-1.015279	-0.884228	-0.995047
H	-1.015279	0.884228	-0.995047
H	1.081535	0.886982	0.372524
H	1.081535	-0.886982	0.372524
H	0.015432	0.000000	2.249929

iPrOH

C	0.140269	1.210556	-0.419612
C	-0.353549	-0.056033	0.278619
C	0.141715	-1.327199	-0.393854
O	0.111849	-0.111789	1.631087
H	-0.220652	2.109123	0.093000
H	1.233343	1.240333	-0.421319
H	-0.211140	1.260817	-1.454716
H	-1.455253	-0.058436	0.272799
H	1.234927	-1.351022	-0.399691
H	-0.213050	-2.205179	0.149759
H	-0.213517	-1.390052	-1.425898
H	-0.194942	0.678880	2.089827

tBuOH

C	-0.604577	1.263356	0.389498
C	0.000103	0.000000	-0.236800
C	1.522181	0.000000	-0.109663
C	-0.604576	-1.263356	0.389498
O	-0.247615	0.000000	-1.654556
H	-1.692406	1.280271	0.258643
H	-0.402605	1.320641	1.463094
H	-0.194788	2.156206	-0.088378
H	1.942472	-0.883441	-0.595806
H	1.942472	0.883438	-0.595811
H	1.831480	0.000003	0.938769
H	-0.194792	-2.156205	-0.088384
H	-0.402597	-1.320645	1.463092
H	-1.692406	-1.280268	0.258650
H	-1.202348	-0.000001	-1.791848

2F-EtOH

O	-1.391303	0.035174	0.788780
C	0.016033	0.072237	0.724627
C	0.527564	0.105730	-0.702846

F	0.001785	-0.976422	-1.379559	C	-1.658936	-0.356830	-1.837230
F	0.110060	1.225760	-1.355415	C	-1.779477	-1.814917	-2.217102
H	-1.696133	-0.697872	0.239942	C	-0.913278	-2.783566	-1.708868
H	0.476832	-0.791923	1.226510	C	-1.055554	-4.121182	-2.079780
H	0.338269	0.978443	1.241002	C	-2.062415	-4.505134	-2.960115
H	1.616893	0.048873	-0.783042	C	-2.932652	-3.541435	-3.470342
3F-EtOH				C	-2.789595	-2.207704	-3.101946
O	-1.413620	-0.081686	0.798024	H	1.770258	1.998446	4.049990
C	-0.009797	-0.093973	0.712859	H	1.034749	3.859914	2.910485
C	0.475392	-0.091233	-0.727796	H	-0.345964	2.806595	3.313330
F	1.820442	-0.012633	-0.780680	H	-0.284686	5.924867	-1.623568
F	0.099707	-1.185048	-1.408305	H	1.473449	5.651294	-1.735235
F	-0.023976	0.983983	-1.390609	H	0.672848	5.658759	-0.142672
H	-1.741103	0.727972	0.388082	H	2.656618	0.542539	-3.041782
H	0.337100	-1.010035	1.191399	H	1.555476	-0.651437	-2.334980
H	0.455854	0.762654	1.217025	H	4.069292	0.306503	0.050373
ManOH				H	6.020226	-1.092799	0.672947
O	1.492357	1.835701	3.143047	H	6.645850	-3.048027	-0.722317
C	0.593373	2.868216	2.751149	H	5.302506	-3.597498	-2.740490
C	0.277889	2.732761	1.273129	H	3.359184	-2.204205	-3.351210
H	-0.580895	3.381213	1.056443	H	-0.410248	-0.181241	3.016879
O	1.420493	3.196044	0.537701	H	-1.074505	-1.090088	1.649178
C	1.282847	3.146222	-0.862565	H	-1.748249	-2.045595	4.253014
H	2.263224	3.451671	-1.244117	H	-3.851094	-2.453048	5.478369
O	0.269453	3.998065	-1.345290	H	-5.861240	-1.072214	5.001572
C	0.556825	5.382008	-1.194745	H	-5.735790	0.724605	3.291789
C	0.949036	1.734730	-1.363148	H	-3.619385	1.125389	2.062877
H	0.762425	1.791480	-2.441741	H	-1.559107	0.251713	-2.748916
O	2.079731	0.920847	-1.094327	H	-2.575480	-0.025993	-1.327212
C	2.412058	-0.005249	-2.117257	H	-0.128883	-2.486970	-1.024259
C	3.594671	-0.843758	-1.695997	H	-0.373416	-4.863085	-1.676014
C	4.349568	-0.541777	-0.561435	H	-2.171717	-5.546282	-3.247472
C	5.443918	-1.334603	-0.215043	H	-3.723052	-3.829761	-4.157215
C	5.795532	-2.431828	-0.996102	H	-3.472484	-1.464030	-3.506555
C	5.042652	-2.738767	-2.129349	GlcOH			
C	3.949062	-1.950960	-2.473209	C	-1.507409	1.651570	-3.686122
C	-0.095247	1.295496	0.873528	O	-0.847635	1.099582	-2.549435
H	0.713492	0.624480	1.166605	C	-1.498969	1.374761	-1.342768
O	-1.306536	0.960501	1.544625	C	-0.624336	0.876284	-0.178540
C	-1.251392	-0.234382	2.313267	O	0.700110	1.380453	-0.205571
C	-2.545724	-0.432406	3.066892	C	0.927381	2.624625	0.445667
C	-2.623019	-1.436940	4.037695	C	0.744134	3.843780	-0.438234
C	-3.807893	-1.668304	4.729431	C	0.344242	5.060654	0.119953
C	-4.935826	-0.893108	4.463305	C	0.235491	6.204664	-0.668767
C	-4.863768	0.112956	3.504012	C	0.519403	6.141023	-2.031305
C	-3.676829	0.342132	2.808517	C	0.913415	4.928847	-2.596426
C	-0.295606	1.202549	-0.635551	C	1.028650	3.787936	-1.805800
H	-1.155571	1.824255	-0.908711	C	-0.543897	-0.657140	-0.176233
O	-0.543552	-0.156832	-0.986279	O	0.046277	-1.150811	1.020917
				C	1.470832	-1.211485	1.076466

C	2.048762	-0.323948	2.158727
C	1.270989	0.115717	3.230648
C	1.830702	0.902052	4.236787
C	3.178528	1.250447	4.189086
C	3.963273	0.810168	3.124485
C	3.400046	0.031371	2.116551
C	-1.941788	-1.286943	-0.266376
O	-1.887982	-2.684938	-0.518356
C	-1.689933	-3.552727	0.595837
C	-0.383487	-4.313874	0.526206
C	0.244545	-4.562978	-0.695501
C	1.417110	-5.314802	-0.746919
C	1.973353	-5.831698	0.421434
C	1.350271	-5.589064	1.644578
C	0.180803	-4.834072	1.694155
C	-2.750094	-0.658168	-1.410446
C	-4.187811	-1.129296	-1.454291
O	-4.734985	-0.737359	-2.708833
O	-2.775322	0.765860	-1.259559
H	-1.576138	2.741783	-3.597007
H	-0.897237	1.397782	-4.552055
H	-2.510244	1.233953	-3.804444
H	-1.702289	2.447687	-1.253465
H	-1.120602	1.189592	0.749621
H	1.962140	2.573181	0.796982
H	0.292734	2.706274	1.337046
H	0.113213	5.115685	1.181001
H	-0.077802	7.142575	-0.220776
H	0.429487	7.028269	-2.650230
H	1.133568	4.871760	-3.658297
H	1.314922	2.839321	-2.244004
H	0.040292	-0.979154	-1.045030
H	1.899714	-0.941922	0.109001
H	1.735481	-2.255966	1.278587
H	0.222374	-0.156023	3.262341
H	1.211657	1.240050	5.062251
H	3.614928	1.859847	4.974348
H	5.014147	1.078446	3.076270
H	4.016122	-0.299956	1.284491
H	-2.462617	-1.099258	0.683892
H	-2.522439	-4.269028	0.586795
H	-1.745385	-2.993431	1.532495
H	-0.188187	-4.156296	-1.602417
H	1.895521	-5.498757	-1.704175
H	2.886708	-6.416782	0.380639
H	1.779778	-5.980245	2.561776
H	-0.293411	-4.641743	2.653175
H	-2.275756	-0.925378	-2.360062
H	-4.735843	-0.670900	-0.619424
H	-4.201505	-2.218445	-1.337718
H	-5.668000	-0.973409	-2.723622

Activator

TfO⁻

S	0.270379	0.882206	0.414833
O	1.696679	0.975628	0.055299
O	-0.011469	0.657497	1.843955
O	-0.620780	1.838176	-0.266618
C	-0.232525	-0.758053	-0.356693
F	-0.061167	-0.759506	-1.696659
F	0.490875	-1.788616	0.133131
F	-1.531991	-1.047333	-0.127248

FSO₃⁻

S	0.000031	0.000000	-0.156998
F	0.000161	0.000000	1.535338
O	-1.434075	0.000000	-0.459598
O	0.716941	1.242035	-0.459372
O	0.716941	-1.242035	-0.459372

MsO⁻

O	-1.441269	-0.000000	-1.271187
S	0.000144	0.000000	-0.909726
O	0.720644	1.248188	-1.271986
C	0.000095	0.000000	0.917589
O	0.720644	-1.248188	-1.271986
H	1.032367	0.000000	1.269581
H	-0.516313	0.893960	1.268858
H	-0.516313	-0.893960	1.268858

Tf₂N⁻

S	0.825785	1.172321	0.099844
O	1.791367	1.712995	1.051931
O	1.246052	0.921706	-1.277113
N	-0.000000	-0.000000	0.837770
S	-0.825785	-1.172321	0.099843
O	-1.791367	-1.712995	1.051930
O	-1.246052	-0.921706	-1.277113
C	0.456422	-2.545965	-0.044252
F	1.506164	-2.168580	-0.780452
F	0.900597	-2.920826	1.162207
F	-0.102933	-3.619846	-0.631049
C	-0.456422	2.545966	-0.044252
F	-0.900597	2.920826	1.162207
F	0.102933	3.619846	-0.631049
F	-1.506164	2.168580	-0.780452

C₃F₆S₂O₄N⁻

O	1.670824	2.476758	0.912300
S	1.256195	1.408058	0.011251
N	1.700913	0.000000	0.672816

S	1.256195	-1.408058	0.011251
C	-0.627469	-1.309374	0.188958
F	-1.194968	-2.352831	-0.461704
F	-0.946009	-1.409690	1.498884
C	-1.246122	0.000000	-0.365166
F	-1.151840	0.000000	-1.710899
F	-2.577352	0.000000	-0.047949
C	-0.627469	1.309374	0.188958
F	-1.194968	2.352831	-0.461704
F	-0.946009	1.409690	1.498884
O	1.478627	-1.563956	-1.424090
O	1.670824	-2.476758	0.912300
O	1.478627	1.563956	-1.424090

Solvent**DCM**

Cl	-1.496181	0.000000	-0.834294
C	0.000000	0.000000	0.151397
H	0.000000	0.898069	0.758595
H	0.000000	-0.898069	0.758595
Cl	1.496181	0.000000	-0.834294

CHCl₃

Cl	1.00141	-0.08214	0.04810
C	2.77273	-0.07859	0.08300
H	3.13708	-0.18292	-0.94223
Cl	3.37971	1.45190	0.73720
Cl	3.37970	-1.44594	1.03208

Toluene

C	0.000000	0.006865	-2.229297
C	0.000000	-0.015533	-0.719333
C	-1.200404	-0.012617	-0.000802
C	-1.203309	-0.000020	1.392028
C	0.000000	0.007441	2.094572
C	1.203309	-0.000020	1.392028
C	1.200404	-0.012617	-0.000802
H	0.000000	1.034698	-2.608759
H	0.882894	-0.489118	-2.639973
H	-0.882894	-0.489118	-2.639973
H	-2.144384	-0.022278	-0.539169
H	-2.146761	0.000062	1.929350
H	0.000000	0.014470	3.179948
H	2.146761	0.000062	1.929350
H	2.144384	-0.022278	-0.539169

tert-butylbenzene

C	1.03252	-0.03386	-0.01238
C	2.57101	0.06688	-0.04893
C	3.11550	0.01937	1.39693

C	3.10889	-1.19200	-0.76695
C	2.96358	1.38576	-0.73824
C	2.73900	2.61951	-0.09606
C	3.07427	3.83282	-0.70426
C	3.63292	3.84322	-1.97696
C	3.85294	2.64083	-2.63949
C	3.52108	1.42675	-2.02805
H	0.70800	-0.96825	0.45996
H	0.61026	-0.00771	-1.02410
H	0.58212	0.79085	0.55167
H	2.89354	-0.94414	1.87106
H	2.67326	0.79070	2.03621
H	4.20302	0.15677	1.41386
H	2.84698	-2.10355	-0.21632
H	4.20137	-1.16603	-0.85537
H	2.68710	-1.29952	-1.77277
H	2.28849	2.65585	0.89306
H	2.89327	4.76853	-0.18214
H	3.89114	4.78488	-2.45299
H	4.28212	2.64268	-3.63826
H	3.70769	0.51820	-2.59331

Anisole

C	1.14586	-0.25066	-0.12817
O	2.51036	0.16600	-0.12800
C	3.10318	-0.03979	-1.34414
C	3.64814	1.07045	-1.98543
C	4.28725	0.91897	-3.21619
C	4.39849	-0.34745	-3.79176
C	3.87873	-1.46208	-3.13317
C	3.23489	-1.31113	-1.90371
H	0.69037	0.10010	0.80287
H	1.06070	-1.34156	-0.15110
H	0.59435	0.19702	-0.96285
H	3.56804	2.05337	-1.52957
H	4.70223	1.78600	-3.72243
H	4.90086	-0.46635	-4.74835
H	3.98401	-2.45069	-3.57284
H	2.86079	-2.18737	-1.38448

MTBE

C	-6.60414	-0.33061	0.05437
O	-5.19935	-0.47809	-0.08379
C	-4.73707	-1.47012	-1.01284
C	-5.18351	-2.87839	-0.60218
C	-5.18352	-1.15255	-2.44498
C	-3.20475	-1.39809	-0.94539
H	-6.78679	0.45666	0.79164
H	-7.06692	-1.24802	0.42589
H	-7.06696	-0.02002	-0.88540
H	-6.26487	-3.00736	-0.71760

H	-4.95143	-3.06928	0.45155
H	-4.69515	-3.64647	-1.21164
H	-6.26487	-1.27618	-2.56612
H	-4.69516	-1.81100	-3.17150
H	-4.95145	-0.11359	-2.70447
H	-2.85013	-1.59460	0.07321
H	-2.85014	-0.39456	-1.20824
H	-2.73237	-2.11922	-1.62071

ACN

C	-2.75374	-0.05943	0.04743
C	-1.22173	-0.05943	0.04743
N	-0.06173	-0.05943	0.04743
H	-3.11040	0.82272	0.53683
H	-3.11040	-0.92433	0.56669
H	-3.11040	-0.07667	-0.96123

α,α,α -trifluorotoluene

F	0.000000	-1.274939	2.657439
C	0.000000	-0.004958	2.185998
C	0.000000	0.030057	0.682890
C	1.209335	0.019966	-0.012490
C	1.206430	-0.002686	-1.404661
C	0.000000	-0.015252	-2.102057
C	-1.206430	-0.002686	-1.404661
C	-1.209335	0.019966	-0.012490
F	-1.087602	0.601128	2.710624
F	1.087602	0.601128	2.710624
H	2.146403	0.037469	0.531451
H	2.147810	-0.007540	-1.943578
H	0.000000	-0.031584	-3.186962
H	-2.147810	-0.007540	-1.943578
H	-2.146403	0.037469	0.531451

1,4-dioxane

O	-1.381564	0.000000	0.295914
C	-0.736678	-1.172467	-0.192174
C	0.736678	-1.172467	0.192174
O	1.381564	0.000000	-0.295914
C	0.736678	1.172467	0.192174
C	-0.736678	1.172467	-0.192174
H	-0.833016	-1.224953	-1.287302
H	-1.262200	-2.023135	0.248095
H	1.262200	-2.023135	-0.248095
H	0.833016	-1.224953	1.287302
H	1.262200	2.023135	-0.248095
H	0.833016	1.224953	1.287302
H	-0.833016	1.224953	-1.287302
H	-1.262200	2.023135	0.248095

References

1. Chatterjee, C.; Pong, F.; Sen, A., Chemical conversion pathways for carbohydrates. *Green Chem.* **2015**, *17* (1), 40-71.
2. Klemm, D.; Heublein, B.; Fink, H.-P.; Bohn, A., Cellulose: Fascinating Biopolymer and Sustainable Raw Material. *Angew. Chem. Int. Ed.* **2005**, *44* (22), 3358-3393.
3. Zhu, Y.; Romain, C.; Williams, C. K., Sustainable polymers from renewable resources. *Nature* **2016**, *540* (7633), 354-362.
4. Werz, D. B.; Seeberger, P. H., Carbohydrates as the next frontier in pharmaceutical research. *Chem.: Eur. J.* **2005**, *11* (11), 3194-3206.
5. Sharon, N.; Lis, H., Carbohydrates in cell recognition. *Sci. Am.* **1993**, *268* (1), 82-89.
6. Davis, B. G.; Fairbanks, A. J., Carbohydrate chemistry. *Oxford Chemistry Primers* **2002**, *99* (1), ALL-ALL.
7. Fischer, E., Ueber die Glucoside der Alkohole. *Ber. Dtsch. Chem. Ges.* **1893**, *26* (3), 2400-2412.
8. van der Vorm, S.; Hansen, T.; van Hengst, J. M.; Overkleeft, H. S.; van der Marel, G. A.; Codée, J. D., Acceptor reactivity in glycosylation reactions. *Chem. Soc. Rev.* **2019**, *48* (17), 4688-4706.
9. Hofmann, J.; Hahm, H. S.; Seeberger, P. H.; Pagel, K., Identification of carbohydrate anomers using ion mobility–mass spectrometry. *Nature* **2015**, *526*, 241.
10. Crich, D., Mechanism of a Chemical Glycosylation Reaction. *Acc. Chem. Res.* **2010**, *43* (8), 1144-1153.
11. Ranade, S. C.; Demchenko, A. V., Mechanism of chemical glycosylation: focus on the mode of activation and departure of anomeric leaving groups. *J. Carbohydr. Chem.* **2013**, *32* (1), 1-43.
12. Hosoya, T.; Takano, T.; Kosma, P.; Rosenau, T., Theoretical foundation for the presence of oxacarbenium ions in chemical glycoside synthesis. *J. Org. Chem.* **2014**, *79* (17), 7889-7894.

-
13. Walvoort, M. T.; van der Marel, G. A.; Overkleeft, H. S.; Codée, J. D., On the reactivity and selectivity of donor glycosides in glycochemistry and glycobiology: trapped covalent intermediates. *Chem. Sci.* **2013**, *4* (3), 897-906.
14. Chatterjee, S.; Moon, S.; Hentschel, F.; Gilmore, K.; Seeberger, P. H., An Empirical Understanding of the Glycosylation Reaction. *J. Am. Chem. Soc.* **2018**, *140* (38), 11942-11953.
15. Nukada, T.; Berces, A.; Zgierski, M. Z.; Whitfield, D. M., Exploring the Mechanism of Neighboring Group Assisted Glycosylation Reactions. *J. Am. Chem. Soc.* **1998**, *120* (51), 13291-13295.
16. Ratner, D. M.; Murphy, E. R.; Jhunjhunwala, M.; Snyder, D. A.; Jensen, K. F.; Seeberger, P. H., Microreactor-based reaction optimization in organic chemistry—glycosylation as a challenge. *Chem. Commun.* **2005**, (5), 578-580.
17. Park, Y.; Harper, K. C.; Kuhl, N.; Kwan, E. E.; Liu, R. Y.; Jacobsen, E. N., Macrocyclic bis-thioureas catalyze stereospecific glycosylation reactions. *Science* **2017**, *355* (6321), 162-166.
18. Fraser-Reid, B.; Wu, Z.; Udodong, U. E.; Ottosson, H., Armed/disarmed effects in glycosyl donors: rationalization and sidetracking. *J. Org. Chem.* **1990**, *55* (25), 6068-6070.
19. Ratcliffe, A. J.; Fraser-Reid, B., Generation of α -D-glucopyranosylacetonitrilium ions. Concerning the reverse anomeric effect. *J. Chem. Soc., Perkin Trans. 1* **1990**, (3), 747-750.
20. Ramshaw, C. In *The incentive for process intensification*, BHR Group Conference Series Publication, Mechanical Engineering Publications Limited: 1995; pp 1-4.
21. Stankiewicz, A.; Moulijn, J. A., *Re-engineering the chemical processing plant: process intensification*. CRC Press: 2003.
22. Yeong, K. K.; Gavriilidis, A.; Zapf, R.; Hessel, V., Experimental studies of nitrobenzene hydrogenation in a microstructured falling film reactor. *Chem. Eng. Sci.* **2004**, *59* (16), 3491-3494.
23. Plutschack, M. B.; Pieber, B. u.; Gilmore, K.; Seeberger, P. H., The hitchhiker's guide to flow chemistry. *Chem. Rev.* **2017**, *117* (18), 11796-11893.
24. Elvira, K. S.; i Solvas, X. C.; Wootton, R. C. R.; deMello, A. J., The past, present and potential for microfluidic reactor technology in chemical synthesis. *Nat. Chem.* **2013**, *5* (11), 905-915.
25. Pastre, J. C.; Browne, D. L.; Ley, S. V., Flow chemistry syntheses of natural products. *Chem. Soc. Rev.* **2013**, *42* (23), 8849-8869.

26. Tsubogo, T.; Oyamada, H.; Kobayashi, S., Multistep continuous-flow synthesis of (R)- and (S)-rolipram using heterogeneous catalysts. *Nature* **2015**, 520 (7547), 329-332.
27. Kim, H.; Min, K.-I.; Inoue, K.; Im, D. J.; Kim, D.-P.; Yoshida, J.-i., Submillisecond organic synthesis: Outpacing Fries rearrangement through microfluidic rapid mixing. *Science* **2016**, 352 (6286), 691-694.
28. Tanaka, S. i.; Goi, T.; Tanaka, K.; Fukase, K., Highly Efficient α -Sialylation by Virtue of Fixed Dipole Effects of N-Phthalyl Group: Application to Continuous Flow Synthesis of α (2-3)- and α (2-6)-Neu5Ac-Gal Motifs by Microreactor. *J. Carbohydr. Chem.* **2007**, 26 (7), 369-394.
29. Tanaka, K.; Mori, Y.; Fukase, K., Practical synthesis of a Man β (1-4) GlcNTroc fragment via microfluidic β -mannosylation. *J. Carbohydr. Chem.* **2009**, 28 (1), 1-11.
30. Volbeda, A. G.; van der Marel, G. A.; Codée, J. D., Protecting Group Strategies in Carbohydrate Chemistry. *Protecting Groups—Strategies and Applications in Carbohydrate Chemistry*, ed. S. Vidal, Wiley-VCH, Weinheim **2019**, 1-28.
31. Wang, T.; Demchenko, A. V., Synthesis of carbohydrate building blocks via regioselective uniform protection/deprotection strategies. *Org. Biomol. Chem.* **2019**, 17 (20), 4934-4950.
32. Matthies, S.; McQuade, D. T.; Seeberger, P. H., Homogeneous gold-catalyzed glycosylations in continuous flow. *Org. Lett.* **2015**, 17 (15), 3670-3673.
33. Kawakami, H.; Goto, K.; Mizuno, M., Multi-step synthesis of a protected monosaccharide unit by iterative reactions in microreactors and fluoruous liquid-phase extractions. *Chem. Lett.* **2009**, 38 (9), 906-907.
34. Jones, R. V.; Godorhazy, L.; Varga, N.; Szalay, D.; Urge, L.; Darvas, F., Continuous-flow high pressure hydrogenation reactor for optimization and high-throughput synthesis. *J. Comb. Chem.* **2006**, 8 (1), 110-116.
35. Ekholm, F. S.; Mándity, I. M.; Fülöp, F.; Leino, R., Rapid, simple, and efficient deprotection of benzyl/benzylidene protected carbohydrates by utilization of flow chemistry. *Tetrahedron Lett.* **2011**, 52 (16), 1839-1841.
36. Tanaka, K.; Fukase, K., Acid-mediated reactions under microfluidic conditions: A new strategy for practical synthesis of biofunctional natural products. *Beilstein J. Org. Chem.* **2009**, 5 (1), 40.
37. Miyagawa, A.; Tomita, R.; Kurimoto, K.; Yamamura, H., Selective deprotection of trityl group on carbohydrate by microflow reaction inhibiting migration of acetyl group. *Synth. Commun.* **2016**, 46 (6), 556-562.

-
38. Webb, D.; Jamison, T. F., Continuous flow multi-step organic synthesis. *Chem. Sci.* **2010**, *1* (6), 675-680.
39. Cancogni, D.; Lay, L., Exploring glycosylation reactions under continuous-flow conditions. *Synlett* **2014**, *25* (20), 2873-2878.
40. Plante, O. J.; Palmacci, E. R.; Seeberger, P. H., Automated solid-phase synthesis of oligosaccharides. *Science* **2001**, *291* (5508), 1523-1527.
41. Naresh, K.; Schumacher, F.; Hahm, H. S.; Seeberger, P., Pushing the limits of automated glycan assembly: synthesis of a 50mer polymannoside. *Chem. Commun.* **2017**, *53* (65), 9085-9088.
42. Andrade, R. B.; Plante, O. J.; Melean, L. G.; Seeberger, P. H., Solid-phase oligosaccharide synthesis: preparation of complex structures using a novel linker and different glycosylating agents. *Org. Lett.* **1999**, *1* (11), 1811-1814.
43. Hewitt, M. C.; Seeberger, P. H., Automated solid-phase synthesis of a branched *Leishmania* cap tetrasaccharide. *Org. Lett.* **2001**, *3* (23), 3699-3702.
44. Wilsdorf, M.; Schmidt, D.; Bartetzko, M.; Dallabernardina, P.; Schuhmacher, F.; Seeberger, P.; Pfrengle, F., A traceless photocleavable linker for the automated glycan assembly of carbohydrates with free reducing ends. *Chem. Commun.* **2016**, *52* (66), 10187-10189.
45. Ganesh, N. V.; Fujikawa, K.; Tan, Y. H.; Stine, K. J.; Demchenko, A. V., HPLC-assisted automated oligosaccharide synthesis. *Org. Lett.* **2012**, *14* (12), 3036-3039.
46. Pistorio, S. G.; Nigudkar, S. S.; Stine, K. J.; Demchenko, A. V., HPLC-assisted automated oligosaccharide synthesis: implementation of the autosampler as a mode of the reagent delivery. *J. Org. Chem.* **2016**, *81* (19), 8796-8805.
47. Satoh, H.; Manabe, S., Design of chemical glycosyl donors: does changing ring conformation influence selectivity/reactivity? *Chem. Soc. Rev.* **2013**, *42* (10), 4297-4309.
48. Nigudkar, S. S.; Demchenko, A. V., Stereocontrolled 1, 2-cis glycosylation as the driving force of progress in synthetic carbohydrate chemistry. *Chem. Sci.* **2015**, *6* (5), 2687-2704.
49. Garcia, A.; Otte, D. A.; Salamant, W. A.; Sanzone, J. R.; Woerpel, K., Acceleration of acetal hydrolysis by remote alkoxy groups: Evidence for electrostatic effects on the formation of oxocarbenium ions. *Angew. Chem. Int. Ed.* **2015**, *54* (10), 3061-3064.
50. Lourenço, E. C.; Ventura, M. R., The effect of electron withdrawing protecting groups at positions 4 and 6 on 1, 2-cis galactosylation. *Tetrahedron* **2013**, *69* (34), 7090-7097.

51. Alabugin, I. V.; Gilmore, K. M.; Peterson, P. W., Hyperconjugation. *Wiley Interdiscip. Rev. Comput. Mol. Sci.* **2011**, *1* (1), 109-141.
52. Alabugin, I. V., *Stereoelectronic effects: a bridge between structure and reactivity*. John Wiley & Sons: 2016.
53. Hoang, K. L. M.; He, J.-x.; Băti, G.; Chan-Park, M. B.; Liu, X.-W., A minimalist approach to stereoselective glycosylation with unprotected donors. *Nat. Commun.* **2017**, *8* (1), 1146.
54. Tvaroška, I.; Bleha, T., Anomeric and exo-anomeric effects in carbohydrate chemistry. In *Adv. Carbohydr. Chem. Biochem.*, Elsevier: 1989; Vol. 47, pp 45-123.
55. Kalikanda, J.; Li, Z., Study of the stereoselectivity of 2-azido-2-deoxygalactosyl donors: Remote protecting group effects and temperature dependency. *J. Org. Chem.* **2011**, *76* (13), 5207-5218.
56. Baek, J. Y.; Lee, B.-Y.; Jo, M. G.; Kim, K. S., β -Directing effect of electron-withdrawing groups at O-3, O-4, and O-6 positions and α -directing effect by remote participation of 3-O-acyl and 6-O-acetyl groups of donors in Mannopyranosylations. *J. Am. Chem. Soc.* **2009**, *131* (48), 17705-17713.
57. Jensen, H. H.; Nordstrøm, L. U.; Bols, M., The disarming effect of the 4, 6-acetal group on glycoside reactivity: torsional or electronic? *J. Am. Chem. Soc.* **2004**, *126* (30), 9205-9213.
58. Huang, M.; Garrett, G. E.; Birlirakis, N.; Bohé, L.; Pratt, D. A.; Crich, D., Dissecting the mechanisms of a class of chemical glycosylation using primary ^{13}C kinetic isotope effects. *Nat. Chem.* **2012**, *4* (8), 663.
59. Crich, D.; Cai, W., Chemistry of 4, 6-O-benzylidene-D-glycopyranosyl triflates: contrasting behavior between the gluco and manno series. *J. Org. Chem.* **1999**, *64* (13), 4926-4930.
60. Crich, D.; Chandrasekera, N. S., Mechanism of 4, 6-O-Benzylidene-Directed β -Mannosylation as Determined by α -Deuterium Kinetic Isotope Effects. *Angew. Chem. Int. Ed.* **2004**, *43* (40), 5386-5389.
61. Schmidt, R. R.; Michel, J., Facile synthesis of α - and β -O-glycosyl imidates; preparation of glycosides and disaccharides. *Angew. Chem. Int. Ed.* **1980**, *19* (9), 731-732.
62. Pozsgay, V.; Jennings, H. J., A new, stereoselective synthesis of methyl 1, 2-trans-1-thioglycosides. *Tetrahedron Lett.* **1987**, *28* (13), 1375-1376.
63. Lemieux, R., The mercaptolysis of glucose and galactose pentaacetates. *Can. J. Chem.* **1951**, *29* (12), 1079-1091.

-
64. Garegg, P. J., Thioglycosides as glycosyl donors in oligosaccharide synthesis. In *Adv. Carbohydr. Chem. Biochem.*, Elsevier: 1997; Vol. 52, pp 179-205.
65. Hashimoto, S.-i.; Honda, T.; Ikegami, S., A rapid and efficient synthesis of 1, 2-trans- β -linked glycosides via benzyl-or benzoyl-protected glycopyranosyl phosphates. *J. Chem. Soc., Chem. Commun.* **1989**, (11), 685-687.
66. Martin, T. J.; Brescello, R.; Toepfer, A.; Schmidt, R. R., Synthesis of phosphites and phosphates of neuraminic acid and their glycosyl donor properties—convenient synthesis of GM 3. *Glycoconjugate J.* **1993**, 10 (1), 16-25.
67. Martin, T. J., Efficient sialylation with phosphite as leaving group. *Tetrahedron Lett.* **1992**, 33 (41), 6123-6126.
68. Kondo, H.; Ichikawa, Y.; Wong, C. H., . beta.-Sialyl phosphite and phosphoramidite: synthesis and application to the chemoenzymic synthesis of CMP-sialic acid and sialyl oligosaccharides. *J. Am. Chem. Soc.* **1992**, 114 (22), 8748-8750.
69. Sim, M. M.; Kondo, H.; Wong, C. H., Synthesis of dibenzyl glycosyl phosphites using dibenzyl N, N-diethylphosphoramidite as phosphitylating reagent: an effective route to glycosyl phosphates, nucleotides, and glycosides. *J. Am. Chem. Soc.* **1993**, 115 (6), 2260-2267.
70. Demchenko, A. V., Stereoselective chemical 1, 2-cis O-glycosylation: from ‘sugar ray’ to modern techniques of the 21st century. *Synlett* **2003**, 2003 (09), 1225-1240.
71. Paulsen, H., Advances in selective chemical syntheses of complex oligosaccharides. *Angew. Chem. Int. Ed.* **1982**, 21 (3), 155-173.
72. Sinay, P.-e., Recent advances in glycosylation reactions. *Pure Appl. Chem.* **1978**, 50 (11-12), 1437-1452.
73. Orgueira, H. A.; Bartolozzi, A.; Schell, P.; Seeberger, P. H., Conformational locking of the glycosyl acceptor for stereocontrol in the key step in the synthesis of heparin. *Angew. Chem. Int. Ed.* **2002**, 41 (12), 2128-2131.
74. Van der Vorm, S.; Hansen, T.; Overkleeft, H.; Van der Marel, G.; Codee, J., The influence of acceptor nucleophilicity on the glycosylation reaction mechanism. *Chem. Sci.* **2017**, 8 (3), 1867-1875.
75. Schumann, B.; Parameswarappa, S. G.; Lisboa, M. P.; Kottari, N.; Guidetti, F.; Pereira, C. L.; Seeberger, P. H., Nucleophile-Directed Stereocontrol Over Glycosylations Using Geminal-Difluorinated Nucleophiles. *Angew. Chem. Int. Ed.* **2016**, 55 (46), 14431-14434.

76. Crich, D., Methodology Development and Physical Organic Chemistry: A Powerful Combination for the Advancement of Glycochemistry. *J. Org. Chem.* **2011**, 76 (22), 9193-9209.
77. Hosoya, T.; Kosma, P.; Rosenau, T., Contact ion pairs and solvent-separated ion pairs from d-mannopyranosyl and d-glucopyranosyl triflates. *Carbohydr. Res.* **2015**, 401, 127-131.
78. Kononov, L. O.; Malysheva, N. N.; Orlova, A. V.; Zinin, A. I.; Laptinskaya, T. V.; Kononova, E. G.; Kolotyckina, N. G., Concentration dependence of glycosylation outcome: a clue to reproducibility and understanding the reasons behind. *Eur. J. Org. Chem.* **2012**, 2012 (10), 1926-1934.
79. Huang, M.; Retailleau, P.; Bohé, L.; Crich, D., Cation clock permits distinction between the mechanisms of α - and β -O- and β -C-glycosylation in the mannopyranose series: evidence for the existence of a mannopyranosyl oxocarbenium ion. *J. Am. Chem. Soc.* **2012**, 134 (36), 14746-14749.
80. Adero, P. O.; Furukawa, T.; Huang, M.; Mukherjee, D.; Retailleau, P.; Bohé, L.; Crich, D., Cation clock reactions for the determination of relative reaction kinetics in glycosylation reactions: Applications to gluco- and mannopyranosyl sulfoxide and trichloroacetimidate type donors. *J. Am. Chem. Soc.* **2015**, 137 (32), 10336-10345.
81. van der Vorm, S.; van Hengst, J. M.; Bakker, M.; Overkleeft, H. S.; van der Marel, G. A.; Codée, J. D., Mapping the Relationship between Glycosyl Acceptor Reactivity and Glycosylation Stereoselectivity. *Angew. Chem.* **2018**, 130 (27), 8372-8376.
82. van der Vorm, S.; Overkleeft, H. S.; van der Marel, G. A.; Codée, J. D., Stereoselectivity of Conformationally Restricted Glucosazide Donors. *J. Org. Chem.* **2017**, 82 (9), 4793-4811.
83. Durantie, E.; Bucher, C.; Gilmour, R., Fluorine-Directed β -Galactosylation: Chemical Glycosylation Development by Molecular Editing. *Chem.: Eur. J.* **2012**, 18 (26), 8208-8215.
84. Rencurosi, A.; Lay, L.; Russo, G.; Caneva, E.; Poletti, L., Glycosylation with trichloroacetimidates in ionic liquids: influence of the reaction medium on the stereochemical outcome. *J. Org. Chem.* **2005**, 70 (19), 7765-7768.
85. Lucero, C. G.; Woerpel, K., Stereoselective C-glycosylation reactions of pyranoses: the conformational preference and reactions of the mannosyl cation. *J. Org. Chem.* **2006**, 71 (7), 2641-2647.
86. Bucher, C.; Gilmour, R., Fluorine-Directed Glycosylation. *Angew. Chem. Int. Ed.* **2010**, 49 (46), 8724-8728.

-
87. Adero, P. O.; Amarasekara, H.; Wen, P.; Boh, L.; Crich, D., The experimental evidence in support of glycosylation mechanisms at the SN1–SN2 interface. *Chem. Rev.* **2018**, *118* (17), 8242-8284.
88. Frihed, T. G.; Bols, M.; Pedersen, C. M., Mechanisms of Glycosylation Reactions Studied by Low-Temperature Nuclear Magnetic Resonance. *Chem. Rev.* **2015**, *115* (11), 4963-5013.
89. Kononov, L. O.; Fedina, K. G.; Orlova, A. V.; Kondakov, N. N.; Abronina, P. I.; Podvalnyy, N. M.; Chizhov, A. O., Bimodal concentration-dependent reactivity pattern of a glycosyl donor: Is the solution structure involved? *Carbohydr. Res.* **2017**, *437*, 28-35.
90. Kumar, A.; Kumar, V.; Dere, R. T.; Schmidt, R. R., Glycoside Bond Formation via Acid–Base Catalysis. *Org. Lett.* **2011**, *13* (14), 3612-3615.
91. Sasaki, K.; Nagai, H.; Matsumura, S.; Toshima, K., A novel greener glycosidation using an acid–ionic liquid containing a protic acid. *Tetrahedron Lett.* **2003**, *44* (30), 5605-5608.
92. Bennett, C. S., *Selective Glycosylations: Synthetic Methods and Catalysts*. John Wiley & Sons: 2017.
93. Kafle, A.; Liu, J.; Cui, L., Controlling the stereoselectivity of glycosylation via solvent effects. *Can. J. Chem.* **2016**, *94* (11), 894-901.
94. Satoh, H.; Hansen, H. S.; Manabe, S.; van Gunsteren, W. F.; Henberger, P. H., Theoretical investigation of solvent effects on glycosylation reactions: stereoselectivity controlled by preferential conformations of the intermediate oxacarbenium-counterion complex. *J. Chem. Theory Comput.* **2010**, *6* (6), 1783-1797.
95. Coley, C. W.; Barzilay, R.; Jaakkola, T. S.; Green, W. H.; Jensen, K. F., Prediction of Organic Reaction Outcomes Using Machine Learning. *ACS Cent. Sci.* **2017**, *3* (5), 434-443.
96. Butler, K. T.; Davies, D. W.; Cartwright, H.; Isayev, O.; Walsh, A., Machine learning for molecular and materials science. *Nature* **2018**, *559* (7715), 547-555.
97. de Almeida, A. F.; Moreira, R.; Rodrigues, T., Synthetic organic chemistry driven by artificial intelligence. *Nat. Rev. Chem.* **2019**, 1-16.
98. Ahneman, D. T.; Estrada, J. G.; Lin, S.; Dreher, S. D.; Doyle, A. G., Predicting reaction performance in C–N cross-coupling using machine learning. *Science* **2018**, *360* (6385), 186-190.
99. Wei, J. N.; Duvenaud, D.; Aspuru-Guzik, A., Neural Networks for the Prediction of Organic Chemistry Reactions. *ACS Cent. Sci.* **2016**, *2* (10), 725-732.

100. Sanchez-Lengeling, B.; Aspuru-Guzik, A., Inverse molecular design using machine learning: Generative models for matter engineering. *Science* **2018**, *361* (6400), 360-365.
101. Zahrt, A. F.; Henle, J. J.; Rose, B. T.; Wang, Y.; Darrow, W. T.; Denmark, S. E., Prediction of higher-selectivity catalysts by computer-driven workflow and machine learning. *Science* **2019**, *363* (6424), eaau5631.
102. Reid, J. P.; Sigman, M. S., Holistic prediction of enantioselectivity in asymmetric catalysis. *Nature* **2019**, *571* (7765), 343-348.
103. Zheng, F.; Zhang, Q.; Li, J.; Suo, J.; Wu, C.; Zhou, Y.; Liu, X.; Xu, L., Machine learning induction of chemically intuitive rules for the prediction of enantioselectivity in the asymmetric syntheses of alcohols. *Chemometrics and Intelligent Laboratory Systems* **2015**, *145*, 39-47.
104. Granda, J. M.; Donina, L.; Dragone, V.; Long, D.-L.; Cronin, L., Controlling an organic synthesis robot with machine learning to search for new reactivity. *Nature* **2018**, *559* (7714), 377.
105. Zhang, Z.; Ollmann, I. R.; Ye, X.-S.; Wischnat, R.; Baasov, T.; Wong, C.-H., Programmable One-Pot Oligosaccharide Synthesis. *J. Am. Chem. Soc.* **1999**, *121* (4), 734-753.
106. Eggensperger, K.; Feurer, M.; Hutter, F.; Bergstra, J.; Snoek, J.; Hoos, H.; Leyton-Brown, K. In *Towards an empirical foundation for assessing bayesian optimization of hyperparameters*, NIPS workshop on Bayesian Optimization in Theory and Practice, 2013; p 3.
107. Skoraczynski, G.; Dittwald, P.; Miasojedow, B.; Szymkuć, S.; Gajewska, E. P.; Grzybowski, B. A.; Gambin, A., Predicting the outcomes of organic reactions via machine learning: are current descriptors sufficient? *Sci Rep* **2017**, *7* (1), 3582.
108. Friedman, J.; Hastie, T.; Rosset, S.; Tibshirani, R.; Zhu, J., Discussion of boosting papers. *Ann. Statist* **2004**, *32*, 102-107.
109. Kumar, A.; Geng, Y.; Schmidt, R. R., Silicon Fluorides for Acid-Base Catalysis in Glycosidations. *Adv. Synth. Catal.* **2012**, *354* (8), 1489-1499.
110. Chatterjee, S.; Guidi, M.; Gilmore, K.; Seeberger, P. H., Automated Radial Synthesis of Organic Molecules. *Nature* **2020**, Accepted.
111. Vibhute, A. M.; Muvvala, V.; Sureshan, K. M., A Sugar-Based Gelator for Marine Oil-Spill Recovery. *Angew. Chem. Int. Ed.* **2016**, *55* (27), 7782-7785.
112. Kitowski, A.; Jimenez-Moreno, E.; Salvadó, M.; Mestre, J.; Castillón, S.; Jimenez-Osés, G.; Boutureira, O.; Bernardes, G. a. J., Oxidative Activation of C–S Bonds with an

Electropositive Nitrogen Promoter Enables Orthogonal Glycosylation of Alkyl over Phenyl Thioglycosides. *Org. Lett.* **2017**, *19* (19), 5490-5493.

113. Schmidt, R. R.; Michel, J.; Roos, M., Glycosylimidate, 12 Direkte Synthese von O- α -und O- β -Glycosyl-imidaten. *Liebigs Ann. Chem.* **1984**, *1984* (7), 1343-1357.

114. Calosso, M.; Tambutet, G.; Charpentier, D.; St-Pierre, G.; Vaillancourt, M.; Bencheqroun, M.; Gratton, J.-P.; Provost, M.; Guindon, Y., Acyclic tethers mimicking subunits of polysaccharide ligands: selectin antagonists. *ACS Med. Chem. Lett.* **2014**, *5* (9), 1054-1059.

115. Zeng, J.; Vedachalam, S.; Xiang, S.; Liu, X.-W., Direct C-glycosylation of organotrifluoroborates with glycosyl fluorides and its application to the total synthesis of (+)-Varitriol. *Org. Lett.* **2010**, *13* (1), 42-45.

116. Kim, S.; Song, S.; Lee, T.; Jung, S.; Kim, D., Practical synthesis of KRN7000 from phytosphingosine. *Synthesis* **2004**, *2004* (06), 847-850.

117. Su, Y.; Xie, J.; Wang, Y.; Hu, X.; Lin, X., Synthesis and antitumor activity of new shikonin glycosides. *Eur. J. Med. Chem.* **2010**, *45* (7), 2713-2718.

118. Norberg, O.; Wu, B.; Thota, N.; Ge, J.-T.; Fauquet, G.; Saur, A.-K.; Aastrup, T.; Dong, H.; Yan, M.; Ramström, O., Synthesis and binding affinity analysis of α 1-2- and α 1-6-O/S-linked dimannosides for the elucidation of sulfur in glycosidic bonds using quartz crystal microbalance sensors. *Carbohydr. Res.* **2017**, *452*, 35-42.

119. Weck, S.; Opatz, T., β -Selective C-mannosylation of electron-rich phenols. *Synthesis* **2010**, *2010* (14), 2393-2398.

120. Tsuda, T.; Arihara, R.; Sato, S.; Koshiba, M.; Nakamura, S.; Hashimoto, S., Direct and stereoselective synthesis of β -D-mannosides using 4, 6-O-benzylidene-protected mannosyl diethyl phosphite as a donor. *Tetrahedron* **2005**, *61* (45), 10719-10733.

121. Cheng, J. M.; Dangerfield, E. M.; Timmer, M. S.; Stocker, B. L., A divergent approach to the synthesis of iGb3 sugar and lipid analogues via a lactosyl 2-azidosphingosine intermediate. *Org. Biomol. Chem.* **2014**, *12* (17), 2729-2736.

122. Wang, Z.; Zhou, L.; El-Boubbou, K.; Ye, X.-s.; Huang, X., Multi-component one-pot synthesis of the tumor-associated carbohydrate antigen Globo-H based on preactivation of thioglycosyl donors. *J. Org. Chem.* **2007**, *72* (17), 6409-6420.

123. Wegmann, B.; Schmidt, R. R., Synthesis of the H-disaccharide (2-O- α -L-fucopyranosyl-D-galactose) via the trichloroacetimidate method. *Carbohydr. Res.* **1988**, *184*, 254-261.

124. Shie, C. R.; Tzeng, Z. H.; Kulkarni, S. S.; Uang, B. J.; Hsu, C. Y.; Hung, S. C., Cu(OTf)₂ as an Efficient and Dual-Purpose Catalyst in the Regioselective Reductive Ring Opening of Benzylidene Acetals. *Angew. Chem. Int. Ed.* **2005**, *44* (11), 1665-1668.
125. Nokami, T.; Shibuya, A.; Tsuyama, H.; Suga, S.; Bowers, A. A.; Crich, D.; Yoshida, J.-i., Electrochemical generation of glycosyl triflate pools. *J. Am. Chem. Soc.* **2007**, *129* (35), 10922-10928.
126. Briner, K.; Vasella, A., Glycosylidene Carbenes. Part 6. Synthesis of alkyl and fluoroalkyl glycosides. *Helv. Chim. Acta* **1992**, *75* (2), 621-637.
127. Liu, X.; Zhang, B.; Gu, X.; Chen, G.; Chen, L.; Wang, X.; Xiong, B.; You, Q.-D.; Chen, Y.-L.; Shen, J., 1, 2-trans-1-Dihydroxyboryl benzyl S-glycoside as glycosyl donor. *Carbohydr. Res.* **2014**, *398*, 45-49.
128. Vidadala, S. R.; Hotha, S., Methyl glycosides are identified as glycosyl donors for the synthesis of glycosides, disaccharides and oligosaccharides. *Chem. Commun.* **2009**, (18), 2505-2507.
129. Toshima, K.; Nagai, H.; Kasumi, K.-i.; Kawahara, K.; Matsumura, S., Stereocontrolled glycosidations using a heterogeneous solid acid, sulfated zirconia, for the direct syntheses of α - and β -manno- and 2-deoxyglucopyranosides. *Tetrahedron* **2004**, *60* (25), 5331-5339.
130. Higashi, K.; Susaki, H., A novel glycosidation promoted by the combination of trimethylsilyl halide and zinc triflate. *Chem. Pharm. Bull.* **1992**, *40* (8), 2019-2022.
131. Chang, G. X.; Lowary, T. L., A glycosylation protocol based on activation of glycosyl 2-pyridyl sulfones with samarium triflate. *Org. Lett.* **2000**, *2* (11), 1505-1508.
132. He, H.; Zhu, X., Thioperoxide-mediated activation of thioglycoside donors. *Org. Lett.* **2014**, *16* (11), 3102-3105.
133. Koshiba, M.; Suzuki, N.; Arihara, R.; Tsuda, T.; Nambu, H.; Nakamura, S.; Hashimoto, S., Catalytic Stereoselective Glycosidation with Glycosyl Diphenyl Phosphates: Rapid Construction of 1, 2-cis- α -Glycosidic Linkages. *Chem. Asian J.* **2008**, *3* (8-9), 1664-1677.